Enhanced ambiguity resolution and integrity monitoring methods for Precise Point Positioning

Altti Samuli Jokinen

A thesis submitted for the Degree of Doctor of Philosophy of Imperial College London and the Diploma of Imperial College London

Centre for Transport Studies

Department of Civil and Environmental Engineering

Imperial College London

August 2014

London, UK

Abstract

Centimetre-level Global Navigation Satellite System (GNSS) based positioning is increasingly relevant for a large number of applications. Currently, this level of GNSS positioning accuracy is most commonly achieved using the conventional Real Time Kinematic (cRTK) method. In order to achieve such high-accuracies with cRTK, the distance (baseline) between the user and reference station must typically be shorter than 50 km for dual-frequency GNSS receivers.

To address the limitations of cRTK, the Precise Point Positioning (PPP) method, which does not require local reference networks, was developed. The principle of PPP is to model and correct error sources such as satellite orbit and clock errors using correction products and error modelling.

PPP is not currently suitable for many applications, because of the long solution convergence time (from 20 to 60 min to achieve 10 cm accuracy), insufficient positioning accuracies and a lack of integrity monitoring. Current fixed ambiguity PPP methods are analysed and tested using the National Oceanic and Atmospheric Administration (NOAA) dataset in this thesis. Based on the analysis, the most reliable existing validation method has unacceptably large rate (12.7%) of incorrect ambiguity resolution. Therefore, this thesis develops an enhanced PPP method.

The enhanced PPP method is based on using the enhanced ambiguity validation method (e.g. time-window based validation) and employing both GLONASS and GPS measurements to calculate a float position solution. In addition, integrity monitoring is improved in terms of failure exclusion and protection level calculation. When employing the enhanced PPP method, the rate of incorrect ambiguity resolution decreases to 5.3% and of correct ambiguity resolution increases to 82.2% when using the (NOAA) dataset. The average horizontal, vertical and 3D position errors at the initial ambiguity resolution epoch are reduced by 40.0%, 23.8% and 31.8%, respectively, compared to the most reliable existing PPP method.

Acknowledgements

I would first like to give special thanks to my PhD supervisors Professor Washington Yotto Ochieng, Dr. Wolfgang Schuster and Dr. Shaojun Feng for helping and providing advice during my PhD studies and thesis writing. I also thank Dr. Khalid Nur and Ramin Moradi for commenting on this thesis.

This research was carried out as a part of iNsight (www.insight-gnss.org), a collaborative research project funded by the UK's Engineering and Physical Sciences Research Council (EPSRC) to extend the applications and improve the efficiency of positioning through the exploitation of new global navigation satellite systems signals. The project was undertaken by a consortium of twelve UK university and industrial groups: Imperial College London, University College London, the University of Nottingham, the University of Westminster, EADS Astrium, Nottingham Scientific Ltd, Leica Geosystems, Ordnance Survey of Great Britain, QinetiQ, STMicroelectronics, Thales Research and Technology UK Limited, and the UK Civil Aviation Authority.

I would like to thank all the university and industrial partners, who participated in the iNsight project, and the UK's Engineering and Physical Sciences Research Council (EPSRC) for funding this PhD research. I want to give a special mention of the following iNsight project members in recognition of their support: Professor Terry Moore, Dr. Chris Hide, Dr. Lei Yang, Dr. Chris Hill, Dr. Zeynep Elmas, Dr. Carl Milner, Professor Izzet Kale, Dr. Yacine Adane, Dr. Alper Ucar, Dr. Burak Bardak, Professor Marek Ziebart, Dr. Paul Groves, Dr. Mojtaba Bahrami, Dr. Ziyi Jiang and Dr. Santosh Bhattarai.

I would also like to thank the following PPP experts for the valuable discussions and ideas: Denis Laurichesse, Dr. Jianghui Geng, Paul Collins and Professor Richard Langley.

In addition, I acknowledge the support of the UK Natural Environment Research Council (NERC) through its British Isles continuous GNSS Facility (BIGF) for providing Ordnance Survey GNSS observation data, the British Atmospheric Data Centre and the UK Met Office for providing Unified Model numerical weather modelling data.

I would also like to thank everyone from the Department of Civil and Environmental Engineering at Imperial College London, and my colleagues from NovAtel Inc. and Nokia Oyj.

Last but not least, my sincere thanks go to my parents, and my wife Yuanshuo Wu.

Declaration of copyright

Declaration of contribution

I hereby declare that the work presented in this thesis is carried by me with advice from my supervisors Professor Washington Yotto Ochieng, Dr. Wolfgang Schuster and Dr. Shaojun Feng and other iNsight project members. I also declare that all referenced work are properly cited and listed.

Table of the contents

List of figures

List of tables

Abbreviations

ANTEX	ANTenna Exchange
BSD	Between-Satellite Difference
BSDFCB	Between-Satellite-Difference Fractional Cycle Bias
C/A	Coarse/Acquisition
CDMA	Code Division Multiple Access
CKFRAIM	Cumulative Kalman Filter Receiver Autonomous Integrity Monitoring
CNES	Centre National d'Etudes Spatiales
CODE	Center for Orbit Determination in Europe
CPU	Central Processing Unit
CRAIM	Carrier Receiver Autonomous Integrity Monitoring
cRTK	conventional Real Time Kinematic
CSAC	Chip-Scale Atomic Clock
DCB	Differential-Code Biases
DDPPP	Double-Differenced PPP
DBT	Dong Bock Test
DORIS	Doppler Orbitography and Radio-positioning Integrated by Satellite
ECEF	Earth Centered Earth Fixed
ECI	Earth-Centered Inertial
EGNOS	European Geostationary Navigation Overlay Service
EKF	Extended Kalman Filter

ENU	East North Up
EU	European Union
ESA	European Space Agency
ESOC	European Space Operations Centre
EWL	Extra-Wide-Lane
FCB	Fractional Cycle Bias
FDMA	Frequency Division Multiple Access
FOC	Full Operational Capability
GAGAN	GPS Aided Geo Augmented Navigation
GBAS	Ground-Based Augmentation System
GBP	Great Britain Pounds
GLONASS	GLObalnaya NAvigatsionnaya Sputnikovaya Sistema
GMF	Global Mapping Function
GEO	Geostationary Earth Orbit
GPT	Global Pressure and Temperature
GSI	Geospatial Information Authority of Japan
GNSS	Global Navigation Satellite System
GPS	Global Positioning System
IAC	Information-Analytical Centre
ICRAIM	Imperial College Carrier Receiver Autonomous Integrity Monitoring
IGS	International GNSS service
IGSO	Inclined Geo-Synchronous Orbit

IERS	International Earth Rotation and Reference Systems Service
ILSC	Integer Least-Squares using Constant ratio test threshold
ILSDNCF	Integer Least-Squares using Doubly Non-Central F-distribution based ratio test threshold
ILSFFS	Integer Least-Squares using Fixed Failure rate ratio test threshold Simulation based method
INS	Inertial Navigation System
iNsight	Innovative Navigation using new GNSS Signals with Hybridised Technologies
IOV	In-Orbit Validation
IPP	Ionosphere Pierce Point
IRC	Integer Recovery Clocks
ITRF	International Terrestrial Reference Frame
ITRS	International Terrestrial Reference System
JGD	Japanese Geodetic Datum
JPL	Jet Propulsion Laboratory
LAMBDA	Least-squares AMBiguity Decorrelation Adjustment
LBS	Location Based Services
LEO	Low Earth Orbit
LTE-4G	Long Term Evolution toward 4th Generation
MCM	Minimum Constellation Method
MEO	Middle Earth Orbiting
MSAS	Multi-functional Satellite Augmentation System

MW	Melbourne-Wubbena
MWWL	Melbourne–Wubbena Wide Lane
NAD	North American Datum
NAE	North Atlantic European
NGS	US National Geodetic Survey
NLOS	Non Line-Of-Sight
NOAA	National Oceanic and Atmospheric Administration
Non-GEO	Non-Geostationary Earth Orbit
NWM	Numerical Weather Modelling
P	Precision
PANDA	Position And Navigation Data Analyst
PCO	Phase Centre Offset
PCV	Phase Centre Variation
PDOP	Position Dilution Of Precision
PLL	Phase Lock Loop
PPP	Precise Point Positioning
PRN	Pseudo Random Noise
PZ-90	Earth Parameters 1990/ Parametry Zemli 1990
QZSS	Quasi Zenith Satellite System
RAIM	Receiver Autonomous Integrity Monitoring
SD	Standard Deviation
RHCP	Right-Hand Circularly Polarized

RICS	Royal Institution of Chartered Surveyors
RMS	Root Mean Square
RTCM	Radio Technical Commission for Maritime Services
RTPP	Real-Time Pilot Project
SBAS	Satellite-Based Augmentation System
SLR	Satellite Laser Ranging
STEC	Slant Total Electron Content
TEC	Total Electron Content
TECR	Total Electron Content Rate
TRIM	Temporally Relative Ionospheric Model
TRS	Terrestrial Reference System
UAS	Unmanned Aircraft Systems
UDFCB	Un-Difference Fractional Cycle Bias
UKMO	UK Met Office
UNAVCO	University Navstar Consortium
UPD	Un-calibrated Phase Delay
USD	United States Dollars
USNO	United States Naval Observatory
UTC	Coordinated Universal Time
V2I	Vehicle to Infrastructure
V2V	Vehicle to Vehicle
VLBI	Very Long Baseline Interferometry

VMF1	Vienna Mapping Function 1
WAAS	Wide Area Augmentation System
WGS	World Geodetic System
WL	Wide-Lane

List of symbols

a	Integer ambiguity candidate vector
$\hat{a}$	Float ambiguity vector
$\check{a}$	Integer ambiguity vector
a_1	GPS carrier-phase standard deviation formula parameter
a_2	GPS carrier-phase standard deviation formula parameter
a_e	Length of the Earth semi-major axis
B	Saastamoinen model specific correction parameter
$B_{L3,r}$	Receiver L3 carrier-phase bias
$B_{L3,s}$	Satellite L3 carrier-phase bias
$B_{P3,r}$	Receiver P3 code-phase bias
$B_{P3,s}$	Satellite P3 code-phase bias
$B_{wl,r}$	Wide-lane receiver FCB
$B_{wl,s}$	Wide-lane satellite FCB
B_{P1-P2}	Bias between the P1 and P2 signals
B_{P1-C1}	Bias between the P1 and C1 signals
B_{P2-C2}	Bias between the P2 and C2 signals
$b_{(c_1,c_2,c_5)}$	Generic triple-frequency combination of float ambiguities
b_3	Ionosphere-free float ambiguity
b_{nl}	Narrow-lane float ambiguity
b_{wl}	Wide-lane float ambiguity

c	Speed of light
c_1	L1 carrier-phase coefficient
c_2	L2 carrier-phase coefficient
c_5	L5 carrier-phase coefficient
C_{E5}	Galileo E5 code-phase measurement
Cor_{C1}	DCB correction to the C1 signal
Cor_{C2}	DCB correction to the C2 signal
D_{layer}	Tropospheric delay in each layer
D_{trop}	Total slant tropospheric delay
D_h^z	Tropospheric dry delay
D_w^z	Tropospheric wet delay
d	Distance between the receiver and satellite
E	Elevation angle of the satellite
E_{hor}	Magnitude of the horizontal position error
E_k	Eccentric anomaly of the satellite orbit
e	Partial pressure of the water vapour
e_g	Geometry based term
e_{LS}	Estimation error
e_s	Satellite orbital eccentricity
F	Frequency index of an observation. F = 1 (GPS/GLONASS L1), F = 2 (GPS/ GLONASS L2), F = 5 (GPS L5) and F = 3 (GPS/GLONASS ionosphere-free L1/L2 measurement combination.

F_r	Constant $-4.442807633 * 10^{-10} \frac{s}{m^{1/2}}$
f_F	Frequency of the GNSS signal. F refers to the frequency index.
f_1	Frequency of the L1 GNSS signal
f_2	Frequency of the L2 GNSS signal
f_5	Frequency of the L5 GNSS signal
$fCent$	Centred chi-square density function
G	Gravitational constant
G_E	Tropospheric gradient to the East direction
G_{E5}	Galileo L5 carrier-phase and E5 code-phase measurement combination
G_N	Tropospheric gradient to the North direction
G_{P1}	Single-frequency code-phase and carrier-phase measurement combination
GM	Gravitational parameter of the Earth
GM_1	Gravitational parameter of the Moon
GM_2	Gravitational parameter of the Sun
H	Design matrix
H_{EKF}	EKF design matrix
HPL	Horizontal protection level
HPL_1	Horizontal protection level 1
HPL_2	Horizontal protection level 2
$HSLOPE$	Linear relation between the magnitude of the test statistic and horizontal position error

h_2	Second degree Shida dimensionless number.
I	Identity matrix or vector
I_1	First-order ionospheric delay
I_2	Second-order ionospheric delay
I_3	Third-order ionospheric delay
I_4	Geometry-free combination ionospheric delay
L_{E5}	Galileo L5 carrier-phase measurement
I_{wl}	Wide-lane combination ionospheric delay
i	Index of the current satellite
j	Index of the base-satellite
$K_{1,2,3}$	Constant for numerical weather modelling
k	Degrees of freedom
$\bar{k}$	Satellite to the receiver unit vector
k_H	Horizontal factor reflecting the probability of missed detection
k_v	Vertical factor reflecting the probability of missed detection
k_r	Ratio test acceptation threshold
L_F	L carrier-phase measurement at the frequency F in metres.
L_1	L1 carrier-phase measurement is metres
L_2	L2 carrier-phase measurement is metres
L_3	L1/L2 ionosphere-free combination of carrier-phase measurements
L_4	L1/L2 geometry-free measurement combination
L_5	L5 carrier-phase measurement is metres

L_{wl}	L1/L2 geometry-dependent wide-lane combination
l_2	Nominal second degree Love dimensionless number
M	Code-phase multipath error
M_e	Mass of the Earth
m	Carrier-phase multipath error
m_4	Carrier-phase multipath in the geometry-free combination
m_{wl}	Carrier-phase multipath error in the wide-lane combination
$m(E)_{azi}$	Tropospheric gradient mapping function
$m(E)_h$	Tropospheric dry delay mapping function
$m(E)_{h/w}$	Tropospheric wet or dry delay mapping function
$m(E)_w$	Tropospheric wet delay mapping function
$N_{(c_1,c_2,c_5)}$	Generic triple-frequency combination of fixed ambiguities
N_{wl}	Wide-lane integer ambiguity
N_{nl}	Narrow-lane integer ambiguity
N_3	Ionosphere-free fixed ambiguity
n	Refractivity
n_a	Number of ambiguities
n_g	Code-phase ionospheric refraction index
n_m	Number of measurements
n_p	Carrier-phase ionospheric refraction index
nominalBias	Chosen nominal bias value
P_F	P code-phase measurement at the frequency F.

P_1	P1 code-phase measurement
$\widetilde{P_1}$	Smoothed P1 code-phase measurement
$\bar{P}_1 - \bar{L}_1$	Mean P1 code-phase minus L1 carrier-phase difference since the last loss of carrier-phase lock (cycle-slip)
P_2	P2 code-phase measurement
P_3	The L1/L2 ionosphere-free combination of P code-phase measurements
P_c	Failure rate of the ambiguity resolution
P_{EKF}^-	EKF predicted variance matrix
P_{EKF}^+	EKF updated variance matrix
P_{FA}	Accepted false alarm rate
P_{local}	EKF P matrix converted into the local (East, North, Up) coordinate system
P_{MD}	Probability of missed detection
P_{parity}	Parity transformation matrix
p	Parity vector
p_d	Partial pressure of the dry
Q	Code-phase measurement noise
$Q_{\hat{a}}$	Variance/co-variance matrix of float ambiguities
Q_{EKF}	EKF system noise matrix
$Q_{\hat{z}}$	Z-transformed ambiguity variance matrix
q	Carrier-phase measurement noise
q_4	Noise of the geometry-free carrier-phase combination

q_{wl}	Noise of the wide-lane combination noise
R_{ca}	Residuals between the fixed ambiguity candidate vectors and float ambiguity vector ($ca = 1$, the best candidate) and ($ca = 2$, the second best candidate)
$\bar{R}$	Unit vector pointing from the receiver to the satellite
R_{EKF}	EKF measurement noise matrix
$\overline{\Delta r}$	Solid earth tides effect
$\overline{r}_{sat}$	Vector from the centre of the Earth to the mass centre of the satellite
$\overline{r}_{Sun}$	Vector from the centre of the Earth to the centre of the Sun
S	Distance which a signal has travelled in the layer
$SLOPE$	Linear relation between the magnitude of the test statistic and position error
$SLOPE_{max}$	Maximum SLOPE value
std	GPS carrier-phase standard deviation
T	Temperature
T_D	Detection threshold
T_{KF}	CKFRAIM test statistic
T_{L1}	L1 carrier-phase test statistic
T_{L1-L2}	Wide-lane carrier-phase test statistic
T_P	Code-phase test statistic
T_{total}	Total test statistic
$TECR$	Total Electron Content Rate
t	Time epoch

$\hat{t}_u$	Time at the linearisation point u
$\bar{R}_j$	Geocentric state unit vectors of the Moon and Sun
$\hat{r}^i$	Distance between the satellite and linearisation point
$\bar{r}$	Geocentric unit state vector of the station
VPL	Vertical protection level
VPL_1	Vertical protection level 1
VPL_2	Vertical protection level 2
$VSLOPE$	Linear relation between the magnitude of the test statistic and vertical position error
W_{EKF}	EKF weight matrix
w	Residual vector
$w_{largest}$	Largest residual
$w_{secondLargest}$	Second largest residual
$\left(X_p - \bar{X}_p\right)$	Pole coordinates variation X component relative to the X mean pole $\bar{X}_p$
$(\bar{z}', \bar{y}', \bar{z}')$	Satellite body coordinate unit vectors
$(\bar{x}, \bar{y}, \bar{z})$	Receiver body coordinate unit vectors
$\bar{x}$	Unit vector pointing from the GNSS receiver to the centre of the mass of the Earth
$\bar{x_{EKF}}$	EKF predicted state
x_{EKF}^+	EKF updated state
x_l^2	LAMBDA method related position constant
$\hat{x}_{LS}$	Least-squares solution

$x_s^i,$	X coordinate of the satellite i
$\hat{x}_u$	X coordinate at the linearisation point u
$(Y_p - \bar{Y}_p)$	Pole coordinates variation: Y component relative to the Y mean pole $\bar{Y}_p$
y	Measurement vector
y_s^i	Y coordinate of the satellite i
$\hat{y}_u$	Y coordinate at the linearisation point u
z	Zenith distance of the satellite
$\hat{z}$	Z-transformed float ambiguity vector
Z	Z-transformation matrix
Z_d	Compressibility factor density of the dry air
Z^n	Integer numbers
z_{EKF}	EKF observation vector
z_l	Z-transformed integer ambiguity vector
z_s^i	Z coordinate of the satellite i
$\hat{z}_u$	Z coordinate at the linearisation point u
Z_w	Compressibility factor density of water vapour
$\beta_{(c_1,c_2,c_5)}$	Generic triple-frequency first-order ionospheric error contribution
Δp	Linearised measurement vector
Δx	Vector of unknown states
Δt	Time difference between two epochs
Δt_r	Relativistic effect correction

Δt_s	Shapiro delay correction
Δt_u	Receiver clock offset difference from the linearisation point
Δx_u	X coordinate difference from the linearisation point
Δy_u	Y coordinate difference from the linearisation point
Δz_u	Z coordinate difference from the linearisation point
$\Delta\phi$	Satellite phase wind-up
φ	Azimuth angle of the satellite
ϕ	Latitude
$\phi_{(c_1,c_2,k)}$	Generic triple-frequency carrier-phase combination
ϕ_1	L1 carrier-phase in cycles
ϕ_2	L2 carrier-phase in cycles
ϕ_5	L5 carrier-phase in cycles
σ	Variance of an ambiguity term
σ_H	Horizontal position uncertainty
σ_V	Vertical position uncertainty
λ	Longitude
λ_1	L1 signal wavelength
λ_3	Ionosphere-free combination wavelength
λ_n	Narrow-lane combination wavelength
λ_{nc}	Non-centrality parameter
λ_{wl}	Wide-lane combination wavelength
θ_g	Greenwich mean sidereal time

Φ_{EKF}	EKF state transition matrix
Φ_{L1}	L1 carrier-phase in cycles
Φ_{L1-L2}	Wide-lane carrier-phase in cycles
ϵ	Error vector
ϵ_1	Range error
δ_R	Saastamoinen model specific correction parameter
$\delta\phi$	Latitude error (EKF state)
$\delta\lambda$	Longitude error (EKF state)
δh	Height error (EKF state)
$\delta\dot{\phi}, \delta\dot{\lambda}, \delta\dot{h}$	Velocities (EKF states)
δdT	Receiver clock offset (EKF state)
δs	Satellite clock error
$\delta d\dot{T}$	Receiver clock offset change (EKF state)
δT_{Trop}	Tropospheric wet delay (EKF state)
$\delta b_3^1,,,\delta b_3^n$	Ionosphere-free float ambiguities (EKF states)
δ_1	Non-centrality parameters of the Chi-square distribution
δ_2	Non-centrality parameters of the Chi-square distribution

List of related publications

JOKINEN, A., FENG, S., MILNER, C., SCHUSTER, W., OCHIENG, W., HIDE, C., MOORE, T. & HILL, C. 2011. Precise Point Positioning and Integrity Monitoring with GPS and GLONASS. The European Navigation Conference (ENC) 2011. London, United Kingdom.

JOKINEN, A., FENG, S., MILNER, C., SCHUSTER, W., OCHIENG, W., HIDE, C., MOORE, T. & HILL, C. 2012. Improving fixed-ambiguity Precise Point Positioning (PPP) convergence time and accuracy by using GLONASS. Proceedings of the 25th International Technical Meeting of, The Satellite Division of the Institute of Navigation (ION GNSS 2012). Nashville, Tennessee.

JOKINEN, A., FENG, S., OCHIENG, W., MILNER, C., SCHUSTER, W., HIDE, C., MOORE, T. & HILL, C. 2012. Fixed ambiguity Precise Point Positioning (PPP) with FDE RAIM. Position Location and Navigation Symposium (PLANS), 2012 IEEE/ION. Myrtle Beach, South Carolina DOI: 10.1109/PLANS.2012.6236939.

JOKINEN, A., FENG, S., SCHUSTER, W., OCHIENG, W., HIDE, C., MOORE, T. & HILL, C. 2013. Fixed Ambiguity Precise Point Positioning (PPP) Using Tropospheric Corrections Based on Numeric Weather Modeling (NWM). ION Pacific PNT. Honolulu, Hawaii.

JOKINEN, A., FENG, S., SCHUSTER, W., OCHIENG, W., HIDE, C., MOORE, T. & HILL, C. 2013. GLONASS aided GPS ambiguity fixed Precise Point Positioning. Journal of Navigation, 66, 399–416 DOI: 10.1017/S0373463313000052.

JOKINEN, A., FENG, S., SCHUSTER, W., OCHIENG, W., HIDE, C., MOORE, T. & HILL, C. 2013. Integrity monitoring of fixed ambiguity Precise Point Positioning (PPP) solutions. Geo-spatial Information Science, 16, 141-148 DOI: 10.1080/10095020.2013.817111.

JOKINEN, A., FENG, S., SCHUSTER, W., OCHIENG, W., YANG, L., MOORE, T. & HILL, C. 2013. Improving Ambiguity Validation and Integrity Monitoring of Precise Point Positioning (PPP). Proceedings of the 26th International Technical Meeting of The Satellite Division of the Institute of Navigation (ION GNSS 2013). Nashville, Tennessee

JOKINEN, A., ELLUM, C., NEUMANN, J., CHAN, D., WEBSTER, I., MASTERSON, S. & MORLEY, T. 2014. Kinematic Performance of NovAtel CORRECT with TerraStar-D Precise Point Positioning (PPP) Service. *Proceedings of the 27th International Technical Meeting of The Satellite Division of the Institute of Navigation (ION GNSS 2014).* Tampa FL (in press).

FENG, S., JOKINEN, A., MILNER, C. & OCHIENG, W. 2013. New methods for dual constellation single receiver positioning and integrity monitoring. *Geo-spatial Information Science,* 16**,** 201-209 DOI: 10.1080/10095020.2013.834112.

FENG, S., JOKINEN, A. & OCHIENG, W. 2014a. Integrity Monitoring for Precise Point Positioning. *Proceedings of the 27th International Technical Meeting of The Satellite Division of the Institute of Navigation (ION GNSS 2014).* Tampa FL.

FENG, S., JOKINEN, A., OCHIENG, W., LIU, J. & ZENG, Q. 2014b. Receiver Autonomous Integrity Monitoring for Fixed Ambiguity Precise Point Positioning. *China Satellite Navigation Conference (CSNC) 2014 Proceedings: Volume II Lecture Notes in Electrical Engineering,* 304**,** 159-169.

FENG, S., JOKINEN, A., OCHIENG, W. & MILNER, C. 2012. Multi-Constellation RAIM in the Presence of Multiple Faults-a Bottom Up Approach. *Proceedings of the 25th International Technical Meeting of The Satellite Division of the Institute of Navigation (ION GNSS 2012).* Nashville, TN.

FENG, S., MILNER, C., JOKINEN, A., OCHIENG, W., HIDE, C., MOORE, T., HILL, C., ZIEBART, M., BAHRAMI, M., GROVES, P. & JIANG, Z. 2011. A Novel Positioning and Integrity Monitoring Algorithm for a Multiple Constellation Receiver. *Proceedings of the 24th International Technical Meeting of The Satellite Division of the Institute of Navigation (ION GNSS 2011).* Portland, OR.

MILNER, C., FENG, S., JOKINEN, A., OCHIENG, W., HIDE, C., HILL, C. & MOORE, T. 2011. A Holistic Approach to Carrier-Phase Receiver Autonomous Integrity Monitoring (CRAIM). *Proceedings of the 24th International Technical Meeting of The Satellite Division of the Institute of Navigation (ION GNSS 2011).* Portland, OR.

MORADI, R., SCHUSTER, W., FENG, S., JOKINEN, A. & OCHIENG, W. 2014. The carrier-multipath observable: a new carrier-phase multipath mitigation technique. *GPS Solutions* DOI: 10.1007/s10291-014-0366-8.

1 Introduction

This chapter provides the motivation for the research carried out in this thesis. The basics of satellite navigation and high accuracy satellite based positioning are discussed. Thereafter, the aims and objectives of the thesis are presented. Finally, the outline of the thesis is given.

1.1 Background

Nowadays, satellite based navigation has a large economic impact. It is estimated that the global market value of the core Global Navigation Satellite System (GNSS) market is 55 billion Great British Pounds (GBP) and global market value of the GNSS enabled market is 132 billion GBP (GSA, 2012). The core GNSS market includes only the value of the products and services which are directly attributable to GNSS. The GNSS enabled market includes the full market value of all GNSS enabled products. The core GNSS market is divided into the following segments: road (54.0 %), Location Based Services (LBS) (43.7%), agriculture (1.0%), surveying (0.6%), aviation (0.5%) and maritime (0.1%) (GSA, 2012). Based on this market research, the consumer-focused road and LBS segments, which currently require typically metre level positioning accuracy, dominate the GNSS market in terms of value. On the other hand, while representing a smaller percentage of the total market share, professional segments such as agriculture, surveying, aviation and maritime require higher accuracy and integrity than consumer applications.

Even though the market share of professional GNSS segments is small, GNSS can provide significant economic benefits in many professional applications such as agriculture and surveying. For example, it is estimated that employing GNSS provides 19.9 billon United States Dollar (USD) benefits for crop farming applications and 9.2 billion USD benefits in the engineering construction (heavy, civil and surveying) applications annually in the USA (Pham, 2011). Therefore, the professional GNSS market is important, despite its small market share compared to the total GNSS market.

1.1.1 Satellite navigation systems

There are currently two Global Navigation Satellite Systems (GNSS) with full operational capability and global coverage: the Global Positioning System (GPS) developed by the USA and GLObalnaya NAvigatsionnaya Sputnikovaya Sistema (GLONASS) developed by Russia (IAC, 2012). In addition, the People's Republic of China is developing the BeiDou system (BeiDou, 2012a) and the European Union (EU) the Galileo system (EU, 2011). However, BeiDou and Galileo cannot currently provide global coverage.

Positioning accuracy of a few metres can be obtained with code-phase measurements using standalone GPS with a dual-frequency surveying-grade receiver (Kaplan and Hegarty, 2006). Modern GNSS receivers can also provide carrier-phase measurements, which can provide centimetre or even millimetre positioning accuracy.

The fundamentals of GNSS positioning and GNSS systems as well as current challenges are discussed in detail in Chapter 3.

1.1.2 High accuracy positioning methods

The feasibility to achieve high accuracy (centimetre level) positioning was demonstrated in the 1980s using the conventional Real Time Kinematic (cRTK) method. The principle of this method is to use a stationary reference receiver with a known location and mitigate errors that are correlated between this receiver and the user (rover) receiver by differencing measurements across these receivers. If errors in the measurements can be cancelled or reduced sufficiently, it is possible to use carrier-phase measurements and achieve millimetre to centimetre-level accuracies (Remondi, 1984, Counselman and Gourevitch, 1981). This however, assumes that measurement errors are correlated between the two receivers. In order for this to be the case, the distance (baseline) between the rover and reference receivers must typically be less than 50 km when employing dual-frequency receivers (Kaplan and Hegarty, 2006). Nevertheless, high ionospheric activity can cause de-correlations even at baselines shorter than 50 km.

The requirement of a reference receiver at a known location makes cRTK expensive in remote areas where there are no existing local GNSS reference networks. In addition, it may

be difficult to build local GNSS reference networks in some areas, because of problems with electricity supply and telecommunications, political instability and difficult natural conditions. Therefore, a different type of method may be more viable: Precise Point Positioning (PPP). Local reference network infrastructure is not required for PPP (Zumberge et al., 1997). In the case of PPP, errors in the measurements are removed or mitigated by employing error modelling and error correction products such as precise satellite orbit and clock error corrections. The principle of PPP was first discussed by Heroux et al. (1993). It was demonstrated in Zumberge et al. (1997) that it is possible to obtain centimetre-level positioning accuracy by employing PPP and post-processing data.

Carrier-phase measurements provide only information on the number of carrier-phase cycles since the receiver has obtained phase lock. To obtain absolute range information, initial integer valued ambiguity terms in carrier-phase measurements must be resolved. To obtain millimetre to centimetre level positioning accuracy using PPP processing, the resolution of the ambiguities is beneficial. Ambiguity resolution was not attempted for the early PPP models such as Zumberge et al. (1997). This was due to Fractional Cycle Bias (FCB) errors in the carrier-phase measurements (Ge et al., 2008). FCBs are non-integer type of bias errors mainly caused by hardware delays (Geng et al., 2010b). FCB erors are also referred to as Un-calibrated Phase Delay (UPD) errors in the literature. Nowadays, it is possible to use global reference networks to generate FCB corrections (Collins, 2008, Ge et al., 2008, Geng, 2009, Laurichesse and Mercier, 2007), thereby resolving this problem. The FCB corrections can be applied at user-level, which enables PPP ambiguity resolution. All required PPP error corrections such as precise satellite orbits and clocks, and FCB corrections can even be generated in real-time (Laurichesse et al., 2010).

Despite the benefits of PPP, it is not suitable for all applications. The primary issue of PPP is the long time required for solution convergence, including ambiguity resolution. Solution convergence and ambiguity resolution are linked, because obtaining correct ambiguity resolution reduces the time required to obtain, for example, smaller than 5 cm position error. However, having a sufficiently converged float solution is required before an initial ambiguity resolution is possible. For example, typically between 20 and 90 minutes are required to obtain an initial ambiguity resolution when employing current PPP models (Geng et al., 2010d, Laurichesse et al., 2010). This is unacceptably long in comparison to the

few second time-period which is needed to fix ambiguities when employing the cRTK method (Kaplan and Hegarty, 2006).

In addition, the resolution and validation of carrier-phase ambiguities can be an issue when employing PPP. Methods to validate carrier-phase ambiguities are presented, for example, in Feng et al. (2012) and Verhagen and Teunissen (2013), but the suitability of the methods for PPP ambiguity validation is not tested widely in the literature. Therefore, the rates for correct and wrong ambiguity resolution when using these methods for real-data PPP processing are not known.

Little research has been carried out on the integrity of PPP. A possible method to monitor the integrity of PPP is presented in Feng et al. (2010). Nevertheless, the method has only been tested with limited data in the literature, insufficient to fully characterise performance.

1.2 Aims and objectives

The aim of this thesis is to develop an improved PPP capability. This is achieved through the objectives to identify applications for high accuracy (centimetre level) positioning, analyse and evaluate current PPP methods, develop an enhanced PPP method to address the issues with the current methods and analyse and test the enhanced PPP method. The most relevant issues are ambiguity resolution, accuracy, convergence time and integrity monitoring.

1.2.1 Identify applications for high accuracy (centimetre-level) positioning

The first aim of this thesis is to identify possible applications and their requirements for centimetre level positioning. The applications are analysed based on their requirements in terms of time criticality, accuracy, integrity, availability and continuity. Time criticality refers to the need for real-time positioning and immediate position solution convergence. Accuracy can be defined at a confidence level (e.g. 95%) of the position error magnitude that all position estimates fall within. Position error refers to the difference between a coordinate estimate and the known reference (true) coordinates. Integrity refers to the ability to warn a user within a given period of time (time-to-alert), if a position error exceeds

the alert limit. This detection must be made with respect to predetermined probabilities of false alert and missed detection. The availability refers to the percentage of time that positioning is available with the required accuracy, integrity and continuity. Continuity refers to the ability to continue positioning with the required accuracy and integrity without non-scheduled interruptions after the required level of accuracy is first achieved (the position solution has already converged to the required accuracy).

1.2.2 Analyse and evaluate the current Precise Point Positioning (PPP) methods

The performance of PPP is dependent on the error correction products and models used. Current correction models and products are analysed and the most suitable models and products are selected based on their accuracy, availability and real-time processing suitability.

Current fixed ambiguity PPP methods are analysed and tested using the most suitable error correction products. The method refers to the algorithm used for position calculation and products refer to error corrections such as precise satellite orbit and clock which are provided by external parties. The suitability of the products is defined based on accuracy, availability and real-time processing suitability.

The analysis criteria for the current fixed ambiguity PPP methods are time required to obtain an initial ambiguity resolution, ambiguity fixing rate, rate of incorrect ambiguity resolution and position error at the initial ambiguity resolution epoch. The most promising methods are chosen based on these criteria.

1.2.3 Develop enhanced PPP method

Taking into account the issues identified based on analysing and testing existing PPP methods, an enhanced PPP method is developed. The enhanced PPP method must provide positioning with the highest possible accuracy, lowest possible rate of wrong ambiguity resolution, shortest possible time required to obtain an initial ambiguity resolution and highest possible integrity. In addition, the enhanced PPP method must be suitable for real-

time use and must use error correction products and models which are openly and freely available on the internet.

1.2.4 Analyse the performance of the new method

The enhanced PPP method is tested using real GNSS data. Its performance is analysed based on the criteria defined in Section 1.2.2 and compared to existing PPP methods.

The performance of the enhanced PPP method must be compared to the requirements of the applications. Based on this analysis, the benefit of the enhanced PPP method is determined and its suitability for select real-life applications analysed.

Finally, the current status and future directions of PPP are analysed.

1.3 Outline

Applications for centimetre level positioning, their requirements and current available positioning methods suitable for these applications are analysed in Chapter 2. GNSS, error sources and current error corrections methods are discussed in Chapter 3. Current PPP methods are presented in Chapter 4.

The current PPP methods are tested and their limitations are evaluated in Chapter 5. To address issues with the current methods, this thesis develops an enhanced PPP method in Chapter 5. The performance of the enhanced method is evaluated and its suitability for different real-life applications is analysed in Chapter 6. Finally, Chapter 7 concludes the thesis and provides an overview of possible future work.

2 Applications for centimetre level positioning

Positioning applications which require centimetre level positioning accuracy or better are discussed in this chapter. The applications are first analysed in Section 2.1, then the requirements for the applications are provided in Section 2.2 and finally, the currently used positioning methods for different applications are analysed in Section 2.3.

2.1 Applications

Applications for centimetre level positioning are identified in this section. The applications can be divided into following categories: surveying, agriculture, scientific, satellite orbit determination, aviation and military, intelligent transport systems, maritime and oil and gas applications.

Surveying is the most well-known application area with centimetre level positioning requirements. High accuracy surveying can be divided into control surveying, where the aim is to obtain positions of control points, which are used as reference points for detail surveying, where the aim is to obtain positions of objects, which need, for example, to be mapped (RICS, 2010).

Agriculture is currently a quickly growing application area (GSA, 2012). There are many agricultural applications which can benefit from centimetre level positioning: precision fertilizer placement, planting, harvesting, laying irrigation tape and automatic steering of farming devices (Buick, 2006). The primary motivation for applying high accuracy positioning to agriculture is to increase efficiency and reduce costs.

There are many scientific applications which can benefit from centimetre level positioning. For example, this level of accuracy is required for tsunami warning systems (Kato et al., 2005). Tsunamis can be detected based on changes in sea level, which can be measured using GNSS receivers placed in buoys in the ocean.

In addition, high accuracy GNSS positioning can also be applied to estimate sources and magnitudes of earthquakes in real-time (Blewitt et al., 2009). The estimation can be done

based on the tidal movements of the GNSS reference stations in the seismic active areas (Blewitt et al., 2009). In addition, high accuracy GNSS positioning can even be applied to predict earthquakes, volcanoes and behaviour of the cryosphere (area covered by ice and snow) (Hammond et al., 2011).

Centimetre level GNSS positioning can also be applied to Low Earth Orbit (LEO) satellite orbit determination, when a GNSS receiver is installed on a satellite (Montenbruck et al., 2005). The motivation of using GNSS for this purpose is to reduce costs compared to conventional satellite tracking technologies such as ground-based radar tracking (Montenbruck et al., 2005).

Centimetre level positioning also has many aviation and military applications. For example, cRTK based positioning is already used commercially for autonomous capture and landing of Unmanned Aircraft Systems (UAS) (Rockwell_Collins, 2012). Other possible aviation related applications are formation flying, mid-air refuelling and airborne photogrammetry (Porretta et al., 2009).

Intelligent transport systems are also a potential application area. The knowledge of the positions of devices can be beneficial, for example, for collision avoidance. It is estimated that up to 80% of collisions caused by impaired drivers can be avoided by employing Vehicle to Vehicle (V2V) and Vehicle to Infrastructure (V2I) technologies, which require accurate knowledge of the positions of the car and other devices (Stephenson et al., 2012). Additional road transportation applications which require centimetre level positioning are, for example, automatic highways, intelligent speed assistance and lane control (Porretta et al., 2009). Railroad applications are typically less challenging compared to road applications, because metre-level positioning accuracy is typically sufficient for railroad applications (Porretta et al., 2009). Therefore, railroad applications are not a particular interest in this thesis.

There are also maritime applications, for example, automatic docking, port operations, dredging and cargo handling. Further applications are maritime surveying, for example, for construction, hydrography and mapping underwater natural resources requires high positioning accuracy (Porretta et al., 2009). In the case of underwater natural resource

mapping, GNSS based methods cannot be used under water, but employing the methods can still be beneficial when doing mapping on the sea surface level.

Oil and gas business is also potential application area for high accuracy GNSS positioning. For example, it is vital to know the locations of oil and gas pipes and platforms with high positioning accuracy (Dixon, 2006). In addition, high accuracy positioning is required in some aviation related applications such as precision approaches to oil and gas platforms.

2.2 Requirements

The requirements for the applications in terms of accuracy, integrity, continuity, time criticality and availability, as defined in Section 1.2.1, are specified in this section. Accuracy requirements in this section refer to the 95% accuracy level, e.g. the magnitude of the position error must be smaller than the required accuracy in the 95% of cases.

For surveying, the required accuracy depends on the specific application. For control surveying, millimetre level accuracy is typically required based on the guidelines given by the Royal Institution of Chartered Surveyors (RICS) (RICS, 2010). For detail surveying, the accuracy requirement is typically between 1 and 10 cm based on the guidelines given by RICS (RICS, 2010). There are no specific integrity, availability or continuity requirements. However, the reliability, availability and continuity of positioning are important in practice. In terms of time criticality, both real-time and post-processing methods can be applied (RICS, 2010). Nevertheless, real-time positioning with immediate convergence is preferable in terms of operating costs.

For agricultural applications, the positioning accuracy requirement is application-dependent. For example, 2.5 cm is used as the pass-to-pass accuracy requirement for precision fertilizer placement, planting, harvesting, laying irrigation tape and automatic steering of farming devices (Buick, 2006). Agricultural applications are usually kinematic. In the case of automatic steering or other means of automatic control, particular attention must be given to integrity monitoring, to assure safety (Porretta et al., 2009). Positioning is carried out in real-time and immediate solution convergence is preferable, because farmers want to minimise the time when their machines cannot operate with full capability. In addition, high

availability and continuity are important because interruptions in service can cause loss of profit.

Centimetre level positioning accuracy is required for tsunami warning applications and positioning must be achieved in real-time (Kato et al., 2005). There are no specific integrity, continuity and availability requirements defined for the systems.

It the case of geodesy applications such as earthquake prediction and early warning systems, particular attention must be paid to the accuracy of positioning. In the case of earthquake prediction systems, millimetre positioning accuracy is required, but positioning can be done in post-processing and the data-rate can be relatively low (between 15 and 30 s) (Blewitt et al., 2009). In the case of earthquake early warning systems, the required positioning accuracy is at the centimetre level, but positioning must be obtained in real-time and with high data-rates at the level of 1 second (Blewitt et al., 2009). In addition, positioning integrity must be monitored to prevent false alerts and misdetections of earthquakes.

The determination of LEO satellite orbits based on GNSS technologies is still in experimental phase. The required positioning accuracy is at centimetre level (Montenbruck et al., 2005). To use GNSS based satellite orbit determination for real-applications, positioning must be achieved in real-time, with high integrity and continuity.

Most military or aviation applications are safety-critical. Thus, integrity is a key consideration. The requirements for aviation applications with high positioning accuracy are shown in Table 2.1. In the table, alert limit refers to the maximum error tolerance which is allowed without issuing an integrity alert, time to alert refers to the maximum time between the onset of a failure (error exceeding the alert limit) and the issuance of an alert. The allowed integrity risk refers to the probability of the position error exceeding the alert limit for a longer time-period than the value defined by the time to alert parameter (Porretta et al., 2009). In addition to the strict accuracy and integrity requirements, positioning must be carried out in real-time and high continuity as well as immediate position convergence even for the initial solution epoch are required (Porretta et al., 2009).

Application	Required accuracy (95%) (m)	Alert limit (m)	Time to alert (s)	Allowed integrity risk	Reference
Automatic landing (a military plane landing to an aircraft carrier)	0.30 (Vertical at touchdown)	1.1 (vertical)	1	10^{-6} (hazardously misleading information)	(Kim et al., 2004)
Mid-air refuel	0.01 (3D)	0.1 (3D)	Not defined	10^{-7} /h	(Porretta et al., 2009)
Formation flying	0.01(3D)	0.1 (3D)	Not defined	10^{-7} /h	
Photogrammetry	0.1 (Horizontal)	0.2 (Horizontal)	10	10^{-5} /h	

Table 2.1 Requirements for aviation applications

The requirements for selected intelligent transport system applications are shown in Table 2.2. It can be seen that although the accuracy requirements as not as strict, the others are similar to those of aviation applications.

Application	Horizontal accuracy (95%) (m)	Alert limit (m)	Time to alert (s)	Allowed integrity risk (1/h)
Automated highway	0.1 – 1.0	1	1	2×10^{-7}
Intelligent speed assistance	0.01 – 1.0	5	2	10^{-5}
Lane control	0.01 – 1.0	1	1	2×10^{-7}

Table 2.2 Requirements for intelligent transport system applications (Porretta et al., 2009)

The requirements for maritime applications are shown in Table 2.3. The accuracy requirements are application-dependent. For example, between 1 and 10 cm accuracy is required for automatic docking, whereas accuracies between 0.1 m and 36 m are acceptable for hydrography. The integrity and continuity requirements depend on the specific application, with some such as automatic docking having specified integrity requirements. Maritime applications can also include maritime surveying, which have similar requirements to land surveying.

Application	Accuracy (95%)	Alert limit (m)	Time to alert (s)	Allowed integrity risk (1/h)
Automatic Docking	0.01 m – 0.1 m(horizontal) and 0.1 kt (speed)	Not defined	10	10^{-6}
Cargo handling	0.1 m – 1 m (horizontal and vertical) and 0.1 kt (speed)	Not defined	10	Not defined
Construction/ offshore surveying	0.1 m – 10 m (horizontal) and 0.1 m and 1 m (vertical)	Not defined	Not defined	Not defined
Dredging	0.1 m – 3 m (horizontal and vertical) and 0.01 kt – 0.1 kt (speed)	Not defined	10 – 60	10^{-6}
Hydrography	0.1 m – 36 m (horizontal) and 0.05 m – 0.2 m (vertical)	Not defined	60	Not defined
Port operations	0.1 m – 1 m (horizontal) and 0.1 kt (speed)	Not defined	10	10^{-6}

Table 2.3 Requirements for maritime applications (Porretta et al., 2009)

The requirements for oil and gas applications are similar to the requirements for land and maritime surveying. Oil and gas applications require typically decimetre to centimetre level positioning accuracy (Dixon, 2006).

The positioning performance requirements are specific for each application. However, based on the analysis, 95% horizontal positioning accuracies between 1 and 10 cm are sufficient for most applications, except for control surveying which required sub-centimetre level accuracy. Moreover, most applications require real-time positioning with immediate convergence. Integrity monitoring is vital for safety critical applications and high continuity and availability are important for all applications.

2.3 Current methods

This section discusses the current high accuracy positioning methods in use. The positioning methods are selected based on accuracy, integrity, continuity, time criticality and availability criteria, specified in Section 1.2.1.

The current high accuracy (centimetre-level) GNSS positioning methods are summarised in Table 2.4: cRTK, PPP, network RTK (Takac and Lienhart, 2008), and PPP with local ionosphere corrections (Chen et al., 2011). The principles of the cRTK and PPP methods are described in Section 1.1.2. The principles of network RTK and PPP with local ionospheric corrections

methods are described below. The PPP category in this section refers to both float and fixed ambiguity PPP methods.

In the case of network RTK, corrections for errors such as atmospheric errors are calculated based on measurements from local GNSS reference networks (Takac and Lienhart, 2008). The benefit of employing network RTK compared to cRTK is improvement in positioning accuracy and the possibility of accommodating longer distances from the nearest reference station. The network enables better modelling of the ionospheric and tropospheric errors. (Takac and Lienhart, 2008).

In the case of PPP with a local ionosphere correction, PPP is employed, together with local ionospheric delay corrections (Chen et al., 2011). The benefit of employing the corrections is to reduce the convergence time of PPP. However, generating sufficiently accurate corrections requires a density of reference stations similar to network RTK (Collins et al., 2012).

Based on the analysis in Table 2.4, close to immediate positioning convergence can be achieved with cRTK, network RTK and PPP with local ionospheric corrections. However, all of these methods require a local reference network and cannot be used globally. On the other hand, PPP can be used globally without local reference networks. However, the position solution convergence time is typically 20 minutes or more (Grinter and Roberts, 2011). Thus, PPP is not suitable for applications which require immediate centimetre level positioning accuracy

The integrity monitoring methodology for centimetre level positioning accuracy for mission critical applications is still under research. Research on the integrity of cRTK has been done in the literature, for example, in Feng et al. (2009) and Langel et al. (2012). For example, it is shown in Schuster et al. (2012) that cRTK integrity monitoring can be applied to kinematic applications, when the length of cRTK baseline was short (between 500 and 8000 m). On the other hand, integrity monitoring for the other methods, is more difficult because anomalies in the correction products need to be taken into account.

It is also difficult to define continuity specifically for other methods such as cRTK, because integrity monitoring is not sufficiently established for these methods. However, if continuity

is defined as the ability to achieve centimetre-level positioning accuracy after initial convergence, cRTK, network RTK and PPP with local ionospheric correction methods can achieve higher continuity than the PPP method, because PPP may require significant time for re-convergence (Geng, 2009).

Method	Time criticality	Coverage area	Integrity	Reference
cRTK	Real-time with close to immediate convergence	Local, typically approximately 50 km maximum distance from the nearest reference station in the case of normal atmospheric conditions	There are integrity monitoring methods such as Feng et al. (2009) and Langel et al. (2012)	(Kaplan and Hegarty, 2006)
Network RTK	Real-time with close to immediate convergence	Local, longer distance to the nearest station possible as in the case cRTK	Some work done, for example, in Chen et al. (2003)	(Takac and Lienhart, 2008)
PPP	Real-time positioning after at least 20 min typical convergence time	Global	Some work done, for example, in Feng et al. (2010)	(Leandro et al., 2011a)
PPP with local ionosphere corrections	Real-time positioning after approximately 30 s convergence time	Local, similar density of reference network required as in the case of network RTK	Some work done, for example, in Feng et al. (2010)	(Chen et al., 2011)

Table 2.4 The current centimetre level accuracy GNSS positioning methods

Each of these methods can be mapped to the applications identified in Section 2.1. In the case of surveying, the positioning method is selected based on the required accuracy and operating environment. For static surveying, any of cRTK, network RTK, or PPP methods can be used. To obtain millimetre level static positioning accuracy, long datasets are required. For example, with a baseline length of 30 km and cRTK, at least 2 hours of data is required to obtain from 5 to 10 millimetre level accuracy (RICS, 2010).

For real-time or kinematic surveying, currently the cRTK or network RTK methods are typically used (RICS, 2010). In addition, some non-GNSS surveying technologies are used in

difficult environments, where the quality or availability of GNSS signals is not sufficient (RICS, 2010).

If centimetre level positioning is required for agricultural applications, the cRTK method is commonly used (GSA, 2012). PPP can also be used for agricultural applications (Chen et al., 2011). However, the primary challenge is the long convergence time of PPP solutions. To overcome this issue, local reference networks can be used with PPP to reduce convergence times (Chen et al., 2011).

In the case of tsunami warning systems, cRTK is used, for example, in Kato et al. (2005). Real-time PPP can also be used for tsunami and earthquake warning and monitoring systems (Blewitt et al., 2009).

The determination of the orbits of LEO satellites is conventionally done using radar based tracking technologies (Montenbruck et al., 2005). Employing PPP to determine satellite orbits based on dual-frequency measurements provided by a GNSS receiver installed to the satellite is demonstrated in Montenbruck et al. (2005) and Laurichesse et al. (2009a). The cRTK method is not a suitable method for the determination of satellite orbits, because there are no GNSS reference networks available in space.

The cRTK method is currently used or at least using it is under research in the case of most aviation, military and intelligent transport applications, which require centimetre level positioning accuracy. PPP is currently not suitable for these applications, because the solution convergence time is unacceptably long and integrity is not sufficient. In general, centimetre-level GNSS positioning for life or safety-critical applications is still under research, this includes integrity monitoring for PPP and cRTK

All of the methods shown in Table 2.4 can be used for static or low dynamics maritime applications, if immediate position solution convergence is not required. For example, PPP is applied to maritime applications in Geng et al. (2010c). In the case of marine applications requiring immediate position solution convergence, cRTK is currently the only suitable method. Similar methods can be used for oil and gas applications as is used for maritime and surveying applications.

Based on the analysis on the requirements of the applications and current centimetre-level positioning methods, an ideal positioning method would provide immediate real-time centimetre level positioning with high integrity, continuity and availability anywhere on Earth. However, it is not possible to fulfil all of these requirements on the basis of any current technology alone. Therefore, different technologies must be used for different applications.

To make PPP more practical for any of the applications discussed, improvements are required in terms of convergence time, integrity, continuity and availability. In terms of accuracy, centimetre level accuracy already achieved after the PPP convergence period is sufficient for most applications.

The primary focus of this thesis is improving PPP compared to the current methods. Therefore, an extensive literature review is carried out on the current PPP methods in Chapter 4 and on the current PPP error correction methods and products in Chapter 3. The PPP method review also includes the current fixed ambiguity PPP methods. In addition, Section 4.1 provides a review of the cRTK method in order to provide a reference for comparison with the current PPP methods

3 Global navigation satellite systems, error sources and corrections

Global Navigation Satellite Systems (GNSS) are discussed in Section 3.1, coordinate systems and frames are discussed in Section 3.2 and the general principle of GNSS positioning is discussed in 3.3. This is to provide a general understanding of the current status of the systems and how they can be used for positioning.

Mitigating different GNSS error sources is particularly important for centimetre-level positioning accuracy, required by the applications discussed in the Chapter 2. All the relevant error sources and most suitable correction methods are discussed in this chapter. The suitability of error correction methods is decided based on the following criteria: 1) best achievable accuracy; 2) availability to the user anywhere on the Earth (i.e. coverage); 3) open and real-time availability of the corrections. Choosing the most suitable error correction method is often a compromise, because, for example, the most accurate method may not be available freely or it is not suitable for real-time processing.

GNSS errors sources and corrections are discussed in Section 3.4. The contribution of each error source to the total error budget before and after applying the most suitable error corrections is discussed in Section 3.5.

3.1 Navigation Satellite Systems and their augmentations

The history of GNSS positioning and different GNSS systems including the Global Positioning System (GPS), GLObalnaya NAvigatsionnaya Sputnikovaya Sistema (GLONASS/ГЛОНАСС), Galileo and BeiDou are discussed in this section. Although designed as a global system, BeiDou currently provides full coverage only in the East Asian region. In addition to global systems, the regional Quasi Zenith Satellite System (QZSS) and GNSS augmentation systems are discussed in this chapter, because they are technically and, from a users perspective, tightly linked to the global systems.

The origins of GNSS date back to the early 1960s, when the United States Department of Defense government organization started to develop a system for three–dimensional position determination (Kaplan and Hegarty, 2006). The USA's Transit system, which

became operational in 1964, and Soviet Union's Tsikada system were the earliest space-based radio navigation systems (Kaplan and Hegarty, 2006). However, the systems were only suitable for low-dynamic applications, because of the long time periods, of the order of hours to obtain a position fix (Kaplan and Hegarty, 2006). The requirement for faster positioning led to the development of the Global Positioning System (GPS).

Similar interest in the Soviet Union led to the development of the GLONASS satellite navigation system (Kaplan and Hegarty, 2006). Following the development of the GPS and GLONASS systems, other countries are currently following suit. The European Union (EU) started to develop the Galileo system, because of the need for a satellite navigation system which is not dependent on other countries and guarantees the performance and availability of the signals (Kaplan and Hegarty, 2006). For the same reasons, the People's Republic of China is in the process of developing the BeiDou global navigation satellite system (BeiDou, 2013).

The structure of the current GNSS systems can be divided into three different parts: space, control and user segments (Kaplan and Hegarty, 2006). The space segment consists of satellites, which broadcast the signals received by the user segment. The control segment monitors the health and status of the satellites, ensures that the satellites are in the correct orbit and generates satellite orbit, clock offset, satellite health and other information broadcast by the satellites. The user segment consists of GNSS receivers, which calculate their positions from GNSS measurements and broadcast data.

3.1.1 The Global Positioning System

The most commonly used GNSS is GPS. Its design started in the late 1960s and reached Full Operational Capability (FOC) in 1995 (Kaplan and Hegarty, 2006). The satellites belonging to the Blocks II-A and IIR broadcast the Coarse/Acquisition (C/A) code at the L1 (1575.42 MHz) frequency and encrypted Precision (P) code (P(Y) code) at the L1 (1575.42 MHz) and L2 (1227.6 MHz) frequencies (GPS, 2014). The P code signals are designed for the U.S. military authorized use only and L1 C/A signal is available for everyone.

The P(Y) signals are broadcast in two different frequencies to enable the elimination of first order ionospheric errors (Grimes, 2007). Methods to eliminate ionospheric delays are

discussed in more detail in Section 3.4.4. In the case of the original GPS constellation, the C/A civilian signal is broadcast only on one frequency. This is an issue for civil users who want to eliminate the second order ionospheric delays. However, modern geodetic quality receivers can receive also the P code signals using semi-codeless techniques (GPS, 2014).

Enabling civilians to receive GPS signals on multiple frequencies is one reason why the USA started to modernise GPS (GPS, 2013b). Additional motivations are providing signals with improved noise and multipath properties, a signal which is suitable for safety-of-life applications and signals with better jamming resistance for military use (GPS, 2013b).

The first step in the modernisation programme was the addition of the M-code military and L2C civilian signals starting with the GPS Block-IIR(M) satellites (GPS, 2013b). The L2C signal (GPS, 2010a) is broadcast on the L2 (1227.6 MHz) frequency and has improved signal properties compared to the L1 C/A signal (GPS, 2013b). The GPS L5 signal (1176.45 MHz) is broadcast on Block II-F satellites (GPS, 2010b). The GPS L5 signal is primarily designed for safety-of-life and other high performance applications (GPS, 2013b).

In the future, the USA will launch Block-III satellites, which will broadcast the GPS L1C signal (GPS, 2010c). The L1C signal is primarily designed for consumer and other civilian applications and Multiplexed Binary Offset Carrier (MBOC) modulation enables improved signal receiving in urban canyon-type environments (GPS, 2013b).

The originally designed number of satellites in the GPS constellation was 24 (Kaplan and Hegarty, 2006). It was selected to provide sufficient availability with sufficiently high Dilution Of Precision (DOP). Nowadays, the number of available satellites is even larger, for example, there were 31 available satellite in August 2013 (IAC, 2013). The number of available satellites has increased mainly because the satellites have lasted longer than their designed operational life.

3.1.2 GLONASS

GLONASS is a satellite navigation system developed by the Soviet Union at approximately the same time as GPS (Chebotarev, 2007). GLONASS first achieved FOC in 1995 (IAC, 2014). However, the number of satellites in the constellation started to decrease, because of

funding problems, and there were only six to eight satellites in 2001 (Chebotarev, 2007). Thereafter, Russia managed to restore the constellation and there were 24 operational satellites restoring FOC in May 2013 (IAC, 2013). The originally designed total number of satellites in the GLONASS system is 24, which is selected based on the need for global coverage (IAC, 2014).

The main difference between GPS and GLONASS is their signal structure: GLONASS uses Frequency Division Multiple Access (FDMA) while GPS uses Code Division Multiple Access (CDMA) signals (IAC, 2013). When using CDMA, signals from all satellites are transmitted on the same frequency, but using different Pseudo Random Noise (PRN) codes (IAC, 2013). On the other hand, when using FDMA, satellites on the same side of the Earth broadcast signals on slightly different frequencies, but using the same PRN code (IAC, 2013).

Using FDMA compared to CDMA makes receiver implementation more complex, because receivers must handle multiple frequencies (Kaplan and Hegarty, 2006). In addition, using FDMA causes frequency dependent biases to signals. On the other hand, FDMA signals are less vulnerable for narrow-band interference than CDMA signals and there is no cross-correlation between signals transmitted from different satellites as in the case of CDMA signals (Kaplan and Hegarty, 2006).

The civilian C/A code signals is transmitted on the L1 frequency and military P-code signals are transmitted on the L1 and L2 frequencies by the GLONASS block one and two satellites, which were launched before 2003. In 2003, Russia started to launch GLONASS-M satellites, which also broadcast civilian C/A signal at the L2 frequency. In addition, the lifetime of the GLONASS-M satellites has increased to seven years, which is at least two times longer than the previous generation of GLONASS satellites.

Russia is adding CDMA signals to new GLONASS satellites primarily to improve interoperability with GPS and other GNSS systems (Revnivykh, 2012). It is easier to design receivers when both GPS and GLONASS use CDMA signals. Russia has added the L3OC test CDMA signal at the L3 (1202.025 MHz) frequency to the GLONASS-K1 satellites, launched starting in 2011 (Revnivykh, 2012). It is planned that Russia will add the L1OC, L2OC and L3OC civilian signals and L1SC and L2SC military signals to GLONASS-K2 satellites, which be

launched starting in 2014 (Revnivykh, 2012). In addition, there is a longer term future plan to add L1OCM and L5OCM civilian signals (Revnivykh, 2012).

3.1.3 Galileo

The European Space Agency (ESA) is developing the Galileo satellite navigation system (ESA, 2010). The primary motivation for its development is to make European GNSS users independent from the GPS and GLONASS systems (EU, 2013). Additional motivations are to improve positioning accuracy and availability through better signal design and increased number of satellites, as well as to provide business opportunities related to GNSS for the European private sector (EU, 2013).

There are four different service levels in the Galileo system: open service, safety-of-life service, public regulated service and commercial service (GSA, 2013). The open service is freely available to anyone. The safety-of-life service provides an integrity function, which will alarm users if the performance of the system does not meet the integrity requirements. Thus, the safety-of-life service is suitable for safety critical applications such as aviation. The public regulated service is an encrypted service for government authorised users. The commercial service is an encrypted service for authorised commercial users.

The Galileo E1 signal at the L1 frequency and E5a, E5b and E5 signals at the L5 frequency can be used for the open service (ESA, 2010). The safety-of-life service uses the E1 and E5b signals (ESA, 2010). The E6 signal is used for the commercial service (ESA, 2010). The E6 service is at the frequency band between 1260 and 1300 MHz. The public regulated service uses the E1 and E6 signals (Palestini, 2014). All Galileo signals use CDMA modulation, which make it easily interoperable with GPS.

It was originally planned that Galileo would achieve FOC be fully in 2008 (DGMOVE, 2007). However, the development of Galileo has been severely delayed and it is currently estimated that 18 Galileo satellites should be available in 2015 (initial operational capability) and the full constellation of 30 satellites should be available in 2020 realising FOC (ESA, 2013). In August 2013, the Galileo systems is still in the In-Orbit Validation (IOV) phase and there are only four satellites available (ESA, 2013). Therefore, tests on the performance of the Galileo using real GNSS are very limited.

3.1.4 BeiDou

BeiDou is a satellite navigation system developed by the People's Republic of China (BeiDou, 2011). Currently, it is providing regional navigation services in China and the surrounding area. There are currently 14 operational satellites: five Geostationary Earth Orbit (GEO), five Inclined Geo-Synchronous Orbit (IGSO) and four Medium Earth Orbiting (MEO) satellites. The current Phase-II BeiDou satellites broadcast civilian signals at the B1 (1561.098 MHz) and B2 (1207.14 MHz) frequencies (Gibbons, 2013). In addition, authorized (military) signals are broadcast at the B1, B2 and B3 (1268.52 MHz) frequencies (Gibbons, 2013). All of the BeiDou signals use the CDMA modulation. The full BeiDou Space Interface Control Document for the B1 civilian signal was published in December 2012.

The Chinese government is currently (in 2013) evaluating the performance of the current BeiDou constellation and it is not currently launching more satellites (Gibbons, 2013). It is planned that there will be five GEO, 27 MEO and three IGSO satellites in the full BeiDou constellation, which will provide global coverage (BeiDou, 2012b). The reason for using GEO satellites in the BeiDou constellation is that they can provide higher availability in China and the surrounding area and provide full BeiDou operability there, even though the full constellation of BeiDou is not ready yet. It is planned that the full constellation of BeiDou satellites will be ready in 2020 (BeiDou, 2013).

3.1.5 Quasi Zenith Satellite System (QZSS)

QZSS is developed by Japan and provides coverage in the East-Asia and Oceania regions, particularly focusing on the Japan area (JAXA, 2013). It is a regional system supplementing GPS. The aims of QZSS are to improve availability, accuracy integrity and continuity of GNSS positioning services (JAXA, 2013). It is designed to provide both ranging and integrity alerting services. QZSS can provide a benefit particularly in urban and mountainous areas, where the blockage of GNSS signals is an issue. The orbits of QZSS satellites are chosen so that the satellites can be seen in high elevation angles when the satellites are over the Japan area. Thus, adding QZSS to a positioning solution can improve accuracy and availability significantly when operating in urban environments.

The primary design criterion for QZSS was to supplement GPS to improve regional performance. Therefore, QZSS broadcasts the same L1 C/A, L1C, L2C and L5 signals as GPS (JAXA, 2013). This makes GPS receiver manufacture easy to be compatible with QZSS. In addition, QZSS broadcasts the L1-SAIF and LEX signals, which provides error corrections and integrity data (JAXA, 2013).

The originally planned number of satellites in the final QZSS constellation was three (JAXA, 2013). However, Japan is nowadays planning to build four-satellite QZSS constellation and it should be completed by 2018 (Inside_GNSS, 2013). It is planned that the additional QZSS satellites will be geostationary (Inside_GNSS, 2013). In August 2013, there is only one available QZSS satellite (Inside_GNSS, 2013).

3.1.6 GNSS augmentation systems

Current GNSS systems alone cannot provide sufficient integrity, for example, for aviation applications. Thus, different organisations have developed Satellite-Based Augmentation Systems (SBAS) or Ground-Based Augmentation Systems (GBAS) (Kaplan and Hegarty, 2006). The systems provide integrity and GNSS error corrections, such as ionospheric delay correction data.

The principle of the augmentation systems is to use reference GNSS receivers to monitor the quality of the GNSS measurements and data (EGNOS, 2011). This information is processed and integrity and error correction information is provided by satellites in the case of the SBAS systems or ground based beacons in the case of the GBAS systems. There are many regional/national SBAS systems, for example, the Wide Area Augmentation System (WAAS) developed by the USA, European Geostationary Navigation Overlay Service (EGNOS) developed by ESA, Multi-functional Satellite Augmentation System (MSAS) developed by Japan and GPS Aided Geo Augmented Navigation (GAGAN) system developed by India (ICAO, 2005).

The current SBAS systems are designed for metre-level code-phase based positioning, they cannot provide integrity information on carrier-phase signals or sufficiently accurate error corrections for centimetre level positioning (EGNOS, 2011). Therefore, using SBAS systems is not currently useful for PPP. However, this may change in the future, if SBAS systems are

used for broadcasting PPP corrections. GBAS systems are also not useful for PPP in most cases, because they can be used only locally and not globally.

3.2 Coordinate systems and frames

Earth-Centred Earth-Fixed (ECEF) coordinate systems are defined by using the centre of the Earth as the origin of the coordinate system and rotating the coordinate system at the rate of Earth rotation (Kaplan and Hegarty, 2006). The xy-plane of the ECEF coordinate systems coincides with the Earth equatorial plane and the z-axis is normal to the xy-plane, pointing to the geographical North Pole. Using ECEF coordinate systems is normally convenient for estimating or mapping positions of rover receivers as the coordinates of the receivers remain fixed in time.

Depending on the positioning methodology, different types of coordinate frames can be used when employing ECEF type of coordinate systems. Coordinate frames differ from each other based on the Earth modelling parameters used. The coordinate frame of GPS broadcast obit predictions is the World Geodetic System (WGS)-84 and of GLONASS broadcast orbit predictions is the Earth Parameters 1990 / Parametry Zemli 1990 (PZ-90) (Dach et al., 2007).

The coordinate frame of the precise satellite orbit corrections depends on the service provider, for example, the coordinate frame of the IGS products is the IGS frame, which have different realisations such as IGS08 (Rebischung et al., 2012). The IGS frame, for example, IGS08 is a realisation of the International Terrestrial Reference Frame (ITRF) 2008 (Rebischung et al., 2012). The aim is that the IGS frame would be as close as possible (ideally sub-millimetre level) to the ITRF frame so that users can employ IGS products to estimate their ITRF coordinates. However, there are differences between the IGS and ITRF frames, because different stations and measurement technologies are used to calculate these frames (Rebischung et al., 2012). Nevertheless, the difference between the frames is at millimetre level and can be ignored by most applications (Rebischung et al., 2012).

IRTF is obtained using GNSS, Very Long Baseline Interferometry (VLBI), Satellite Laser Ranging (SLR) and Doppler Orbitography and Radio-positioning Integrated by Satellite (DORIS) measurement from a global ground station network (Altamimi et al., 2011). There

are different yearly realizations of ITRF such as ITRF2005 or ITRF2008 which are obtained by accumulating data from the past to the realisation year (Altamimi et al., 2011). There are differences between the realisations, because different stations, datasets and modelling methods are used depending on the realisation.

Other coordinate systems are fixed to a specific tectonic plate, for example, The North American Datum (NAD) 1983 (Schwarz and Wade, 1990) or the Japanese Geodetic Datum (JGD) 2000 (GSI, 2004). These are affected amongst others by Earthquakes. For example, the Geospatial Information Authority of Japan (GSI) had to define a new version of the JGD following the Tohoku Earthquake, on 11 March 2011 (GSI, 2011).

In the case of PPP an output position from the processing depends on the coordinate frame of satellite orbit corrections used. Therefore, the output position from PPP processing is typically in the IGS frame as satellite orbit corrections are provided in the IGS frame in the case of most correction products. Conversion to other systems can be achieved on the basis of parameters published by relevant organisations (Snay and Pearson, 2010). However, the conversion of coordinates between coordinates system may cause decrease of positioning accuracy, if the conversion parameters are not known in sufficient accuracy.

3.3 The principle of GNSS positioning

The general principle of standalone GNSS positioning is discussed in this section. It involves using code-phase measurements obtained from a receiver and broadcast orbit and clock correction data, satellite health information and ionosphere corrections received from satellites. Based on a test done in 2004, the expected 3D positioning accuracy (95%) of standalone GPS positioning is between 3 and 5 m when using measurements from a dual-frequency receiver (Kaplan and Hegarty, 2006). Nowadays (2013), higher accuracy is expected if using GLONASS and BeiDou dual-frequency measurements in addition to GPS measurements. However, the typical accuracy of standalone GNSS positioning is still at metre-level and the accuracy cannot be guaranteed.

Each GNSS satellite is equipped with a highly stable atomic clock, which are synchronised between satellites of a given constellation to the constellation system time (Kaplan and Hegarty, 2006). The satellite specific clock offsets from the constellation system time are

estimated by the control segment and broadcasted for users by the satellites (GPS, 2010a). Thus, each satellite is synchronised to the system time with metre level accuracy. A distance between the satellite and receiver can be obtained based on the signal propagation time from the satellite to the receiver. In practice, the receiver can measure the propagation time by correlating a replica PRN code with the code received from the satellite (Kaplan and Hegarty, 2006). Thereafter, the propagation time can be converted to distance by multiplying the time with the speed of light.

If the receiver clock was perfectly synchronised with the GNSS time, three code-phase measurements are sufficient to determine the position of the antenna in three dimensions. Nevertheless, perfectly synchronised clocks are normally not the case, because inexpensive oscillators are typically used as receiver clocks. Therefore, at least four measurements are required for position determination, because three of those measurements are required to solve the position and one measurement is required to solve the offset between the receiver local time and GNSS system time. When employing a highly stable atomic clock as a receiver clock, at least four measurements are required at the first epoch to determine the position and solve the receiver clock offset, but after synchronisation, only three measurements are required.

The iterative least-squares method can be used for position determination (Kaplan and Hegarty, 2006). Position determination can be initiated by choosing a linearisation point ($\hat{x}_u$, $\hat{y}_{u,}$, $\hat{z}_u$, $\hat{t}_u$), which can be the centre of the Earth ($\hat{x}_u = 0$, $\hat{y}_u = 0$, $\hat{z}_u = 0$, $\hat{t}_u = 0$) if there is no other more accurate estimate of the initial position. A linearised code-phase measurement for the satellite i is calculated using equation (3.1), where P_1^i is the measured L1 P code-phase provided by the receiver and (x_s^i, y_s^i, z_s^i) is the position of the satellite obtained based on the broadcast orbit prediction. In the equation, $\hat{x}_u$ is the X coordinate of the linearisation point, $\hat{y}_{u,}$ the Y coordinate of the linearisation point, $\hat{z}_u$ the Z coordinate of the linearisation point, $\hat{t}_u$ the receiver clock at the linearisation point and c the speed of light. Satellite orbit errors and their corrections are discussed in detail in Section 3.4.1.

$$\Delta P_1^i = P_1^i - \sqrt{(x_s^i - \hat{x}_u)^2 + (y_s^i - \hat{y}_u)^2 + (z_s^i - \hat{z}_u)^2} - c\hat{t}_u \tag{3.1}$$

The design matrix (H) and its terms are calculated using equations (3.2) and (3.3), where $\hat{r}^i$ refers to the distance between the satellite and linearisation point. The linearised measurement vector (Δp) is calculated using equation (3.4).

$$H = \begin{bmatrix} a_x^1 & a_y^1 & a_z^1 & 1 \\ a_x^2 & a_y^2 & a_z^2 & 1 \\ a_x^3 & a_y^3 & a_z^3 & 1 \\ a_x^4 & a_y^4 & a_z^4 & 1 \end{bmatrix} \tag{3.2}$$

$$\begin{cases} a_x^i = \dfrac{x_s^i - \hat{x}_u}{\hat{r}^i} \\ a_y^i = \dfrac{y_s^i - \hat{y}_u}{\hat{r}^i} \\ a_z^i = \dfrac{z_s^i - \hat{z}_u}{\hat{r}^i} \end{cases} \tag{3.3}$$

$$\Delta p = \begin{bmatrix} \Delta P_1^1 \\ \Delta P_1^2 \\ \Delta P_1^3 \\ \Delta P_1^4 \end{bmatrix} \tag{3.4}$$

The vector of unknowns to estimate (Δx) is shown in equation (3.5). The unknowns are: Δx_u is the x coordinate difference from the linearisation point, Δy_u is the y coordinate difference from the linearisation point, Δz_u is the z coordinate difference from the linearisation point and Δt_u is the receiver clock offset difference from the linearisation point.

$$\Delta x = \begin{bmatrix} \Delta x_u \\ \Delta y_u \\ \Delta z_u \\ -c\Delta t_u \end{bmatrix} \tag{3.5}$$

The $\Delta \boldsymbol{x}$ vector is solved as shown in equation (3.6). The output position is obtained by summing the position of the linearization point ($\hat{x}_u$, $\hat{y}_u$, $\hat{z}_u$) and the computed coordinate differences ($\Delta x_u, \Delta y_u, \Delta z_u$). The least-squares calculation is carried out iteratively using the position of the previous output as the new linearisation point as long the magnitudes of the coordinate differences are below a predetermined threshold. The simplest example of GNSS based positioning is illustrated in Figure 3.1: navigation signals are broadcasted by four satellites belonging to the same constellation and received by a GNSS receiver. At least four

satellites are required for position estimation, because three coordinate offsets ($\hat{x}_u$, $\hat{y}_{u,}$, $\hat{z}_u$) and the system time offset (Δt_u) must be solved.

$$\Delta \boldsymbol{x} = H^{-1}\Delta p \tag{3.6}$$

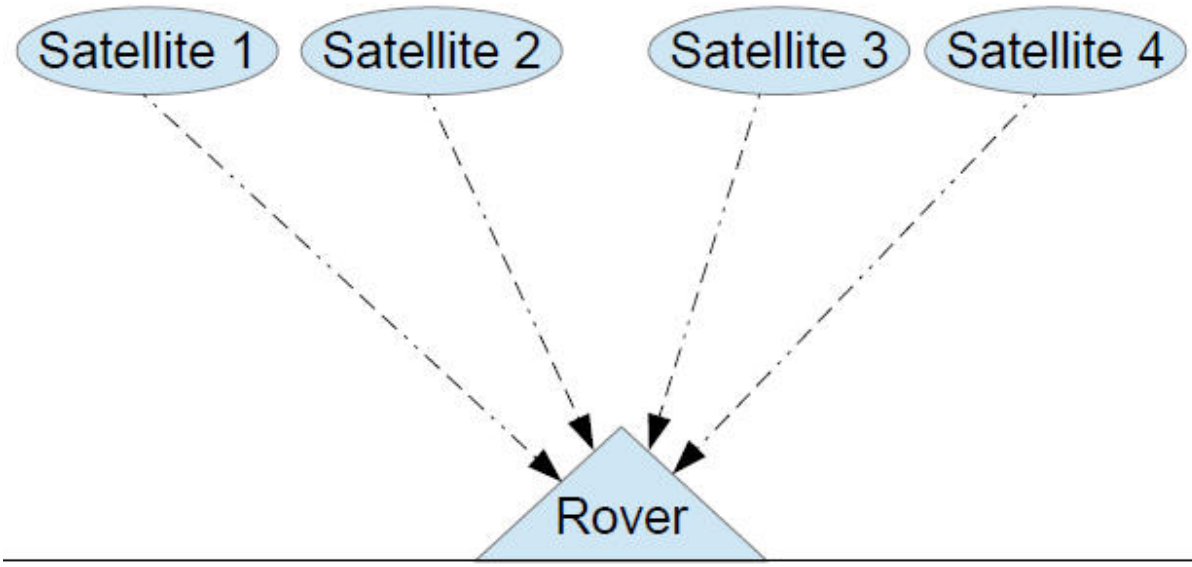

Figure 3.1 GNSS positioning using four satellites

In practice, GNSS positioning is not as simple as described above. GNSS measurements are prone to errors which must be accounted for in the computation of the position solution. For example, satellite clock errors and tropospheric and ionospheric delays must be taken into account. This is particularly relevant to PPP, because error sources even with magnitudes smaller than 10 cm are significant. GNSS observations and error sources are discussed more detail in the following sections.

3.3.1 GNSS observations

Geodetic quality GNSS receivers produce multiple-frequency carrier and code-phase measurements (Kaplan and Hegarty, 2006). Code-phase measurements have centimetre to decimetre level noise and metre level multipath errors. On the other hand, carrier-phase measurements have millimetre-level noise and centimetre level multipath error, but there is an unknown ambiguity term in carrier-phase measurements.

GNSS measurements are vulnerable to the error sources shown in Figure 3.2. The satellite and signal generation related error sources are: orbit error (Section 3.4.1), clock error

(Section 3.4.2), antenna error (Section 3.4.6), satellite antenna phase wind-up (Section 3.4.9), differential code biases (Section 3.4.7) and fractional cycle biases (Section 3.4.3). Receiver, antenna and local environment errors sources are: multipath (Section 3.4.11), measurement noise (Section 3.4.14), receiver antenna errors (Section 3.4.6), receiver clock error (Section 3.4.13) and receiver antenna phase wind-up (Section 3.4.9). Site displacement errors are: solid earth tides (Section 3.4.8.1), ocean loading (Section 3.4.8.3) and polar tides (Section 3.4.8.2). GNSS signals are also affected by ionosphere (Section 3.4.4) and troposphere (Section 3.4.5), because the signals pass through these atmospheric layers when broadcasted from the satellite to the receiver.

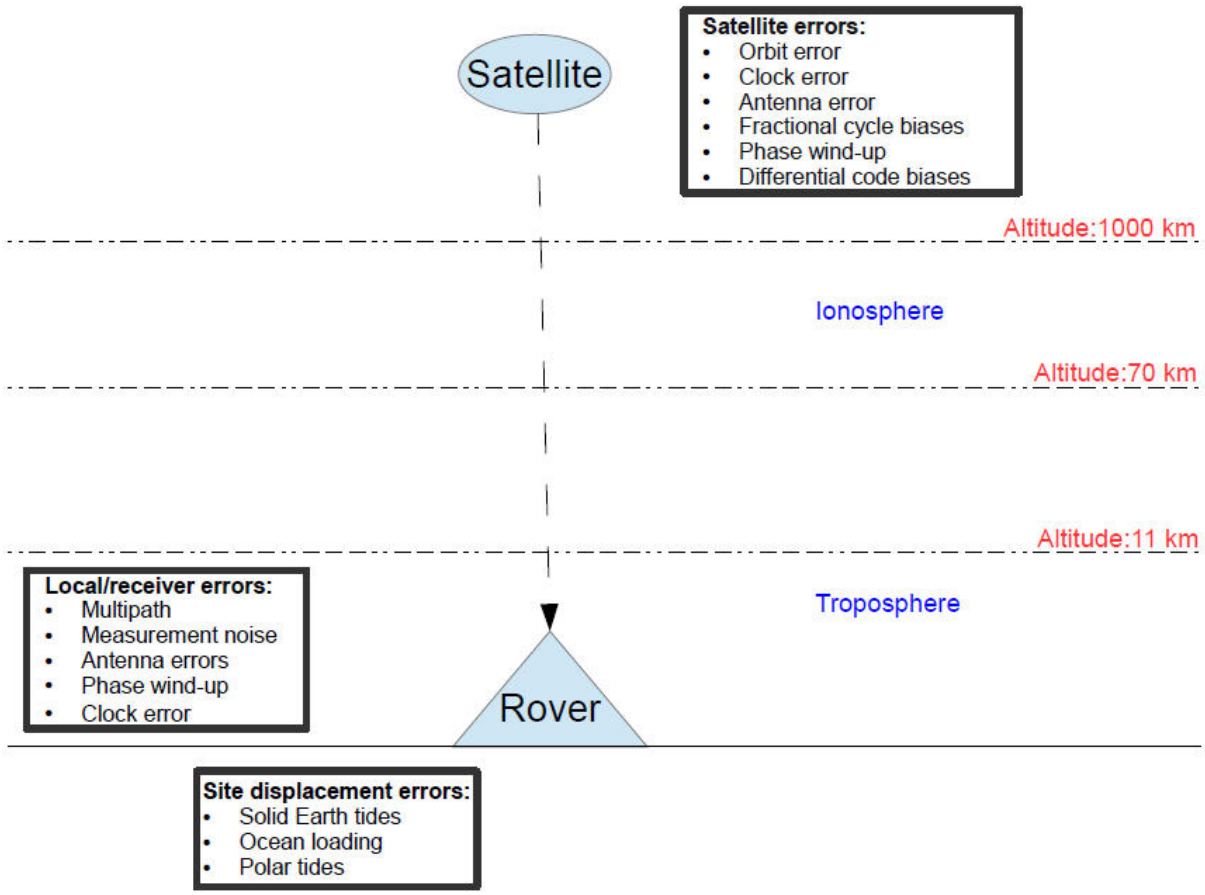

Figure 3.2 GNSS error sources

GNSS observation equations establish the relationship between measurements provided by the receiver, geometric range from the satellite to the receiver and error sources. The code-phase measurements are further divided into P and C code measurements. The P-code measurements are obtained using the GPS or GLONASS P1 or P2 signals, which are primarily designed for military-purposes. The C-code measurements are obtained using the GPS L1

C/A, L2C or L5, GLONASS L1 or L2 C/A or Galileo E1, E5a, E5b or E5 signals, which are primarily for civilian use. Each of the code-phase signals has different biases, because the signals are generated separately in the satellite. Thus, the difference between signals must be taken into account, if eliminating the biases is required in the position estimation. Equation (3.7) presents GNSS P code-phase measurements (P_F, in metres) and equation (3.8) presents GNSS carrier-phase measurements (L_F, in metres).

$$P_F^i = d^i + \delta dT - \delta s^i + \frac{I_1^i}{f_F^2} + \frac{I_2^i}{f_F^3} + \delta T_{Trop}^i + M_{PF}^i + Q_{PF}^i + B_{PF,R} - B_{PF,S}^i \tag{3.7}$$

$$L_F^i = d^i + \delta dT - \delta s^i - \frac{I_1^i}{f_F^2} - \frac{I_2^i}{f_F^3} + \delta T_{Trop}^i + m_F^i + q_F^i + \lambda_F(N_F^i + B_{LF,R} - B_{LF,S}^i) \tag{3.8}$$

where:

i denotes the satellite identity.

F is the index of the GNSS frequency. For GPS satellites, the indices are $F = 1$ (GPS L1), $F = 2$ (GPS L2) and $F = 5$ (GPS L5). For GLONASS satellites, the indices are $F = 1$ (GLONASS L1) and $F = 2$ (GLONASS L2). For Galileo satellites, the indices are $F = 1$ (GALILEO E1), $F = 5$ (GALILEO E5), $F = 6$ (GALILEO E6), $F = 7$ (GALILEO E5a) and $F = 8$ (GALILEO E5b)

f_F is the GNSS frequency in Hertz.

d^i is the geometric distance from the receiver to the satellite.

δdT is the receiver clock error.

δs^i is the satellite clock error.

I_1^i is the first-order ionospheric error term.

I_2^i is the second-order or higher ionospheric error term.

δT_{Trop}^i is the tropospheric error.

M_{PF}^i is the multipath error for the P code-phase measurements.

Q_{PF}^i is the noise for the P code-phase measurements.

m_F^i is the multipath error for the carrier-phase measurements.

q_F^i is the noise for the carrier-phase measurements.

N_F^i is the carrier-phase ambiguity term.

$B_{LF,S}^i$is the satellite-side Fractional Cycle Bias (FCB), also referred to as Un-calibrated Phase Delay (UPD) in the literature.

$B_{LF,R}$ is the receiver-side FCB.

λ_F is the wavelength of the signal.

$B^i_{PF,S}$ is the satellite code-phase bias for the P code-phase measurements.

$B_{PF,R}$ is the receiver code-phase bias for the P code-phase measurements.

3.4 GNSS error sources and corrections

GNSS error sources and corrections are discussed in this section. This includes satellite orbit errors in Section 3.4.1, satellite clock errors in Section 3.4.2 and Fractional Cycle Bias (FCB) errors in Section 3.4.3. This is followed by atmospheric effects in the forms of ionospheric errors in Section 3.4.4 and tropospheric errors in Section 3.4.5. Antenna errors are discussed in Section 3.4.6, Differential Code Biases (DCBs) in Section 3.4.7, site displacement effects in Section 3.4.8, phase wind-up in Section 3.4.9, satellite eclipsing sessions in Section 3.4.10, multipath errors in Section 3.4.11 and relativistic effects in Section 3.4.12. Finally, receiver clock errors are discussed in Section 3.4.13 and measurement noise in Section 3.4.14.

3.4.1 Satellite orbits

In the case of standalone GNSS positioning such as described in Section 3.3, the coordinates of satellites are obtained based on ephemeris data broadcast by GNSS satellites. Satellite ephemeris broadcast data including orbit and clock predictions is typically updated and uploaded to the satellite every 24 hours in the case of GPS (Warren and Raquet, 2003). Therefore, orbit corrections broadcast by the satellites are typically between 0 and 24 hours old.

The orbits of the satellites are predicted using a curve fit at the time when an upload operation is carried out (Kaplan and Hegarty, 2006). The error in the ephemeris data is generally smallest in the radial direction compared to the along-track and cross-track directions (Warren and Raquet, 2003). The reason for this is that observing the along-track and cross-track components is more difficult for the control segments than observing the radial component. The impact on the receiver positioning accuracy depends on the satellite orbit error projection onto the direction of the line of sight between the receiver and

satellite. Based on the analysis of historical GPS ephemeris data, the typical range-level RMS error of broadcast satellite orbit corrections is 1.1 m (Warren and Raquet, 2003).

The accuracy of broadcast orbit corrections is not sufficient for PPP. As a result, various organisations have developed precise satellite orbit correction products. Table 3.1 shows examples of some of the freely available products. In addition, there are many other organisations such as the Information-Analytical Centre (IAC, 2012) and European Space Agency (ESA, 2011) that provide GPS and GLONASS satellite orbit predictions. The International GNSS service (IGS) products are the combination of products provided by different service providers, for example, the Centre National d'Etudes Spatiales (CNES) or Center for Orbit Determination in Europe (CODE) (Kouba, 2009a).

The suitability of a given product is application-dependent. The IGS or CODE final or rapid products are suitable for post-processing, because both provide the highest possible accuracy when the latency of the products is not a limiting factor. On the other hand, real-time or ultra-rapid products must be used for real-time PPP. Currently, the IGS and CNES real-time products are most suitable for this purpose, because they provide satellite orbit corrections with centimetre level accuracy in real-time.

Provider	Type	Constellations	Latency	Accuracy	Correction interval	Reference
International GNSS service (IGS)	Ultra-rapid (predicted)	GPS	Real-time (predicted six hours ahead)	5 cm (3D RMS error)	15 min	(IGS, 2009)
	Ultra-rapid (Observed)	GPS	3-9 hours	3 cm (3D RMS error)	15 min	
	Rapid	GPS	17 - 41 hours	2.5 cm (3D RMS error)	15 min	
	Final	GPS and GLONASS	12 - 18 days	2.5 cm (GPS), 5.0 cm (GLONASS) (3D RMS error)	15 min	
Center for Orbit Determination in Europe (CODE)	Final	GPS and GLONASS	Two weeks	2.5 cm (GPS)	15 min	(Griffiths and Ray, 2009, BERN, 2012)
Centre National d'Etudes Spatiales (CNES)	Real-time	GPS and GLONAS	Real-time, based on Ultra-rapids	4 cm (3D RMS error)	5 min	(Laurichesse et al., 2010)
European Space Operations Centre (ESOC)	Real-time	Multi-GNSS	Real-time (3-4 s), making orbit prediction every 2 hours	Between 3 and 4 cm (RMS against the IGS rapid products)	5 s	(Enderle et al., 2013)
Jet Propulsion Laboratory (JPL)	Final	GPS	14 days	2 cm (3D precision)	5 min	(Desai et al., 2014, JPL, 2014)
International GNSS service (IGS)	Real-time	GPS	Real-Time (15 s) interpolation, based on IGS Ultra-rapid.	4.1 cm (in 2010)	5 or 60 s	(Caissy et al., 2012, MacLeod and Caissy, 2010)

Table 3.1 Precise satellite orbit correction products

Ultra-rapid predicted products are generated by predicting satellite orbits on the basis of previously recorded GNSS data. There can be up to six hours delay between the time when orbits are predicted and used for positioning, because new ultra-rapid products are only generated every six hours (IGS, 2009). The long prediction period may compromise the accuracy of the orbit corrections, for example, when there is a large number of satellites in the eclipse season (Laurichesse, 2011). The satellite eclipsing refers to the satellite not being at the nominal attitude (Kouba, 2009b). The satellite eclipsing is discussed in more detail in Section 3.4.10

In the case of the IGS real-time service, ultra-rapid predicted satellite orbit products are used. To address the accuracy issue of real-time orbit products, some analysis centres participating in the IGS real-time service carry out orbit predictions on a more frequent basis, such as every one to two hours (Caissy et al., 2012). It is also proposed that the ultra-rapid orbit corrections can be improved by estimating correction terms relative to the ultra-rapid orbit corrections when estimating real-time satellite clock corrections in real-time using a Kalman filter (Laurichesse, 2011). To obtain the best possible accuracy, satellite orbit corrections should be generated every few minutes. However, the problem with shorter correction generation intervals is the high computational resources required (Laurichesse, 2011).

A global geographically diverse GNSS reference network is used to obtain the data needed for orbit determination (Dach et al., 2007). The locations of the GNSS stations used to collect data for the CNES orbit and clock correction estimation are shown in Figure 3.3. In addition, Satellite Laser Ranging (SLR) data can be used as an input for the orbit determination (Dach et al., 2007). The determination can be done using the measurement data, broadcast GNSS orbit predictions and geo-potential, third-body (the positions of the Sun and Moon), solar radiation pressure, tidal force and relativity models (Dach et al., 2007, CODE, 2012).

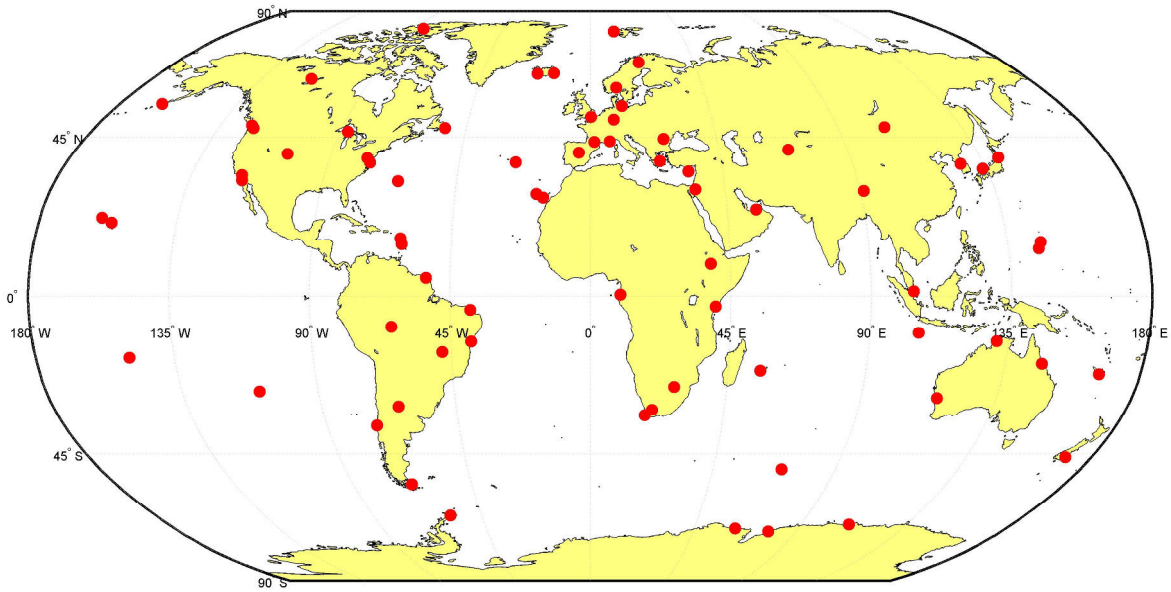

Figure 3.3 The locations of the reference stations used to collect data for the CNES satellite orbit and clock correction estimation (Laurichesse, 2013)

Trimble CenterPoint RTX (Leandro et al., 2012b) is an example of commercially available real-time GNSS satellite orbit prediction system. They claim that it provides orbit predictions with a few minutes delay and a typical accuracy of 2.5 cm (RMS error compared to the IGS rapid products), which is better than the accuracy of real-time IGS or CNES products. However, their products are not freely available and the quality of their products cannot be analysed openly.

The correction products from CNES are used in this thesis, because they are freely available in real-time and their products include FCB corrections, which enable fixed-ambiguity PPP. FCB corrections are discussed in detail in Section 3.4.3. In early 2013, CNES was the only well-established provider of open products suitable for fixed-ambiguity PPP.

3.4.2 Satellite clock error

In the case of standalone GNSS based position determination as discussed in Section 3.3, the position is estimated based on code-phase measurements, which are obtained based on the transmission and reception times of the signals. To obtain correct distance measurements, the reception and transmission times of the signals must be measured in the same time reference, e.g. GNSS time.

GNSS time refers to the time scale of the atomic clocks in the GNSS satellites and ground stations. It is obtained by statistical processing of atomic clock timing data from satellites and ground stations. In the case of the GPS, its system time is fixed to the Coordinated Universal Time (UTC) United States Naval Observatory (USNO) within 1 μs modulo 1 s accuracy (GPS, 2010a). In the cases of other GNSS, their system time is typically also fixed to UTC time. Even though GNSS satellites are equipped with highly stable atomic clocks, the difference between the time of a given satellite clock and GNSS system time can be as large as 1 ms (Kaplan and Hegarty, 2006). This translates into 300 km ranging error. Therefore, it is absolute vital to correct the offset between the satellite specific time and GNSS system time.

Similar to the GPS satellite orbit data, satellite clock corrections are uploaded to satellites every 24 hours (GPS, 2010a). The broadcast satellite clock corrections are estimated by the GPS/GNSS control segment based on the observed and modelled clock behaviour. The

magnitude of the clock error after applying broadcast corrections varies depending on the age of the clock data, because atomic clocks drift against the GPS/GSSS system time. The error is smallest immediately after the upload operation, when typical values are approximately 0.8 m (in the case of the GPS system); however after 24 hours, the error can be as large as 1.0-4.0 m (in the case of the GPS system) (Kaplan and Hegarty, 2006).

The magnitude of the error after applying GNSS broadcast clock corrections is too large for PPP. Therefore, various organisations have developed precise GNSS satellite clock corrections. The primary improvements in precise clock corrections compared to the broadcast corrections are: precise clock corrections are provided with short update rates (e.g. at intervals of 5 s); a larger number of reference stations is used to monitor satellites when generating precise products; and carrier-phase measurements, which have only millimetre-level noise, are used to estimate precise products. Thus, precise products have significantly higher accuracy than broadcast products. It is beneficial to provide satellite clock corrections with a short as possible update interval and latency, because atomic clocks in GNSS satellites drift, which will cause errors to the position estimation (Hadas and Bosy, 2014).

Examples of freely available satellite clock correction products are shown in Table 3.2. In the case of the IGS Ultra-rapid predicted products, the typical RMS error is 0.9 m. The reason for this magnitude is that satellite clocks can drift rapidly over the six-hour period between the prediction and usage of the clock corrections. Therefore, satellite clock corrections for high accuracy real-time PPP must be generated and delivered in real-time.

Provider	Type	Constellations	Latency	RMS error	Sampling interval	Reference
International GNSS service (IGS)	Ultra-rapid (predicted)	GPS	Real-time (predicted over six hours ahead)	90 cm (against to the IGS time-scale)	15 min	(IGS, 2009)
International GNSS service (IGS)	Ultra-rapid (Observed)	GPS	3-9 hours	4.5 cm (against to the IGS time-scale)	15 min	
International GNSS service (IGS)	Rapid	GPS	17 - 41 hours	2.3 cm (against to the IGS time-scale)	5 min	
International GNSS service (IGS)	Final	GPS, GLONASS	12 - 18 days	2.3 cm (against to the IGS time-scale)	30 s	
Center for Orbit Determination in Europe (CODE)	Final	GPS	Two weeks	Similar to the IGS products	5 s	(Griffiths and Ray, 2009, BERN, 2012)
Centre National d'Etudes Spatiales (CNES)	Real-time	GPS,GLONAS	Real-time (6-8 s)	3.6 cm (against to the IGS rapid products)	5 s	(Laurichesse, 2011)
European Space Operations Centre (ESOC)	Real-time	Multi-GNSS	Real-time (3-4 s)	3 cm (against to the IGS rapid products)	5 s	(Enderle et al., 2013)
Jet Propulsion Laboratory (JPL)	Final	GPS	14 days	1.8 cm (precision)	30 s	(Desai et al., 2014, JPL, 2014)
International GNSS service (IGS)	Real-time	GPS	Real-Time (15 s)	4.2 cm (against to the IGS rapid products, in June 2011)	5 s	(Caissy et al., 2012)

Table 3.2 Satellite clock correction products

Based on the information in Table 3.2, the CNES or IGS real-time clock corrections are the most suitable choice for real-time PPP, because they provide the lowest possible RMS error in real-time. In addition, they are the only openly available real-time products at the time (early 2013) of writing this thesis. For post-processing, the final clock correction products such as the CODE final products are the most suitable choice, because they can provide the best possible accuracy.

It possible use telecommunication satellites to broadcast real-time precise clock and orbit corrections. For example VERIPOS Apex provides this kind of service (VERIPOS, 2013). In a theory, precise clock corrections could be broadcast by a GNSS itself, but the issues in practice, are the limited bandwidth of the broadcast message at least with current signals and limited coverage of tracking network and upload stations. In addition, it would require advanced processing techniques at the control segment.

Similar to satellite orbit corrections, products from CNES are used in this thesis, because they are freely available in real-time and are suitable for fixed ambiguity PPP. In 2013, CNES was the only established provider of open products suitable for fixed ambiguity PPP.

3.4.3 Fractional Cycle Bias (FCB)

The Fractional Cycle Bias (FCB) errors, which are also referred to as Un-Calibrated Phased Delays (UPD) in the literature, are mainly caused by hardware delays in the satellite and receiver (Geng et al., 2010b). The FCB errors are not entirely stable, with potentially unknown variations over time of their magnitude.

In the case of cRTK, FCB errors are cancelled entirely by double-differencing the measurements across receivers and satellites (Ge et al., 2008). However, this is not an option for PPP. If these errors are not corrected, carrier-phase ambiguity resolution becomes difficult. The magnitude of the FCB errors can vary between minus one half and plus one half of a carrier-phase cycle, if the FCB is defined as a fractional part, when the float ambiguity is rounded to the nearest integer.

GNSS measurements from a global reference network with 50 stations or more can be used to estimate FCB errors. FCB corrections generated by the reference network can be provided as fractional part corrections for Between-Satellite-Difference (BSD) wide-lane and narrow-lane ambiguities (Geng et al., 2010d). The BSD operation is done by selecting one satellite as a base-satellite and differencing its measurements with the other satellites measurements. The operation removes receiver clock and FCB errors. In case of the carrier-phase ambiguity resolution wide-lane and narrow-lane carrier-phase signals combinations are used, this is discussed more in Sections 4.3.1.1 and 4.3.2.2. The second commonly used way to provide FCB corrections is assimilating narrow-lane FCB corrections into the satellite

clock corrections. In a theory, both methods are expected to correct FCB errors to a similar level of accuracy (Geng et al., 2010b).

The issue with the methods presented above is that the FCB corrections are dependent on the signal combination used for ambiguity resolution. There is the dependency, because the FCB corrections are calculated separately for the wide-lane and narrow-lane combinations or narrow-lane FCB corrections are assimilated into the satellite clock corrections. In addition, new signals in the future will enable making more signal combinations. Therefore, it is proposed in Laurichesse (2012) that FCB corrections should be provided separately for each carrier-phase signal such as L1 and L2. The benefit of this is that FCB corrections are carrier-phase signal specific and not dependent on the ambiguity resolution method used. In addition, code-biases are provided also in a signal specific way in the Radio Technical Commission for Maritime Services (RTCM) standard (RTCM, 2013), which makes adding carrier-phase corrections more compatible with the standard.

In this thesis, the CNES FCB correction product is used, because it is currently the only one fully openly available. In the future, there will likely be additional service providers which provide FCB corrections without charge.

3.4.4 Ionospheric error

The ionosphere is located between approximately 70 km and 1000 km above the surface of the Earth (Kaplan and Hegarty, 2006). In the ionospheric region, gas molecules are ionised by ultraviolet rays from the sun. This causes a release of free electrons, which induces delays in the code-phase measurements and advances in the carrier-phase measurements.

The magnitude of the ionospheric delay depends on the electron density and the frequency of the GNSS signals (Kaplan and Hegarty, 2006). The refraction index provides a measure of the impact of the ionosphere on GNSS measurements. For carrier-phase observations, the refraction index (n_p) can be defined as in equation (3.9):

$$n_p = 1 + \frac{I_1}{f^2} + \frac{I_2}{f^3} + \frac{I_3}{f^4} \dots \tag{3.9}$$

For code-phase observations, the refraction index (n_g) can be defined as in equation (3.10):

$$n_g = 1 - \frac{I_1}{f^2} - \frac{2I_2}{f^3} - \frac{3I_3}{f^4} \dots \quad (3.10)$$

In the above equations, I_1 is the first-order ionospheric delay term, I_2 the second-order ionospheric delay term, I_3 the third-order ionospheric delay term and f is the frequency of the GNSS signal. The first-order Ionospheric error ($\frac{I_1}{f^2}$) can be eliminated using the Ionosphere-free measurement combination, using measurements from at least two GNSS frequencies. The measurement combination in equation (3.11) can be used for code-phase measurements and measurement combination in equation (3.12) can be used for carrier-phase measurements, where units are expressed in metres (Dach et al., 2007). In the equations, P_3 refers to ionosphere-free code-phase combination in metres, L_3 refers to ionosphere-free carrier-phase combination in metres, P_1 refers to P code-phase measurements at the L1 frequency, P_2 refers to P code-phase measurements at the L2 frequency, L_1 refers to carrier-phase measurements (in metres) at the L1 frequency, L_2 refers to carrier-phase measurements (in metres) at the L2 frequency, f_1 refers to the L1 GNSS frequency and f_2 refers to the L2 GNSS frequency.

$$P_3 = \frac{1}{f_1^2 - f_2^2}(f_1^2 P_1 - f_2^2 P_2) \quad (3.11)$$

$$L_3 = \frac{1}{f_1^2 - f_2^2}(f_1^2 L_1 - f_2^2 L_2) \quad (3.12)$$

The magnitude of the ionospheric delay is typically between 5 and 15 m, but in the periods of extreme solar activity, it can be as large as 150 m (Elsobeiey and El-Rabbany, 2009). 99.9% of the ionospheric error magnitude can be mitigated employing the ionosphere-free combination, which eliminates the first-order ionospheric delay (Hofmann-Wellenhof et al., 2008). However, higher order ionospheric-delay terms can still cause centimetre-level errors, which may increase the convergence time and decrease the accuracy of a PPP solution (Elsobeiey and El-Rabbany, 2009).

The second-order ionospheric delay can be eliminated using triple-frequency measurements when employing the measurement combination which eliminates both first and second order ionospheric errors (Hoque and Jakowski, 2008). However, correcting second order

ionospheric error using triple-frequency measurement is not currently practical, because there are only a few satellites broadcasting signals in three frequencies.

A model for correcting the second-order ionospheric delay is presented in Elsobeiey and El-Rabbany (2011). The model is based on taking into account the interaction of the ionosphere with the Earth's magnetic field, on which the second-order ionospheric delay is dependent. The second order ionospheric delay can be calculated based on the magnetic field vector and ionospheric Slant Total Electron Content (STEC) at the Ionosphere Pierce Point (IPP) (Elsobeiey and El-Rabbany, 2011). The IPP is the intersection of the receiver to the satellite vector and ionosphere, when ionosphere is modelled as one single layer.

The estimation of the second or higher order ionospheric delay requires knowledge of the ionosphere Slant Total Electron Content (STEC) (Elsobeiey and El-Rabbany, 2011). This information can be obtained from dual-frequency GNSS measurements or external ionospheric correction products. The measurement based STEC estimation method requires the knowledge of receiver P1/P2 Differential Code Biases (DCB), which are the code-phase biases between the GNSS P1 and P2 signals (Dach et al., 2007). DCB are discussed more detail in Section 3.4.7. Obtaining receiver DCB information is difficult or even impossible, if the receiver is not used for a network solution, because it is not possible to separate receiver DCB from other unknowns in single receiver processing. Alternatively, external ionospheric correction products are a potential source of the STEC, provided that the products are generated in real-time and with a sufficient level of accuracy.

It is possible to use different kinds of external products such as the IGS ionospheric grid maps (Kouba, 2009a) to correct ionospheric errors. With such products, it is possible to correct most of the ionospheric errors even with single frequency GNSS measurements. However, in typical cases it is not possible to correct ionospheric errors as accurately with ionospheric models as by using dual-frequency GNSS measurements.

Currently, there are also services which can provide real-time ionospheric corrections products. According to Juan et al. (2012), their service can provide real-time ionospheric correction with centimetre-level accuracy. However, a reference network with high station density is required to generate such accurate corrections. Therefore, this kind of service is not suitable for remote areas.

According to Caissy et al. (2012), the IGS is also developing real-time ionospheric correction products. However, their service also requires local reference networks to generate accurate ionospheric delay corrections.

In this thesis, the aim is to develop a PPP method suitable for use in remote areas. Thus, local ionospheric corrections are not typically available, due to a lack of local reference networks. For PPP, employing the ionosphere-free combination is therefore, the most suitable method to remove the first order ionospheric errors, because no external corrections are needed. In addition, the second or higher order ionospheric delays are ignored in this thesis, a typical approach of most PPP implementations. The reason is that the correction of these higher orders would require the knowledge of the receiver DCB or the use of external ionospheric corrections. Receiver DCB are not available for rover receivers which are not part of a network solution and it is not possible to provide sufficiently accurate external ionospheric correction products in remote area where there are not local reference networks. Therefore, it is not feasible to correct higher order ionospheric error terms in real-time PPP processing. Ignoring these terms may cause few centimetre extra error to the position solution, if ionospheric activity is high (Elmas et al., 2011).

3.4.5 Tropospheric error

The lower part of the atmosphere is called the troposphere (Kaplan and Hegarty, 2006). The delay caused by the troposphere is not a function of the frequency of the GNSS signal, because the troposphere is non-dispersive for frequencies below 15 GHz. In addition, the magnitude of the tropospheric delay is similar both for carrier-phase and code-phase measurements. The magnitude of the tropospheric delay depends on the temperature, relative humidity and pressure along the signal path. Therefore, for low elevation satellites, the relatively long paths of the signal within the troposphere result in correspondingly large troposphere delays. The troposphere delay can be of the order of 2.4 m for a satellite at the zenith, but as large as 25 m for a satellite at an elevation angle of 5 degrees (Kaplan and Hegarty, 2006).

The tropospheric delay can be divided into two components: hydrostatic (dry) and non-hydrostatic (wet) (Kaplan and Hegarty, 2006). Approximately 90% of the tropospheric delay is caused by the hydrostatic component in the hydrostatic equilibrium, and is usually referred to as the dry delay. The dry delay can be modelled accurately, for example, by the Saastamoinen model (Saastamoinen, 1973). In contrast, determining the wet delay, which is mainly caused by water vapour, is more difficult because of the uncertainties and dynamics in its distribution. Therefore, tropospheric delay correction for PPP is achieved as follows. The values of tropospheric delay (wet and dry) are obtained using tropospheric models as discussed in Section 3.4.5.1. The zenith delays are mapped into the receiver-to-satellite range direction using tropospheric mapping functions as discussed in Section 3.4.5.2. The residual tropospheric wet delay is estimated as a Kalman filter state. The benefit of estimating residual tropospheric wet delay as a Kalman filter states is to take the variation in the wet delay into account.

3.4.5.1 Tropospheric models

The Saastamoinen model (Saastamoinen, 1973) is one of the state-of-the-art methods to calculate tropospheric wet and dry delays based on meteorological parameters. In the Saastamoinen model, the tropospheric dry delay (D_h^z) is estimated using equation (3.13), where p is the total barometric pressure (mbar). The tropospheric wet delay (D_w^z) is estimated using equation (3.14), where e is the partial pressure of the water vapour (mbar) and T is the absolute temperature (Kevin). The total tropospheric delay, including both the dry and wet parts, can be calculated for a satellite using equation (3.15), where z is the zenith distance of the satellite and B and δ_R are Saastamoinen model specific correction parameters. The input values of the temperature, pressure or partial water vapour pressure are not specified in the original Saastamoinen model paper.

$$D_h^z = 0.002277p \tag{3.13}$$

$$D_w^z = 0.002277\left(\frac{1255}{T} + 0.05\right)e \tag{3.14}$$

$$D_{trop} = 0.002277 \sec z \left(p + \left(\frac{1255}{T} + 0.05 \right) e - B * \tan^2 z \right) + \delta_R \quad (3.15)$$

When correcting the tropospheric delay, the meteorological information, i.e. temperature, pressure and partial water vapour pressure, are often not available. Therefore, different models have been developed to estimate the meteorological parameters, which are used when calculating the tropospheric delay using the Saastamoinen model.

One commonly used model is the EGNOS tropospheric model (RTCA, 1999), in which the tropospheric delay is calculated based on the total pressure, temperature, water vapour pressure, temperature lapse rate, water vapour lapse rate and height of the receiver above the mean sea level. The meteorological parameters are obtained from a look-up table based on the receiver latitude (Penna et al., 2001).

The UNB3m model (Leandro et al., 2006) has a look-up table for barometric pressure, relative humidity, temperature, temperature lapse rate and water vapour pressure height factor values based on the latitude of the receiver. Compared to the EGNOS model or previous UNB3 model, relative humidity data is used instead of water vapour pressure data to obtain more realistic water vapour pressure estimates. The parameter values in the look-up table are obtained based on the U.S. Standard Atmosphere Supplements 1966.

The Global Pressure and Temperature (GPT) model (Boehm et al., 2007) is an empirical model to estimate the temperature and pressure anywhere on the Earth's surface. It is one of the most advanced models for the estimation. Nevertheless, it does not provide the relative humidity information provided by the UNB3m model.

For PPP processing, the Saastamoinen model can be used to calculate tropospheric delay estimates based on the meteorological parameter values obtained, for example, from the UNB3m or GPT models. According to the results based on data from 125 IGS stations presented in Li et al. (2012), the magnitude of the bias and RMS errors of the zenith tropospheric delay after correcting the delay are: EGNOS model (bias: 2.0 cm, RMS: 5.4 cm), UNB3m model (bias: 0.7 cm, RMS: 5.0 cm) and IGGtrop model (bias: -0.7 cm, RMS: 4.0 cm). The results show that the new IGGtrop model (Li et al., 2012) provides the smallest bias and RMS errors. However, the IGGtrop model is not suitable to use in this thesis, because it is not available in the public domain.

The UNB3m model is used in this thesis. It is chosen, because it is one of most advanced tropospheric models available in the literature and its implementation is freely available.

3.4.5.2 Tropospheric mapping functions

The total tropospheric slant delay for a satellite (D_{trop}) can be calculated by combining tropospheric wet and dry delay estimates using equation (3.16), where $m(E)_h$ and $m(E)_w$ are the mapping functions for the tropospheric dry and wet delay and E is the elevation angle of the satellite. There are many different mapping functions available. The Saastamoinen mapping function (Saastamoinen, 1973) is shown in equation (3.17), where *z* is the zenith distance of the satellite. The Saastamoinen mapping function is the simplest only using satellite elevation as an input. The same mapping function is used for both the wet and dry delays.

$$D_{trop} = m(E)_h D_h^z + m(\varepsilon E)_w D_w^z \tag{3.16}$$

$$m(E)_h = m(E)_w = \sec z \tag{3.17}$$

As shown in Niell (1996), simple tropospheric mapping functions such as the Saastamoinen function are not optimal when attempting to obtain high accuracy, because they do not accurately map the tropospheric delay for low-elevation satellites (particularly below 10 degrees) and they do not provide a separate mapping for the dry and wet components. It is difficult to accurately map tropospheric delay, particularly for low elevation satellites, because even the dry part of tropospheric delay is highly variable (Kouba, 2009c).

To map the tropospheric delay accurately, many different tropospheric mapping functions have been developed, for example, the Herring mapping function (Herring, 1992), Ifadis mapping function (Ifadis, 1992) and Niell mapping function (Niell, 1996). The Niell tropospheric dry delay mapping function coefficients are dependent on the latitude and height (above sea level) of the station and on the day of the year (Niell, 1996). The Niell wet delay coefficients are only dependent on the latitude of the station. In addition, both the dry and wet delay mapping functions depend on the elevation of the satellite (Niell, 1996). The Niell mapping function maps tropospheric delay more realistic way compared to the Ifadis and Herring functions, because it is not dependent on the surface temperature (Kleijer,

2004). Mapping tropospheric delay based on the surface temperature can lead to inaccurate results, because the temperature of tropospheric layers which are located higher than 2000 m is not necessary dependent on the surface temperature (Niell, 1996).

However, the Niell mapping function has a number of weaknesses, including not accounting for the longitude of a station, resulting in systematic errors, and latitude-dependent biases. The biases are largest in the high southern latitudes. To address these weaknesses, the Global Mapping Function (GMF) (Boehm et al., 2006a) was developed, and shown to provide a higher accuracy than the Niell mapping function. Depending on the elevation of a satellite, time of year, meteorological conditions and location of a station, the improvement provided by GMF compared to the Niell mapping function in terms of the receiver to the satellite range-level error can be up-to few centimetres (Boehm et al., 2006a).

The Vienna Mapping Function 1 (VMF1) is a tropospheric mapping function, which uses also real meteorological data for calculation (Boehm et al., 2006b). In specific stations, the availability of meteorological data such as pressure measurements enables the use of VMF1 However, typically the lack of meteorological data precludes the use of VMF1 and the GMF or Niell mapping functions are used instead.

For PPP, GMF is the most suitable choice when real meteorological data is not available. It is widely accepted and used, for example, by the CODE analysis centre (CODE, 2012), when generating precise satellite orbit and clock corrections. GMF is used in this thesis, because it is the most accurate currently available mapping function which does not require meteorological data It is not possible to estimate real tropospheric wet delays with sufficient accuracy based on statistical meteorology data models (Kouba, 2009a). Therefore, the tropospheric wet delay must be estimated as an unknown in the least-squares or Kalman filter based estimation.

3.4.5.3 Tropospheric gradient models

To improve the tropospheric error estimation accuracy, the troposphere azimuthal inhomogeneity must also be taken into account. It can be accounted for to a certain extent,

by linearly estimating the tropospheric gradients in the North and East directions. The total tropospheric error estimation formula, including the tropospheric gradients to the North (G_N) and East (G_E) directions, is show in equation (3.18), where $m(E)_{azi}$ is the tropospheric gradient mapping function, φ is the azimuth angle of the satellite and E is the elevation angle of the satellite (Zhang and Gao, 2006). The tropospheric gradient terms can be estimated, for example, as Kalman filter states. Based on the results shown in Zhang and Gao (2006), tropospheric gradient modelling can reduce latitude, longitude and height errors by few millimetres depending on the location of a station and atmospheric conditions.

$$D_{trop} = m(E)_h D_h^z + m(E)_w D_w^z + m(E)_{azi}(G_N \cos(\phi) + G_E \sin(\phi)) \quad (3.18)$$

There are two commonly used tropospheric gradient mapping functions: the Chen mapping function (Chen and Herring, 1997) as in equation (3.19) and Wet mapping function (MacMillan, 1995, Bar-Sever et al., 1997) as in equation (3.20) where $m(E)_{h/w}$ is either the wet or dry delay mapping function. According to Zhang and Gao (2006), both the Chen and Wet mapping functions provide similar performance. The Chen mapping function is used in this thesis, because it is the state-of-the-art mapping function used widely in the literature.

$$m(E)_{azi} = \frac{1}{\sin E \cos E + 0.0032} \quad (3.19)$$

$$m(E)_{azi} = m(E)_{h/w} \frac{1}{\tan E} \quad (3.20)$$

3.4.5.4 Tropospheric correction products

In a typical PPP processing case, tropospheric delays are modelled locally in the rover receiver without input of real-time meteorological data as discussed in Sections 3.4.5.1 and 3.4.5.2. However, tropospheric conditions can change rapidly and therefore, statistical tropospheric models and mapping functions are not capable of estimating sufficiently accurate temperature, pressure, relative humidity and other meteorological parameters. This may still cause inaccurate tropospheric estimation, even though tropospheric wet delay and gradients are modelled as Kalman filter states. To address the issue, tropospheric delay correction methods based on real (measured) meteorological data are discussed next.

An example of real-time GNSS network based tropospheric delay estimation is shown in Iwabuchi et al. (2006). The system can provide millimetre level accurate troposphere corrections compared to measurements made by radiosonde stations. A radiosonde is a device which can be used to measure atmosphere parameters. However, estimating tropospheric delay as accurately (millimetre level) as in Iwabuchi et al. (2006) requires high reference station density, which is typically only available in high population density areas such as Japan.

In the case of Numerical Weather Modelling (NWM), meteorological information is collected from ground meteorological stations, radiosonde weather balloons, commercial aircraft and remote sensing weather satellites, and assimilated into numerical weather models (Yang et al., 2011). The primary use of the NWM products is weather forecasting, but employing these products also enables estimating tropospheric delay. The benefit of using NWM products to estimate tropospheric delays is that it enables calculating tropospheric delay based on real meteorological parameters. In addition, by employing NWM based estimations, the troposphere azimuthal inhomogeneity is considered on individual satellite-to-receiver lines of sight, and not in a simple linear model as in the case of tropospheric gradient models shown in Section 3.4.5.3. This typically improves the accuracy of the tropospheric delay estimation.

The North Atlantic European (NAE) model in the Unified Model from the UK Met Office (UKMO) can be used to provide values for meteorological parameters (Yang et al., 2011). This model is regional, as indicated by its name, and the weather parameters are provided in three dimensions. Horizontally, there are 600 by 360 (~12.3km) grids, and vertically there are 15 different geo-potential layers at [1000, 950, 925, 850, 700, 600, 500, 400, 300, 250, 200, 150, 100, 70 and 30] mbar. This model is dynamic, with information updated every 6 hours. It is currently obtained by post-processing, but a real-time version of it is under research.

The tropospheric delay calculation based on NWM is explained in Yang et al. (2011). For estimating tropospheric delay, the useful parameters obtained from NWM at each geo-potential layer (pressure layer) are temperature (T), geo-potential height and relative humidity. The parameters are used in calculating the refractivity (n) as in equation (3.21). In

this equation, p_d is the partial pressure of the dry air, e is the partial pressure of water vapour, $K_{1,2,3}$ are constants, Z_d is the compressibility factor density of the dry air and $Z_w$is the compressibility factor density of water vapour (Orliac, 2009). The calculation of p_d, e, Z_d and Z_w is based on the pressure, temperature, geo-potential height and relative humidity data, and is explained in Mendes (1999), Davis et al. (1985), WMO (1988) and Orliac (2009).

$$n = K_1 \times \frac{p_d}{T} \times Z_d^{-1} + K_2 \times \frac{e}{T} \times Z_w^{-1} + K_3 \times \frac{e}{T^2} \times Z_w^{-1} \tag{3.21}$$

In the NWM based tropospheric delay calculation algorithm used in this thesis, the vertical space between each geo-potential layer is split into many thin layers, and it is assumed that the interpolated parameters remain constant in each layer (Yang et al., 2011). The tropospheric delay in each layer (D_{layer}) is calculated as in equation (3.22), where n is the refractivity and S is the distance which the signal has travelled in the layer (Yang et al., 2011).

$$D_{layer} = S \times n \tag{3.22}$$

The total tropospheric delay for each satellite is obtained by summing over the tropospheric delays from each of the relevant layers through which the signal has travelled. NWM models are not used in this thesis except in Section 6.3, where the impact of employing NWM based corrections is tested.

3.4.6 Antenna errors

Satellite and receiver antenna phase centre errors can be separated into two terms: a satellite Phase Centre Offset (PCO) and satellite Phase Centre Variation (PCV) (Kouba, 2009a). PCO is a constant offset for the specific antenna. On the other hand, PCV is not a constant and its magnitude varies depending on the path of the signal passing through the antenna.

Satellite PCO refers to an offset between the centre of mass of a GNSS satellite and phase centre of the GNSS satellite (Kouba, 2009a). The satellite PCO must be corrected, because the IGS orbit products refer to the centre of the mass, whereas the GNSS range measurements are done with respect to the phase centre of the GNSS satellite (Kouba, 2009a). The magnitude of satellite PCO can be metre level (Kouba, 2009a). Therefore, this error needs to be corrected for PPP.

The satellite PVC term is dependent on the azimuth and nadir angles in which the station is located relative to the satellite. Despite the similar style of design of the satellites within the same block, for example, the GPS block II or GPS block IIR, it is not possible to provide block specific PCO and PCV corrections. This is because the magnitude of the PCO and PCV errors is specific to each satellite even within the same block of satellites (Schmid et al., 2005). To ensure the highest accuracy, PCO and PCV corrections must be provided for each satellite separately.

Receiver antenna phase centre error is caused by the difference between the antenna reference point and actual phase centre (Bilich and Mader, 2010). The error can be separated into the PCO and PCV components (Bilich and Mader, 2010). The PCV component depends on the type of the antenna, frequency, elevation and azimuth of the received signal. In contrast, the PCO component is a constant, depending only on the type of the antenna and frequency.

Receiver antenna phase centre estimation for a specific antenna type can be achieved, for example, by using a five metre-long baseline between two GNSS antennas (Bilich and Mader, 2010). These antennas are connected to a GNSS receiver which supports multiple antenna inputs. In practice, it is possible to remove almost all errors which are common to both antennas by differencing the measurements, because the baseline is short. Therefore, the remaining error is related to the antenna phase centres. If PCO and PCV are calibrated for one of the antennas, it is possible to estimate PCO and PCV for the second antenna.

IGS provides satellite and receiver antenna phase centre error corrections in the ANTenna Exchange (ANTEX) format. Corrections in the Isg05.atx format were used between 5 November 2006 and 16 April 2011 (Ray, 2011). From 17 April 2011, antenna phase centre error corrections in the Igs08.atx format are used (Ray, 2011).

The antenna phase centre corrections provided by IGS are the most suitable for PPP processing, because they are openly available and the error can be removed almost completely (sub-millimetre level) using the products. The products from IGS used with most PPP implementations, are used in this thesis.

3.4.7 Differential Code Biases (DCB)

There are various types of GNSS receivers: P1/P2 providing the C1, P1 and P2 observations; C1/X2 providing the C1 and cross correlated linear combination X2 observations; and C1/P2 providing the C1 and P2 observables (Dach et al., 2007). The magnitudes of hardware delays vary depending on the observables. Precise satellite clock corrections are typically provided relative to the ionosphere-free P1/P2 signal combination (Dach et al., 2007). Thus, precise clock corrections contain the ionosphere-free combination of the P1 and P2 code-phase biases. Therefore, if other observables are used, corrections DCBs are required.

The Center for Orbit Determination in Europe (CODE) provides products to correct satellite DCBs. The DCB corrections provided by CODE are the biases between the P1 and P2 signals (B_{P1-P2}), between the P1 and C1 signals (B_{P1-C1}) and between the P2 and C2 signals (B_{P2-C2}) (Schaer and Dach, 2010). DCB corrections can directly be applied to the C1 and C2 code-phase measurements using equations (3.23) and (3.24), respectively. Cor_{C1} refers to the DCB correction for the C1 signal and Cor_{C2} refers to the DCB correction for the C2 signal. However, correcting the B_{P1-P2} bias is not required when using the Ionosphere-free or Melbourne-Wubbena measurement combinations (Kouba, 2009a).

$$Cor_{C1} = \frac{f_2^2}{f_1^2 - f_2^2} B_{P1-P2} + B_{P1-C1} \tag{3.23}$$

$$Cor_{C2} = \frac{f_1^2}{f_1^2 - f_2^2} B_{P1-P2} + B_{P2-C2} \tag{3.24}$$

Receiver hardware delays may also cause DCBs, but in a typical case these biases are similar for all measurements and can be absorbed into the receiver clock bias (Leandro et al., 2011b). Thus, the receiver side DCB is eliminated from the solution.

In the future, there will be a need to provide DCB corrections also for new GNSS signals, for example, the GPS L5 or Galileo signals. CODE has already started to develop a system to estimate the GPS L5 DCB corrections (Schaer and Dach, 2010).

DCB corrections are provided as monthly files because they are fairly stable. For example, the approximate day by day reproducibility of C1/P1 DCB is 1.5 cm (RMS) (Dach et al., 2007). In the case of PPP, correcting DCB is particularly important when employing the Melbourne-

Wubbena combination to estimate wide-lane ambiguities, because the impact of DCBs can be up to 1.2 m (1.4 wide-lane cycles) (Dach et al., 2007).

In this thesis, C1/P1 and C2/P2 DCB are corrected using products from CODE. DCB can be eliminated with centimetre-level accuracy with these corrections. This is sufficient, because DCBs affect code-phase measurements alone.

3.4.8 Site displacement effects

The site displacement effects cause periodic movement of a station with respect to its International Terrestrial Reference Frame (ITRF) coordinates (Kouba, 2009a). Because most of the periodic movements are largely the same for stations over broad areas of the Earth, the site displacement effects do not need to be considered when using cRTK over short (less than 100 km) baselines. For longer baselines or for PPP, the site displacement effects cannot be sufficiently cancelled by differencing measurements across receivers. Therefore, modelling and correcting site-displacement effects are required. In the case of typical PPP implementations, the solid earth tides, polar tides and ocean loading effects are only corrected (Kouba, 2009a). Other site displacement effects, for example, the atmospheric pressure, ground water and snow build-up loading, which have typically magnitudes smaller than 1 cm, are ignored.

In addition, the use of the Earth rotation parameter corrections (sidereal time, precession and nutation) are required, when making a conversion from the ITRF frame to the inertial frame (Kouba, 2009a). If working directly in the ITRF frame, the Earth rotation parameters are not required.

3.4.8.1 Solid earth tides

The solid earth tide effect is caused by the disturbances in the gravitational force similar to the forces which cause the ocean tide effect. The solid earth tide effect can cause an error as large as 30 and 5 cm in the radial and horizontal directions, respectively (Kouba, 2009a). Therefore, the effect must be corrected when employing PPP. The solid earth tides effect ($\overline{\Delta r}$) can be corrected using equation (3.25) with a 5 mm level precision according to the

International Earth Rotation and Reference Systems Service (IERS) conventions (IERS, 2003). GM is the gravitational parameter of the Earth. GM_1 is the gravitational parameter for the Moon and GM_2 is the gravitational parameter for the Sun. $\bar{r}$ is the geocentric unit vector of the station and $\bar{R}_j$ refers to the geocentric unit vectors of the Moon and Sun. l_2 is the nominal second degree Love dimensionless number and h_2 is the second degree Shida dimensionless number. ϕ is the latitude of the site and λ is the longitude of the site. θ_g is the Greenwich mean sidereal time. The correction as shown here is used in this thesis.

$$\overline{\Delta r} = \sum_{j=2}^{3} \frac{GM_j}{GM}\frac{r^4}{R_j^3}\left\{\left[3l_2\left(\bar{R}_j \cdot \bar{r}\right)\right]\bar{R}_j + \left[3\left(\frac{h_2}{2} - l_2\right)\left(\bar{R}_j \cdot \bar{r}\right)^2 - \frac{h_2}{2}\right]\bar{r}\right\} + \left[-0.025 * \sin\phi * \cos\phi * \sin(\theta_g + \lambda)\right]\bar{r} \tag{3.25}$$

3.4.8.2 Polar tides

The polar tide effect is caused by the changes of the Earth's spin axis relative to the Earth's crust. The maximum displacement error which can be caused by the polar tide effect is 25 and 7 mm in the vertical and horizontal directions, respectively (Kouba, 2009a). Equation (3.26) corrects the latitude component from the polar tide effect, equation (3.27) corrects the longitude and equation (3.28) corrects the station height (IERS, 2003). These corrections are used in this thesis. The required input data to calculate the corrections are the latitude (ϕ) and longitude (λ) of the station. In addition, the X and Y pole coordinate variations $\left(X_p - \bar{X}_p\right)$ and $(Y_p - \bar{Y}_p)$ relative to the mean poles $(\bar{X}_p, \bar{Y}_p)$ are required.

$$\Delta\phi = -9\cos 2\phi\left[\left(X_p - \bar{X}_p\right)\cos\lambda - (Y_p - \bar{Y}_p)\sin\lambda\right] \tag{3.26}$$

$$\Delta\lambda = 9\sin\phi\left[\left(X_p - \bar{X}_p\right)\sin\lambda + (Y_p - \bar{Y}_p)\cos\lambda\right] \tag{3.27}$$

$$\Delta h = -33\sin 2\phi\left[\left(X_p - \bar{X}_p\right)\cos\lambda - (Y_p - \bar{Y}_p)\sin\lambda\right] \tag{3.28}$$

3.4.8.3 Ocean loading

The ocean loading effect is caused by the load of the ocean tides on the underlying crust of the Earth (Kouba, 2009a). The ocean loading effect can cause for example, a 5 cm position error, but the magnitude of the error is dependent on the distance from the coast (Kouba, 2009a). The magnitude of the error is larger for stations in coastal regions compared to stations inland.

The service provided by the Chalmers University of Technology can be used to calculate the ocean loading corrections, which are also used in this thesis (Bos and Scherneck, 2011). The corrections are calculated based on the latitude, longitude and height of the station.

3.4.8.4 Atmospheric pressure loading

The atmospheric pressure loading effect is caused by the movement of the pressure systems over the Earth (Urquhart, 2009). The magnitude of the atmospheric pressure loading error can occasionally reach up to 3 cm in the vertical direction (Urquhart, 2009). Nevertheless, the pressure loading error is not normally corrected in GNSS analysis.

There are two main methods to correct the atmospheric pressure loading error: the geophysical and empirical approach (Urquhart, 2009). The principle of the geophysical approach is to use a global gridded atmospheric pressure model to calculate the correction for each site. This approach can provide both horizontal and vertical displacement terms, but the correction cannot be provided in real-time. The empirical approach is based on using local pressure data to calculate the correction. The benefit of this approach is that the correction can be provided in real-time. However, only the vertical correction can be provided.

It is shown in Urquhart (2009) that correcting the atmospheric pressure loading error can reduce position errors in PPP. Nevertheless, a significant number of issues remain, for example, the accuracy of global gridded pressure fields, response of the oceans to the pressure loading and the structure of the earth in the corrections.

The atmospheric pressure loading effect is ignored in PPP in this thesis, because it is difficult to correct in real-time.

3.4.9 Phase wind-up

The antenna phase wind-up effect is caused by the relative rotation of the receiver and satellite antennas (Banville and Tang, 2010). GNSS signals are Right-Hand Circularly Polarized (RHCP) and the relative rotation between the receiver and transmitter antennas causes changes in phase measurements. The phase wind-up effect causes errors only to carrier-phase measurements and not to code-phase measurements. The wind-up effect is cumulative. Thus, if the antenna is rotated *n* times, the magnitude of the wind-up effect is the wavelength of the signal times *n*.

In practice, the receiver phase wind-up effect can cause centimetre to decimetre level position errors (Banville and Tang, 2010). The satellite antenna phase wind-up effect can cause a range error up to 0.5 carrier-phase cycles, which is equal to, for example, 9.5 cm for the GPS L1 carrier-phase signal (Kouba, 2009a). Thus, the wind-up effect must be taken into account in PPP processing

The satellite phase wind-up effect ($\Delta\phi$, in radians) can be calculated using equation (3.29). Equations (3.30), (3.31) and (3.32) are required to calculate input values for equation (3.29) (Wu et al., 1992). The vector $\bar{k}$ is the satellite to the receiver unit vector. The vectors $\bar{x}'$, $\bar{y}'$and $\bar{z}'$ are the current satellite body coordinate unit vectors and vectors $\bar{x}$, $\bar{y}$ and $\bar{z}$ are the receiver coordinate system unit vectors. Continuity of consecutive phase observation segments must be ensured by adding or subtracting 2π from the phase wind-up correction when it is necessary.

$$\Delta\phi = sign(\varsigma)cos^{-1}(\bar{D}' \cdot \bar{D}/(|\bar{D}'||\bar{D}|)) \tag{3.29}$$

$$\varsigma = \bar{k} \cdot (\bar{D}' \times \bar{D}) \tag{3.30}$$

$$\bar{D}' = \bar{x}' - \bar{k}\left(\bar{k} \cdot \bar{x}'\right) - \bar{k} \times \bar{y}' \tag{3.31}$$

$$\bar{D} = \bar{x} - \bar{k}\left(\bar{k} \cdot \bar{x}\right) - \bar{k} \times \bar{y} \tag{3.32}$$

If a satellite is in the nominal yaw attitude, the satellite body-fixed attitude vector directions are as follows: the $\bar{z}'$ vector points to the Earth, $\bar{y}'$ vector is perpendicular to the direction to the Sun and is along the satellite solar panels and $\bar{x}'$ vector points away from the Sun in

the case of Block IIR GPS satellites and towards the Sun in the case of Block II or Block IIA GPS satellites (Kouba, 2009b). If the satellite is not in the nominal yaw attitude, it may add centimetre-level errors to the phase wind-up calculation.

The local receiver unit vectors ($\bar{x}$,$\bar{y}$,$\bar{z}$) can be calculated using equations (3.33), (3.34), and (3.35) (Drake, 2004). The vector $\bar{x}$ is points to the North, $\bar{y}$ to the East and $\bar{z}$ to the up direction. ϕ is the geodetic latitude of the receiver and λ is the longitude of the receiver.

$$\bar{x} = (-\sin(\phi)\cos(\lambda), -\sin(\phi)\sin(\lambda), \cos(\phi)) \tag{3.33}$$

$$\bar{y} = (-\sin(\lambda), \cos(\lambda), 0) \tag{3.34}$$

$$\bar{z} = (\cos(\phi)\cos(\lambda), \cos(\phi)\sin(\lambda), \sin(\phi)) \tag{3.35}$$

The satellite wind-up correction model as in Wu et al. (1992) is used with most PPP models and it is also used in this thesis. The model can remove the effect of phase wind-up almost completely (sub millimetre-level).

Correcting the receiver phase wind-up error is possible using external information on antenna rotation (Banville and Tang, 2010). As an alternative method, the error can be corrected without any external information using the de-coupled clock model (Collins, 2008). The main principle of the de-coupled clock model is to estimate separate receiver code-phase and carrier-phase clock values instead of estimating a common receiver clock error value as in the case of traditional PPP models. According to experiments presented in Banville and Tang (2010), it is possible to remove the effect of the receiver phase wind-up using the de-coupled clock model.

In addition, the receiver antenna phase wind-up can also be removed by differencing measurements between satellites (as explained in Section 4.3.2.2), because the receiver phase wind-up value is the same for all carrier-phase measurements. This method is used in this thesis.

3.4.10 Satellite eclipsing sessions

Satellite eclipsing occurs when the Earth is between the satellite and Sun (Kouba, 2009b). The Earth blocks sunlight from the satellite making it difficult for the satellite hardware to maintain its nominal attitude (Mervart, 1995). The nominal yaw attitude is defined for GPS satellites with respect to the satellite body-fixed Z-axis pointing to the Earth, X-axis pointing toward the Sun in the case of GPS Block II or IIA satellites or away from the Sun in the case GPS Block IIR satellites and the Y-axis at 90 degrees angle to the Sun direction and along the satellite solar panels (Kouba, 2009b).

The satellite eclipsing phase can be detected using equations (3.36) and (3.37) (Mervart, 1995). $\overline{r}_{sat}$ is a vector from the centre of the Earth to the mass centre of the satellite. $\overline{r}_{Sun}$ is a vector from the centre of the Earth to the centre of the Sun. a_e is the length of the Earth semi-major axis (6378137.0 m). The satellite is in the eclipsing phase if both conditions defined by equations (3.36) and (3.37) are true (Mervart, 1995). There are two eclipsing sessions per satellite each year. Each of the sessions lasts approximately seven weeks. However, the satellite is in the eclipse phase only for a part of the day.

$$\cos\gamma = \frac{\overline{r}_{sat} \cdot \overline{r}_{Sun}}{|\overline{r}_{sat}||\overline{r}_{Sun}|} < 0 \tag{3.36}$$

$$|\overline{r}_{sat}|\sqrt{1-\cos^2\gamma} < a_e \tag{3.37}$$

When the satellite is in the eclipsing phase, the attitude of the satellite is not nominal. This can cause errors, including in: satellite orbit prediction, satellite phase wind-up correction and satellite phase offset correction (Kouba, 2009b). For user-side processing, satellites which are in the eclipsing phase can be excluded from the solution (Kouba, 2009b). However, this cannot be done in network processing (Kouba, 2009b). In this case, satellite yaw-attitude models for GPS satellites as in Kouba (2009b) and for GLONASS satellites as in Dilssner et al. (2010) can be used during eclipsing sessions.

Satellites in the eclipsing phase are excluded in this thesis, as is done in most other PPP models.

3.4.11 Multipath and Non Line-Of-Sight (NLOS) signals

Multipath errors are caused by the reflection or diffraction of the signal, whilst travelling from the satellite to the GNSS receiver (Kaplan and Hegarty, 2006). It may be possible that the direct path of the signal is blocked and it is only possible to receive the signal travelling via an indirect path, known as Non Line-Of-Sight (NLOS). Nevertheless, the more likely situation in typical environments is that the signal is received both by the direct and indirect paths. In this case, the direct signal is received before the indirect one. If the receiver can separate the direct signal from the indirect one, multipath will not cause large errors. It may be difficult to detect which signal is travelling by the direct path, because the indirect signal may be stronger. This may occur when the direct signal is almost blocked, but the indirect signal is reflected.

The magnitude of multipath depends on the environment surrounding the GNSS receiver, receiver signal processing, antenna gain pattern, satellite elevation and signal characteristics. The magnitude of multipath is typically larger for low elevation satellites compared to high elevation satellites. The typical magnitude of the 1-sigma multipath can be 20 cm for code-phase measurements and 2 cm for carrier-phase measurements (Kaplan and Hegarty, 2006). However, the magnitude of the multipath can be much larger in extreme multipath environments such as some urban canyons. For example, in the case of GPS L1 C/A positioning, using consumer level GNSS equipment in difficult environments, where there may be only reflected signals, the multipath error for code measurements may be larger than one C/A code chip, which is equal to approximately 293 m (Kaplan and Hegarty, 2006).

The mitigation of the multipath can be achieved by combining multiple methods. Antenna design and placement can be used to reduce multipath (Kaplan and Hegarty, 2006). Antennas can be designed to reduce multipath errors caused by reflections near or below the horizon. Choke-ring antennas are an example of this kind of design. In addition, it is possible to reduce the multipath error by receiver design (Kaplan and Hegarty, 2006). The receiver-side multipath mitigation technologies are divided into parametric and non-parametric techniques. The design goal with the non-parametric technologies is to make receiver discriminator design less sensitive to multipath, for example, by a narrower early-

late correlator spacing. The objective of the parametric techniques is to estimate parameters related to multipath, and then to remove the effects of multipath.

Currently, multipath mitigation is an active research interest. For example, it is proposed that dual-polarization antennas can be used to mitigate multipath (Groves et al., 2010). Alternatively, modifications to GNSS reference station antennas are proposed to reduce multipath (Kerkhoff et al., 2010).

In addition, it is possible to weight measurements based on estimated multipath magnitude (Lau and Cross, 2006). 3D-city models can also be used to detect and identify the measurements affected by multi-path (Wang et al., 2012).

When employing cRTK, the magnitude of multipath can be mitigated using the method developed in Moradi et al. (2013). The method is based on using between receiver and frequency differenced measurements to estimate the multipath error. However, the method is not suitable for PPP, because it requires the mitigation of ionospheric error by differencing measurements across receivers, which is not possible when employing PPP.

New GNSS signals such as the GPS L5 and Galileo E5a, E5b and E5 are less vulnerable to code-phase multipath compared to the GPS L1 C/A signal (Kaplan and Hegarty, 2006). This is due to the improved signal structure, for example, the BPSK-R(10) modulation is used for the GPS L5 signal as the BPSK-R(1) modulation is used for the GPS L1 C/A signal. The type of modulation used has a significant effect on the vulnerability of the signal to multipath.

In conclusion, there are no multipath mitigation methods which can be used in all cases. The primary issue with the current multipath methods is that they are dependent on the receiver and antenna used as well as the environment where the GNSS receiver is used. However, the situation with the code-phase multipath is becoming better in future, because of the new GNSS signals such as GPS L5 and Galileo E5 are less vulnerable to multipath than the currently used GPS L1 C/A, GPS P1/P2 and GLONASS signals.

3.4.12 Relativistic effects

When designing GNSS, the impact of the general and special relativity must be taken into account (Kaplan and Hegarty, 2006). The latter is required, because the satellites and

receivers are normally moving relative to the chosen isotropic light speed frame. The general relativistic effects must be corrected, because the satellites and receivers are normally located at different gravitational potentials. The effects can be corrected by adjusting the satellite clock frequency to 10.22999999543 MHz. Thus, the frequency observed by the user at the sea level is 10.23 MHz.

Additionally, the effect caused by the slight eccentricity of the satellite orbits also needs to be taken into account. This effect causes the satellite clock to run slower when the satellite is at the perigee and to run faster when the satellite is at the apogee. The correction (Δt_r) can be calculated using the following equations (Kaplan and Hegarty, 2006):

$$\Delta t_r = F_r e_s \sqrt{a_e} \sin E_k \tag{3.38}$$

where

$F_r = -4.442807633 * 10^{-10} \frac{s}{m^{1/2}}$, e_s is the satellite orbital eccentricity, a_e is the semi-major axis of the satellite orbit and E_k is the eccentric anomaly of the satellite orbit.

The Sagnac effect is caused by the rotation of the Earth during the time of the signal transmission (Kaplan and Hegarty, 2006). The error caused by the Sagnac effect can reach 30 m, if left uncompensated. The Sagnac effect can be eliminated by carrying out all calculations in the Earth-Centered Inertial (ECI) coordinate system. The ECI frame is obtained by freezing the ECEF at the time when the receiver makes measurements to a set of visible satellites.

The Shapiro delay is caused by the signals travelling around a sufficiently massive object, for example, the Earth. Equation (3.39) can be used to correct the Shapiro delay (Δt_s) (Parkinson et al., 1996).

$$\Delta t_s = -\frac{2GM_e}{c^3} \log(1 - \bar{R} \cdot \bar{x}) \tag{3.39}$$

where G is the gravitational constant, c is the speed of light, M_e is the mass of the Earth, $\bar{R}$ is the unit vector pointing from the receiver to the satellite, $\bar{x}$ is the unit vector pointing from the GNSS receiver to the centre of the mass of the Earth.

3.4.13 Receiver clock error

The receiver clock error corresponds to the difference between the receiver local time and GNSS time (Weinbach and Schön, 2011). Typically, the receiver clock error is estimated as an unknown in a least-squares or Kalman filter solution. The estimation is carried out at every epoch. Another common way to eliminate or reduce the receiver clock error is to apply the Between-Satellite-Difference (BSD) operation (Section 4.3.1.1) to GNSS measurements.

Usually oscillators in GNSS receivers are inexpensive quartz crystal oscillators. Solving the receiver clock error must be done at each epoch when using this kind of oscillator, because it is unstable. The drawback of this method is the need for one extra observation to solve the clock error. In addition, using the method degrades the accuracy of the height component, particularly, in kinematic cases, because of the correlation between the station height, receiver clock and tropospheric parameters (Weinbach and Schön, 2011).

It is possible to use a highly stable atomic clock as a GNSS receiver clock (Weinbach and Schön, 2011). For example, the Symmetricom Chip-Scale Atomic Clock (CSAC) is suitable. When using an atomic clock as the GNSS receiver clock, only an initial synchronization to GNSS time is needed. Thereafter, there is no need to solve the receiver clock error at each epoch. Instead, the atomic clock behaviour can be modelled using a simple quadratic clock polynomial. This kind of polynomial can be valid for up to 24 hours without degrading the positioning accuracy (Weinbach and Schön, 2011).

Using an atomic clock as the receiver clock instead of a quartz crystal oscillator does not provide much benefit for static positioning (Weinbach and Schön, 2011). In contrast, using it for kinematic positioning may provide improvements, particularly, for the height component accuracy (Weinbach and Schön, 2011).

3.4.14 Measurement noise

There is always noise in GNSS measurements. The main sources of code-phase noise are the thermal noise jitter and effects of interference (Kaplan and Hegarty, 2006). The typical magnitude of code-phase noise is at decimetre level. Carrier-phase noise is caused by the phase jitter and dynamic tress error. The magnitude of carrier-phase errors under nominal

conditions is, for example, 1.6 mm when tracking the GPS P(Y) code and 1.2 mm when tracking the GPS C/A code (Kaplan and Hegarty, 2006). In general, the magnitude of the measurement noise depends on the design of the GNSS receiver and type of the GNSS signal.

Interference in GNSS measurements can be caused intentionally or un-intentionally. Intentional interference includes jamming, disturbance, meaconing and spoofing. As an example of jamming, North Korea used a GNSS jammer close to the South Korean border and caused blockage and attenuation of signals on the South-Korean side (GPS_World, 2012a). Un-intentional interference can be caused, for example, by other signals broadcast in the same frequency band as the GNSS signals. For example, the LightSquared Company tried to obtain a permission to build a Long Term Evolution towards 4th Generation (LTE-4G) broadband network in the USA in the same frequency band as the GPS L1 signal. The application was not approved because the broadband network would have caused interference to the GNSS signals (GPS, 2013a).

The modernisation of the GPS system and Galileo systems provide new signals such as GPS L5 and Galileo E5/E5a, which have significantly lower noise than the GPS L1 C/A signal (Bakker et al., 2012). In addition, improvements in receiver technologies have provided benefits in terms of reducing measurement noise. This can be seen in Table 3.3, which shows one sigma measurement standard deviation values for the Septentrio PolaRx4/PolaRx4TR receiver. The noise values for the modern Septentrio receiver are lower than the values published in Kaplan and Hegarty (2006). In addition, the table shows that the noise standard deviation of the Galileo E5 code-phase signal is significantly lower than of any other currently specified GPS, Galileo or GLONASS signal.

System	Measurement	1 sigma noise standard deviation
GPS	C/A code-phase (smoothed)	5 cm
GPS	C/A code-phase (non-smoothed)	16 cm
GPS	P2 code-phase (non-smoothed)	10 cm
GPS	L5 code-phase (non-smoothed)	6cm
GPS /GLONASS/Galileo	L1 and L2 carrier-phase	1 mm
GPS/Galileo	L5 carrier-phase	1.3 mm
GLONASS	C/A code-phase (smoothed)	7 cm
GLONASS	C/A code-phase (non-smoothed)	25 cm
GLONASS	P code-phase (non-smoothed)	10 cm
Galileo	E1 code-phase (non-smoothed)	8 cm
Galileo	E5a/E5b code-phase (non-smoothed)	6 cm
Galileo	E5 code-phase (non-smoothed)	1.5 cm

Table 3.3 One sigma measurement noise standard deviation values for the Septentrio PolaRx4/PolaRx4TR receiver (Septentrio, 2011)

The noise in code-phase measurements can be reduced using the code-phase smoothing method (Dach et al., 2007). Carrier-phase measurements have low noise, but there is an unknown ambiguity term in each carrier-phase measurement. Nevertheless, the ambiguity term can be removed by time-differencing measurements and carrier-phase measurements can be employed to smooth code-phase measurements. The principle of the code-phase smoothing method is that code-phase measurements are replaced with carrier-phase measurements, but the carrier-phase measurements are shifted by the mean difference code minus phase. Equation (3.40) shows how code-phase smoothing is achieved for measurements in the L1 frequency band (Dach et al., 2007). $\widetilde{P_1}(t)$ is the P1 smoothed code-phase measurement at the current epoch t. $L_1(t)$ and $L_2(t)$ are carrier-phase measurements at the current epoch t at the L1 and L2 frequencies, respectively. f_1 is the GNSS L1 frequency and f_2 is the GNSS L2 frequency. $\bar{P}_1 - \bar{L}_1$ is the mean P1 code-phase minus L1 carrier-phase difference since the last loss of carrier-phase lock (cycle-slip).

$$\widetilde{P_1}(t) = L_1(t) + \bar{P}_1 - \bar{L}_1 + 2\frac{f_2^2}{f_1^2 - f_2^2}\left((L_1(t) - \bar{L}_1) - (L_2(t) - L_2)\right) \tag{3.40}$$

When estimating a position, Kalman filters as originally presented in Kalman (1960) or other filtering techniques can be used to mitigate measurement noise. The principle of the Kalman filter is to minimise the error variance. It gives an optimal solution when the noise is

Gaussian and white. Thus, the Kalman filter is optimal for GNSS position estimation in a theory, but in practice there may be correlations between the GNSS noise and error sources such as multipath. This makes the estimation sub-optimal and may cause position estimation errors.

3.5 Total error budget

Table 3.4 shows the magnitude of error sources in the case of standalone positioning using GPS L1 only and in the case of using the most suitable error correction products and dual-frequency GPS L1 and L2 measurements. The definition for the most suitable error correction is that the correction must provide the best accuracy compared to other corrections according to the literature and must be available for real-time use free of charge globally. Thus, this definition excludes commercially available error correction products or products which are only available for some specific regions. In addition, this table shows error magnitudes in a typical case, when there are no problems with generating error corrections and the satellite being analysed is not in the eclipsing phase.

Error source	Typical range error (GPS L1)	Typical residual range error corrected by the most suitable product	The most suitable product
Atmospheric pressure loading	Normally insignificant (mm level)	Normally insignificant (mm level)	No suitable real-time products
Differential code biases (DCB) B_{P1-C1} (code-phase only)	4 ns = 1.2 m	0.05 ns = 0.015 m	CODE DCB products (Dach et al., 2007)
Fractional Cycle Bias (FCB) (carrier-phase only)	One cycle	~mm level	CNES phase satellite clock corrections (Laurichesse, 2011)
Ionosphere	7.0 m (1σ)	mm to cm level, higher for low elevation satellites	The first order: the Ionosphere-free combination (Kaplan and Hegarty, 2006) The higher order: ignoring it
Multipath	Code-phase: 20 cm (1σ), carrier-phase: 1 cm (1σ)	Depends on the environment, typical impact on carrier-phase measurements is few cm or less.	Antenna and receiver design. Measurement weighting and excluding measurements, which have high magnitude of multipath.
Measurement noise	Code-phase : ~dm Carrier-phase: ~mm	Code-phase : ~dm Carrier-phase: ~mm	The impact of measurement noise on position solutions can be reduced, for example, by Kalman filtering (Kalman, 1960).
Ocean loading	5 cm position error	~mm level	(Bos and Scherneck, 2011)
Polar tides	Position error: 25 mm radial and 7 mm horizontal	~mm level	(Kouba, 2009a)
Receiver antenna phase centre	Can be more than 10 cm	< 1 mm	IGS ANTEX (Kouba, 2009a)
Receiver antenna phase wind-up (carrier-phase only)	Possible many metres, if rotating the receiver antenna.	~mm level	The De-coupled clock model (Banville and Tang, 2010) or applying the Between-Satellite-Difference (BSD) operation to measurements.
Receiver clock	< 1 mm, error can be solved	< 1 mm, error can be solved	Solving the error as an unknown each epoch or differencing measurements between satellites
Relativistic effects	< 1 mm	< 1 mm	(Kaplan and Hegarty, 2006)
Satellite antenna phase centre	No error respect to the broadcast GPS orbits.	< 1 mm	IGS ANTEX (Kouba, 2009a)
Satellite antenna phase wind-up (carrier-phase only)	0.5 cycle	< 1 mm	(Wu et al., 1992)
Satellite clock	1.1 m (1σ)	IGS 4.2 cm (RMS), CNES 3.6 cm (STD) Not necessary as large range level error	IGS Real-Time (Caissy et al., 2012) or CNES real-time (Laurichesse, 2011)
Satellite orbit	0.8 m (1σ)	4 cm (RMS) Not necessary as large range level error	CNES Real-Time (Laurichesse et al., 2010) or IGS Ultra-Rapid products
Solid Earth tides	Position error: 30 cm radial and 5 cm horizontal.	~mm level	(Kouba, 2009a)
Troposphere	0.2 m (1σ)	mm level – cm level, after convergence	The UNB3m model (Leandro et al., 2006), Global Mapping Function (GMF) (Boehm et al., 2006a). The Chen (Chen and Herring, 1997) or Wet (MacMillan, 1995) tropospheric gradient mapping functions

Table 3.4: Total error budget

As shown in Table 3.4, the dominating error sources after applying the most suitable error corrections are the satellite orbit, satellite clock and multipath. In the case of satellite orbit and clock errors, the error in the user to satellite direction is typically smaller than the estimated error in the correction products. In typical cases, other error sources such as ionospheric and tropospheric errors are not significant compared to satellite clock, satellite orbit and multipath errors.

In conclusion, the accuracy of the current error corrections is sufficient compared to, for example, the wavelength of narrow-lane combination (10.7 cm), which is a relevant threshold when attempting PPP ambiguity resolution.

4 Current Precise Point Positioning (PPP) methods

Chapter 2 has identified a number of positioning applications which require centimetre-level accuracy. In Chapter 3, a review of the Global Navigation Satellite Systems (GNSS) has been performed focusing on their error sources and the associated mitigation techniques. This chapter reviews the current Precise Point Positioning (PPP) methods.

Depending on the type of carrier-phase ambiguity resolution, PPP methods can be classified into float PPP and fixed ambiguity PPP categories. In this thesis, particular interest is placed on ambiguity resolution using the GPS L1 and L2 signals since the full constellation of GPS satellites broadcasting L5 or Galileo constellation is not yet ready. Furthermore, this chapter also reviews the current integrity monitoring algorithms suitable for PPP.

Section 4.1 provides a review of the cRTK method in order to provide a reference for comparison with the current PPP methods. A current float PPP model is analysed in Section 4.2. The performance of the model is important, because ambiguity resolution is carried out based on the estimated float ambiguities.

The current fixed ambiguity PPP methods in terms of product generation and rover side implementation are discussed in Section 4.3. In general, PPP ambiguity resolution is more complicated than ambiguity resolution for cRTK, because FCBs in the measurements are not removed and ionospheric delays not mitigated.

When using PPP for the applications discussed in Chapter 2, the correct resolution of carrier-phase ambiguities is vital. The current ambiguity resolution and validation methods are analysed in Section 4.4. Integrity monitoring methods suitable for PPP are analysed in Section 4.5. Current research and commercial PPP services and software are compared in Section 4.6. Finally, a summary of the main issues in this chapter is given in Section 4.7.

4.1 Conventional Real Time Kinematic (cRTK)

The cRTK method exploits the differential GNSS concept which is based on cancelling or mitigating common errors between two or more GNSS receivers by differencing their

measurements across the receivers (Remondi, 1984, Counselman and Gourevitch, 1981). At least one GNSS receiver must be used as a reference receiver, which must be at a known location. To obtain high positioning accuracy, carrier-phase measurements must be used. While carrier-phase measurements have low noise (millimetre level), they exhibit an unknown ambiguity term which needs to be resolved.

It is possible to obtain centimetre level positioning accuracy using cRTK in real-time (Kaplan and Hegarty, 2006). However, cRTK cannot be used everywhere on Earth. The distance (baseline) between the rover whose position is required, and reference receiver must typically be shorter than 50 km, depending on the ionospheric conditions, even if dual-frequency GNSS receivers are used (Kaplan and Hegarty, 2006). This presents a challenge if high accuracy positioning is needed in remote areas. In addition, employing cRTK requires frequent communication between the rover and reference receivers using, for example, radio-links or cellular networks. This is in order to transmit the required correction parameters to the rover.

When employing the cRTK model in this thesis, the wide-lane combination is calculated by subtracting L2 carrier-phase from L1 carrier-phase measurements in cycles (Kaplan and Hegarty, 2006). The longer wavelength of the combination (86 cm) makes ambiguity resolution easier compared to using the original L1 or L2 measurements with 19 and 24 cm wavelengths, respectively. The reason for this is that ambiguity resolution is easier when wavelength is larger in comparison to the total magnitude of the errors. Both wide-lane and L1 ambiguities are resolved using the Least-squares AMBiguity Decorrelation Adjustment (LAMBDA) method, which is based on making ambiguity resolution computationally efficient by de-correlating ambiguities (Teunissen, 1993). The LAMBDA method is discussed in detail in Section 4.4.3.1.

The principle of cancelling errors by differencing measurements across receivers can also be applied to baselines longer than 50 km by employing the wide-area RTK method (Blewitt, 1989). However, as the length of the baseline increases, errors become less correlated between the receivers. Thus, error modelling and corrections must be applied and ambiguity resolution must be carried out on ionosphere-free measurements (Blewitt, 1989).

This approach is similar to that of PPP ambiguity resolution which is discussed in Section 4.3.2.

The performance of cRTK is tested using real-data in Section 5.2.1. This is to provide a performance reference for the PPP method analysis.

4.2 Float Precise Point Positioning (PPP)

The Precise Point Positioning (PPP) method can be used to obtain centimetre level positioning accuracy using only one GNSS receiver. This effectively addresses the limitations of cRTK where at least one reference receiver at a known location is required. Instead of mitigating errors by differencing measurements as in the case of cRTK, PPP methods apply error modelling and corrections (Kaplan and Hegarty, 2006). The relevant error sources and most suitable error correction methods are discussed in Chapter 3.

Heroux et al. (1993) applied precise satellite orbit corrections to improve the accuracy of single-point positioning. Centimetre level accuracy was obtained by Zumberge et al. (1997) by post-processing data, estimating carrier-phase ambiguities and employing precise satellite orbit and clock corrections and the ionosphere-free measurement combination. Their pioneering work demonstrated the ability to obtain centimetre level accuracy by processing data from a single GNSS receiver. In the case of float PPP models, carrier-phase ambiguities are estimated as float values and ambiguity resolution is not attempted. An example of a typical float PPP model is presented in Héroux and Kouba (2001), where measurements from the GPS L1 and L2 frequencies are used. The ionosphere-free measurement combination is used to remove the first-order ionospheric error and inter-frequency biases from carrier-phase and code-phase measurements.

In general, the aim in PPP is to model and correct measurement errors as accurately as possible. Different float PPP models apply corrections for different errors. For example, precise satellite orbit and clock, tropospheric, site-displacement, antenna phase centre offset and phase wind-up corrections are applied in Héroux and Kouba (2001). However, delays in the provision of error models and computational power requirements may compromise the accuracy of PPP error corrections.

For example, the least-squares method or Kalman filter (Kalman, 1960) can be used to solve for the position and other unknowns when employing PPP. In the case of employing an Extended Kalman Filter (EKF) (Larson et al., 1967, Wishner et al., 1969), the observation vector $z_{EKF}(t)$ corresponds to the difference between observed and predicted ionosphere-free measurements, where t is the current time epochs. The predicted measurements are calculated based on the current receiver position, satellite positions and error estimates. The EKF states x_{EKF} as in equation (4.1) are the latitude error ($\delta\phi$), longitude error ($\delta\lambda$), height error (δh), velocities ($\delta\dot{\phi}, \delta\dot{\lambda}, \delta\dot{h}$), receiver clock offset (δdT), receiver clock offset change ($\delta d\dot{T}$), tropospheric wet delay (δT_{Trop}) and ionosphere-free float ambiguities ($\delta b_3^1,,,\delta b_3^n$) (Abdel-salam, 2005). There is one EKF state per each ionosphere-free ambiguity (per each ionosphere-free carrier-phase measurement combination).

$$x_{EKF} = [\delta\phi, \delta\lambda, \delta h, \delta\dot{\phi}, \delta\dot{\lambda}, \delta\dot{h}, \delta dT, \delta d\dot{T}, \delta T_{Trop}, \delta b_3^1,,,\delta b_3^n]^T \quad (4.1)$$

The EKF prediction step is described by equations (4.2) and (4.3). $x_{EKF}^-(t)$ is the predicted state vector, $x_{EKF}^+(t-1)$ the state vector estimated based on the measurements from the previous epoch, Φ_{EKF} the state transition matrix, $P_{EKF}^-(t)$ the predicted state vector variance/covariance matrix, $P_{EKF}^+(t-1)$ the state vector variance/covariance estimated based on the measurements from the previous epoch and Q_{EKF} the variance/covariance matrix of the system noise (Abdel-salam, 2005).

$$x_{EKF}^-(t) = \Phi_{EKF} x_{EKF}^+(t-1) \quad (4.2)$$

$$P_{EKF}^-(t) = \Phi_{EKF} P_{EKF}^+(t-1) \Phi_{EKF}^T + Q_{EKF} \quad (4.3)$$

The EKF update step is described by equations (4.4), (4.5) and (4.6) (Abdel-salam, 2005). $K_{EKF}(t)$ is the Kalman gain, $R_{EKF}(t)$ the measurement noise matrix and $H_{EKF}(t)$ the design matrix. The design matrix presents the relation between the measurements and EKF states. For example, it shows the relation between the code-phase measurements and the position.

$$x_{EKF}^+(t) = x_{EKF}^-(t) + K_{EKF}(t)[z_{EKF}(t) - H_{EKF}(t) x_{EKF}^-(t)] \quad (4.4)$$

$$P_{EKF}^+(t) = [I - K_{EKF}(t) H_{EKF}(t)] P_{EKF}^-(t) \quad (4.5)$$

$$K_{EKF}(t) = P_{EKF}^-(t) H_{EKF}^T(t) [H_{EKF}(t) P_{EKF}^-(t) H_{EKF}^T(t) + R_{EKF}(t)]^{-1} \quad (4.6)$$

The final inputs from float PPP are the EKF states $x_{EKF}^{+}(t)$, which are updated with the latest measurements at each epoch (Abdel-salam, 2005). These states include, for example, latitude, longitude and altitude.

For the float PPP tests carried out in this thesis, an EKF is used. The estimated states and their initial values, initial standard deviations and process noise, are shown in Table 4.1. The initial standard deviation and process noise parameter values are chosen empirically. The Between-Satellite-Difference (BSD) operation is applied to both carrier-phase and code-phase measurements as shown in equations (4.7) and (4.8), respectively. The operation is done to eliminate the receiver clock error. The BSD is calculated by selecting a satellite (typically the highest elevation satellite) as a base-satellite (j) and differencing its measurements with respect to measurements from other satellites' (i) (Gabor and Nerem, 1999). It would also be possible to process measurements as un-differenced and estimate the receiver clock error as an unknown, but the BSD operation is used to enable the use of the same float PPP model in fixed-ambiguity tests presented in Section 5.2.3. This ensures that the float model used in float and fixed ambiguity tests does not cause differences in results.

State	**Initial value**	**Initial standard deviation**	**Process noise standard deviation**
Latitude	Based on the least square solution.	10000 m (the East component)	0.0 $\frac{m}{\sqrt{s}}$ (the East component)
Longitude	Based on the least square solution.	10000 m (the North component)	0.0 $\frac{m}{\sqrt{s}}$ (the North component)
Height	Based on the least square solution.	10000 m	0.0 $\frac{m}{\sqrt{s}}$
Troposphere wet delay (residual)	0	0.1 m	$10^{-4}\ \frac{m}{\sqrt{s}}$
Troposphere gradient G_N	0	0.001 m	$3.1667 * 10^{-6}\ \frac{m}{\sqrt{s}}$
Troposphere gradient G_E	0	0.001 m	$3.1667 * 10^{-6}\ \frac{m}{\sqrt{s}}$
Carrier-phase ambiguities (ionosphere-free)	Based on the difference between the estimated and predicted ranges	10000 cycles	0

Table 4.1 The estimated EKF states and their initial values, initial standard deviations and process noise for the case of float PPP.

$$L_F^{i,j} = L_F^{\,i} - L_F^{\,j} \tag{4.7}$$

$$P_F^{i,j} = P_F^{\,i} - P_F^{\,j} \tag{4.8}$$

The first order ionospheric delay is eliminated using the ionosphere-free combination as discussed in Section 3.4.4. The combination is calculated as shown in equations (3.11) and (3.12) for BSD code-phase and carrier-phase measurements, respectively.

The most suitable error corrections selected in Chapter 3 are used. These are the CNES real-time satellite orbit and clock corrections, UNB3m tropospheric model, GMF tropospheric mapping function, Chen tropospheric gradient mapping function, ANTEX antenna phase centre offset and variation corrections, Wu phase wind-up correction model, site displacement corrections (Kouba, 2009a) and relativistic effects (Kaplan and Hegarty, 2006). Residual tropospheric wet delay and tropospheric gradients are estimated as EKF states.

Cycle-slip detection is carried out before position estimation. Cycle-slip detection is based on detecting changes in the ionospheric Total Electron Content Rate (TECR) as shown in equation (4.9) and Melbourne–Wubbena Wide Lane (MWWL) ambiguities as shown in equation (4.10) between the current and previous measurement epochs (Liu, 2011). The Melbourne-Wubbena ambiguities are calculated using equation (4.11) (Melbourne, 1985, Wubbena, 1985). In the equations, t is the current time epoch, Δt the time-difference between the current and previous epochs, $TECR$ the total electron content rate, f_1 the GNSS L1 frequency, f_2 the GNSS L2 frequency, b_{WL} the float Melbourne-Wubbena wide-lane ambiguity, L_1 the carrier-phase measurement at the L1 frequency, L_2 the carrier-phase measurement at the L2 frequency, P_1 the code-phase measurement at the at the L1 frequency, P_2 the code-phase measurement at the L2 frequency and λ_{wl} the wavelength of the wide-lane ambiguity (86 cm). When there are no cycle-slips, both TECR ($\left[\lambda_1 \nabla N_1^i(t) - \lambda_2 \nabla N_2^i(t)\right]$) and MWWL ($\left[\nabla N_1^i(t) - \nabla N_2^i(t)\right]$) differences between the epochs are small. When ionospheric activity is high, TECR can have the approximate magnitude of 0.03TECU/s. That is low compared to the magnitude of TECR (−0.514TECU/s) when 1Hz data-rate is used and there is a cycle-slip with the magnitude of one cycle (Liu, 2011). The magnitude of MWWL is below one cycle, if there are no cycle-slips and the magnitude of the code-phase multipath is not large (Liu, 2011). The MWWL difference gives reliable results except when

the cycle-slip has the same magnitude both in the L1 and L2 frequencies. TECR gives reliable results except when the special cycle-slip combinations (Liu, 2011) such as (L1 =77N, L2 = 60N) occurs. Therefore, both the MW and TECR difference tests must be used jointly to provide robust cycle-slip detection.

$$\left[\lambda_1 \nabla N_1^i(t) - \lambda_2 \nabla N_2^i(t)\right] = \frac{40.3 * 10^{16} \left(\frac{f_1^2}{f_2^2} - 1\right) \Delta t * TECR(t)}{f_1^2} \tag{4.9}$$

$$\left[\nabla N_1^i(t) - \nabla N_2^i(t)\right] = b_{WL}^i(t-1) - b_{WL}^i(t) \tag{4.10}$$

$$b_{wl}^i = \frac{\frac{f_1 L_1^i - f_2 L_2^i}{f_1 - f_2} - \frac{f_1 P_1^i + f_2 P_2^i}{f_1 + f_2}}{\lambda_{wl}} \tag{4.11}$$

If a cycle-slip is detected, a correction method, mainly based on the work presented in Banville and Langley (2009), is applied. The magnitude of the cycle-slip on the L1 and L2 measurements is estimated based on the change of the geometry-dependent wide-lane ambiguity and TECR between the current and previous epoch. Thereafter, the cycle-slip is corrected based on the geometry dependent wide-lane and TECR estimates. The geometry-dependent wide-lane is used for cycle-slip correction instead of MWWL because it has smaller multipath and noise errors. Cycle-slip corrections are validated by checking the TECR and geometry-dependent wide-lane difference between the current and previous epochs.

GPS carrier-phase measurement standard deviations (std) are obtained using equation (4.12), where a_1 is 0.003 m, a_2 is 0.003 m and E is the elevation angle of the satellite. The formula and parameters are similar to those used in the RTKLIB software (Takasu, 2012). It is assumed that the standard deviation for GPS code-phase measurement is 100 times larger than for carrier-phase measurements, because code-phase measurements have significantly larger noise and multipath compared to carrier-phase measurements.

$$std = a_1 + \frac{a_2}{\sin(E)} \tag{4.12}$$

The performance of this float PPP model tested in Section 5.2.3 using a dataset of 10 stations and 96 one hour time periods.

4.3 Fixed ambiguity Precise Point Positioning (PPP)

The primary motivations to develop PPP ambiguity resolution methods have been to reduce convergence time and improve accuracy. PPP carrier-phase ambiguity resolution is not possible without correcting for FCBs from carrier-phase measurements. This is because float carrier-phase ambiguities do not have an integer nature without correcting for FCBs when employing PPP (Geng et al., 2010d). FCBs still exist in the float carrier-phase ambiguity estimates, even though the float position solution has converged and float ambiguities are stabilised close to some float value. This is not a problem for cRTK, because FCB errors are cancelled by differencing measurements across receivers and satellites (double-differencing), which then enables the ambiguities to be resolved (Kaplan and Hegarty, 2006).

The general principle of the fixed ambiguity PPP product generation is to estimate FCB corrections using data from a global reference network. The corrections are delivered to users (rovers), for example, over a cellular data connection. Users can then apply the corrections and attempt PPP ambiguity resolution. The PPP error corrections (Chapter 3) and ambiguity resolution methods (Section 4.3.2) used in the rover side are not necessarily dependent on the server side FCB correction generation method (Section 4.3.1) used.

Gabor et al. (1999) showed that measurements from a reference network can be used to estimate satellite FCBs. They managed to estimate FCB corrections sufficiently accurately to enable geometry-free wide-lane ambiguity resolution in a single receiver (i.e. without differencing measurements across receivers). Nevertheless, they did not manage to estimate narrow-lane FCBs with sufficient accuracy to enable narrow-lane ambiguity resolution, which is necessary in order to obtain a fixed-ambiguity position solution.

It is shown in Wang and Gao (2006), using simulated GNSS data, that PPP ambiguity resolution can be achieved when FCBs are corrected with the sufficient accuracy. In a theoretical case where all other error sources as FCBs would be eliminated, correcting FCBs with better than 0.5 cycle accuracy would be sufficient to enable correct ambiguity resolution. However, float ambiguities are impacted by multiple error sources such as multipath and noise in addition to FCBs. Therefore, 0.25 cycles are often used as a tolerance for the FCB accuracy in the literature such as Geng et al. (2010d). In general, obtaining FCB corrections with the smallest possible error is important for reducing the probability of

incorrect ambiguity resolution. Measurements from a reference network are used to estimate both wide-lane and narrow-lane FCBs (Ge et al., 2006, Ge et al., 2008). They managed to estimate FCBs with sufficient accuracy to enable fixed-ambiguity positioning in most cases.

Currently, there are four methods to generate correction products to enable PPP ambiguity resolution using the GPS L1 and L2 signals. The methods are: the Between-Satellite-Difference Fractional Cycle Bias (BSDFCB) estimation (Ge et al., 2008, Geng et al., 2010d), Integer Recovery Clocks (IRC) (Laurichesse and Mercier, 2007, Collins, 2008), Double-Differenced PPP (DDPPP) (Bertiger et al., 2010) and Un-Differenced Fractional Cycle Bias (UDFCB) estimation (Li and Zhang, 2012). The principles of these methods are discussed in Section 4.3.1.

Rover (user) side PPP ambiguity resolution methods on the basis of GPS L1 and L2 signals are discussed in Section 4.3.2. The use of GLONASS for PPP ambiguity resolution is discussed in Section 4.3.3. The use of new GNSS signals such as GPS L5 and new systems such as Galileo are discussed in Section 4.3.4.

4.3.1 Product generation when using GPS L1 and L2

Current methods to generate correction products which enable PPP ambiguity resolution are discussed in this section. The methods using the GPS L1 and L2 signals are included in this analysis, because the aim in this thesis is to use signals which are already available.

4.3.1.1 The Between-Satellite-Difference Fractional Cycle Bias (BSDFCB) estimation method

The principle of the Between-Satellite-Difference Fractional Cycle Bias (BSDFCB) estimation method is to use data from a reference network to estimate wide-lane and narrow-lane FCBs (Geng et al., 2010d). The literature also refers to these FCBs as Un-calibrated Phase Delay (UPD) errors.

When employing the BSDFCB method, the Between-Satellite-Difference (BSD) operation is applied to measurements to remove the receiver clock error and receiver side FCB from

carrier-phase measurements, and receiver clock error and receiver side code-phase biases from code-phase measurements. The BSD is calculated using equation (4.7) for carrier-phase measurements and equation (4.8) for code-phase measurements. One satellite is selected as the base-satellite (j) and its measurements are subtracted from the measurements from other satellites (i) (Gabor and Nerem, 1999).

The first step in the FCB estimation is the application of the Melbourne-Wubbena combination (Melbourne, 1985, Wubbena, 1985) to estimate float wide-lane ambiguities $(b_{wl}^{i,j})$. The computation of the combination is carried out for each satellite pair (i,j), as shown in equation (4.11).

The sine components in equation (4.13) and cosine components in equation (4.14) of the wide-lane ambiguities are summed based on the data from each reference station belonging to the network. The summing is done for each possible combination of satellites. The wide-lane satellite FCB $(B_{wl,s}^{i,j})$ estimates are then calculated based on the sum of the sine and cosine components using equation (4.15) (Gabor and Nerem, 1999).

$$\sum_{sin} = \sum \sin[2\pi b_{wl}^{i,j}] \tag{4.13}$$

$$\sum_{cos} = \sum \cos[2\pi b_{wl}^{i,j}] \tag{4.14}$$

$$B_{wl,s}^{i,j} = \frac{1}{2\pi}\, arctan2(\sum_{sin}, \sum_{cos}) \tag{4.15}$$

After obtaining sufficiently stable FCB corrections, wide-lane ambiguity resolution is attempted at each station. The stability of the corrections from the network estimation is defined, for example, based on their standard deviation. The float wide-lane ambiguities corrected with FCBs are rounded to the nearest integers using equation (4.16) (Geng et al., 2010d). The decision on whether the ambiguities have been correctly fixed is based on the Dong Bock Test (DBT) presented in Dong and Bock (1989). The test makes the fixing decision based on the standard deviation of the float ambiguity and its distance from the closest integer. The ambiguity can only be fixed, when the probability of wrong fixing is sufficiently small. For example, the allowed probability of the wrong ambiguity fixing can be 0.1%.

$$N_{wl}^{i,j} = round(b_{wl}^{i,j} - B_{wl,s}^{i,j}) \quad (4.16)$$

Float ionosphere-free ambiguities ($b_3^{i,j}$) are estimated using equation (4.17), where $e_g^{i,j}$ refers to a geometry based term and λ_1 refers to the L1 signal wavelength. The narrow-lane float ambiguities ($b_{nl}^{i,j}$) for each satellite pair at each station can then be calculated based on the fixed wide-lane ($N_{wl}^{i,j}$) and float ionosphere-free ambiguities ($b_3^{i,j}$), as shown in equation (4.18) (Ge et al., 2008).

$$L_3^{i,j} = \frac{f_1^2}{f_1^2 - f_2^2} L_1^{i,j} - \frac{f_2^2}{f_1^2 - f_2^2} L_2^{i,j} = e^{i,j} + \lambda_1 b_3^{i,j} \quad (4.17)$$

$$b_{nl}^{i,j} = \frac{f_1 + f_2}{f_1} b_3^{i,j} - \frac{f_2}{f_1 - f_2} N_{wl}^{i,j} \quad (4.18)$$

Narrow-lane FCBs are obtained using a similar approach to that for the wide-lane FCBs. Narrow-lane ambiguities for each satellite pair from each station are calculated using equation (4.18) (Ge et al., 2008). Following this, the sum of the cosine and sine components of the ambiguities is calculated using equations (4.13) and (4.14). In the calculation, the wide-lane terms are replaced by the narrow-lane terms. Then, narrow-lane FCBs are calculated using the method applied to the wide-lane FCBs using equation (4.15).

Narrow-lane FCBs can change quickly. Therefore, their corrections must be provided using a data rate of between 5 seconds and 15 minutes (Geng, 2009). A high data-rate such as 5 seconds is preferable, because it prevents the magnitude of FCB error increasing unacceptably during the correction interval. However, providing FCB corrections at a high data rate is not always possible, because of the data connection bandwidth limitations. On the other hand, wide-lane FCBs can be provided as daily corrections, because they are very stable (Geng, 2009).

Ambiguity resolution can be attempted at the rover level when both wide-lane and narrow-lane FCB corrections are available for a satellite pair (Geng et al., 2010d). The same set of FCB corrections cannot be used globally because the satellite which has been used as the base-satellite in the reference network must also be available at the rover (Geng et al.,

2010d). The same satellite orbit, clock and DCB corrections used in the product generation must be used by the rover, because the type of correction products employed impacts on the magnitude of estimated FCBs.

The quality of FCB corrections can be improved by carrying out the estimation based on a network solution, instead of on separate float PPP solutions for each of the stations as described above (Geng et al., 2012). The network solution is obtained by first differencing measurements between satellites and secondly between stations and then attempting ambiguity resolution. There are no FCBs in the double-differenced solution and hence, it is possible to attempt ambiguity resolution. After the double-differenced ambiguities are resolved, the BSD ambiguities in each station can be re-calculated based on the fixed-ambiguity network solution. Thereafter, FCB estimates can be obtained based on the fractional parts of the BSD ambiguities. The benefit of this method is obtaining FCB corrections with a small error magnitude compared to the conventional BSDFCB method (Geng et al., 2012). Based on the results shown in Geng et al. (2012), the new method reduced the RMS error of the east position component by 0.4 mm compared to the conventional method when FCBs were used for fixed ambiguity PPP. GNSS data from 248 stations and 359 days were used in the test.

4.3.1.2 The Integer Recovery Clocks (IRC) method

The Integer Recovery Clocks (IRC) method is presented in Laurichesse and Mercier (2007), Laurichesse et al. (2008, 2009a, 2010), Laurichesse (2011), Collins (2008) and Collins et al. (2008). In Collins (2008) and Collins et al. (2008), the IRC method is referred to as the De-coupled clock model. The general principle of the IRC method is to provide separate code-phase and carrier-phase satellite clock corrections. This eliminates FCBs from carrier-phase measurements and enables ambiguity resolution.

The ionosphere-free measurement combination is calculated as shown in equations (3.11) and (3.12) for code-phase and carrier-phase measurements in metres, respectively. When the ambiguity term (b_3^i) in the ionosphere-free measurement combination is solved in equations (4.19) and (4.20), the ambiguity term includes carrier-phase ($B_{L3,r} - B_{L3,s}^i$) and

code-phase ($B^i_{P3,s} - B_{P3,r}$) biases (Collins, 2008). Therefore, the ambiguity term (b^i_3) is not an integer even when all measurement errors excluding carrier and code-phase biases are corrected perfectly and the distance between the receiver and satellite is known exactly (Collins, 2008). The symbols in the equations are following: d^i is the distance between the receiver and satellite, δdT_3 the receiver clock error, δs^i the satellite clock error, ${D_{trop}}^i$ the tropospheric error, M^i_3 the code-phase multipath error, m^i_3 the carrier-phase multipath error, Q^i_3 the code-phase measurement noise, q^i_3 the carrier-phase measurement noise, $B_{P3,r}$ the receiver code-phase bias term, $B^i_{P3,s}$ the satellite code-phase bias term, $B_{L3,r}$ the receiver carrier-phase bias term, $B^i_{L3,s}$ the satellite carrier-phase bias term and i the satellite.

$$\begin{cases} P^i_3 = d^i + \delta dT_{P3} - \delta s^i_{P3} + {D_{trop}}^i + M^i_3 + Q^i_3 \\ L^i_3 = d^i + \delta dT_{P3} - \delta s^i_{P3} + {D_{trop}}^i + m^i_3 + q^i_3 + b^i_3 \end{cases} \quad (4.19)$$

$$\begin{cases} \delta dT_{P3} = \delta dT + B_{P3,r} \\ \delta s^i_{P3} = \delta s^i + B^i_{P3,s} \\ b^i_3 = \lambda_3(N^i_3 + B_{L3,r} - B^i_{L3,s}) + B^i_{P3} - B_{P3,r} \end{cases} \quad (4.20)$$

The motivation to develop the IRC method was to prevent ambiguities from being affected by code biases when employing the traditional float solution PPP model, which is similar to the model used in Section 4.2 (Collins, 2008). Satellite and receiver clock errors are estimated separately for the carrier-phase and code-phase measurements when employing the IRC method. The measurement model for the IRC method is shown in equations (4.21) and (4.22), where δdT_{P3} is the receiver code-phase clock error, δs^i_{P3} the satellite code-phase clock error, δdT_{L3} the receiver carrier-phase clock error, δs^i_{L3} the satellite carrier-phase clock error and λ_3 the wavelength of the ionosphere-free combination (Collins, 2008). The benefit of estimating the separate code-phase and carrier-phase clock errors, compared to the traditional model in equation (4.19), is that ambiguities have an integer nature. This enables carrier-phase ambiguity resolution.

$$\begin{cases} P^i_3 = d^i + \delta dT_{P3} - \delta s^i_{P3} + {D_{trop}}^i + M^i_3 + Q^i_3 \\ L^i_3 = d^i + \delta dT_{L3} - \delta s^i_{L3} + {D_{trop}}^i + m^i_3 + q^i_3 + \lambda_3 N^i_3 \end{cases} \quad (4.21)$$

$$\begin{cases} \delta dT_{P3} = \delta dT + B_{P3,r} \\ \delta s^i_{P3} = \delta s^i + B^i_{P3,s} \\ \delta dT_{L3} = \delta dT + \lambda_3 B_{L3,r} \\ \delta s^i_{L3} = \delta s^i + \lambda_3 (B^i_{L3,s}) \end{cases} \quad (4.22)$$

Expressing the ionosphere-free fixed ambiguity term (N_3^i) in equation (4.21) as multiples of 6 mm, which is the wavelength of the ionosphere-free combination, is possible in a theory (Dach et al., 2007). However, it is not practical because the wavelength is too short compared to the typical total magnitude of the errors. Therefore, it is not possible to resolve the ambiguity term (N_3^i) directly in practice. To overcome the issue, the ionosphere-free ambiguity term (N_3^i) is decomposed into the wide-lane (N_{wl}^i) and narrow-lane (N_{nl}^i) terms as in equation (4.23) (Collins, 2008). The wavelength of the wide-lane combinations is 86 cm and the wavelength of the narrow-lane combination is 10.7 cm (Collins, 2008).

$$N_3^i = \frac{f_1}{f_1 + f_2}\left(N_{nl}^i\right) + \frac{f_1 f_2}{f_1^2 - f_2^2} N_{wl}^i \quad (4.23)$$

Wide-lane ambiguities are estimated using the Melbourne-Wubbena combination (Melbourne, 1985, Wubbena, 1985). The combination is calculated using equation (4.11). The magnitude of noise and multipath in the wide-lane estimates depends on the receiver, antenna and environment around the receiver (Collins, 2008).

Narrow-lane float ambiguities are calculated based on the float ionosphere-free ambiguities and fixed wide-lane ambiguities as shown in equation (4.18) (Collins, 2008). The fixed ionosphere-free ambiguity (N_3^i) can be obtained after fixing both the wide-lane (N_{wl}^i) and narrow-lane (N_{nl}^i) ambiguities for the satellite as described in equation (4.23) (Collins, 2008).

Data from a global GNSS reference network is required for IRC correction estimation. For example, data from 32 reference stations (Collins, 2008) or from 50 stations (Laurichesse et al., 2010) are used to estimate IRC corrections. It is beneficial to use as many geographically diverse located stations as possible in the calculation in order to improve the accuracy of the corrections (Ge et al., 2012). In general, the larger number of stations adds redundancy to the estimation and geographical diversity ensures that as many satellites as possible are tracked by the stations. Nevertheless, increasing the number of stations also increases the

amount of computational power required, which could make real-time processing impossible (Ge et al., 2012). Real-time IRC correction generation is demonstrated, for example, in Laurichesse (2010).

In the network processing, float wide-lane ambiguity estimates, obtained using the Melbourne-Wubbena combination, can be filtered using a sliding window to reduce measurement noise. Equation (4.11), which is used to estimate wide-lane ambiguities, is singular, because the wide-lane ambiguity (N_{wl}^{i}), wide-lane receiver FCB ($B_{wl,r}$) and wide-lane satellite FCB ($B_{wl,s}^{i}$) terms cannot be separated (Mercier and Laurichesse, 2008). Having a singular equation means that an infinite number of solutions is possible.

A method to perform un-differenced wide-lane estimation using data from a GNSS receiver network is shown in Laurichesse et al. (2009c). To address the singularity issue, the FCB is first estimated for a station with a stable receiver FCB. At the station, the receiver FCB ($B_{wl,r}$) is set to zero. Thereafter, wide-lane ambiguities are fixed by rounding the ambiguities to the nearest integers and the satellite FCBs are estimated as shown in equation (4.24). The satellite wide-lane FCBs are then applied in the other stations. In these stations, the receiver FCB can be estimated using the least-squares method and the initial value for the receiver FCB can be obtained based on equation (4.25), where N_{wl}^{i} is the closest integer. The ambiguity term must be rounded to the closest integer to separate ambiguity from receiver FCB. Finally, the batch least-squares method is employed all over the network to obtain new estimates of the receiver and satellite FCBs (Laurichesse et al., 2009c). The previous FCB estimates are used as initial values in the estimation.

$$B_{wl,s}^{i} = \; b_{wl}^{i} - \; N_{wl}^{i} \tag{4.24}$$

$$B_{wl,r} \; = \; b_{wl}^{i} - N_{wl}^{i} - B_{wl,s}^{i} \tag{4.25}$$

IRC corrections can be estimated using the Kalman filter method as in Laurichesse et al. (2010) or the least-squares method as in Collins (2008). The number of Kalman filter states estimated for 34 satellites using 50 stations is shown in Table 4.2 (Laurichesse et al., 2010).

Kalman filter state type	Quantity	Total number
Satellite carrier-phase clock error	One per satellite	1×34
Station carrier-phase clock error	One per station	1×50
Satellite code-phase clock error	One per satellite	1×34
Station code -phase clock error	One per station	1×50
Tropospheric wet delay	One per station	1×50
Station coordinate corrections	Three per station	3×50
Satellite orbit corrections	Three per satellite	3×34
Narrow-lane carrier-phase ambiguities	12 per station	12×50
Total number of states		1070

Table 4.2 Kalman filter states for IRC corrections estimation (Laurichesse et al., 2010)

For the IRC correction estimation, initial satellite orbit estimates can be calculated based on the IGS Ultra-rapid orbit predictions (Laurichesse et al., 2010). However, the accuracy of these predictions is not always sufficient (with errors larger than 10.7 cm) (Laurichesse et al., 2010). Therefore, additional orbit corrections which are relative to the IGS Ultra-rapid corrections are estimated using EKF when estimating satellite clock corrections (Laurichesse et al., 2010).

Station coordinates can be fixed to the known values in the estimation (Laurichesse et al., 2010). Tropospheric wet delay is estimated as a Kalman filter state at each station. The IRC correction estimation begins with wide-lane and narrow-lane float ambiguity estimation. The wide-lane ambiguities must be fixed first, for example, after 30 minutes in the case of the implementation presented in Laurichesse et al. (2010). The reason for not fixing wide-lane ambiguities immediately is to let ambiguities to converge to ensure stability of the float ambiguity solution.

The system used to estimate IRC corrections is singular, because of the singularity between the receiver carrier-phase clock error, satellite carrier-phase clock error and narrow-lane ambiguity and singularity between the receiver and satellite code-phase clock errors (Collins, 2008). Therefore, one station with a stable receiver clock error is selected and the receiver clock errors are fixed to zero for this station. To remove the singularity between the narrow-lane ambiguities and carrier-phase clock error, one narrow-lane ambiguity in each station is fixed to an arbitrary value.

IRC corrections with, for example 5 s data-rate can be estimated using a Kalman filter (Laurichesse et al., 2010). Selecting the data-rate is a compromise between the

computational power requirement and performance of the corrections. The corrections delivered to rovers are wide-lane FCB and code-phase and carrier-phase clocks for each satellite. The satellite wide-lane FCBs can be delivered as daily files while code-phase and carrier-phase clock corrections are updated, for example, every five seconds (Laurichesse et al., 2010).

4.3.1.3 The Double-Differenced PPP (DDPPP) method

The Double-Differenced PPP (DDPPP) method (Bertiger et al., 2010) estimates the positions of GPS reference stations and positions and clock error of GPS satellites based on a network solution, which is calculated using data from 209 globally located reference stations. In the network solution, wide-lane float ambiguities are estimated using the Melbourne-Wubbena combination (Melbourne, 1985, Wubbena, 1985) as shown in equation (4.11). Ionosphere-free float ambiguity estimation is carried out using equation (3.12). Narrow-lane float ambiguities are obtained using equation (4.18) based on the float ionosphere-free and fixed wide-lane ambiguities. The fractional parts of the wide-lane and narrow-lane float ambiguity estimates are calculated at each station and provided for rovers.

In the rover receiver, precise satellite orbit and clock corrections are obtained from the network. The BSD operation is applied to the measurements to remove the receiver FCB. This is done by selecting one satellite as the base-satellite and subtracting its measurements from the measurements from the other satellites. The approach to float ionosphere-free and wide-lane ambiguity estimation in the rover is similar to that used for the network. To remove satellite FCBs from the ambiguities, the float ambiguities obtained from the rover and fractional parts of the ambiguities obtained from the reference network are differenced. Typically, the fractional parts of the ambiguities from the closest station belonging to the network are used to maximise the number of common satellites tracked by the rover and reference station. The major difference between the DDPPP and cRTK methods is that only the fractional parts of the ambiguities are obtained from the reference station in the case of DDPP while raw measurements are obtained in the case of cRTK.

Ambiguity resolution can be attempted in the rover after the double-differenced ambiguities are calculated (Bertiger et al., 2010). The FCB errors are cancelled or reduced

from the double-differenced ambiguities. Therefore, the ambiguities have an integer nature and ambiguity resolution can be attempted. After resolving both wide-lane and narrow-lane ambiguities, fixed ionosphere-free ambiguities are calculated and used to constrain the position estimation (Bertiger et al., 2010).

4.3.1.4 The Un-Differenced Fractional Cycle Bias (UDFCB) estimation method

When employing the Un-Differenced Fractional Cycle Bias (UDFCB) estimation method, un-differenced FCBs are estimated based on data from a global reference network (Li and Zhang, 2012). Similar to the IRC method discussed in Section 4.3.1.2, un-differenced float ionosphere-free ambiguities are computed using equation (3.12) and wide-lane Melbourne-Wubbena ambiguities (Melbourne, 1985, Wubbena, 1985) using equation (4.11). In the network processing, existing satellite clock corrections are used, station coordinates are fixed to the known values and other errors sources are corrected using the current correction methods.

Firstly, wide-lane FCBs are estimated (Li and Zhang, 2012). For example, wide-lane FCBs are calculated for *n* satellites using data from *m* stations. Thus, there are *m times n* equations similar to equation (4.11). There are *n times m* known float wide-lane ambiguities (b_{wl}^{i})*, n times m* unknown wide-lane integer ambiguities (N_{wl}^{i}), *m* unknown receiver wide-lane FCBs and *n* unknown satellite wide-lane FCBs. However, there is a singularity between the terms, which prevents direct solution of the equations.

To overcome the singularity, the receiver wide-lane FCB must be set to zero in one of the stations (Li and Zhang, 2012). In that station, wide-lane integer ambiguities are obtained by rounding the ambiguities to the nearest integers. Thereafter, initial wide-lane satellite FCBs are obtained using equation (4.24). The initial receiver wide-lane FCBs are obtained in the other stations as shown in equation (4.25). This is done using the initial satellite wide-lane FCBs from the first station to correct the float wide-lane ambiguities and then rounding the ambiguities to the closest integers (N_{wl}^{i}). Thereafter, the initial wide-lane FCBs can be estimated for the satellites not tracked by the first station, but tracked by the other stations.

The estimation is based on using the initial wide-lane receiver FCB estimates and defining N_{wl}^{i}as the closest integer.

After obtaining the initial receiver and satellite FCBs, wide-lane ambiguity resolution can be attempted. After that, the least-squares method is used to estimate FCBs again based on the fixed wide-lane ambiguities and float ambiguities which are not yet fixed. The least-squares method is used in an iterative loop and more wide-lane ambiguities are fixed to integers during the iterations if that is possible with sufficient reliability. The ambiguity fixing decision can be made based on the standard deviation of the ambiguity and distance from the nearest integer. After the final iteration, wide-lane FCBs can be delivered to rovers and narrow-lane FCB estimation can be initiated in the network.

Narrow-lane float ambiguity estimates (b_{nl}^{i}) are obtained using equation (4.18), based on the float ionosphere-free ambiguities (b_{3}^{i}) and fixed wide-lane ambiguities (N_{wl}^{i}) (Li and Zhang, 2012). Narrow-lane FCB estimation is done in a similar way to the wide-lane FCB estimation. The total magnitude of the errors in the float ambiguity estimates must be smaller than half of the narrow-lane wavelength (10.7 cm) for an accurate estimate of the narrow-lane FCB.

It is sufficient to provide wide-lane FCBs for rovers as daily corrections, but narrow-lane FCBs must be delivered using relatively short update interval such as ten minutes (Li and Zhang, 2012) or 5 seconds (Laurichesse et al., 2010). The reason is that narrow-lane FCBs can change quickly while, on the other hand, wide-lane FCBs are stable for long time periods (Li and Zhang, 2012). Narrow-lane FCBs can change quickly because of the short (10.7 cm) wavelength which makes them more sensitive to errors.

4.3.1.5 Comparison between the correction product generation methods

All the correction product generation methods (i.e. BSDFCB (Section 4.3.1.1), IRC (Section 4.3.1.2), DDPPP (Section 4.3.1.3) and UDFCB (Section 4.3.1.4) enable the elimination or reduction of FCBs in carrier-phase measurements. This enables attempting PPP ambiguity resolution. It can be assumed that all of the methods provide similar positioning accuracy, because FCBs are removed or reduced. For example, the BSDFCB and IRC methods were tested in Geng et al. (2010b) and the IRC method provided one millimetre smaller east and

up position errors based on analysing a large dataset. Therefore, it can be concluded that the BSDFCB and IRC methods provide approximately similar performance.

However, there are many differences between the product generation methods. The IRC and UDFCB methods provide un-differenced FCB corrections. Therefore, the same FCB corrections can be used anywhere on the Earth. The BSDFCB method provides the corrections for (rover-reference BSD) satellite pairs. Thus, the visibility of common satellites between the reference network and rovers limits the area where BSDFCB corrections can be applied. Therefore, the BSDFCB method can only provide corrections which are used in some specific regions of the size of the UK. This makes the BSDFCB method unsuitable for global use, which would require generating BSDFCB corrections for all possible satellite pairs. The DDPPP method has also the same limitations as the BSDFCB method (i.e. the need for a sufficient number of common satellites which are tracked both by the rover and reference station).

In terms of implementation complexity, the DDPPP method is the simplest because only the fractional parts of ambiguities from the nearest reference station are required. The second simplest method is the BSDFCB method, because the BSD operation eliminates the receiver clock error and FCB, making the FCB estimation simpler compared to the IRC and UDFCB methods. The most complex methods to implement are the IRC and UDFCB. This is because the receiver clock error and FCB must be taken into account when estimating the corrections.

On the whole, the IRC and UDFCB methods are the most suitable, because they can provide un-differenced corrections and the same set of corrections can be used globally. When employing the IRC or UDFCB methods, FCB corrections can be provided for each carrier-phase signal separately, instead of providing code-phase and carrier-phase satellite clock corrections or wide-lane and narrow-lane FCB corrections (Laurichesse, 2012). The method and its benefits are discussed in Section 3.4.3.

4.3.2 Rover side implementation when using GPS L1 and L2

As discussed in Section 4.3.1, the correction products can be used to enable PPP ambiguity resolution. They are delivered to rover receivers in real-time using, for example, cellular

data connection or telecommunication satellites. The bandwidth limitations and reliability of the data connections must be taken into account when designing correction formats and specifying the correction update interval.

Obtaining a sufficiently accurate float PPP solution is a prerequisite for ambiguity fixing. Therefore, as discussed in Chapter 3, the error sources must be corrected or modelled. In practice, the error sources that are taken into account depend on the PPP model applied. For example, satellite orbit and clock errors, first-order ionospheric delay, relativistic effects, site-displacement effects, tropospheric delay, satellite phase-windup and antenna offsets are typically eliminated, corrected or modelled (Laurichesse and Mercier, 2007). When narrow-lane ambiguity (with 10.7 cm wavelength) resolution is attempted, the total magnitude of the errors in the range domain must be smaller than half of the narrow-lane wavelength to enable correct ambiguity resolution (Blewitt, 1989).

The current rover side ambiguity fixing methods when employing the GPS L1 and L2 signals are: un-differenced dual-frequency ionosphere-free (Collins et al., 2008, Laurichesse and Mercier, 2007), Between-Satellite-Differenced (BSD) dual-frequency ionosphere-free (Ge et al., 2008), Double-Differenced (DD) dual-frequency ionosphere-free (Bertiger et al., 2010), Dual-frequency with ionospheric corrections (Collins et al., 2012, Juan et al., 2012, Odijk et al., 2012, Geng et al., 2010a), Single-frequency with ionospheric corrections (Odijk et al., 2012) and Single-frequency without ionospheric corrections (Laurichesse et al., 2009b). These are discussed in the next sections.

4.3.2.1 Un-differenced dual-frequency ionosphere-free

Rover side PPP processing and ambiguity resolution can be based on un-differenced approaches when the corrections are generated using the IRC (Section 4.3.1.2) or UDFCB (Section 4.3.1.4) methods. Obviously, employing un-differenced ambiguity resolution in the rover requires the use of un-differenced FCB corrections. In the literature, un-differenced ambiguity resolution is used, for example, in Laurichesse and Mercier (2007) and Collins et al. (2008).

An Extended Kalman Filter (EKF) (Larson et al., 1967, Wishner et al., 1969) is used for float PPP estimation as described in Section 4.2. The rover position, ionosphere-free (b_c^i) and

wide-lane (N_{wl}^{i}) carrier-phase float ambiguities, tropospheric wet delay, wide-lane receiver FCB and receiver code-phase and carrier-phase clocks are estimated as EKF states (Laurichesse, 2011).

Ionosphere-free measurements calculated using equation (3.12) are used as inputs to the EKF. The Melbourne-Wubbena (Melbourne, 1985, Wubbena, 1985) combination is used to estimate float wide-lane ambiguities as shown in equation (4.11) and the estimates can be input to EKF to minimise their noise. FCBs are corrected from the wide-lane float estimates using the correction products.

When employing un-differenced PPP processing, there is singularity between the wide-lane ambiguities and receiver wide-lane FCB term (Collins, 2008). Therefore, one wide-lane ambiguity must be fixed to an arbitrary value in order to allow for the singularity to be removed. For other wide-lane ambiguities, fixing can be done using DBT as discussed in Section 4.3.1.1.

Narrow-lane float ambiguities are calculated based on the float ionosphere-free and fixed wide-lane ambiguities as in equation (4.18) (Laurichesse et al., 2010). To remove the singularity between the ionosphere-free ambiguities and receiver carrier-phase clock state, wide-lane and narrow-lane ambiguities must be fixed to an arbitrary value for one satellite (Collins, 2008).

When using the UDFCB method, FCB corrections must be applied to float narrow-lane ambiguities to enable ambiguity resolution (Li and Zhang, 2012). This is not required when employing the IRC method because correcting satellite code and carrier clocks separately and estimating receiver phase and code clocks makes ambiguities integers (Collins, 2008). If FCB corrections are provided specifically for each carrier-phase signal as in Laurichesse (2012), FCB corrections can be applied directly to the carrier-phase measurements before formulating the measurement combinations.

In the literature, for example, the integer rounding (Section 4.4.1) or LAMBDA (Section 4.4.3.1) methods are used for ambiguity resolution. The former was applied, for example in Laurichesse (2010) and latter in Collins et al. (2008). The current PPP ambiguity resolution and validation methods are discussed in detail in Section 4.4.

After fixing both the narrow-lane and wide-lane ambiguities, the fixed ionosphere-free ambiguity is calculated based on the fixed narrow-lane (N_{nl}^{i}) and fixed wide-lane ambiguities (N_{wl}^{i}) as shown in equation (4.23) (Laurichesse et al., 2010). Thereafter, the position can be estimated using fixed ambiguities.

4.3.2.2 Between-Satellite-Differenced (BSD) or Double-Differenced (DD) dual-frequency ionosphere-free

When employing rover side BSD ambiguity resolution, the BSD operation is applied to measurements to remove the receiver clock error and receiver FCB (Ge et al., 2008). The BSD operation is based on selecting one satellite as a base satellite and subtracting its measurements from the other satellite's measurements.

The BSD PPP processing and ambiguity resolution is suitable to use when the product generation is performed using the IRC, BSDFCB or UDFCB methods. When the DDPPP method is used for product generation, the fractional parts of the ambiguities obtained from a network station are differenced with the ambiguities estimated by the rover (double differencing the ambiguities) (Bertiger et al., 2010). Hence, the method's name is Double-Differenced PPP. Nevertheless, the processing is similar to the BSD PPP method, after the differencing operation.

The BSD operation is applied to carrier- and code-phase measurements as in equations (4.7) and (4.8), respectively (Ge et al., 2008). If FCB corrections are provided separately for each carrier-phase signal as in Laurichesse (2012), the corrections are applied before the BSD operation.

Ionosphere-free measurements are calculated as shown in equation (3.12) (Ge et al., 2008). Wide-lane ambiguities are estimated using the Melbourne-Wubbena combination (Melbourne, 1985, Wubbena, 1985) as in equation (4.11). The FCBs from wide-lane ambiguities must be corrected using the products, unless the FCBs are already corrected from raw carrier-phase measurements or the DDPPP method is employed. Depending on the implementation, position, tropospheric wet delay and ionosphere-free and wide-lane

float ambiguity estimation can be done using EKF or the least-squares method. Similar to float PPP, discussed in Section 4.2, the current PPP error corrections and models must be applied.

Wide-lane ambiguities can be fixed to integers using DBT as discussed in Section 4.3.1.1. Narrow-lane float ambiguities are calculated using equation (4.18) based on the float ionosphere-free ambiguities ($b_c^{i,j}$) and fixed wide-lane ambiguities ($N_{wl}^{i,j}$) (Ge et al., 2008). FCBs from narrow-lane float ambiguities must be corrected unless the IRC or DDPPP methods are used or FCBs are already correction from raw carrier-phase measurements. For example, narrow-lane ambiguity resolution can be done using the LAMBDA method and validation using the ratio test (Euler and Schaffrin, 1990). Finally, fixed ionosphere-free ambiguities are calculated based on the fixed wide-lane and narrow-lane ambiguities as shown in equation (4.23) (Ge et al., 2008).

BSD processing by the rover is simpler than the un-differenced processing (Section 4.3.2.1) because the BSD operation eliminates the receiver clock error and FCB. When using the BSD approach, there is no singularity in the system. Although BSD processing requires handling base-satellite changes, a similar type of handling is also required when employing the un-differenced processing method. In that case the handling is necessary, if the carrier-phase lock is lost to the satellite which has narrow-lane and wide-lane ambiguities fixed to arbitrary values and none of the other ambiguities are fixed.

4.3.2.3 Dual-frequency with ionospheric corrections

When using a dual-frequency GNSS receiver, the first-order ionospheric error can be removed by forming the ionosphere-free measurement combination as discussed in Section 3.4.4. However, solving ambiguities in the ionosphere-free way (Sections 4.3.2.1 and 4.3.2.2) using the Melbourne-Wubbena (Melbourne, 1985, Wubbena, 1985) wide-lane and ionosphere-free combinations takes a long time (e.g. at least 30 min) (Geng et al., 2010d). When employing the ionosphere-free ambiguity resolution method, the first order ionospheric error is completely eliminated, but the magnitude of measurement noise is large.

Wide-lane ambiguity resolution is achieved in a geometry-free way using the Melbourne-Wubbena combination when employing the methods discussed in Sections 4.3.2.1 and 4.3.2.2. Noise, multipath and code and phase biases are the only remaining major error sources in the geometry-free estimation. The estimated position is not directly dependent on the wide-lane ambiguities when using the geometry-free wide-lane estimation (Geng et al., 2010d). This is the opposite to cRTK, where the estimated position is dependent on the wide-lane ambiguities (Kaplan and Hegarty, 2006). The dependency enables constraining the position estimates by fixing the wide-lane ambiguities, because having ambiguities fixed to integers enable more accurate position estimation. It typically leads to faster narrow-lane or L1 ambiguity resolution (Kaplan and Hegarty, 2006). This approach enables centimetre-level positioning within a few seconds. When employing cRTK, geometry-dependent wide-lane ambiguity resolution is typically possible, because the ionospheric delay is mitigated by differencing measurements across receivers (Kaplan and Hegarty, 2006). Nevertheless, ionospheric delay is not always correlated between two receivers, if the base-line (distance) between the receivers is long (over 50 km) or ionospheric activity is high. This may make geometry-dependent wide-lane ambiguity resolution impossible or lead to wrong ambiguity resolution.

The same wide-lane ambiguity resolution method used in cRTK can also be applied to PPP, if ionospheric delay estimates are provided to the rover from a reference network or receiver nearby (Collins et al., 2012). The geometry-dependent wide-lane combination (L_{wl}^{i}) is calculated using equation (4.26), where q_{wl}^{i} is the wide-lane noise, m_{wl}^{i} wide-lane multipath and I_{wl}^{i} the slant (receiver to satellite) wide-lane ionospheric delay (Collins et al., 2012). The geometry-dependent wide-lane is estimated by the rover and corrections are used to mitigate ionospheric delay. Thereafter, the wide-lane ambiguity resolution is carried out using the LAMBDA method (Teunissen, 1993). Ambiguity resolution can typically be achieved within five seconds (Collins et al., 2012).

$$L_{wl}^{i} = \frac{f_1 L_1^i - f_2 L_2^i}{f_1 - f_2} = e_g^i + \lambda_{wl} * \left(B_{wl,r} - B_{wl,s}^{i} - N_{wl}^{i}\right) + q_{wl}^{i} + m_{wl}^{i} + I_{wl}^{i} \quad (4.26)$$

Juan et al. (2012) also proposed a method to accelerate PPP ambiguity resolution based on using slant ionospheric delay estimates from a reference network. When employing this method, the geometry-free combination (L_4^i) shown in equation (4.27), where I_4^i is the slant

ionospheric delay, q_4^i geometry-free combination noise and m_4^i geometry-free combination multipath, is used by the rover. Wide-lane ambiguities are estimated using the Melbourne-Wubbena combination (Melbourne, 1985, Wubbena, 1985). After fixing the wide-lane ambiguities, ionosphere-free ambiguities can be estimated based on the geometry-free combination (L_4^i), the fixed wide-lane ambiguities (N_{wl}^i) and the ionospheric slant delay corrections (I_4^i) from the network as shown in equation (4.28), where $b_3^{i,j}$ is the ionosphere-free ambiguity and λ_n the narrow-lane wavelength. When employing the method, the convergence time to 10 cm accuracy can be reduced to a few minutes, while otherwise the convergence would take approximately 30 minutes (Juan et al., 2012).

$$L_4^i = L_1^i - L_2^i = I_4^i + \lambda_1 N_1^i + \lambda_2 N_2^i + q_4^i + m_4^i \tag{4.27}$$

$$L_4^i - I_4^i = \frac{\lambda_1 \lambda_2}{\lambda_{wl} \lambda_n} (\lambda_{wl} N_{wl}^i - \lambda_1 b_3^{i,j}) \tag{4.28}$$

Ionospheric-delay corrections from a reference network are also used in Odijk et al. (2012), where ambiguities can typically be fixed immediately when employing a dual-frequency GNSS receiver. This is similar to the performance of cRTK or the method presented in Collins et al. (2012).

Based on the results presented in the literature, using external ionospheric corrections for dual-frequency PPP can make typical PPP convergence time similar to cRTK. However, calculating sufficiently accurate ionospheric delay corrections requires a reference network density similar to cRTK (Collins et al., 2012). This is against the main principle of PPP that only a global reference network with approximately 50 stations is required (Collins et al., 2012). Another downside is that using ionospheric corrections causes an additional integrity risk when ionospheric conditions change quickly. The methods using external ionospheric information are out of scope in this thesis, because the aim is to develop a method what can be used in remote areas, where local reference networks do not exist.

A method to accelerate PPP re-convergence is presented in Geng et al. (2010a). When employing the method, slant ionospheric delay is estimated locally and the estimates are saved each epoch by the rover when ambiguities are fixed (Geng et al., 2010a). When ambiguity fixing is lost, the saved slant ionospheric delay estimates help re-convergence. Geometry-dependent wide-lane ambiguities which are corrected with the saved slant

ionospheric delay are estimated and their fixing is attempted (Geng et al., 2010a). The geometry-dependent wide-lane ambiguities constrain the position similar to the approach for cRTK, which enable fast narrow-lane ambiguity resolution and convergence. The limitation of the method is that ionospheric conditions may change quickly during the time period when the ambiguity fix is lost. This can make rapid re-convergence impossible and cause an additional integrity risk.

4.3.2.4 Single-frequency with ionospheric corrections

Slant ionospheric delay corrections obtained from a reference network can also be used for fixed-ambiguity single-frequency PPP. It is shown in Odijk et al. (2012) that it takes an average of four minutes to obtain an initial ambiguity resolution when using single-frequency measurements from a high-grade GNSS receiver and employing slant ionospheric delay corrections provided by the network.

The primary limitation of single-frequency PPP ambiguity resolution is that local reference networks with high station density are required for the slant ionospheric delay correction generation (Odijk et al., 2012).

4.3.2.5 Single-frequency without ionospheric corrections

Single-frequency PPP carrier-phase ambiguity resolution can be achieved even without external ionospheric corrections (Laurichesse et al., 2009b). The principle of the method is to use the single-frequency code-phase and carrier-phase measurement combination (G_{P1}) as shown in equation (4.29) (Gao and Shen, 2001). The first-order ionospheric delay is cancelled in this combination because the ionospheric delay in the code and carrier-phase measurements has the same order of magnitude but opposite sign.

$$G_{P1} = \frac{P_1 + L_1}{2} \tag{4.29}$$

The negative aspect of this method is that the magnitude of the noise in the measurement combination is large due to the use of code-phase measurements. This makes ambiguity resolution lengthy and even impossible in some cases. In particular, ambiguity resolution is difficult when the magnitude of the code-phase noise and multipath is large. Therefore, this

method is not very practical, particularly when using measurements from inexpensive single-frequency receivers which can only provide L1 C/A code-phase and carrier-phase measurements (Laurichesse et al., 2009b).

4.3.2.6 Methods comparison

The ionosphere-free ambiguity resolution methods discussed in Sections 4.3.2.1 and 4.3.2.2 can be used globally because no location specific correction products, such as ionospheric delay corrections, are required. In terms of the performance, there is no difference between the Un-differenced (Section 4.3.2.1) and BSD (Section 4.3.2.2) methods. However, the BSD method is simpler to implement, because the receiver clock and FCB errors are cancelled using the BSD operation and there is no singularity in the system. The negative aspect of the ionosphere-free ambiguity resolution methods is that the time required to obtain an initial ambiguity resolution is typically long (approximately 30 minutes).

Using a dual-frequency receiver and external slant ionospheric delay corrections enables fast ambiguity resolution. Nevertheless, generating sufficiently accurate ionospheric corrections requires a reference network station density similar to that used for cRTK. Therefore, the method is not suitable in remote areas where there are no dense reference networks. Fixing ambiguities is possible even using single-frequency measurements, but it is not practical, because it relies upon high accuracy local ionospheric corrections or the use of the noisy code plus carrier-phase measurement combination.

The ionosphere-free BSD ambiguity resolution method discussed in Section 4.3.2.2 is used in this thesis, because it enables PPP ambiguity resolution without external ionospheric corrections and is simper to implement than the un-differenced ionosphere-free method discussed in Section 4.3.2.1.

4.3.3 Using GLONASS

It is shown that the combination of GPS and GLONASS for float PPP can reduce convergence time compared to GPS alone (Cai and Gao, 2013). Particularly, using GLONASS with GPS is useful when the number of visible GPS satellites is small (less than six) (Li et al., 2009).

The major difference between GPS and GLONASS is that GLONASS uses the Frequency Division Multiple Access (FDMA) modulation while GPS uses the Code Division Multiple Access (CDMA) modulation (Dach et al., 2007). This refers to separating GPS signals broadcasted from different satellites in the same frequency band from each other using different PRN codes. On the other hand, GLONASS satellites use the same PRN code but signals from different satellites are broadcasted in different frequencies.

The FDMA modulation of GLONASS signals makes carrier-phase ambiguity resolution more difficult because of the satellite/frequency/receiver type specific inter-frequency biases in measurements (Reussner and Wanninger, 2011). Satellite FCBs and code-phase biases can be handled in a similar way as is done in GPS alone PPP. In addition, receiver inter-frequency carrier-phase biases can be calibrated. However, receiver code-phase biases can vary even between receivers of a given type. Thus, calibrating receiver code biases is difficult or almost impossible (Reussner and Wanninger, 2011).

The Melbourne-Wubbena combination (Melbourne, 1985, Wubbena, 1985) is used to estimate wide-lane ambiguities in the case of fixed-ambiguity PPP. Using both code-phase and carrier-phase measurements is necessary when formulating the combination. Therefore, correcting code biases with sufficient accuracy is vital. Currently, it is not possible to calibrate the GLONASS code biases with an accuracy sufficient for the Melbourne-Wubbena combination to enable ambiguity resolution (Reussner and Wanninger, 2011).

Trimble has claimed that solving both GPS and GLONASS ambiguities using PPP is possible using the Trimble CenterPoint RTX system (Leandro et al., 2011a). GLONASS biases are estimated and calibrated using their global GNSS reference network which consist of Trimble GNSS receivers alone (Doucet et al., 2012). The method used for GLONASS ambiguity resolution in the CenterPoint RTK system is not publicly available

GLONASS ambiguity resolution is not employed in this thesis, because there are no suitable correction products available openly and the code bias behaviour of the different receiver types is not known with sufficient accuracy.

4.3.4 Using new GNSS signals and systems

Most current PPP implementations use the GPS L1 (C/A, P) and L2 (P) signals, even though some also support the GPSL2C signal and GLONASS. As presented in Section 3.1, the modernisation of GPS and GLONASS is on-going while the EU and China are building their own GNSS (i.e. Galileo and BeiDou, respectively).

The GPS modernisation and new satellite systems provide three main benefits: new signals with better noise and multipath properties as discussed in Sections 3.4.11 and 3.4.14, an increased number of possible signal combinations and better satellite geometry due to the larger number of visible satellites. The modernised GPS system will broadcast the new L1C, L2C and L5 signals, BeiDou will broadcast the B1, B2 and B3 signals and Galileo will broadcast the E1, E5a, E5b and E5 civilian signals.

In December 2012, there were only three GPS satellites broadcasting the L5 signal, ten satellites broadcasting the L2C signal and no satellites broadcasting the L1C signal (IAC, 2012). At the same time, there were three Galileo In-Orbit Validation (IOV) satellites broadcasting signals (GPS_World, 2012b). For the BeiDou systems, there were at least 14 satellites available (BeiDou, 2011). The GLONASS CDMA L3 signal transmission is available for testing on only one satellite: the GLONASS-K #701 satellite (IAC, 2012).

Currently, the number of GPS satellites broadcasting the new signals or Galileo satellites is limited, which makes it difficult or even impossible to verify the benefits of GNSS modernisation using real data. The full constellation of modernised satellites is required in order to understand the full benefit of new signals. However, some studies have already been done based on a theory, simulations or using data from these few satellites which already broadcast the modernised signals. The benefits of the new signals and systems are discussed in Sections 4.3.4.1 and 4.3.4.2.

In this thesis, only the GPS and GLONASS L1 and L2 signals are used, due to the lack of availability of other signals and their corresponding PPP correction products.

4.3.4.1 Other possible signal combinations

For the GPS L1 and L2 signals (Sections 4.3.2.1 and 4.3.2.2), the Melbourne-Wubbena (Melbourne, 1985, Wubbena, 1985) wide-lane and ionosphere-free combinations are typically used. Ambiguity resolution is carried out in two steps: wide-lane and narrow-lane resolution, where narrow-lane ambiguities are obtained based on the float ionosphere-free and fixed wide-lane ambiguities. The wavelength of the wide-lane and narrow-lane ambiguities is 86.2 cm and 10.7 cm, respectively. The short wavelength of the narrow-lane combination makes ambiguity resolution difficult, because the total magnitude of the errors in float narrow-lane ambiguity estimates must typically be less than the half of the wavelength.

The increased number of signals, from GPS modernisation and the new Galileo system, enables a large number of signals combinations with varying properties (Li et al., 2010). For example, the signal combinations can have different wavelengths, ionospheric behaviour, noise properties and geometry-based error dependency.

There are multiple ways to achieve PPP or long-baseline cRTK ambiguity resolution when using triple-frequency GPS signals. For example, the method presented in Li et al. (2010) achieves ambiguity resolution using an approach which is both geometry and ionosphere-free. The first step of the ambiguity resolution process is using the Melbourne-Wubbena combination (Melbourne, 1985, Wubbena, 1985) to estimate the wide-lane ambiguities ($b^i_{(1,-1,0)} = b^i_{wl}$) using equation (4.11), which has 86 cm wavelength, and extra-wide-lane ambiguities ($b^i_{(0,1,-1)}$) using equation (4.30), which has 586 cm wavelength. The carrier-phase combinations ($\phi_{(c_1,c_2,k)}$) are calculated using equation (4.31) and ambiguity combinations using equation (4.32), where $N_{(c_1,c_2,c_5)}$ refers to fixed ambiguities and $b_{(c_1,c_2,c_5)}$ to float ambiguities. In the equations, c_1 refers to the L1 carrier-phase coefficient, c_2 refers to the L2 carrier-phase coefficient and c_5 refers to the L5 carrier-phase coefficient.

$$b^i_{(0,1,-1)} = \frac{\frac{f_2 L^i_2 - f_5 L^i_5}{f_2 - f_5} - \frac{f_2 P^i_2 + f_5 P^i_5}{f_2 + f_5}}{\lambda_{(0,1,-1)}} \tag{4.30}$$

$$\phi_{(c_1,c_2,k)} = \frac{c_1 * f_1 * \phi_1 + c_2 * f_2 * \phi_2 + c_5 * f_5 * \phi_5}{c_1 * f_1 + c_2 * f_2 + c_5 * f_5} \quad (4.31)$$

$$N_{(c_1,c_2,c_5)} = c_1 * f_1 * N_1 + c_2 * f_2 * N_2 + c_5 * f_5 * N_5 \quad (4.32)$$

The wide-lane ($b^i_{(1,-1,0)}$) and extra-wide-lane ($b^i_{(0,1,-1)}$) ambiguities can be fixed by rounding the ambiguities to the nearest integers. Thereafter, the extra-wide lane term $N^i_{(1,-6,5)}$ is calculated based on the fixed wide-lane $N^i_{(1,-1,0)}$ and extra-wide-lane ($N^i_{(0,1,-1)}$) ambiguities using equation (4.33). L1 float carrier phase ambiguities are estimated using equation (4.34), in which the factors a_1 and a_2 are computed using equation (4.35), where the combination is both ionosphere- and geometry-free. The first-order ionospheric error contribution ($\beta_{(c_1,c_2,c_5)}$) is calculated using equation (4.36). L1 float carrier-phase ambiguities can be fixed using the DBT method (Section 4.3.1.1), because they are obtained in a way which is ionosphere and geometry-free and the only remaining main error sources are noise, multipath and higher order ionospheric terms. Thereafter, an ambiguity fixed position solution is obtained after fixing the L1, wide-lane and extra-wide-lane ambiguities. The important benefit of the method is that ambiguity resolution is geometry and ionosphere-free in all the steps (Li et al., 2010).

$$N^i_{(1,-6,5)} = N^i_{(1,-1,0)} - 5\,N^i_{(0,1,-1)} \quad (4.33)$$

$$b^i_{(1,0,0)} = \frac{a_1\phi^i_{(0,1,-1)} + a_2\phi^i_{(1,-6,5)} - \phi^i_{(1,0,0)}}{\lambda_{(1,0,0)}} \quad (4.34)$$

$$\begin{cases} a_1\beta_{(0,1\,-1)} + a_2\beta_{(1,-6,5)} = \beta_{(1,0,0)} \\ a_1 + a_2 = 1 \end{cases} \quad (4.35)$$

$$\beta_{(c_1,c_2,c_5)} = \frac{f_1^2 * (\frac{c_1}{f_1} + \frac{c_2}{f_2} + \frac{c_5}{f_5})}{c_1 * f_1 + c_2 * f_2 + c_5 * f_5} \quad (4.36)$$

There are multiple possible measurement combinations and methods to fix ambiguities when using triple-frequency GPS or Galileo signals (Li et al., 2010). The optimal signal combination depends on the specific scenario, for example, ionosphere reduced signal combinations may be optimal when ionospheric corrections are available.

Some preliminary results on ambiguity resolution using triple-frequency GPS signals are presented in Laurichesse (2012). The method presented is based on the stepwise resolution of extra-wide-lane, wide-lane and L1 ambiguities in a geometry and ionosphere-free approach. Results based on real GNSS data show that L1 ambiguity fixed position solution can be obtained within 5 minutes. However, it is currently difficult to assess the performance using real data because there are only three GPS satellites broadcasting the L5 signal (in 2012). In addition, the exact method of ambiguity fixing is not presented in Laurichesse (2012).

4.3.4.2 Improved noise and multipath properties

As discussed in Sections 3.4.11 and 3.4.14, due to improved signal design, the modernised GNSS signals are significantly less vulnerable to multipath and have significantly lower measurement noise than the GPS L1 (C/A or P) or L2 (P) signals.

For example, the structure of the GPS L2C signal, enables better tracking in more difficult environments such as urban canyons (GPS, 2013b). Based on the tests shown in Elsobeiey and El-Rabbany (2010), using the GPS L2C signal for PPP could be beneficial compared to using the GPS P2 signal in terms of obtaining shorter convergence times.

The significantly lower noise and multipath errors of the Galileo E5 signal, discussed in Sections 3.4.11 and 3.4.14, enable the use of single-frequency processing models which are not practical when using the GPS L1 C/A signal alone. For example, this kind of processing model is single-frequency PPP ambiguity resolution using the combination of code and carrier-phase measurements as discussed in Section 4.3.2.5.

Forming the single-frequency code plus carrier combination, which is already discussed in Section 4.3.2.5, eliminates the first-order ionospheric error. Because code-phase measurements are used when forming the combination, the magnitude of noise in the combination is large and the combination is vulnerable to multipath. Using the combination becomes more practical when employing the Galileo E5 signal, because of its improved noise and multipath properties (Schüler et al., 2011). The combination for the Galileo E5 signal (G_{E5}) is calculated using equation (4.37), where C_{E5} is the Galileo E5 code-phase and L_{E5} the Galileo E5 carrier-phase measurement.

$$G_{E5} = \frac{C_{E5} + L_{E5}}{2} \tag{4.37}$$

For example, according to the specification of the Septentrio PolaRx4/PolaRx4TR receiver (a geodetic quality GNSS receiver) the standard deviation of the non-smoothed GPS L1 C/A measurements is 16 cm and standard deviation of the non-smoothed Galileo E5 measurements is 1.5 cm (Septentrio, 2011). The potential benefit of the Galileo E5 signal is tested using simulated data, which is cRTK processed using a 300 km base-line (Schüler et al., 2011). The results should be closely similar to PPP because the ionospheric error is not cancelled or reduced significantly when the length of the baseline is 300 km. The code plus carrier combination is calculated as shown in equation (4.37) using the GPS L1 C/A and Galileo E5 signals. When processing a 3600 s data-set, the magnitude of the 3D-position error at the end of the processing stage was 12.9 cm and 3.8 cm for the GPS L1 C/A and Galileo E5 signals, respectively (Schüler et al., 2011). In comparison, the 3D-position error was 1.0 cm when processing the GPS L1 and L2 measurements using the ionosphere-free combination (Schüler et al., 2011).

Based on these results, it can be concluded that the Galileo E5 signal can bring a clear improvement over the GPS L1 C/A signal for single-frequency processing (Schüler et al., 2011). This can be beneficial particularly for consumer applications since the cost of single-frequency Galileo E5 receivers is typically less compared to dual or multiple-frequency GNSS receivers (Schüler et al., 2011).

4.4 Carrier-phase ambiguity resolution and validation

Carrier-phase ambiguity resolution and validation is a major challenge in fixed-ambiguity PPP. Suitable current methods for PPP processing using the GPS L1 and L2 signals are discussed next. In general, the approach to ambiguity resolution and the validation methods used in cRTK can also be applied to PPP. However, PPP ambiguity resolution is more challenging, because the geometry-dependent wide-lane combination cannot be used to constrain the position (without employing external ionospheric corrections as discussed in Section 4.3.2.3) as is done in cRTK. For PPP, ambiguity resolution must be done directly for the geometry-dependent narrow-lane combination, which has only a wavelength of 10.7 cm.

The short wavelength makes PPP ambiguity resolution vulnerable to the error sources discussed in Chapter 3.

The first step of ambiguity resolution is to estimate the float position and ambiguities. The rover-side implementations suitable for this are discussed in Section 4.3.2. The outputs from the estimation, which are required for ambiguity resolution, are the float ambiguity vector $(\hat{a})$ and variance matrix of the float ambiguities $(Q_{\hat{a}})$ (Jonge and Tiberius, 1996).

Based on the float ambiguity solution, for example, the Integer Least-Squares (ILS) method (Teunissen, 1993) is used to obtain an integer ambiguity vector $(\breve{a})$. Thereafter, the correctness of the integer ambiguity vector is validated using, for example, the ratio test (Verhagen, 2005). As a final step, the position solution is calculated using the fixed ambiguity vector, if the ambiguity fixing has been accepted by the validation method. Otherwise, ambiguities are kept as float.

The current ambiguity resolution and validation methods are analysed next. The integer rounding method is discussed in Section 4.4.1, integer bootstrapping in Section 4.4.2 and ILS in Section 4.4.3. The Least-squares AMBiguity Decorrelation Adjustment (LAMBDA) method (Teunissen, 1993) to make the ILS search computationally efficient is discussed in Section 4.4.3.1. Ambiguity validation when employing the ILS method is discussed in Section 4.4.4.

4.4.1 Integer rounding

Integer rounding is the simplest method for integer ambiguity resolution (Teunissen, 1998, Verhagen, 2005). When employing the method, each ambiguity in the float ambiguity vector $(\hat{a})$ is rounded to the nearest integer as shown in equation (4.38), where $[\cdot]$ is the rounding to the nearest integer operator and n_a is the number of ambiguities. The integer rounding method does not take correlations between the ambiguities into account, which makes the method non-optimal particularly for geometry-dependent ambiguity estimation.

$$\breve{a} = \begin{pmatrix} [\hat{a}_1] \\ . \\ . \\ . \\ [\hat{a}_{n_a}] \end{pmatrix} \tag{4.38}$$

Depending on the implementation, ambiguities are rounded to the nearest integer without or with validation. For example, the DBT method (Section 4.3.1.1) can be employed for ambiguity validation.

4.4.2 Integer bootstrapping

The bootstrapping method is better than the integer rounding method, because it takes into account some correlation between the ambiguities (Verhagen, 2005). The bootstrapping ambiguity resolution is computed as shown in equation (4.39), where σ is the variance/co-variance of the ambiguities, $\hat{a}_{i|I}$ a factor based on the previously sequentially rounded ambiguities and I an identity matrix defined as $I = \{1, \ldots, (i-1)\}$. In practice, the bootstrapping ambiguity estimation is started by rounding the ambiguity with the smallest variance to the closest integer. Thereafter, the float ambiguity vector and their variance/co-variance matrix are updated based on the fixed ambiguity and the next ambiguity is rounded to the nearest integers. This process is repeated until all float ambiguities in the vector are resolved (Teunissen, 1998).

$$\begin{aligned} \breve{a}_1 &= [\hat{a}_1] \\ \breve{a}_2 &= \left[\hat{a}_2 - \sigma_{\hat{a}_2\hat{a}_1}\sigma_{\hat{a}_1}^{-2}\,(\hat{a}_1 - \breve{a}_1)\right] \\ &\vdots \\ \breve{a}_{n_a} &= \left[\hat{a}_{n_a} - \sum_{i=1}^{n_a-1} \sigma_{\hat{a}_{n_a}\hat{a}_{i|I}}\sigma_{\hat{a}_{i|I}}^{-2}\,(\hat{a}_{i|I} - \breve{a}_i)\right] \end{aligned} \tag{4.39}$$

Ambiguity validation can, for example, be based on the variance of the ambiguity and distance from the nearest integer (Dong and Bock, 1989, Blewitt, 1989).

4.4.3 Integer Least-Squares (ILS)

The standard deviation of float ambiguities can be large (many cycles) and the ambiguities are highly correlated particularly when only short sets of data (less than few minutes) are used to estimate the ambiguities in a geometry-dependent way. Therefore, the correct integer ambiguities cannot be obtained by simply rounding ambiguities to the closest integers. To take the correlation and geometry-dependency of the ambiguities properly into account, the ILS method must be employed. The principle of the method is to minimise the

least-squares distances between the float ($\hat{a}$) and fixed (a) ambiguity vectors as shown in equation (4.40), where ($Q_{\hat{a}}$) is the variance/co-variance matrix of the float ambiguities and $\in Z^n$ refers to the ambiguity vector (a) elements being integers (Teunissen, 1993).

$$min_a \|\hat{a} - a\|^2_{Q_{\hat{a}}^{-1}}, a \in Z^n \tag{4.40}$$

The least-squares ambiguity search requires large computational resources, if the search is done directly in the float ambiguity space (Teunissen, 1993). To overcome the computational efficiency issue of the ILS search, the LAMBDA method was developed (Teunissen, 1993).

4.4.3.1 The Least-squares AMBiguity Decorrelation Adjustment (LAMBDA) method

The theoretical description of the LAMBDA method was first presented in Teunissen (1993) while its practical implementation was described in Jonge and Tiberius (1996). The first step of the LAMBDA method is to make the Z-transformation for the float ambiguity vector as shown in equation (4.41) and for the variance/co-variance matrix of the float ambiguities as shown in equation (4.42). Thereafter, the ILS search is carried out in the Z-domain as described in equation (4.43), where (x_l^2) must be a positive constant. In the equations, Z refers to the Z-transformation matrix, $\hat{z}$ Z-transformed float ambiguity vector, z_l Z-transformed integer ambiguity vector and $Q_{\hat{z}}$ Z-transformed ambiguity variance matrix. The ILS search can be carried out significantly more efficiently in the Z-level, because the float ambiguities are de-correlated and the search space is significantly smaller. After completing the search operation, the integer ambiguity vector which has the smallest least-squares error is transformed back.

$$\hat{z} = Z\hat{a} \tag{4.41}$$

$$Q_{\hat{z}} = ZQ_{\hat{a}}Z \tag{4.42}$$

$$(\hat{z} - z_l)Q_{\hat{z}}^{-1}(\hat{z} - z_l) \leq x_l^2 \tag{4.43}$$

Ambiguity validation is done after completing the ILS search as discussed next. If the ambiguity candidate vector is accepted, the position solution can be recalculated using the fixed ambiguities.

4.4.4 Integer Least-Squares ambiguity validation

A number of methods to validate ambiguities, such as the ratio test (Euler and Schaffrin, 1990) and difference test (Tiberius and Jonge, 1995), have been presented in the literature. The ratio test is currently the most commonly used ambiguity validation method. The ratio test statistic is calculated as shown in equation (4.44), where R_2 are the residuals of the second best integer ambiguity candidate vector, R_1 the residuals of the best integer ambiguity candidate vector and k_r the ratio test acceptation threshold. The residuals R_{ca} between the fixed ambiguity candidate vectors and float ambiguity vector are obtained using equation (4.45).

$$\frac{\mathrm{R}_2}{\mathrm{R}_1} > k_r \tag{4.44}$$

$$\mathrm{R}_{ca} = (\hat{a} - \check{a}_{ca})^T Q_{\hat{a}}^{-1} (\hat{a} - \check{a}_{ca}) \tag{4.45}$$

Empirical constant ratio test thresholds such as 2.0 or 3.0 are used in many PPP or RTK software implementations. The problem with using constant thresholds is that there is no credible theoretical or practical justification for it (Teunissen and Verhagen, 2009). In addition, the same constant threshold is not always suitable. For example, different threshold values should be used depending on the number of ambiguities. The current ambiguity resolution and validation methods presented in the literature are analysed theoretically in Verhagen (2005). It is first shown that the ILS is the optimal method for ambiguity resolution, because it maximises the probability of correct integer estimation (Teunissen, 1999). Thereafter, ambiguity validation methods are analysed and the integer aperture theory is presented. The optimal integer aperture estimator is defined based on the aperture theory (Verhagen, 2005). This estimator maximises the success rate of ambiguity validation for a given fixed failure rate, as described next.

Employing the optimal integer aperture estimator requires calculating probability densities of ambiguity residuals and simulating aperture parameters for the given fail rate (Verhagen, 2005). Thus, using the method requires high computational resources, which makes it impractical for real-time GNSS ambiguity estimation (Verhagen, 2005).

It is shown, based on the integer aperture theory, that the ratio test (Euler and Schaffrin, 1990) and difference test (Tiberius and Jonge, 1995) are close in performance to the integer aperture estimator, if the test thresholds are defined based on the fixed failure rate (Verhagen, 2005). Therefore, it is attractive to use these tests for real-life GNSS applications as they do not require complex computational operations.

Current methods to calculate the ratio test threshold based on the required failure rate are discussed next.

4.4.4.1 Doubly Non-Central F-distribution (DNCF) based method

The Doubly Non-Central F-distribution (DNCF) based method (Feng et al., 2010, Feng et al., 2012) provides the ratio test acceptance threshold based on the required fixed failure rate and number of float ambiguities in the ambiguity candidate vector. The ratio test statistic can be written as shown in equation (4.46). It is assumed that both R_2 and R_1 obey the Chi-square distribution (Feng et al., 2010). Therefore, if R_2 and R_1 are independent, the ratio $\frac{\mathrm{R}_2}{\mathrm{R}_1}$ obeys the double non-central F-distribution as shown in equation (4.47), where δ_1 and δ_2 are the non-centrality parameters of the Chi-square distribution and n_a is the number of ambiguities. Nevertheless, R_2 and R_1may not always be completely independent in reality which may compromise the performance of the test.

$$\frac{\mathrm{R}_2}{\mathrm{R}_1} = \frac{\mathrm{R}_2/(n_a\sigma^2)}{\mathrm{R}_1/(n_a\sigma^2)} \tag{4.46}$$

$$\frac{\mathrm{R}_2}{\mathrm{R}_1} \sim F(n_a, n_a, \delta_2, \delta_1) \tag{4.47}$$

The failure rate P_c of the ambiguity resolution is calculated using equation (4.48), where n_a is the number of ambiguities and δ_1 and δ_2 are the F-distribution parameters which are calculated based on the defined false alarm and missed detection rates (Feng et al., 2010, Feng et al., 2012). Calculating the integral in equation (4.48) is complicated and solving it requires numerical integration.

$$P_c = \int_0^{\frac{\mathrm{R}_2}{\mathrm{R}_1}} F(x|n_a, n_a; \delta_2, \delta_1)dx \tag{4.48}$$

In practice, using the DNCF method does not require calculating complicated mathematic operations. Instead, a constant look-up table can be used, which is calculated offline (Feng et al., 2010, Feng et al., 2012).

4.4.4.2 Fixed Failure rate Simulation (FFS) based method

When employing the Fixed Failure rate Simulation (FFS) based method (Verhagen and Teunissen, 2013, Teunissen and Verhagen, 2009) to calculate the ratio test threshold, it is assumed that float carrier-phase ambiguities obey the normal distribution. To determine the thresholds for each failure rate, simulations are performed for different combinations of satellite geometry, number of epochs, number of frequencies, baseline length, measurement noise and quality of the atmospheric corrections. Thereafter, the results with the same failure rate and number of ambiguities are combined and analysed. Based on the combined results, a relation between the ILS failure rate and ratio test threshold value is defined. The upper bound of the ILS failure rate is calculated based on the failure rate of the integer bootstrapping ambiguity resolution (Verhagen and Teunissen, 2013).

The simulations can be done offline and a look-up table is created based on the results. In the table, there are ratio test acceptance thresholds for each combination of the fixed failure rate, ILS failure rate and degrees of freedom (Verhagen and Teunissen, 2013).

4.4.4.3 Methods comparison

Both the DNCF and FFS methods make assumptions when calculating the ratio test threshold. The DNCF method assumes that the ratio test statistic obeys the double non-central F-distribution. The FFS method assumes that float ambiguities are normally distributed. Furthermore assumptions are made on the positioning model used. In the literature, no comparisons between the two methods have been carried out on the basis of real-data. However, it is likely that the difference in performance between the methods depends on the data-set and GNSS processing model used. The performance of the existing fixed ambiguity PPP methods is tested in Section 5.2.4.

4.5 Integrity

Reliability of positioning is a major challenge when employing PPP or any other positioning method. For example, there can be errors in the code and carrier-phase signals broadcast by a satellite. Thus, it is vital to detect such errors in order to provide a position solution with high reliability (integrity). Integrity refers to the ability that a user can be alerted within a given period of time (the time-to-alert), if a position error exceeds a given threshold, the alert limit. In addition, it is necessary to provide position solution continuity. For example, if there is an error which causes an integrity alert, the error must be detected and it must be excluded within the allowed time-to-alert from the position calculation to maintain continuity.

Early approaches to monitoring the integrity autonomously within the receiver include range and position comparison methods (Lee, 1986). When employing the range comparison method, there must be measurements to at least five satellites in good geometry and position estimates are calculated based on all possible four satellite subsets. Following this, measured ranges to the satellites are compared to the predicted ranges calculated based on the position estimates, which are obtained based on the measured ranges to the four other satellites. In the position comparison method, the position is calculated first using all five satellites and then using all possible four-satellite combinations. The position calculated using five satellites is then compared to the position estimates calculated using the four-satellite combinations.

Other more advanced current within receiver integrity monitoring methods are discussed next. The Receiver Autonomous Integrity Monitoring (RAIM) method (Brown and Chin, 1998), which can be used to monitor integrity of least-squares solutions when using code-phase measurements only, is discussed in Section 4.5.1. RAIM is extended for the case of carrier-phase measurements in Section 4.5.2 with the presentation of the Imperial College Carrier Receiver Autonomous Integrity Monitoring (ICRAIM) (Feng et al., 2009) and Cumulative Kalman Filter Receiver Autonomous Integrity Monitoring (CKFRAIM) (Joerger and Pervan, 2012) methods.

4.5.1 Receiver Autonomous Integrity Monitoring (RAIM)

Conventional RAIM techniques analyse code-phase only positioning solutions (Brown and Chin, 1998). The principle of the RAIM technique is to use an over-determined position solution to detect and exclude errors. In the standalone GPS case, at least four measurements are required to obtain a position solution. When employing the RAIM techniques, at least five measurements are required when attempting to detect errors and at least six measurements are required to attempt error exclusion.

When employing RAIM, the system can be described by equation (4.49), where y is the measurement vector, H the design matrix, Δx the state vector and ϵ the error vector (Brown and Chin, 1998). However, the error vector is not known when using real GNSS data. A least-squares solution ($\hat{x}_{LS}$) is calculated using equation (4.50) and the estimation error (e_{LS}) using equation (4.51). However, calculating the position error is not possible in the case of real-life systems, unless the correct position is known. A residual vector (w) of the least-squares estimate can be calculated using equations (4.52) or (4.53).

$$y = H\Delta \boldsymbol{x} + \epsilon \tag{4.49}$$

$$\hat{x}_{LS} = (HH)^{-1}H^T y \tag{4.50}$$

$$e_{LS} = \hat{x}_{LS} - \Delta x = (H^T H)^{-1}H^T \epsilon \tag{4.51}$$

$$w = y - H\hat{x}_{LS} \tag{4.52}$$

$$w = (I_n - H(H^T H)^{-1}H^T)y \tag{4.53}$$

RAIM uses the magnitude of the parity (p) or residual vector (w) as the test statistic (T_{total}) as shown in equation (4.54), because it is not possible to monitor the position error directly when processing real GNSS data (Brown and Chin, 1998). The parity vector can be obtained as shown in equations (4.55), (4.56) and (4.57) based on the measurement vector y (y), measurement residual vector (w) and range level error vector (ϵ). The parity transformation matrix P_{parity} is calculated by carrying out the QR factorisation, which refers to decomposing a matrix to an orthogonal matrix Q and upper triangular matrix R, for the H

matrix and taking the (*n-4*) lower rows from the transpose of the *Q* matrix (Brown and Chin, 1998, Kaplan and Hegarty, 2006). The magnitude of the parity vector p or equivalent magnitude of the residuals vector *w* is used as the test statistic as shown in equation (4.58) (Brown and Chin, 1998).

$$T_{total} = |p| = |w| \tag{4.54}$$

$$p = P_{parity} y \tag{4.55}$$

$$p = P_{parity} w \tag{4.56}$$

$$p = P_{parity} \epsilon \tag{4.57}$$

$$p^T p = w^T w \tag{4.58}$$

However, the magnitude of the test statistic is not directly related to the magnitude of the position error. A linear relation between the magnitude of the test statistic and horizontal position error for the satellite (i) can be described by the $SLOPE$ value calculated using equations (4.59), (4.60) and (4.61) (Brown and Chin, 1998). The magnitude of the horizontal position error ($E_{hor}(i)$) which is caused by a failure in satellite i can be calculated using equation (4.62).

$$SLOPE(i) = \frac{\sqrt{A_{1i}^2 + A_{2i}^2}}{\sqrt{S_{ii}}}, i = 1,2, \ldots . n \tag{4.59}$$

$$A = H(H^T H)^{-1} H^T \tag{4.60}$$

$$S = I_n - H(H^T H)^{-1} H^T = {P_{parity}}^T P_{parity} \tag{4.61}$$

$$E_{hor}(i) = SLOPE(i) * w(i) \tag{4.62}$$

The test statistic (T_{total}) is compared to the detection threshold (T_D) (Brown and Chin, 1998). If the test statistic is larger than the threshold, an integrity alert is raised. The detection threshold is defined based on the accepted false alarm rate (P_{FA}), degrees of freedom and

standard deviation of measurement noise (Brown and Chin, 1998). The magnitude of the parity vector is the square sum of normally distributed variables. Therefore, it obeys the chi-square distribution with (number of satellites – 4) degrees of freedom. In the case of five satellites in a view, the distribution can be treated as normally distributed, because the chi-square distribution with one degree of freedom is equal to the standard deviation. To calculate the normalised detection threshold, the density function of the parity vector (i.e. the centred chi-square density function ($fCent$) described in (4.63)) is integrated using equation (4.64) by assuming that the total magnitude of the integrated area is equal to P_{FA}. k refers to the degrees of freedom. The detection threshold (T_D, in metres) is calculated using equation (4.65), where σ is the standard deviation of the noise.

$$\begin{cases} fCent(x) = \dfrac{x^{\left(\left(\frac{k}{2}\right)-1\right)}e^{-\frac{x}{2}}}{2^{\frac{k}{2}}\Gamma(\frac{k}{2})}, x > 0 \\ 0, x \leq 0 \end{cases} \tag{4.63}$$

$$\int_a^{\infty} fCent(x)dx = P_{FA} \tag{4.64}$$

$$T_D = \sigma\sqrt{a} \tag{4.65}$$

The horizontal protection level (HPL) for RAIM represents the magnitude of the horizontal error which is detected for the given probability of missed detection (P_{MD}) (Brown and Chin, 1998). The non-centrality parameter (λ_{nc}) is defined by shifting the central chi-square distribution until the central chi-square distribution area, between zero and the detection threshold (T_D), is equal to P_{MD}. After defining the λ_{nc}, HPL is calculated using equation (4.66), where $SLOPE_{max}$ is the largest SLOPE value from the group of the used satellites and σ is the noise standard deviation.

$$HPL = SLOPE_{max}\sigma\sqrt{\lambda_{nc}} \tag{4.66}$$

When the RAIM test statistic is larger than the detection threshold, an integrity alert is raised. In this case, the specified navigation performance is no longer satisfied. Therefore, it would be beneficial to identify and exclude the failure. The failure can be identified, if the magnitude of the parity vector (p) or residual vector (w) element corresponding to the

problematic measurement is sufficiently large compared to the total magnitude of the vector (Pervan et al., 1998). The most difficult cases occur when the magnitude of the vector is approximately evenly divided between all satellites, then it is not possible to identify the failed satellite.

In conclusion, the RAIM method as in Brown and Chin (1998) is suitable when using code-phase measurements alone and the position solution is calculated using the least-squares method. However, the RAIM method is only designed for cases when there is only one unacceptable error. The RAIM method presented in Brown and Chin (1998) is therefore, not suitable for PPP or cRTK, because it is not designed for use when employing EKF and attempting to fix carrier-phase ambiguities.

4.5.2 Carrier Receiver Autonomous Integrity Monitoring (CRAIM)

The standard RAIM method is not suitable when using both code and carrier-phase measurements, because it does not take into account the correlation of measurements (in the case of single or double differenced observables), ambiguity resolution, ambiguity validation, cycle-slip detection and potential simultaneous failures. Pervan et al. (1996, 1998) presented an integrity monitoring method which is suitable to use with carrier-phase measurements. However, the method assumes that carrier-phase ambiguities are known. The RAIM method developed by Chang et al. (2001) can be used with carrier-phase measurements but only when ambiguities are float. To enable integrity monitoring both for float and fixed ambiguity PPP, two algorithms have been developed, namely the Imperial College Carrier Receiver Autonomous Integrity Monitoring (ICRAIM) and Cumulative Kalman Filter Receiver Autonomous Integrity Monitoring (CKFRAIM). These are presented in Sections 4.5.2.1 and 4.5.2.2, respectively.

4.5.2.1 Imperial College Carrier Receiver Autonomous Integrity Monitoring (ICRAIM)

The ICRAIM method uses EKF to estimate position and carrier-phase ambiguities (Feng et al., 2009). The principle of the EKF employed, including its equations and symbols, is already explained in Section 4.2.

Different measurement types (P is code-phase, Φ_{L1-L2} is wide-lane carrier-phase and Φ_{L1} is carrier-phase on the L1 frequency) are grouped in the EKF as shown in equation (4.67). Their variance matrix is shown in equation (4.68). The measurements can be double differenced as in Feng et al. (2009) when employing cRTK or un-differenced as in Feng et al. (2010) when employing PPP.

$$z_{EKF} = \begin{bmatrix} \nabla\Delta P \\ \nabla\Delta\Phi_{L1-L2} \\ \nabla\Delta\Phi_{L1} \end{bmatrix} \tag{4.67}$$

$$R_{EKF} = \begin{bmatrix} R_{EKF,P} & 0 & 0 \\ 0 & R_{EKF,L1} + R_{EKF,L2} & R_{EKF,L1} \\ 0 & R_{EKF,L1} & R_{EKF,L1} \end{bmatrix} \tag{4.68}$$

The ICRAIM test statistics are calculated based on subsets of the measurements (Feng et al., 2009). The reason for using the measurement subset specific test statistics is to detect and exclude errors associated with different types of measurements. For example, the carrier-phase only test statistic can be used to detect cycle-slips. The total test statistic (T_{total}) and test statistic for code-phase (T_P), wide-lane (T_{L1-L2}) and L1 carrier-phase (T_{L1}) measurements are calculated using equations (4.69), (4.70), (4.71), (4.72), (4.73), respectively. The selection of test statistics depends on the observation model used. For example, if the ionosphere-free combination is used, a test statistic specific to it should be used. The measurement residuals (w) used in the test statistics calculations are obtained from equation (4.74).

$$W_{EKF} = (H_{EKF} P_{EKF}^{-} H_{EKF}^{T} + R_{EKF})^{-1} \tag{4.69}$$

$$T_{total} = \sqrt{w^T W_{EKF} w} \tag{4.70}$$

$$T_P = \sqrt{w_P^T R_{EKF,P}^{-1} w_P} \tag{4.71}$$

$$T_{L1-L2} = \sqrt{w_{L1-L2}^T (R_{EKF,L1} + R_{EKF,L2})^{-1} w_{L1-L2}} \tag{4.72}$$

$$T_{L1} = \sqrt{w_{L1}^T R_{EKF,L1}^{-1} w_{L1}} \tag{4.73}$$

$$w = z_{EKF} - H_{EKF} x_{EKF}^{+} \tag{4.74}$$

As in the case of the traditional RAIM, it is assumed that the test statistics obey the chi-square distribution. Therefore, error detection thresholds can be determined based on the probability of false alarm, noise standard deviation and degrees of freedom (Feng et al., 2009). The degrees of freedom used with ICRAIM are calculated based on the number of measurements.

Two separate horizontal and vertical protection levels are calculated. The horizontal protection level (HPL_1) is calculated using equation (4.77), where the horizontal position uncertainty (σ_H) is calculated using equation (4.75) and k_H is a factor which reflects the probability of missed detection (Feng et al., 2009). The vertical protection level (VPL_1) is calculated using equation (4.78), where the vertical position uncertainty (σ_V) is obtained using equation (4.76) and k_v is a factor reflecting the probability of missed detection (Feng et al., 2009). The factor k_H and k_v values are different, because the impact of a missed detection is not the same on the vertical and horizontal levels. In the equations, P_{local} is the EKF P matrix (P_{EKF}) converted into the local (East, North, Up) coordinates, $P_{local,11}$ refers to the P_{local} matrix row and column 1, $P_{local,22}$ refers to the P_{local} matrix row and column 2 and $P_{local,33}$ refers to the P_{local} matrix row and column 3.

$$\sigma_H = \sqrt{P_{local,11} + P_{local,22}} \tag{4.75}$$

$$\sigma_V = \sqrt{P_{local,33}} \tag{4.76}$$

$$HPL_1 = k_H \sigma_H \tag{4.77}$$

$$VPL_1 = k_V \sigma_V \tag{4.78}$$

The *HSLOPE* and *VSLOPE* are calculated using equations (4.79), (4.80) and (4.81), respectively (Feng et al., 2009). They provide information on the relationship between the test statistic and position error (Feng et al., 2009). The larger the *SLOPE* value for a given satellite, the smaller is the impact of an error associated with the satellite on the test statistic. Thus, it is most difficult to detect errors associated with a satellite which has the

largest *SLOPE* value. Therefore, the horizontal protection level using equation (4.83) and vertical protection level using equation (4.84) are determined for the most pessimistic case (i.e. when the error occurs for the satellite with the largest SLOPE value). The standard deviation used is calculated based on satellite (i) with the largest slope value as in equation (4.82). The P_{Bias} value is obtained by numerically integrating the probability density function of the parity vector (Section 4.5.1) based on the allowed probability of missed detection (Brown and Chin, 1998).

$$S = (I - H_{EKF}K_{EKF})^T (I - H_{EKF}K_{EKF}) \tag{4.79}$$

$$HSLOPE(i) = \sqrt{\frac{K_{1i}^2 + K_{2i}^2}{S_{ii}}} \tag{4.80}$$

$$VSLOPE(i) = \frac{K_{3i}}{\sqrt{S_{ii}}} \tag{4.81}$$

$$\sigma = \sqrt{\sum_{j=1}^{n} R_{i,j}} \tag{4.82}$$

$$HPL_2 = HSLOPE_{MAX} P_{Bias} \sigma \tag{4.83}$$

$$VPL_2 = VSLOPE_{MAX} P_{Bias} \sigma \tag{4.84}$$

The final protection levels are calculated using equations (4.85) and (4.86) in order to cover the worst case scenario (Feng et al., 2009). As presented in Feng et al. (2009, 2010), the ICRAIM method is suitable both for float and fixed ambiguity RTK and PPP.

$$HPL = \max(HPL_1, HPL_2) \tag{4.85}$$

$$VPL = \max(VPL_1, VPL_2) \tag{4.86}$$

4.5.2.2 Cumulative Kalman Filter Receiver Autonomous Integrity Monitoring (CKFRAIM)

The principle of Cumulative Kalman Filter Receiver Autonomous Integrity Monitoring (CKFRAIM) presented in Joerger and Pervan (2011, 2012) is to take into account measurement residuals provided by the EKF from the current and previous epochs. This is different from ICRAIM, where residuals from only the current epoch are used. The benefit of taking residuals from the previous epochs into account is to improve the detection of errors which persist over time (Joerger and Pervan, 2012).

The CKFRAIM test statistic (T_{KF}) is calculated based on the sum of weighted squared norms of residuals from the current and previous epochs as shown in equation (4.87), where t is the current epoch, w the measurement residual vector for the epoch t_k and W the measurement weight matrix for the epoch t_k obtained from EKF (Joerger and Pervan, 2012). The calculation can be done in practice by adding the current residual component to the test statistic at each epoch. It is assumed that the measurement residuals obey the non-central chi-square distribution. Thus, the detection threshold can be calculated based on the assumed distribution, degrees of freedom and assumed rate of false alarm.

$$T_{KF} = \sum_{t_k=1}^{t} \|w(t_k)\|^2_{W(t_k)^{-1}} \tag{4.87}$$

CKFRAIM is used for cRTK integrity monitoring in Joerger and Pervan (2012). At least in a theory, CKFRAIM can also be applied to PPP using a similar approach to that of the ICRAIM method.

4.6 PPP software and methods

The currently available PPP software packages, services and methods are discussed in this section. They are divided into the fixed ambiguity PPP (research) and other model categories. The fixed ambiguity PPP (research) category shows the current PPP methods presented in conference or journal papers. The other models category includes the most interesting open source and commercial PPP implementations.

4.6.1 Fixed ambiguity PPP (research)

The fixed ambiguity PPP implementations presented in the literature are compared in Table 4.3. They are compared in terms of the PPP correction product type (Section 4.3.1), application area, time required to obtain an initial ambiguity resolution, accuracy and the ambiguity resolution and validation methods used. The applicable area criteria divides PPP implementations into categories based on the area where they can be used with the same error correction products. The categories are: global, regional (for example, California) and local (distance from the reference network < 100 km). For example, if the model uses local ionospheric corrections, the same corrections can only be used in the same local area. All PPP implementations presented in the table use the GPS L1 and L2 measurements. The comparison is only done at a high level, because PPP implementations in the papers are typically not described in detail.

Reference	PPP correction product type	Applicable area	Time required to obtain an initial ambiguity resolution	Accuracy	Ambiguity resolution and validation	Remarks
(Collins et al., 2008)	IRC, post-processing.	Global	3600 s to obtain centimetre level accuracy	Centimetre level.	The LAMBDA method, no ambiguity validation.	Ambiguity resolution is carried out every epoch. Float solution is maintained independently.
(Collins et al., 2012)	IRC, post-processing. Local ionosphere corrections	Local	Few seconds	Horizontal error: one sigma 1 cm, two sigma 2 cm	The LAMBDA method, the confidence level based ratio test	
(Geng et al., 2010d)	BSDFCB, real-time.	Regional	1500-1800 s	East: 0.8 cm North: 0.9 cm Up: 2.5 cm	The Ratio test, threshold: 2 (Geng et al., 2010a)	
(Juan et al., 2012)	UDFCB, real-time. Local ionosphere corrections	Local	Approximately 300 s	Centimetre level	The LAMBDA method and confidence level based ratio test	Integrity monitoring
(Laurichesse et al., 2010)	IRC, real-time.	Global	At least 1800 s	Horizontal: approximately 1 cm	Based on rounding ambiguities and checking their co-variance	
(Li, 2012)	UDFCB, real time. Ionospheric corrections	Global	1300 s without ionospheric corrections, 900 s with ionospheric corrections	Horizontal: 2.2 cm without ionospheric corrections, 1.9 cm with ionospheric correction	Not presented in the paper	The performance of the method depends on the quality of ionospheric maps
(Shi and Gao, 2010)	IRC, post-processing.	Global	Approximately 1800 s	Not available	The ratio test	
(Shi and Gao, 2012)	IRC, post-processing.	Global	Approximately 1500 s	Not available	Partial ambiguity fixing, validation by the ratio test and success rate test	

Table 4.3: PPP method comparison (static case)

As shown in Table 4.3, it takes between 1300 and 3600 seconds to fix ambiguities depending on the PPP implementation used when external ionospheric corrections are not used. When local ionospheric corrections are used, ambiguities can be fixed in a few seconds (Collins et al., 2012). However, the density of local reference network stations similar to that for cRTK is required to generate sufficiently accurate ionospheric corrections (Collins et al., 2012). Typically, centimetre level position accuracy is obtained when using the PPP models employing external ionospheric corrections after the ambiguities are fixed.

There are numbers of factors that impact PPP results: implementation, dataset, available error corrections, processing settings and approach used in the performance evaluation. For example, only datasets which provide good results may be presented in some PPP papers or the cases when ambiguity resolution fails are excluded. In addition, only small datasets are used for testing in many papers. When using datasets with smaller errors less strict ambiguity validation settings can be used, leading to an apparent better performance. However, using loose ambiguity validation settings with more challenging datasets, which have, for example, large multipath errors, can lead to wrong ambiguity resolution.

Based on the results presented in the literature, the model in Li (2012) appears to provide the shortest time needed to fix the ambiguities. However, it is impossible to make a fair comparison between the various PPP implementations, because of the different datasets used (which are not in the public domain) and lack of knowledge about the exact processing settings used. Therefore, in reality it is impossible to identify the best PPP model based on the results presented in the literature.

4.6.2 Other models and software

The current PPP software packages and services are shown in Table 4.4. There are four global commercial PPP services: VERIPOS Apex^2, TERRASTAR-D, OmniSTAR G2, NavCom StarFire and Trimble CenterPoint RTX. All of the services broadcast real-time PPP corrections using telecommunication satellites. The PPP-Wizard and RTKLIB are the most interesting research software packages because they are open source and provide at least some support for PPP ambiguity resolution. The source code and functionality of the PPP-Wizard and RTKLIB software packages were studied as a part of the research project. However, the software was not tested in this thesis.

Name	Reference	Type	Supported GNSS systems	Ambiguity estimation
Bernese	(Dach et al., 2007)	Research	GPS and GLONASS	Float
GPSTk	(Tolman et al., 2004)	Research, open source	GPS, GLONASS and Galileo	Float
OmniSTAR G2	(OmniSTAR, 2012)	Commercial	GPS and GLONASS	Float
NavCom StarFire	(NavCom, 2012)	Commercial	GPS and GLONASS	Float
Novatel GrafNav	(Novatel, 2012)	Commercial	GPS and GLONASS	Float
PANDA	(Shi et al., 2010)	Research	GPS	Float and fixed (depending on the version)
PPP-Wizard	(Laurichesse, 2011)	Research, open source	GPS	Fixed
TERRASTAR-D	(TerraStar, 2013)	Commercial	GPS and GLONASS	Float
Trimble CenterPoint RTX	(Leandro et al., 2012a)	Commercial	GPS, GLONASS and QZSS	Fixed
RTKLIB	(Takasu, 2012)	Research, open source	GPS, GLONASS, QZSS and Galileo	Float, fixed (experimental)
VERIPOS Apex[2]	(VERIPOS, 2013)	Commercial	GPS and GLONASS	Float

Table 4.4: Available PPP software and solutions

4.7 Conclusion

The current PPP methods have been discussed in this chapter. To provide a performance reference, cRTK was presented in Section 4.1, because it is currently the most commonly used high accuracy positioning method. cRTK can typically provide centimetre-level positioning with a few seconds convergence time. However, employing it requires dense local GNSS reference networks, which are expensive. Therefore, it is not a suitable method to use in remote areas.

A current float PPP method was presented in Section 4.2. The current fixed ambiguity PPP methods including product generation and rover side implementations were discussed in Section 4.3. In terms of product generation using the GPS L1 and L2 signals, the IRC and UDFCB methods were chosen as the most suitable, because they can generate un-differenced corrections which can be used anywhere on the Earth while there were no significant differences in terms of performance between the product generation methods. In terms of the rover side implementation using the GPS L1 and L2 signals, the BSD and un-differenced dual-frequency ionosphere-free methods are the most suitable. The BSD method is used in this thesis, because it is easier to implement and provides similar performance to the un-differenced method. In addition, PPP ambiguity resolution using triple-frequency signals was discussed. This can provide centimetre-level accuracy with a

convergence time of 5 minutes or shorter. However, triple-frequency PPP is not currently a suitable method, because there are no suitable correction products available and the number of satellites broadcasting triple-frequency signals is not sufficient. PPP using external ionospheric corrections was also discussed. It can typically provide centimetre level positioning with immediate convergence, but requires a dense reference networks as in the case for cRTK. Thus, PPP using external ionospheric corrections is not suitable method to use in this thesis.

Current carrier-phase ambiguity resolution and validation methods were discussed in Section 4.4. The discussion included the integer rounding, integer bootstrapping and ILS methods. In the case of ILS, the LAMBDA method can be employed to make an ILS search in a computationally efficient way and ratio test to validate ambiguities. A constant ratio test decision threshold can be used or the threshold can be defined using the DNCF or FFS based methods.

The current integrity monitoring methods were discussed in Section 4.5. Based on the analysis, the ICRAIM method is suitable for monitoring integrity of PPP.

Finally, the current PPP methods, software and services were discussed in Section 4.6. The discussion included both research type models published in scientific papers and other available commercial or openly available PPP implementations. It was concluded that it is impossible to make a fair comparison between the various PPP implementations, because of the different datasets used (which are not available in the public domain) and lack of knowledge about the exact processing settings used. In case of scientific papers, the exact processing methods are not typically explained in detail and in case of commercial software the methods are typically commercial secrets.

5 Development of the enhanced Precise Point Positioning (PPP) method

This thesis develops an enhanced PPP method to address the issues with the existing methods. The POINT software used to test the existing PPP methods and develop the enhanced PPP method is first discussed in Section 5.1. Thereafter, the performance of the current methods is tested in Section 5.2 to understand their weaknesses. This includes testing a current cRTK method (discussed in Section 4.1), float PPP method (Section 4.2) and current fixed ambiguity PPP methods (Section 4.4). The primary focus on testing the existing fixed ambiguity PPP method is ambiguity validation.

To address the issues with the existing PPP methods, this thesis develops the enhanced PPP method in Section 5.3. A particular focus is to make ambiguity validation more reliable.

5.1 POINT software

The POINT software is used in this thesis for cRTK and PPP processing. The software has been developed as a part of the innovative Navigation using new GNSS signals with hybridised technologies (iNsight) project (http://www.insight-gnss.org/index.html). The software is written in the C++ language and it runs in Microsoft Windows.

The general architecture of the software is shown in Figure 5.1. Raw GNSS data in the Receiver Independent Exchange Format (RINEX) format (Reussner and Wanninger, 2011) is read in the RINEXReceiver module. The RINEX data is forwarded to the GNSSReceiver module, which combines the data with the relevant error corrections: satellite orbit corrections (Section 3.4.1) from the EphemeridesSP3 module, satellite clock corrections (Section 3.4.2) from the IGS_ClkData module, tropospheric mapping function and initial delay values (Section 3.4.5) from the Troposphere module, FCB corrections (Section 3.4.3) from the CNES_biases module and antenna phase centre error corrections (Section 3.4.6) from the ANTEX module. The DCB (Section 3.4.7) and satellite antenna phase wind-up (Section 3.4.9) corrections are applied directly in the GNSSReceiver module. In addition, the GNSSReceiver module handles calculating the relevant measurement combinations such as

the ionosphere-free (Section 3.4.4) and Melbourne-Wubbena (Section 4.3.1.1) combination. The errors corrections employed are the correction chosen as the most suitable in Chapter 3.

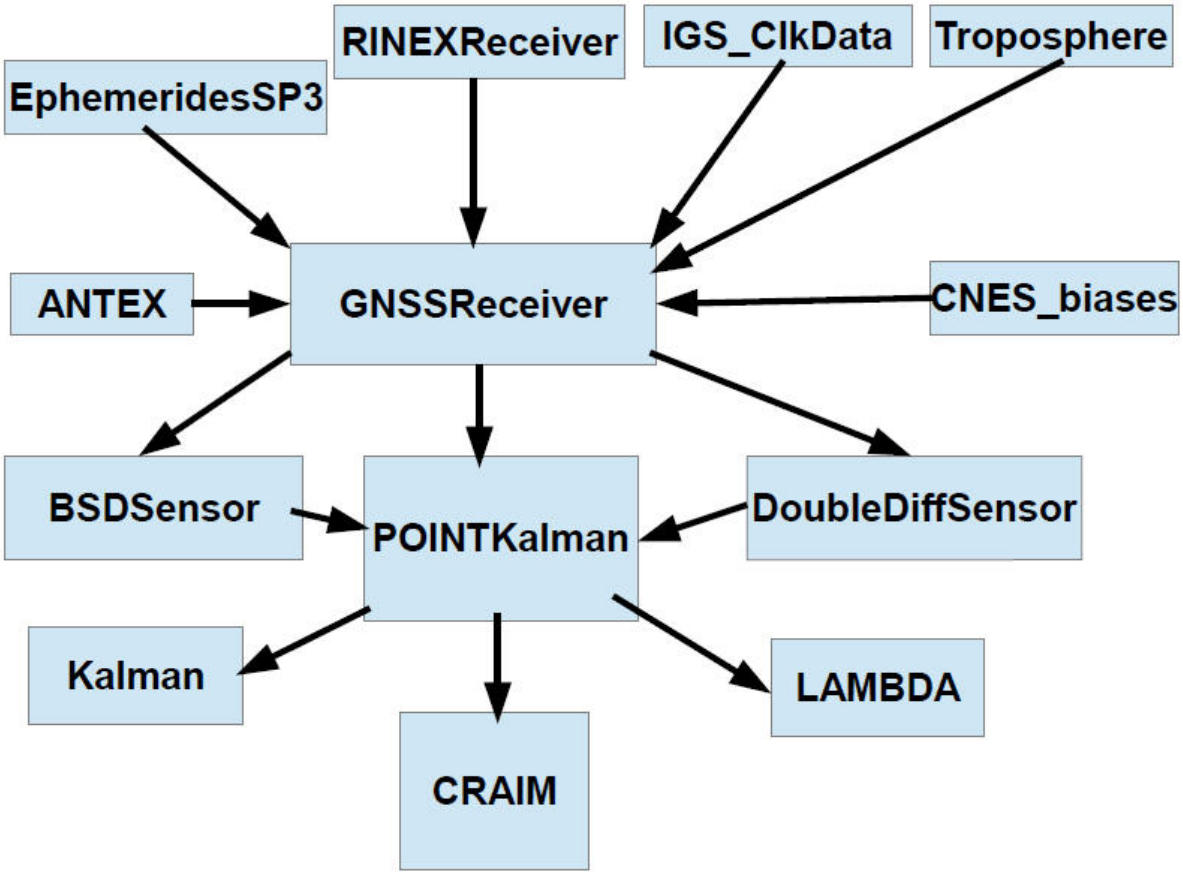

Figure 5.1 The architecture of the POINT software

The POINTKalman module estimates a position using an Extended Kalman Filter (EKF) (Section 4.2). A generic EKF is implemented in the Kalman module. Un-differenced measurements and corrections obtained directly from the GNSSReceiver module are employed when making un-differenced PPP estimation. When using BSD (Section 4.3.2.2) measurements for PPP, the differencing is done in the BSDSensor module based on the un-difference measurements and corrections provided by the GNSSReceiver module. Thereafter, the BSD measurements and corrections are fed into the POINTKalman module. When employing cRTK (Section 4.1), a double-differencing operation is applied in the DoubleDiffSensor module to the un-differenced measurements obtained from the GNSSReceiver module. Thereafter, the information is fed into the POINTKalman module.

PPP and cRTK carrier-phase ambiguity resolution and validation is done in the POINTKalman module. The Least-squares AMBiguity Decorrelation Adjustment (LAMBDA) method (Section

4.4.3.1) is implemented in the LAMBDA module. The Imperial College Carrier Receiver Autonomous Integrity Monitoring (ICRAIM) method (Section 4.5.2.1) is implemented in the CRAIM module.

An initial version of the POINT software supporting cRTK and float PPP was primary developed by the University of Nottingham and University College London. The primary contribution in this thesis for the POINT software is implementing the existing fixed ambiguity PPP methods (Sections 4.3.2 and 4.4) and enhanced PPP method (Section 5.3). In addition, a large amount of other implementation work was completed as a part of the research leading to this thesis. This implementation work includes: support for using BSD measurements, CNES FCB corrections, CNES satellite clock corrections, DCB corrections and GMF tropospheric mapping function (Section 3.4.5), implementing failure exclusion for ICRAIM (Section 5.3.4.1), antenna phase centre variation correction (Section 3.4.6), PPP fast re-convergence after signal blockages (Section 4.3.2.3), tropospheric gradient correction (Section 3.4.5.3), satellite eclipsing detection (3.4.10), cycle-slip detection and correction (Section 4.2) and cRTK (Section 4.1) for long baselines.

5.2 Performance of the current methods

The performance of the cRTK method is first tested in the next section to provide a reference for comparison with the current PPP methods. The National Oceanic and Atmospheric Administration (NOAA) dataset used to test the existing PPP methods. A current float PPP method is tested in Section 5.2.3. The current fixed ambiguity PPP methods are tested in Section 5.2.4. ICRAIM is tested in Section 5.2.5. Finally, the limitations of the current PPP methods are discussed in Section 5.2.6.

5.2.1 cRTK

The performance of the cRTK method (Section 4.1) is demonstrated using 1 Hz GNSS data from 20 one hour time-periods. The KIRU IGS station is used as a reference station, and KIR0 IGS station as the rover. The distance (baseline) between the stations is 4.5 km and both stations are located in Sweden. A small dataset is used, because the aim is only to give an example of cRTK performance in a typical case. The data is processed using POINT software.

The average time required to obtain an initial ambiguity resolution is shown in Figure 5.2 and the position error at the initial ambiguity resolution epoch in Figure 5.3. It is shown that carrier-phase ambiguities can be fixed on average within a few seconds and with 0.9 cm horizontal and 2.8 cm vertical average position error against the know coordinates of the stations. However, the performance of cRTK is dependent on the dataset. For example, high ionospheric activity can make it much worse because ionospheric errors can significantly affect ambiguity resolution. It should be noted that ambiguities could have been fixed even faster, but a minimum of six seconds carrier-phase lock-time is required in the software implementation before attempting ambiguity resolution. The standard deviation of the time required to fix ambiguities is approximately 4 s and standard deviations of horizontal and vertical position errors are 0.5 and 1.0 cm, respectively. That is an example of typical variation of the cRTK performance, because it varies, for example, depending on the atmospheric conditions and number of available satellites.

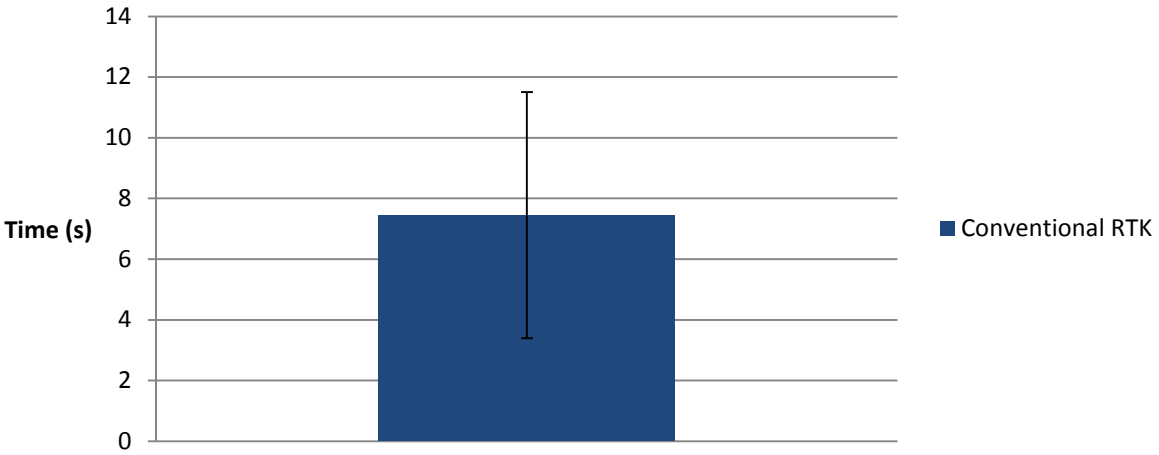

Figure 5.2 The average time required to obtain an initial ambiguity resolution (cRTK) (one sigma standard deviation as error bars)

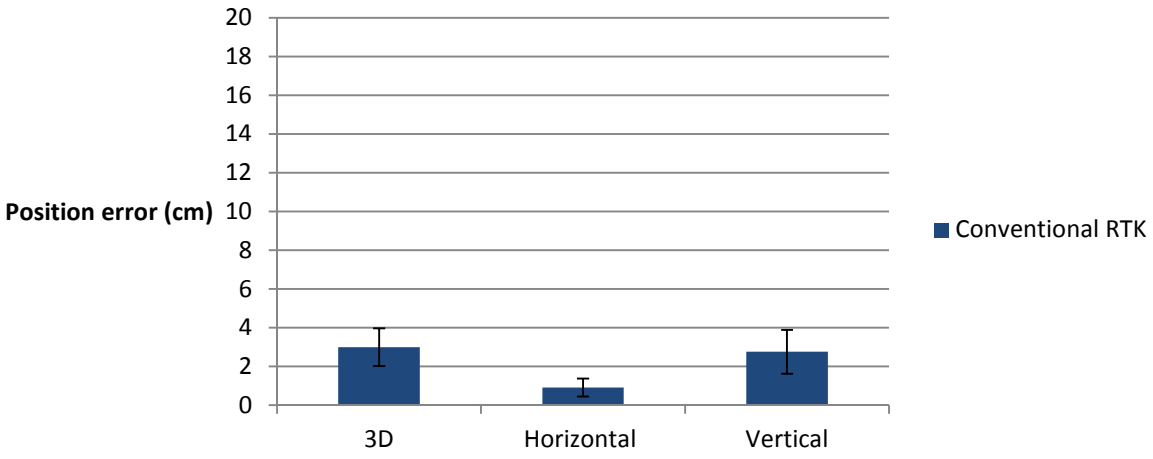

Figure 5.3 The average position error at the initial ambiguity resolution epoch (cRTK) (one sigma standard deviation as error bars)

Although the results above are obtained using a small dataset, they clearly demonstrate the ability of cRTK to provide centimetre-level positioning with a few seconds convergence time. However, employing cRTK requires dense GNSS reference networks, which are expensive to build. Therefore, cRTK is not suitable to use in remote areas.

5.2.2 National Oceanic and Atmospheric Administration dataset

The float PPP test in the next section is carried out using the National Oceanic and Atmospheric Administration (NOAA) (NOAA, 2013) dataset. It is also used to test the existing PPP carrier-phase ambiguity resolution and validation methods and enhanced PPP method. The dataset contains data from 10 NOAA stations (Table 5.1) and 96 one hour time periods (Table 5.2). The locations of the NOAA dataset stations are shown in Figure 5.4.

Stations at different locations of the Earth are selected to provide geographic diversity. This is important because geographical-dependent error sources such as tropospheric and ionospheric delay, multipath, and site-displacement effects vary by location. Therefore, the use of multiple locations makes testing more representative of the performance which can be obtained anywhere on the earth. The stations are selected so that they are not part of the reference network (Figure 3.3) that provides data for the CNES clock correction generation. This prevents any correlations between the test data and the data used for the generation of corrections. The number of stations and time periods to test is a compromise

between the amount of data and time required for data processing. To reduce the processing time, eight hours of data per day is processed as shown in Table 5.2.

Station code	Location	Receiver	Antenna
BDOS	Barbados	LEICA GRX1200GGPRO	ASH700936E_C
BJCO	Benin	TRIMBLE NETR5	TRM59800.00
CHIN	Florida, the USA	TRIMBLE NETR5	TRM55971.00
ICT5	Kansas, the USA	LEICA GRX1200GGPRO	LEIAX1202GG NONE
ISER	Iraq	TRIMBLE NETR5	TRM57971.00
ISNA	Iraq	TRIMBLE NETR5	TRM57971.00
MIQE	Michigan, the USA	LEICA GRX1200+GNSS	LEIAT504GG
SCWT	South Carolina, the USA	TRIMBLE NETR9	TRM55971.00 NONE
SUAF	Alaska, the USA	LEICA GRX1200GGPRO	LEIAX1202GG
MTDT	Montana, the USA	TRIMBLE NETR5	TRM57971.00

Table 5.1 The stations, locations of the stations, receivers and antennas for the National Oceanic and Atmospheric Administration (NOAA) dataset

Year	Month	Day	Hours
2013	02	10	1-2, 4-5, 7-8, 10-11, 13-14, 16-17, 19-20 and 22-23
2013	02	11	1-2, 4-5, 7-8, 10-11, 13-14, 16-17, 19-20 and 22-23
2013	02	12	1-2, 4-5, 7-8, 10-11, 13-14, 16-17, 19-20 and 22-23
2013	02	13	1-2, 4-5, 7-8, 10-11, 13-14, 16-17, 19-20 and 22-23
2013	03	01	1-2, 4-5, 7-8, 10-11, 13-14, 16-17, 19-20 and 22-23
2013	03	02	1-2, 4-5, 7-8, 10-11, 13-14, 16-17, 19-20 and 22-23
2013	03	03	1-2, 4-5, 7-8, 10-11, 13-14, 16-17, 19-20 and 22-23
2013	03	04	1-2, 4-5, 7-8, 10-11, 13-14, 16-17, 19-20 and 22-23
2013	03	05	1-2, 4-5, 7-8, 10-11, 13-14, 16-17, 19-20 and 22-23
2013	03	06	1-2, 4-5, 7-8, 10-11, 13-14, 16-17, 19-20 and 22-23
2013	03	07	1-2, 4-5, 7-8, 10-11, 13-14, 16-17, 19-20 and 22-23
2013	03	08	1-2, 4-5, 7-8, 10-11, 13-14, 16-17, 19-20 and 22-23

Table 5.2 The testing time-periods for the National Oceanic and Atmospheric Administration (NOAA) dataset

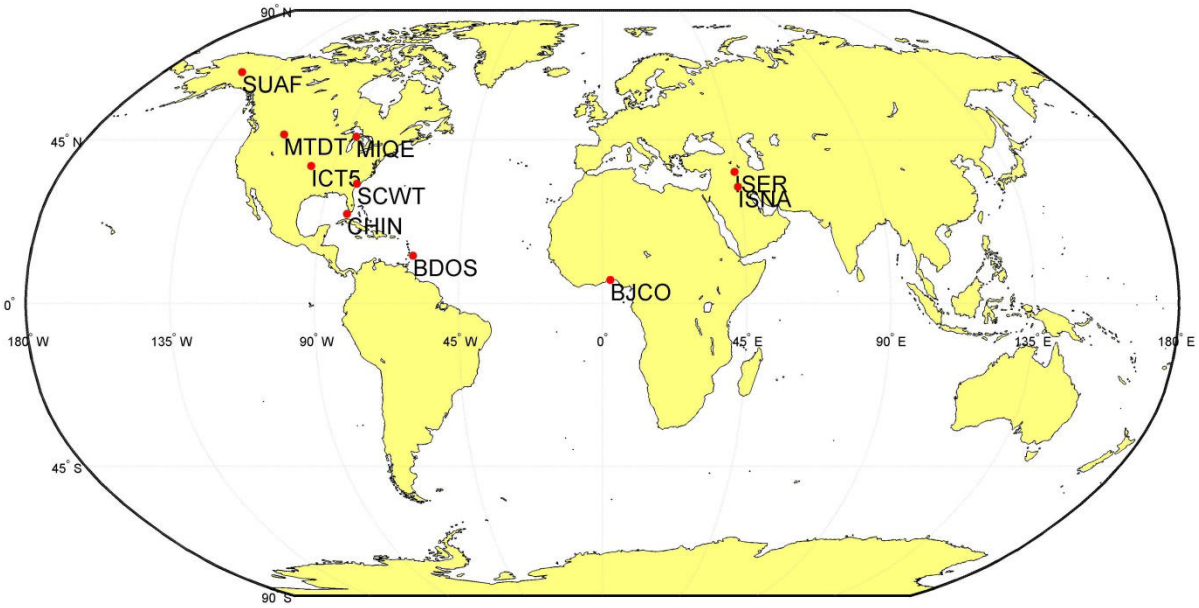

Figure 5.4 The locations of the NOAA dataset stations

The accuracy of the position estimates is evaluated by comparing the computed location with the known IGS08 coordinates of the stations. The coordinates are provided by NOAA (NOAA, 2013) and their accuracy is at millimetre level. Vertical position error in this thesis refers always to the absolute value of the vertical error.

5.2.3 Float PPP

The performance of the current float PPP method presented in Section 4.2 is tested using the NOAA dataset. The primary motivation of testing float PPP is to provide a comparison against fixed ambiguity PPP. The float PPP results are analysed in terms of the time required to obtain better than 10 and 5 cm position errors (convergence time) and success rates of obtaining such position errors. The results for the 10 cm convergence criterion and data from all time periods are shown in Figure 5.5.

The time required to obtain better than 10 cm 3D, horizontal and vertical position errors varies between 1200 and 2700 s, 800 and 1800 s and 800 and 2100 s, respectively, depending on the station. The location-dependent variation may have been caused by the different satellite geometries and varying multipath and troposphere conditions at different locations. It is not possible to proof that these factors had been the reasons for the variation, but it is commonly known that the satellites geometry, tropospheric conditions and

multipath impacts the results of GNSS analysis. It is shown in Hilla and Cline (2003) that different NOAA stations have the varying magnitude of the multipath error. In addition, the different antenna and receiver types used may also impact the results. It is not possible to proof the impact of the receiver and antenna types in these specific tests, but it is shown in Geng et al. (2010d) that the type of antenna and receiver can have a significant impact on PPP performance. The standard deviations of the horizontal and vertical convergence times vary between 660 and 810 s and between 500 and 860 s, respectively, depending on the station. The large standard deviations may have been caused by the varying quality of the CNES corrections and time dependent satellite geometry and atmospheric conditions. It is shown in Laurichesse (2011) that the accuracy of CNES satellite orbit corrections is occasionally worse than the typical accuracy shown in Table 3.1. Therefore, it can be speculated that the longer than usual convergence time in some test cases may have been caused by the insufficient quality of the CNES products.

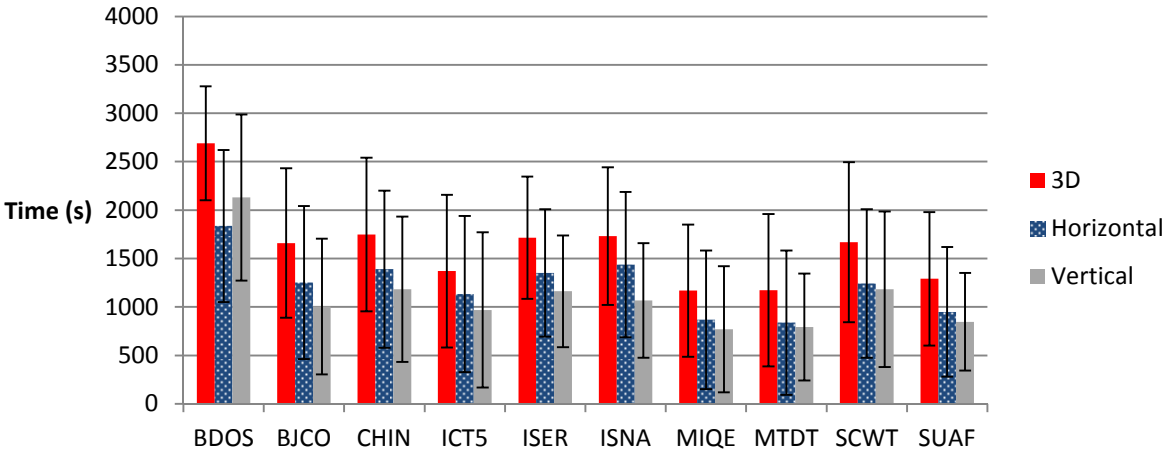

Figure 5.5 The average time required to obtain smaller than 10 cm position error at different stations when employing float PPP (one sigma standard deviation as error bars)

The success rate of obtaining better than 10 cm 3D position error is shown in Figure 5.6. The success rate refers to the percentage of the tests achieving better than 10 cm position error. The rate varies between 73% and 97% depending on the station. The variation of the rate may have been caused by the same reasons as the variation of the convergence time. The convergence time to 10 cm error using all data is shown in Figure 5.7. It takes an average of 1600, 1200 and 1100 s to obtain better than 10 cm 3D, horizontal and vertical position errors, respectively. The standard deviations of the horizontal, vertical and 3D convergence times over all stations are large, because the standard deviations at all stations are large and

average convergence times also vary by the station. The success rate of obtaining better than 10 cm position error using all data is shown in Figure 5.8. The rate is 88% for 3D position error, 94% for horizontal position error and 95% for vertical position error.

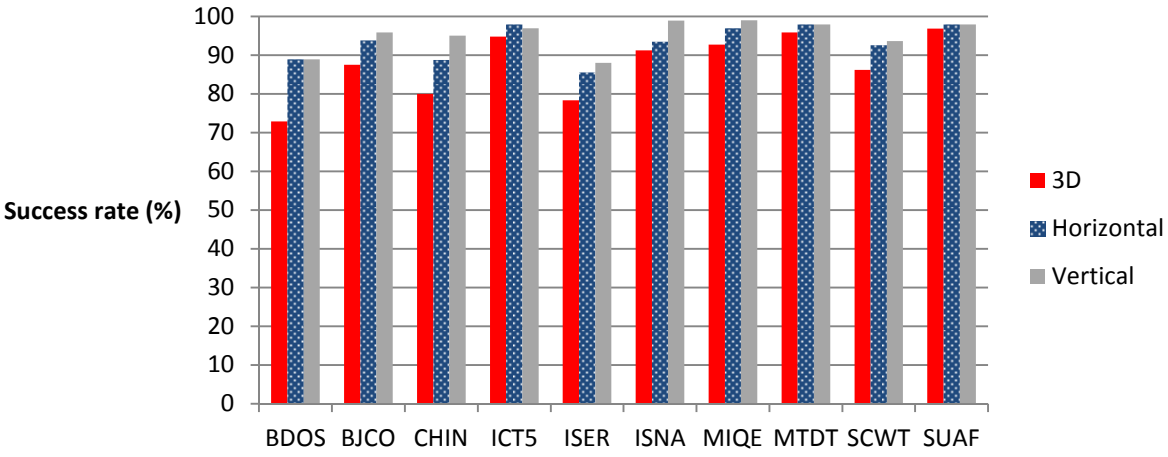

Figure 5.6 The success rate of obtaining better than 10 cm position error at different stations

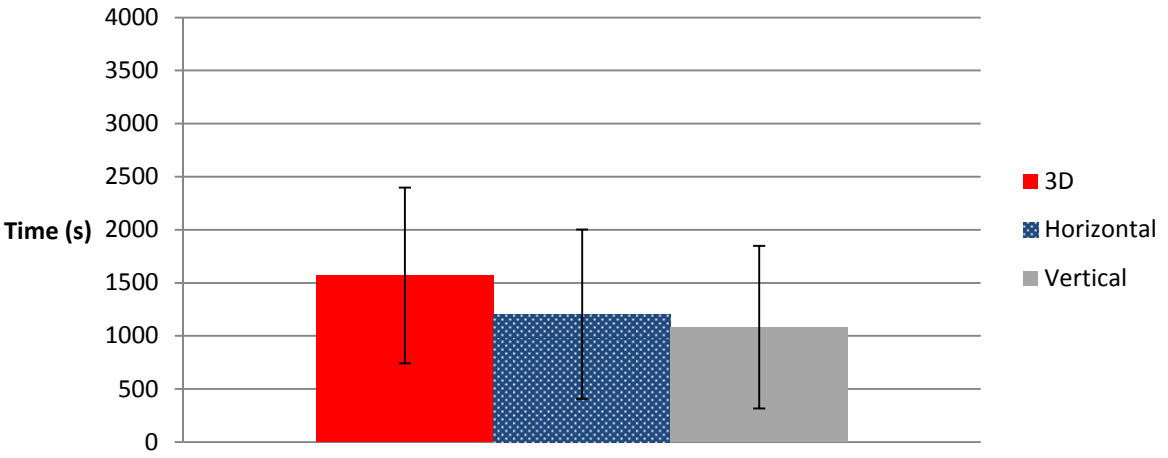

Figure 5.7 The average time needed to obtain better than 10 cm position error using all data when employing float PPP (one sigma standard deviation as error bars)

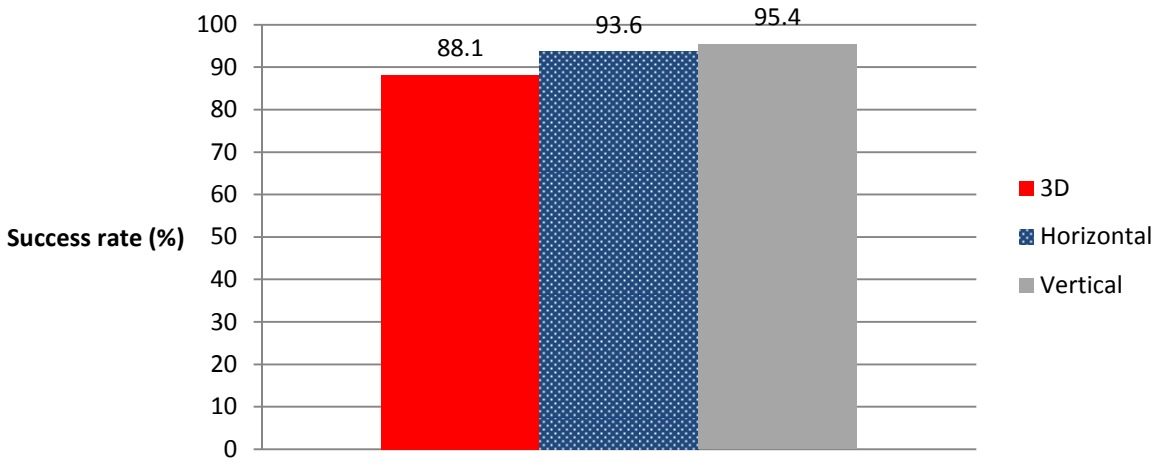

Figure 5.8 The success rate of obtaining better than 10 cm position error using all data

The convergence time to achieve 5 cm error for different stations using data from all time-periods is shown in Figure 5.9. Based on the data from all stations and time-periods, the convergence time to achieve 5 cm error is shown in Figure 5.10. The longest average convergence time to 5 cm error is 3100 s (at the BDOS station) and shortest convergence time is 2000 s (at the MTDT station). Based on all the data, the average 5 cm convergence time of the 3D position error is 2400 s. In general, the convergence time to 5 cm error is significantly longer than the convergence time to 10 cm error. This is due that the total magnitude of PPP error sources divided by the required error level (e.g. 5 or 10 cm) becomes larger as the required error level increases. For example, assuming that the standard deviation of the noise in the L1 and L2 carrier-phase measurements is 0.5 cm, which based on equation (3.12) refers to the 1.49 cm standard deviation of the ionosphere-free carrier-phase combination. Therefore, the total magnitude of the noise is significantly larger compared to the 5 cm than to the 10 cm error level. The increasing convergence time as the required error level becomes smaller is a common known property of PPP and it is discussed, for example, in Bisnath and Gao (2009). Similar to the standard deviation of 10 cm convergence time, the standard deviation of 5 cm convergence time is large. The standard deviations of the horizontal, vertical and 3D convergence times vary between 610 and 840 s, 660 and 890 s and 370 and 730 s, respectively, depending on the station. The large standard deviations may have been caused by the varying quality of the CNES corrections products and varying satellite geometry and atmospheric conditions.

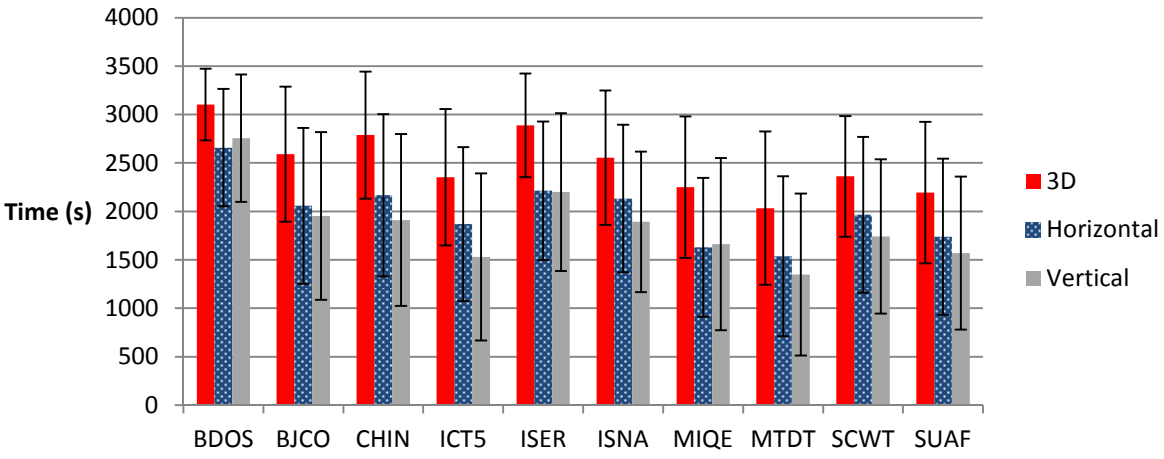

Figure 5.9 The average time needed to obtain better than 5 cm position error at different stations when employing float PPP (one sigma standard deviation as error bars)

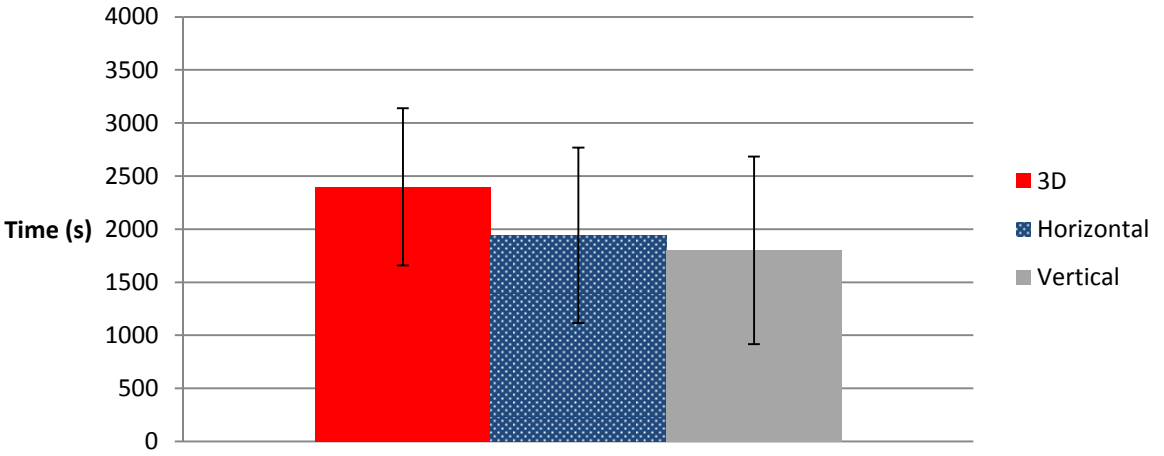

Figure 5.10 The average time needed to obtain better than 5 cm position error using all when employing float PPP (one sigma standard deviation as error bars)

The success rate of obtaining better than 5 cm error using data from different stations is shown in Figure 5.11 and using all data is shown in Figure 5.12. The success rate varies between 20% and 76% depending on the station. Based on all data, the success rates of obtaining better than 5 cm 3D, horizontal and vertical position errors are 55%, 76% and 79%, respectively. This is significantly lower than the rate of obtaining smaller than 10 cm position errors. The long convergence time to 5 cm position error is a clear weakness when employing the float PPP method to support applications with high positioning accuracy requirements (better than 5cm).

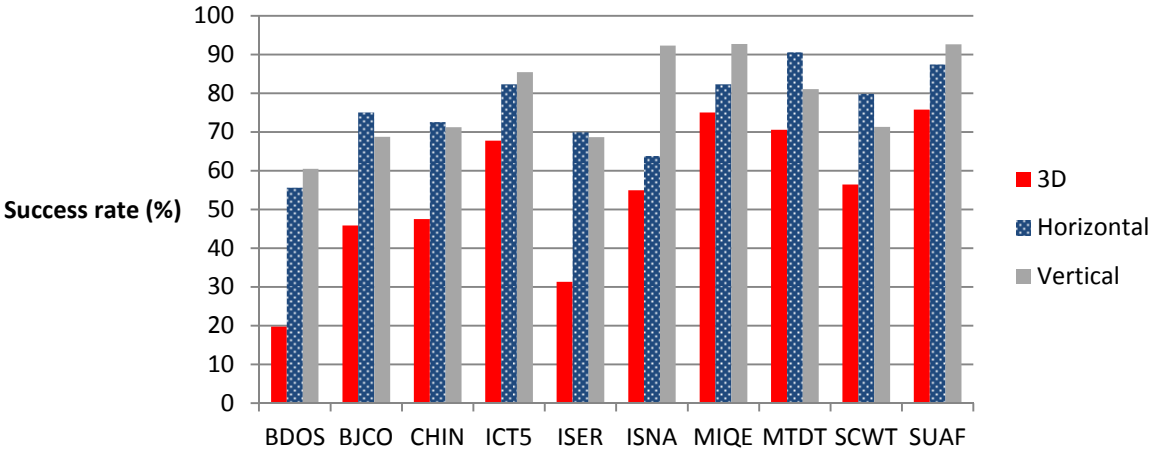

Figure 5.11 The success rate of obtaining better than 5 cm position error at different stations

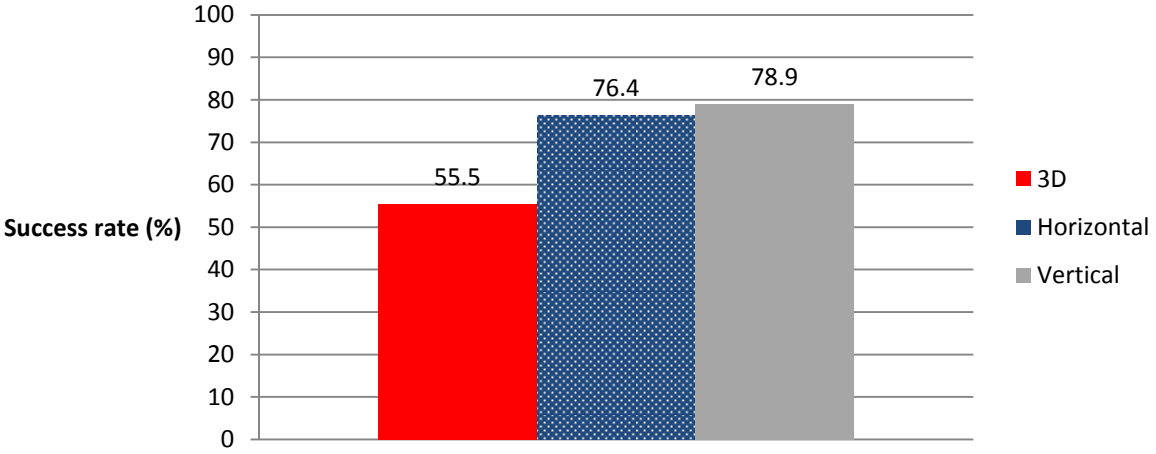

Figure 5.12 The success rate of obtaining better than 5 cm position errors using all data

Employing float PPP does not require local reference networks, as in the case of cRTK. However, the convergence time to 5 cm position error is significantly longer. For example, it takes on average 7 s to obtain 3 cm 3D position error using cRTK. In contrast, it takes an average 2400 s to obtain better than 5 cm 3D position error using float PPP. The success rate of obtaining better than 5 cm 3D position error is only 55% when float PPP processing is applied to one hour datasets. This makes float PPP impractical for many of the applications discussed in Chapter 2.

5.2.4 Fixed ambiguity PPP

The performance of the current ambiguity resolution and validation methods is tested using the NOAA dataset, previously used to test float PPP methods. The dataset is explained in in Section 5.2.2.

The same PPP error correction and modelling methods as those used to test float PPP in the previous section are employed. This includes the CNES satellite clock corrections that are generated using the IRC model discussed in Section 4.3.1.2. The rover-side BSD dual-frequency ionosphere-free model discussed in Section 4.3.2.2 is used.

The PPP ambiguity resolution and validation methods discussed in Section 4.4 are tested. This includes the integer bootstrapping in Section 5.2.4.1, ILS using Constant ratio test threshold (ILSC) in Section 5.2.4.2, ILS using Doubly Non-Central F-distribution based ratio test threshold (ILSDNCF) in Section 5.2.4.3 and ILS using Fixed Failure rate Simulation based method (ILSFFS) in Section 5.2.4.4. The results using these methods are analysed in terms of the time required to obtain an initial ambiguity resolution, rates of correct and incorrect ambiguity resolution and magnitude of the position error at the initial ambiguity resolution epoch. The initial ambiguity resolution epoch is defined as the epoch when at least four narrow-lane ambiguities are fixed to integers. In a theory, the definition could be any number of ambiguities. However, it is required in this thesis that four narrow-lane ambiguities are fixed initially, because four has been chosen as the threshold and the LAMBDA method implementation employed requires fixing at least four ambiguities initially. Fixing wide-lane ambiguities alone is not counted as ambiguity resolved solution, because the wide-lane ambiguities are geometry-free (Section 4.3.2.2) and they do not impact the position error. It is defined that incorrect ambiguity resolution occurs when the magnitude of the 3D position error at the initial ambiguity resolution epoch is larger than 10.7 cm, corresponding to the wavelength of the narrow-lane signal combination. On the other hand, if the 3D error is 10.7 cm or less at the initial ambiguity resolution epoch, then ambiguity resolution is defined as being correct. The test results shown are based on using all data from the NOAA dataset. Conclusions from the comparison of the methods are drawn in Section 5.2.4.5.

5.2.4.1 Integer bootstrapping

The integer bootstrapping method presented in Section 4.4.2 is used. The validation parameters are chosen to match the values used in Laurichesse et al., (2010) and the PPP-wizard software (Laurichesse, 2011). The parameter values are: the satellite elevation mask is 15 degrees, float position solution must have converged at least 30 minutes prior to attempting wide-lane or narrow-lane ambiguity resolution, and maximum difference between the float ambiguities and closest integer is set to 0.25 cycles. Ambiguities are validated using the DBT method (Section 4.3.1.1).

From the results, the average time required to obtain an initial ambiguity resolution is 2030 s and its Standard Deviation (SD) is 400 s. The ambiguity resolution rate is 74% which refers to the percentage of the tested cases where the initial ambiguity resolution is obtained. The average position error at the initial ambiguity resolution epoch is shown in Figure 5.13. The average 3D, horizontal and vertical errors are 12.4 (SD: 13.7 cm), 5.8 (SD: 7.3 cm) and 9.9 cm (SD: 12.4 cm), respectively. The large magnitude of the position errors is mainly caused by incorrect ambiguity resolution. SD of the position errors is large, because of the high rate of incorrect ambiguity resolution. The distribution of the 3D position error at the initial ambiguity resolution epoch is divided into different error categories, as presented in Figure 5.14. The 3D position error at the initial ambiguity resolution epoch is larger than 10.7 cm in 36.9% of the cases where ambiguities were fixed.

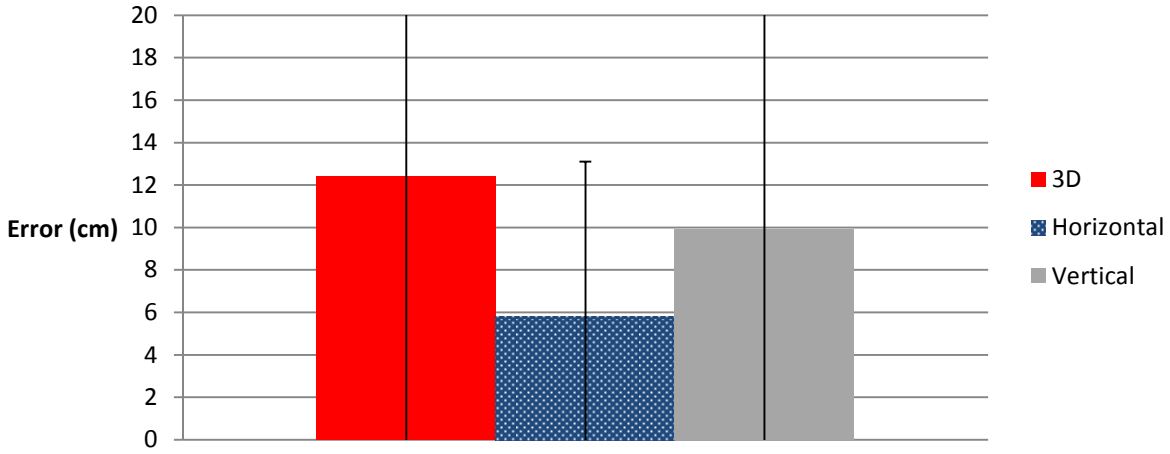

Figure 5.13 The average position error at the initial ambiguity resolution epoch when using the integer bootstrapping method (one sigma standard deviation as error bars)

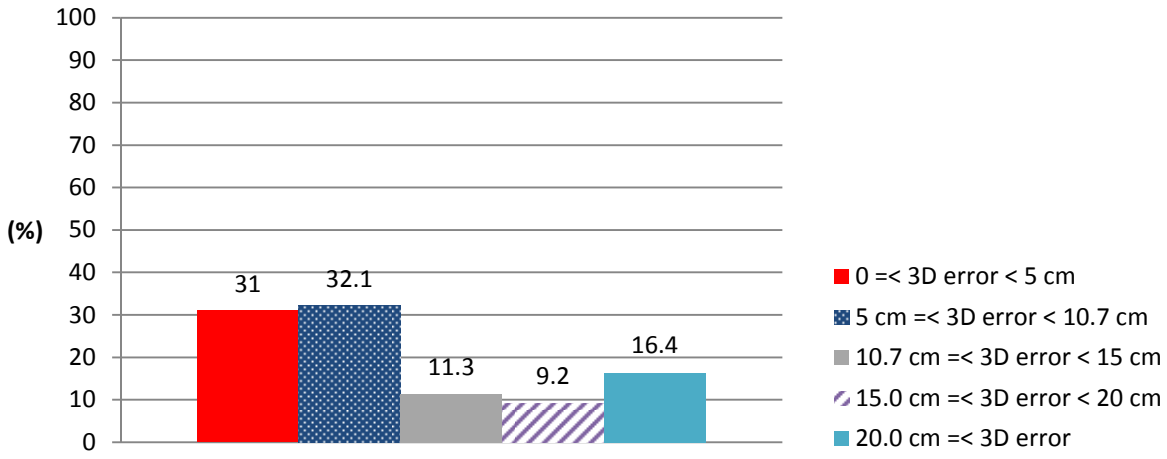

Figure 5.14 The distribution of 3D position error at the initial ambiguity resolution epoch when using the integer bootstrapping method

Based on the results, the most serious problem is the large percentage (36.9%) of the cases where the 3D position error at the initial ambiguity resolution epoch is larger than 10.7 cm, as seen in Figure 5.14. This has been caused by incorrect fixing of the narrow-lane ambiguities. This makes the integer bootstrapping method unsuitable for real-life applications.

The major problem with the integer bootstrapping method is that it does not adequately take into account the correlations between ambiguities. Therefore, the method is unsuitable for geometry-dependent ambiguity resolution where the position is dependent on the ambiguities. Nevertheless, the integer bootstrapping method is suitable for geometry-free or network processing ambiguity resolution, where the exact position of the stations is known.

5.2.4.2 Integer Least-Squares using Constant ratio test threshold (ILSC)

The ILS method as discussed in Section 4.4.3 and ratio test ambiguity validation using a constant test threshold (Section 4.4.4) are employed. The ambiguity validation and other parameter values are similar to those used in Geng et al. (2009, 2010d). The ratio test acceptance threshold is 3.0, the satellite elevation mask is 7.0 degrees, ambiguity resolution is only attempted for satellites above 15 degree elevation angle and a minimum of 1200 s carrier-phase lock time is required before attempting initial wide-lane or narrow-lane ambiguity resolution. Partial narrow-lane ambiguity resolution is used in this test: ambiguity

resolution is tested for all possible narrow-lane ambiguity combinations (Geng et al., 2009). The partial ambiguity fixing method was initially developed as the Minimum Constellation Method (MCM) in Schuster et al. (2012).

From the results, the average time required to obtain an initial ambiguity resolution is 1400 s and its SD is 460 s. The ambiguity resolution rate is 94%. The average position error at the initial ambiguity resolution epoch is shown in Figure 5.15. The average 3D, horizontal and vertical position errors are 8.2 (SD: 10.5 cm), 5.1 (SD: 8.9 cm) and 5.4 cm (SD: 6.6 cm), respectively.

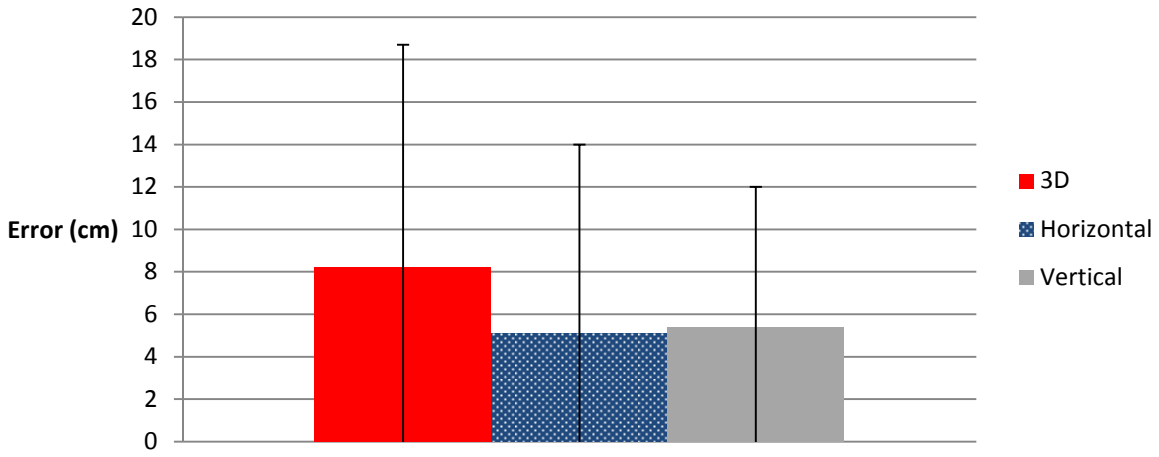

Figure 5.15 The average position error at the initial ambiguity resolution epoch using the ILSC method (one sigma standard deviation as error bars)

The distribution of the 3D position error at the initial ambiguity resolution epoch is divided into different categories in Figure 5.16. The 3D position error is larger than 10.7 cm in 20.8% of the cases where ambiguities are fixed.

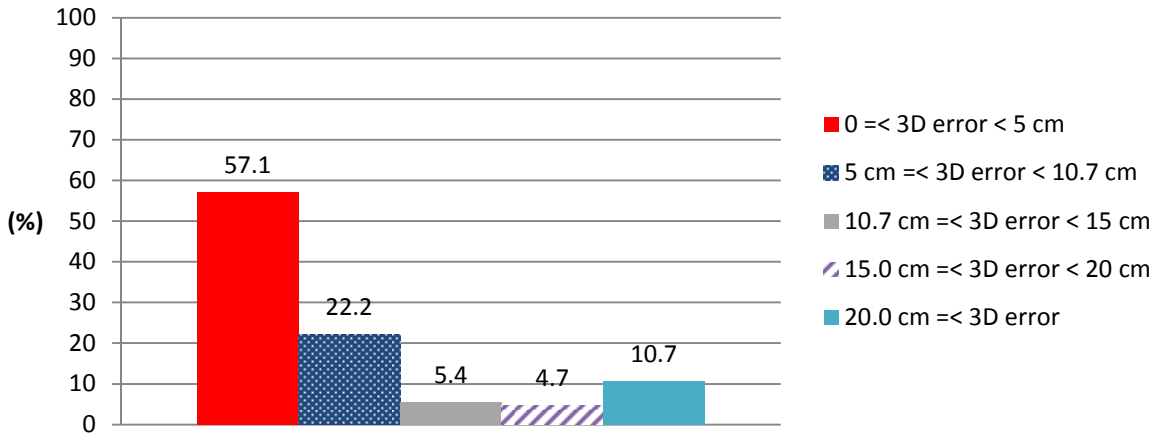

Figure 5.16 The distribution of 3D position error at the initial ambiguity resolution epoch using the ILSC method

Based on the results, the ILSC method provides better performance than the integer bootstrapping method in all aspects: the time needed to obtain an initial ambiguity resolution is shorter, ambiguity fixing rate is higher and average position error at the initial ambiguity resolution epoch and its SD are smaller. For example, the average 3D position error is 12.4 cm (SD: 13.7 cm) when employing the integer bootstrapping method and 8.2 cm (SD: 10.5 cm) when employing the ILSC method. There is a significant difference when comparing the distribution of the 3D position error at the initial ambiguity resolution epoch between the integer bootstrapping and ILSC methods, which can be seen in Figures 5.14 and 5.16. The rate of incorrect ambiguity resolution is significantly lower when using the ILSC method compared to the integer bootstrapping method.

Nevertheless, the ILSC method still suffers from various weaknesses: the rate of incorrect ambiguity resolution is high at 20.8 %. This is too large for real-life applications. In addition, there is no theoretical justification for using a constant ratio test threshold value of 3.0, chosen based on empirical experience. The lack of theoretical justification makes it is difficult to prove that the ILSC method is suitable for all possible situations such as the varying number of visible satellites or allowed failure rate.

5.2.4.3 Integer Least-Squares using Doubly Non-Central F-distribution based ratio test threshold (ILSDNCF)

The ILS method presented in Section 4.4.3 is employed. The ratio test is used for narrow-lane ambiguity validation and its acceptance threshold is calculated based on the assumed Doubly Non-Central F-distribution discussed in Section 4.4.4.1. This validation is carried out as described in Feng et al. (2012). Wide-lane ambiguity validation is done using the DBT method (Section 4.3.1.1). The elevation mask used is 5 degrees and ambiguity fixing is attempted for satellites with elevation angles higher than 10 degrees.

The required confidence level (1 - failure rate) for an initial narrow-lane ambiguity resolution is 99.9%. The MCM is employed and it is required that at least four narrow-lane ambiguities can be fixed initially.

Based on the results, an initial narrow-lane ambiguity resolution can be obtained on average in 194 s and the ambiguity fixing rate is 99.9%. However, the ambiguity resolution is incorrect in most cases as shown in Figure 5.17. The percentage of the cases where the 3D position error at the initial ambiguity resolution is larger than 10.7 cm is 95.0%.

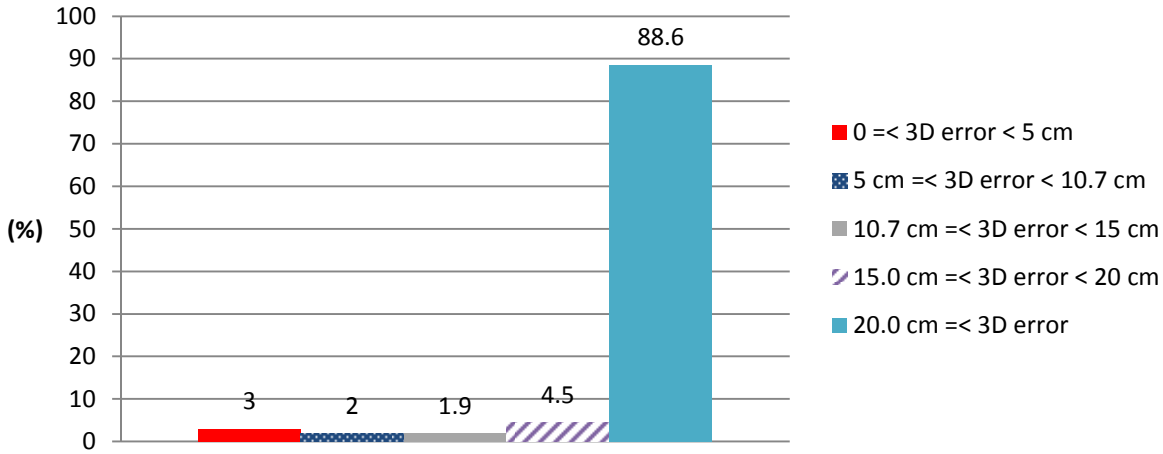

Figure 5.17 The distribution of 3D position error at the initial ambiguity resolution epoch using the ILSDNCF method

The issue is that it is too risky to fix narrow-lane ambiguities while the float position solution is still converging. It is often possible that an integer ambiguity candidate vector is sufficiently close to the float ambiguity vector, which causes the ratio test to be accepted

with a high confidence level. Nevertheless, the float ambiguities are far from the correct values. This leads to wrong ambiguity resolution.

To reduce the likelihood of incorrect ambiguity resolution, a minimum of 1200 s carrier-phase lock time is imposed before attempting initial ambiguity resolution. The requirement is similar to the ILSC method and is used also in Geng et al. (2010d). The lock-time requirement was not introduced when the ILSDNCF method was originally presented in Feng et al. (2010, 2012).

The average time required to obtain an initial ambiguity resolution is now 1560 s and its SD is 570 s. The ambiguity resolution rate is 87%. The average position error at the initial ambiguity resolution epoch is shown in Figure 5.18. The average 3D, horizontal and vertical errors are 6.3 (SD: 7.8 cm), 4.0 (SD: 6.7 cm) and 4.2 cm (SD: 4.7 cm), respectively. Compared to the integer bootstrapping and ILSC methods, the ILSDNCF method with the 1200 s lock time requirement provides the smaller magnitude of the position errors and their SDs.

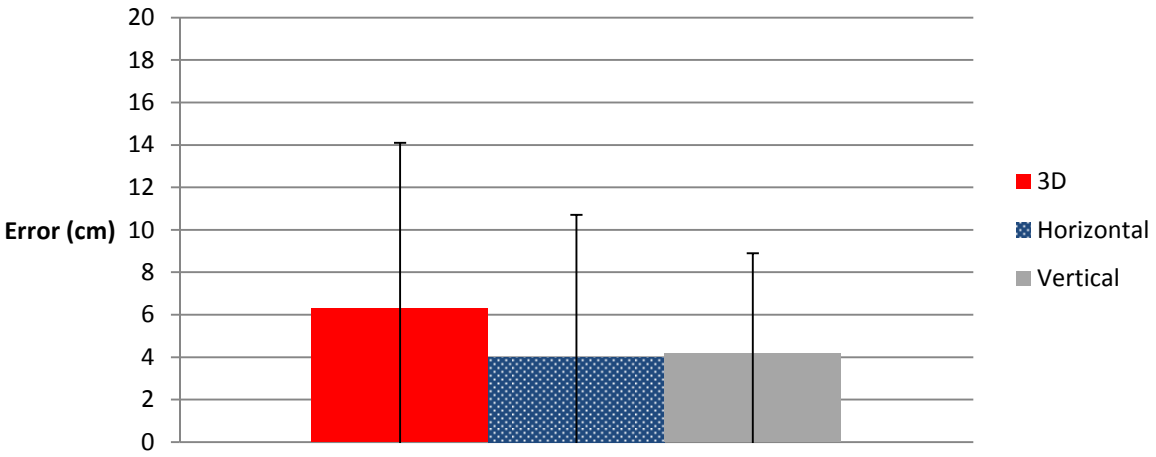

Figure 5.18 The average position error at the initial ambiguity resolution epoch using the ILSDNCF method with the 1200 s lock time requirement (one sigma standard deviation as error bars)

The distribution of the 3D position error at the initial ambiguity resolution epoch is shown in Figure 5.19. The position error at the initial ambiguity resolution epoch is larger than 10.7 cm in 14.6 % of the cases where ambiguities were fixed.

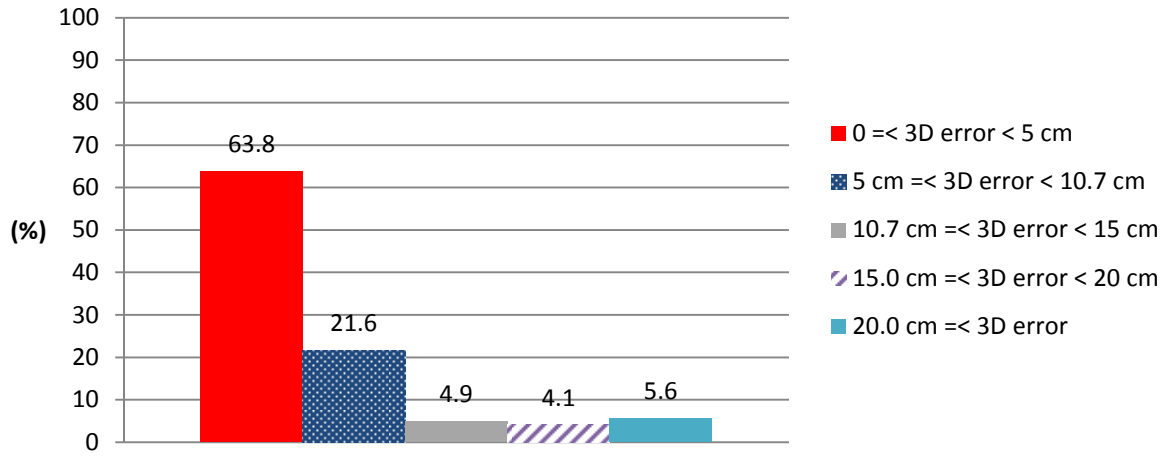

Figure 5.19 The distribution of 3D position error at the initial ambiguity resolution epoch using the ILSDNCF method with the 1200 s lock time requirement

Compared to the ILSC method, using the ILSDNCF method with the 1200 s lock time requirement reduced the average 3D position error at the initial ambiguity resolution epoch by 23.2% and reduced the percentage of cases with larger than 10.7 cm position error from 20.8% to 14.6%. The average time required to fix ambiguities increased by 11.4% and the ambiguity fixing rate decreased from 94% to 87%. The decrease in the overall ambiguity fixing rate reflects the smaller percentage of cases where ambiguities were fixed incorrectly.

5.2.4.4 Integer Least-Squares using Fixed Failure rate Simulation based method (ILSFFS)

The ratio test acceptance threshold is calculated using an approach similar to that in Verhagen and Teunissen (2013), based on the fixed failure rate, degrees of freedom and ILS failure rate. The allowed failure rate in this test is 0.1%. The MCM is employed. It is required that at least four narrow-lane ambiguities can be fixed initially. A similar ambiguity fixing and validation method is also used in Shi (2012). The elevation mask used is 5 degrees and ambiguity fixing is attempted for satellites with elevation angles higher than 10 degrees.

From the results, the time required to obtain an initial ambiguity resolution is 710 s with a standard deviation of 320 s. The ambiguity fixing rate is 99%. The position error at the initial ambiguity resolution epoch is shown in Figure 5.20, where the average 3D, horizontal and vertical errors are 16.7 (SD: 19.3 cm), 10.9 (SD: 15.2 cm) and 10.6 cm (SD: 13.8 cm), respectively. The large magnitude of the position error and its standard deviation is caused

by the large number of cases where ambiguities were fixed incorrectly. The distribution of the 3D position error at the initial ambiguity resolution epoch is shown in Figure 5.21. Based on the results, ambiguities are fixed very quickly and fixing can be performed in 99% of the cases. Nevertheless, ambiguities are fixed incorrectly in 42.2% of the cases. The reasons for the high rate of incorrect ambiguity resolution when employing the ILSFFS method are discussed later in this section.

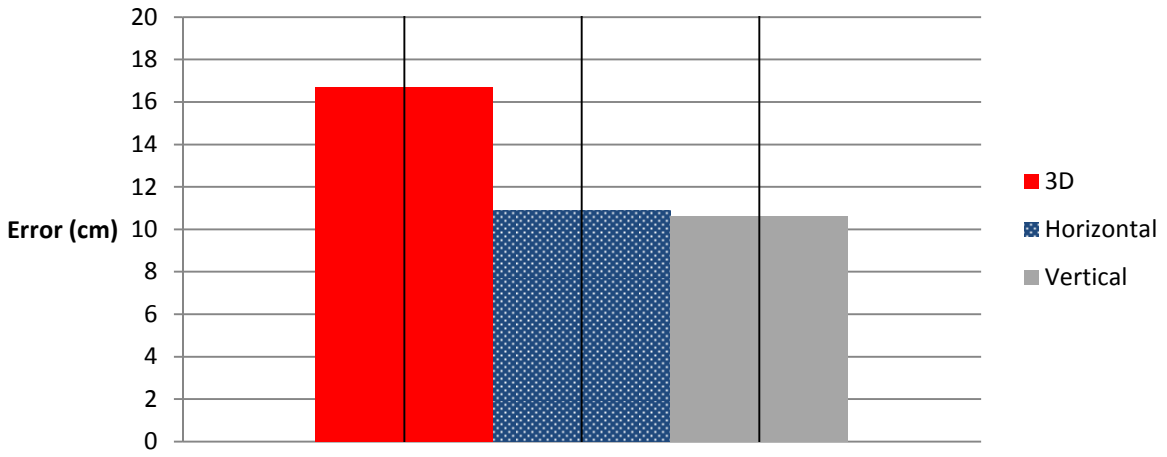

Figure 5.20 The average position error at the initial ambiguity resolution epoch using the ILSFFS method (one sigma standard deviation as error bars)

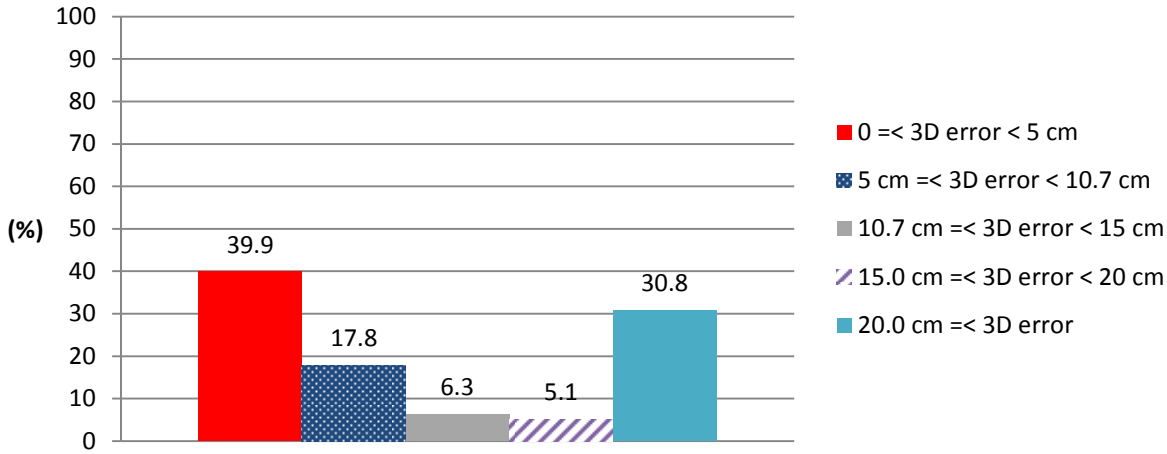

Figure 5.21 The distribution of the 3D position error at the initial ambiguity resolution epoch using the ILSFFS method

The ambiguity resolution test is carried out again by requiring at least a 1200 s carrier-phase lock time before attempting ambiguity resolution, similar to the tests carried out for the ILSC and ILSDNCF methods in the previous sections. The time required to obtain an initial ambiguity resolution was found to be 1310 s and the standard deviation 330 s. The position

error at the initial ambiguity resolution epoch is shown in Figure 5.22. The average 3D, horizontal vertical position errors are 9.7 (SD: 12.5 cm), 6.2 (SD: 10.5 cm) and 6.3 cm (SD: 7.9 cm), respectively. The distribution of the 3D position error at the initial ambiguity resolution epoch is shown in Figure 5.23. Ambiguity resolution can be obtained in 97% of the tested cases. The 3D position error at the initial ambiguity resolution epoch is larger than 10.7 cm in 25.2% of the cases when the ambiguities were fixed.

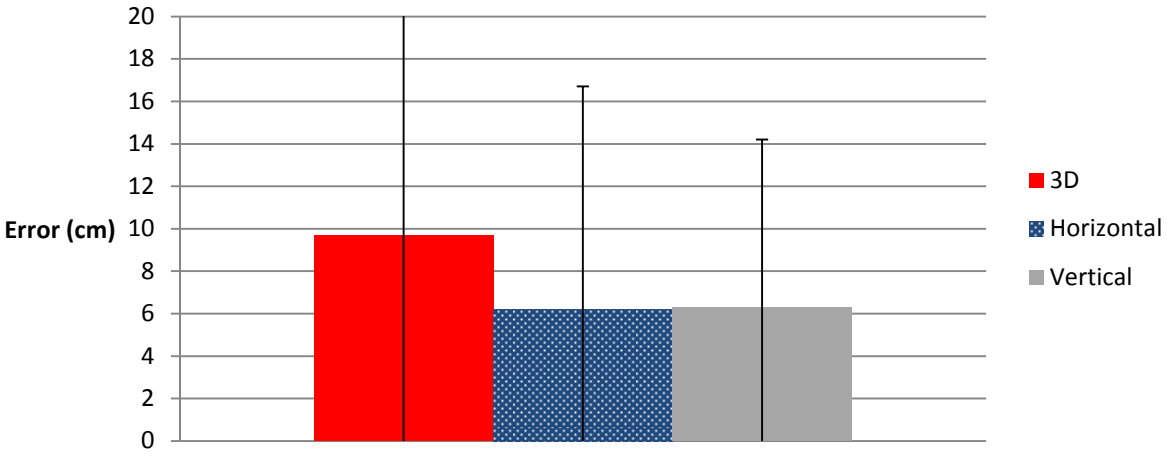

Figure 5.22 The average position error at the initial ambiguity resolution epoch using the ILSFFS method with 1200 s lock time requirement (one sigma standard deviation as error bars)

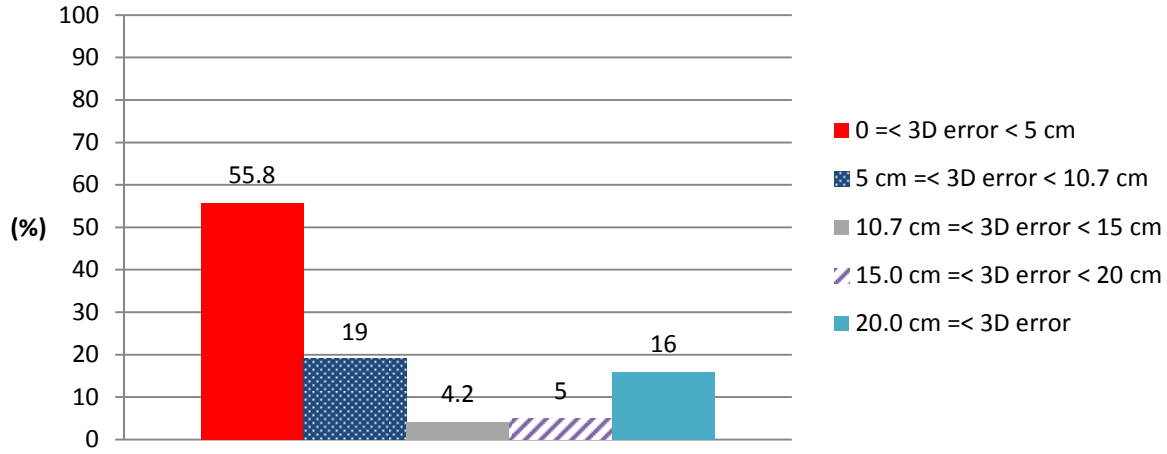

Figure 5.23 The distribution of 3D position error at the initial ambiguity resolution epoch using the ILSFFS method with 1200 s lock time requirement

Based on the results, introducing the 1200 s carrier-phase lock-time requirement does not reduce the rate of incorrect ambiguity resolution significantly, unlike in the case of the ILSDNCF method. When employing the ILSFFS method, the ratio test threshold is calculated based on the allowed failure-rate, degrees of freedom and ILS failure rate. The ILS failure

rate is estimated based on the success rate of the integer bootstrapping. However, calculating the integer bootstrapping success rate in a realistic way is not always possible when employing EKF for float PPP estimation. The reason for this is that the success rate is calculated based on the variance of float narrow-lane ambiguities, which is typically underestimated by EKF (Shi, 2012). This leads to unrealistically low ILS failure rates after the solution has converged for a few hundred seconds.

Using unrealistically low ILS failure rates is problematic when calculating the ratio test threshold, because it leads to very low ratio test thresholds. This increases the risk of incorrect ambiguity resolution, the primary problem of the ILSFFS method.

The ILSFFS method ratio test thresholds used in this experiment are the same as used in the Lambda software version 3.0 (Verhagen and Teunissen, 2013). It may be possible that the simulated thresholds are not optimal, because the simulation parameters may not reflect reality. It impossible to simulate a ratio test threshold for each particular ambiguity resolution case, because the simulation has large computational requirements. Even though the simulation would reflect the ambiguity resolution case perfectly, estimating realistic ILS failure rates is still a problem, when the aim is to use the method for fixed-ambiguity PPP.

5.2.4.5 Summary on the comparison of the methods

The results from the ambiguity resolution and validation tests are summarised in Table 5.3, where the ambiguity fixing rate, rate of correct ambiguity resolution, rate of incorrect ambiguity resolution, time required to obtain an initial ambiguity solution and position error at the initial ambiguity fix are shown for each method. The ambiguity resolution is identified as incorrect, if the 3D position error at the initial ambiguity resolution epoch is larger than 10.7 cm and as correct, if the position error at the initial ambiguity resolution epoch is smaller or equal to 10.7 cm. The elevation mask, ambiguity resolution elevation mask and carrier-phase lock-time requirement parameter values (Table 5.4) for the integer bootstrapping and ILSC methods are the same as used in literature. For the other methods, no any parameter values were given in the literature. Therefore, parameter values which are assumed to be suitable are used.

Method	Rate of ambiguity resolution (%)	Rate of correct ambiguity resolution (%)	Rate of incorrect ambiguity resolution (%)	Time to obtain an initial ambiguity resolution and its standard deviation (s)	Average position error 3D/Horizontal/ Vertical and their standard deviations (cm)
Integer bootstrapping	74.4	47.0	27.4	2030 (SD: 400 s)	12.4/5.8/9.9 (SD: 13.7/7.3/12.4)
ILSC	94.0	74.5	19.5	1400 (SD: 460 s)	8.2/5.1/5.4 (SD: 10.5/8.9/6.6)
ILSDNCF, no lock time requirement	99.9	5.0	94.9	190 (SD: 300 s)	63.8/39.3/43.7 (SD: 46.1/28.6/44.0)
ILSDNCF, 1200 s lock time requirement	86.9	74.2	12.7	1560 (SD: 570 s)	6.3/4.0/4.2 (SD: 7.8/6.7/4.7)
ILSFFS, no lock time requirement	99.4	57.4	42.0	710 (SD: 320 s)	16.7/10.9/13.8 (SD: 19.3/15.2/13.8)
ILSFFS, 1200 s lock time requirement	97.0	72.5	24.5	1310 (SD: 330 s)	9.7/6.2/6.3 (SD: 12.5/10.5/7.9)

Table 5.3: The summary of PPP ambiguity resolution and validation result

Method	Elevation mask (deg)	Ambiguity resolution elevation mask (deg)	Carrier-phase lock-time requirement (s)	Reference
Integer bootstrapping	15	15	1800	The PPP-wizard software (Laurichesse, 2011)
ILSC	7	15	1200	Geng et al. (2009, 2010d)
ILSDNCF, no lock time requirement	5	10	0	No any parameter values given in the literature
ILSDNCF, 1200 s lock time requirement	5	10	1200	
ILSFFS, no lock time requirement	5	10	0	
ILSFFS, 1200 s lock time requirement	5	10	1200	

Table 5.4: PPP ambiguity resolution and validation test parameters

Based on the results, the ILSDNCF method provides the smallest rate of incorrect ambiguity resolution when the 1200 s minimum lock time is required. The second best method in terms of the ambiguity resolution reliability is the ILSC method with a 1200 s lock-time requirement, which has a 19.5% rate of incorrect ambiguity resolution. The other methods are significantly worse in terms of the reliability of the ambiguity resolution. In terms of the correct ambiguity resolution rate, the ILSC method gives the highest rate of 74.5%. Nevertheless, the rate is only 0.3% percentage higher than the ILSDNCF method with the 1200 s minimum lock time requirement.

In terms of the average position error at the initial ambiguity resolution epoch and its standard deviation, the ILSDNCF method with 1200 s lock time requirement provides the smallest magnitude. In general, the standard deviation of the average position error is linked to the rate of incorrect ambiguity resolution. The standard deviation increases when the rate of incorrect ambiguity resolution increases. In addition, the standard deviation of the average position error is also linked to the float PPP performance discussed in Section 5.2.3. For example, large position errors in a float PPP solution impact also ambiguity resolution, because the errors may cause wrong ambiguity fixing.

The results in were based on using method specific parameter values. For a fair comparison, the results generated using the same parameters for all the methods are shown Table 5.5. The parameters used for the results in are: elevation mask of 5 degrees; the ambiguity resolution is carried out for the satellites above 10 degrees elevation and a 1200 s carrier-phase lock-time is required before attempting initial ambiguity resolution. There are no significant differences compared to the previous results shown in Table 5.3.

Method	Rate of ambiguity resolution (%)	Rate of correct ambiguity resolution (%)	Rate of incorrect ambiguity resolution (%)	Time to obtain an initial ambiguity resolution and its standard deviation (s)	Average position error 3D/Horizontal/ Vertical and their standard deviations (cm)
Integer bootstrapping	91.1	52.3	38.8	1490 (SD: 460 s)	13.3/8.0/9.2 (SD: 15.3/10.0/12.8)
ILSC	95.9	74.5	21.4	1330 (SD: 370 s)	8.3/5.4/5.3 (SD: 10.4/9.1/6.1)
ILSDNCF, 1200 s lock time requirement	86.9	74.2	12.7	1560 (SD: 570 s)	6.3/4.0/4.2 (SD: 7.8/6.7/4.7)
ILSFFS, 1200 s lock time requirement	97.0	72.5	24.5	1310 (SD: 330 s)	9.7/6.2/6.3 (SD: 12.5/10.5/7.9)

Table 5.5: The summary of PPP ambiguity resolution and validation results using the same parameters

Based on the analyses, the ILSDNCF with the 1200 s lock time requirement is chosen as the most promising method, because it provides the smallest rate of incorrect ambiguity resolution while achieving close to the highest rate of correct ambiguity resolution. This method is therefore, used for ambiguity validation in the enhanced PPP method developed later in this Chapter.

5.2.5 Imperial College Carrier Receiver Autonomous Integrity Monitoring (ICRAIM)

The ICRAIM method is tested in this thesis using four hours of real GNSS data recorded at the UNB3 IGS station on 30 December 2011 between 10 am and 2 pm UTC time. The same float PPP model with the same EKF implementation, PPP error corrections and filter and standard deviation parameters as in Section 5.2.3 is used. No failures are added to the data. Nevertheless, the data may include some failures caused, for example, by multipath or errors in satellite orbit and clock corrections. The position error is calculated based on the difference between the PPP estimated coordinates and the known IGS08 coordinates of the station.

The horizontal position error and its protection levels (HPL_1 and HPL_2) are shown in Figure 5.24. Based on the figure, the magnitude of the position error is larger than both the

protection levels most of the time. The possible reason for this may be the non-Gaussian nature of errors, such as tropospheric delay, site-displacement effects and satellite orbit and clock errors. For example, it is shown in Laurichesse (2011) that the accuracy of CNES satellite orbit corrections is occasionally worse than the typical accuracy shown in Table 3.1. Standard deviation parameters used in the PPP estimation are selected based on the typical accuracy of the error corrections. Therefore, the position standard deviation is underestimated, if the errors in the correction products are larger than assumed. The underestimated position standard deviation leads to underestimated protection levels. Calculating realistic protection levels is more difficult when employing PPP than cRTK, because non-Gaussian errors are not cancelled by differencing measurements across receivers.

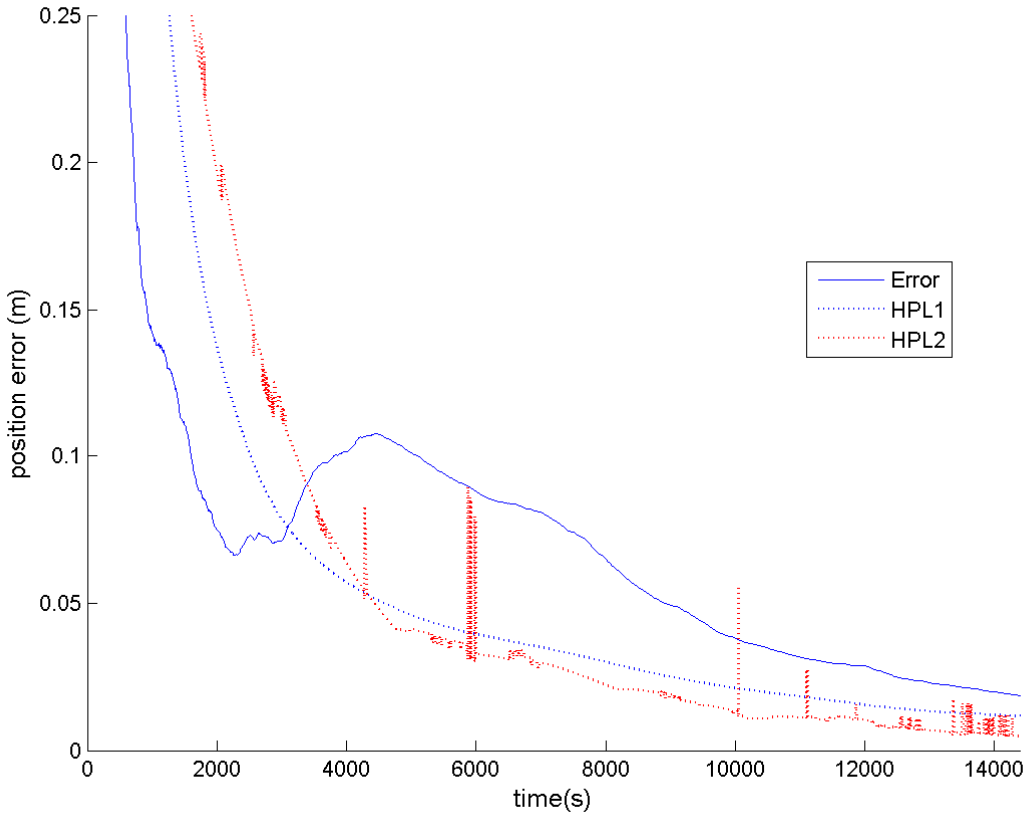

Figure 5.24 Horizontal position error and protection levels in the case of the ICRAIM test for the UNB3 IGS station

The vertical position error and its protection levels (VPL_1 and VPL_2) are shown in Figure 5.25. Based on the figure, VPL_1 is always larger than the position error, but VPL_2 is smaller than the position error during some time-periods. The reason for this is that VPL_2 is

calculated based on the Kalman gain, which has a small magnitude when the solution has converged. This is a feature of EKF, because when the magnitude of the EKF process noise is zero or small, the impact of new measurements is small after the solution has converged. Thus, the magnitude of the Kalman gain is small after solution convergence.

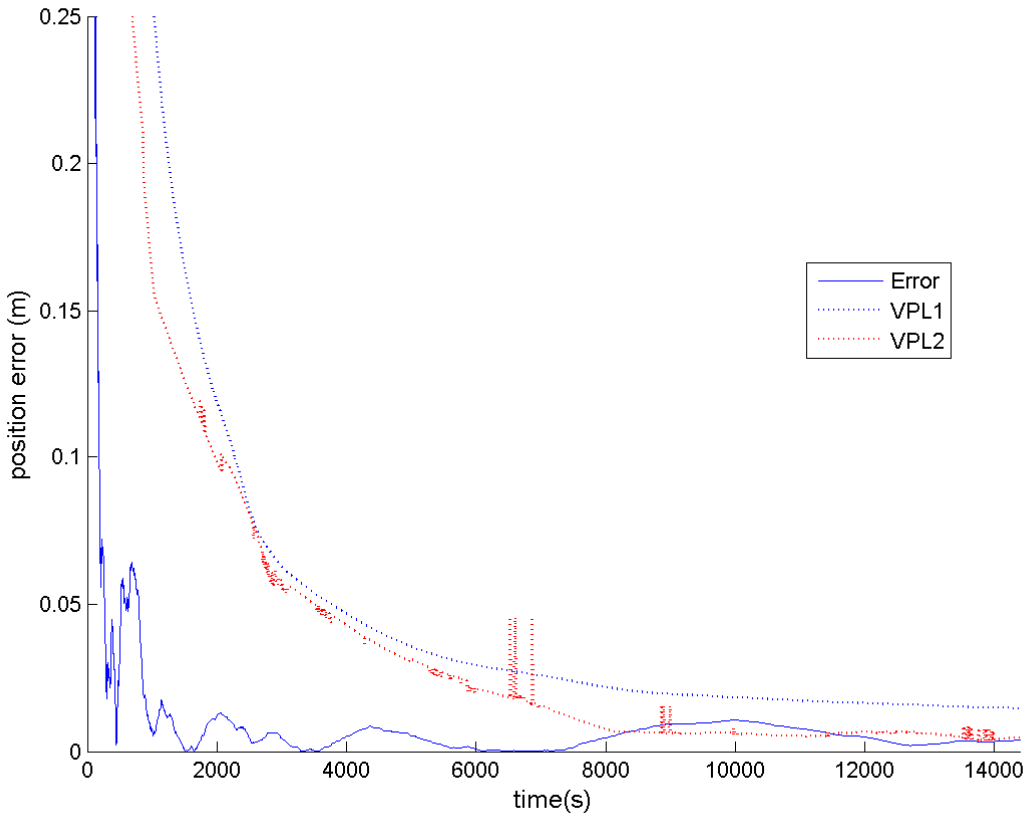

Figure 5.25 Vertical position error and protection levels in the case of the ICRAIM test for the UNB3 IGS station

This test demonstrates the difficulties associated with PPP integrity monitoring. The test case has been chosen intentionally to show that the non-Gaussian nature of the errors makes calculating realistic protection levels difficult. ICRAIM can provide realistic protection levels when errors are normally distributed.

5.2.6 Limitations of current Precise Point Positioning (PPP) methods

The limitations of the current PPP methods are analysed based on the results shown above. The performance of current methods is compared to the requirements of the applications, discussed in Chapter 2. The analysis is carried out on the basis of the solution convergence

time (Section 5.2.6.1), carrier-phase ambiguity resolution and validation approach (Section 5.2.6.2), positioning accuracy (Section 5.2.6.3), integrity monitoring performance (Section 5.2.6.4) and availability and performance of correction products (Section 5.2.6.5).

5.2.6.1 Solution convergence time

Based on the results from the float PPP tests in 5.2.3, it takes on average 1570 s to obtain 3D position error smaller than 10 cm and on average 2400 s to obtain 3D error smaller than 5 cm. The success rates of obtaining better than 10 or 5 cm 3D position errors are 88.0% and 55.4%, respectively, for the one hour datasets used.

Based on the fixed ambiguity PPP tests in Section 5.2.4, the ILSDNCF method with a 1200 s minimum lock time requirement was found to be the most suitable. The average time required to obtain an initial ambiguity resolution was found to be 1560 s, rate of correct ambiguity resolution 74.2% and rate of incorrect ambiguity resolution 12.7%. The time required to obtain 3D position errors better than 10 and 5 cm is 1310 and 1780 s, respectively. The success rates of obtaining 3D position errors better than 10 and 5 cm are 83.0% and 66.3%, respectively.

The results show that typical PPP solution convergence times are unacceptably long compared to the requirements of most applications. For example, many agricultural, aviation and LSB applications require immediate solution convergence to centimetre level accuracy. The long convergence time is the most important limiting factor which prevents the wider use of PPP.

The ionosphere-free combination is used by the PPP methods tested. The combination eliminates the first order ionospheric error, but magnifies measurement noise. The large magnitude of the noise makes convergence slow. In addition, the current fixed ambiguity PPP methods discussed in 4.3 employ GPS alone. In terms of the solution convergence, it would be beneficial to use also other GNSS systems such as GLONASS, to improve satellite geometry and increase measurement redundancy.

The insufficient quality of the error correction products such as satellite orbit and clocks and error models such as tropospheric models also impacts convergence in a negative way,

because it causes the position estimation to be sub-optimal. It is possible that the insufficient the quality of the error correction products is the reason why 10 cm position accuracy is not achieved in 12.0% of the tested cases in the float PPP tests in Section 5.2.3. The PPP performance issues caused, for example, by the insufficient accuracy of satellite orbit corrections are discussed in Laurichesse (2011). To achieve the best possible convergence, all error sources should be eliminated. However, this is impossible in practice.

Solution convergence time is also linked to the speed and reliability of initial ambiguity resolution. When employing PPP, correct narrow-lane ambiguity resolution can improve convergence to the 5 cm accuracy, because resolved ambiguities constrain the position error. However, as shown in Section 5.2.4, the reliability of the current fixed ambiguity PPP methods is not sufficient. The limitations of the current PPP ambiguity resolution methods are discussed in detail in the next Section.

5.2.6.2 Carrier-phase ambiguity resolution and validation

Ambiguity resolution and validation are the main challenges when employing fixed ambiguity PPP. Based on the tests in Section 5.2.4, the ILSDNCF method with a 1200 s lock time requirement is the most reliable method. However, the rate of incorrect ambiguity resolution is still 12.7%, unacceptably high for real-life applications.

The ratio test based on the ILSC, ILSDNCF and ILSFFS methods (Section 4.4.4) do not test the absolute correctness of the fixed ambiguity candidate vector. Instead they provide information on the closeness of the integer ambiguity candidate vector to the float ambiguity vector (Teunissen and Verhagen, 2008). Therefore, the integer ambiguity candidate vectors accepted could be incorrect, if the float ambiguity vector is incorrect, for example, as a result of multipath, insufficiently accurate correction products or other error sources.

In reality, it is often possible that a float position solution has large errors. For example, in the float PPP test in Section 5.2.3, 10 cm position accuracy is not achieved in 12.0 % of the cases. Therefore, the possibility of wrong float solution must be taken into account when validating carrier-phase ambiguities.

For example, when employing the ILSDNCF method with a 1200 s lock time requirement and using data recorded at the BDOS NOAA station on 12 February 2013 between 04:00 and 05:00, wrong ambiguity resolution occurs at the 1200 s epoch, as shown in Figure 5.26. The values of fixed and float ambiguities at the initial ambiguity resolution epoch are shown in Table 5.6. It can be seen that the float ambiguity values are close to integers. Thus, the ratio test accepts the fixed ambiguity candidate vector with the test statistic value of 19.47, when the threshold is 10.71. However, the float ambiguity values are far from correct, because the float position solution is still converging and the magnitude of the 3D position error is approximately 0.3 m. The correct float ambiguity values correspond to the case where the magnitude of the position error is zero. However, it is not possible to know the exact correct float ambiguity values when using real data. Thus, it is assumed that float ambiguities are far from correct when the position error is large (3D error more than 10.7 cm). In summary, this case shows that wrong ambiguity resolution may occur when using the ratio test alone and the float ambiguities are far from the correct values.

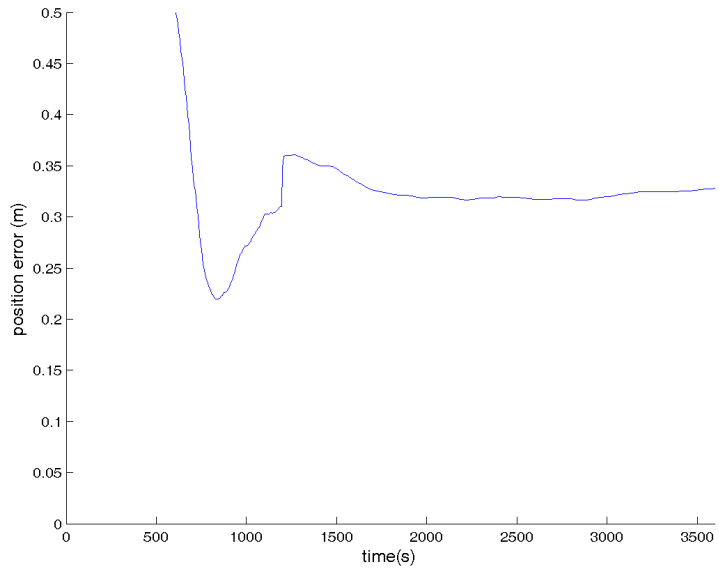

Figure 5.26 3D position error in the case of fixing ambiguities incorrectly

Satellite Pseudo Random Noise (PRN) Code	Base satellite Pseudo Random Noise (*PRN*) *Code*	Float ambiguity value (Narrow-lane cycles)	Fixed ambiguity value(Narrow-lane cycles)
16	11	97.29	97
19	11	7.99	8
30	11	-15.50	-16
23	11	-42.24	-42

Table 5.6 Ambiguity values in a wrong ambiguity resolution case

The reliability of ambiguity resolution is important when using PPP for real-life applications. The large incorrect ambiguity resolution rate of 12.7% is not acceptable even for non-life-critical applications such as land surveying. To make fixed-ambiguity PPP useful for practical applications, the incorrect ambiguity resolution rate closer to the cRTK method is required.

PPP ambiguity resolution with the GPS L1 and L2 signals without external ionospheric corrections is typically significantly more difficult than cRTK ambiguity resolution. The reason is that constraining the position error by employing the geometry-dependent wide-lane combination with the 86 cm wavelength and fixing the wide-lane ambiguities is not possible when employing PPP. Ionospheric errors affect the geometry-dependent wide-lane combination significantly as shown in equation (5.1), where $\frac{I_1}{f_1^2}$ and $\frac{I_1}{f_2^2}$ are the magnitudes of the first order ionospheric delays at the L1 and L2 frequencies, respectively, in metres. Based on this, the magnitude of the ionospheric delay in the geometry-dependent wide-lane combination can be at the metre level when measurements are not differenced across receivers. Thus, the combination cannot be used in PPP. This is the reason why geometry-dependent PPP ambiguity resolution must be carried out directly using the narrow-lane combination, which has a 10.7 cm wavelength. Measurement errors and inaccurate float solutions aggravate narrow-lane ambiguity resolution significantly more than wide-lane resolution, because of the short narrow-lane wavelength.

$$I_{wl} = \frac{1}{f_1 - f_2}\left(f_1 \frac{I_1}{f_1^2} - f_2 \frac{I_1}{f_2^2}\right) \tag{5.1}$$

The 10.7 cm wavelength of the narrow-lane combination is a limiting factor which prevents fast ambiguity resolution compared to cRTK. As discussed in 4.3.4, using the new GNSS signals and systems adds more possible geometry-dependent signal combinations which have longer wavelength than the GPS L1/L2 narrow-lane. As discussed in Section 4.3.4.1,

employing longer wavelength geometry-dependent signal combinations enables faster ambiguity resolution. However, the signals and systems are not currently available and cannot be used for practical applications.

Fixing GLONASS ambiguities when employing PPP is not practical as discussed in Section 4.3.3, because of the satellite/frequency/receiver type specific inter-frequency biases in GLONASS measurements. However, it is possible to use both GPS and GLONASS for the float solution estimation and fix GPS ambiguities as discussed in Section 5.3.3.

In conclusion, the major issues with the current ambiguity validation methods are the vulnerability for inaccurate float solutions, a high rate of wrong ambiguity resolution and low rate of correct ambiguity resolution.

5.2.6.3 Accuracy

There are applications such as control surveying which require millimetre-level accuracy. However, most applications require positioning accuracy between 1 and 10 cm. Based on the tests, fixed-ambiguity PPP can fulfil the requirement of accuracy between 1 and 10 cm in 3D, horizontal and vertical levels, if carrier-phase ambiguities are fixed correctly.

Similar to the solution convergence time, the quality of error correction products and models also impacts accuracy. If the magnitude of the residual error after applying correction products and models is significantly large compared to the total error budget shown in Table 3.4, the PPP solution may not converge to the required accuracy and correct narrow-lane carrier-phase ambiguity resolution may not be possible.

Wrong ambiguity resolution can also result insufficient positioning accuracy. Based on the example shown Section 5.2.6.2, where ambiguities were fixed incorrectly at the initial ambiguity resolution epoch, horizontal and vertical position errors and protection levels are shown in Figures 5.27 and 5.28. This shows that the ICRAIM method cannot be used to detect errors caused by wrong ambiguity resolution, because the position solution is self-consistent with the wrongly fixed ambiguities. The reason for the self-consistency is that the position solution is re-calculated based on the incorrectly fixed ambiguities. Therefore, the

magnitude of the measurement residuals is small and the solution can pass the ICRAIM based integrity check.

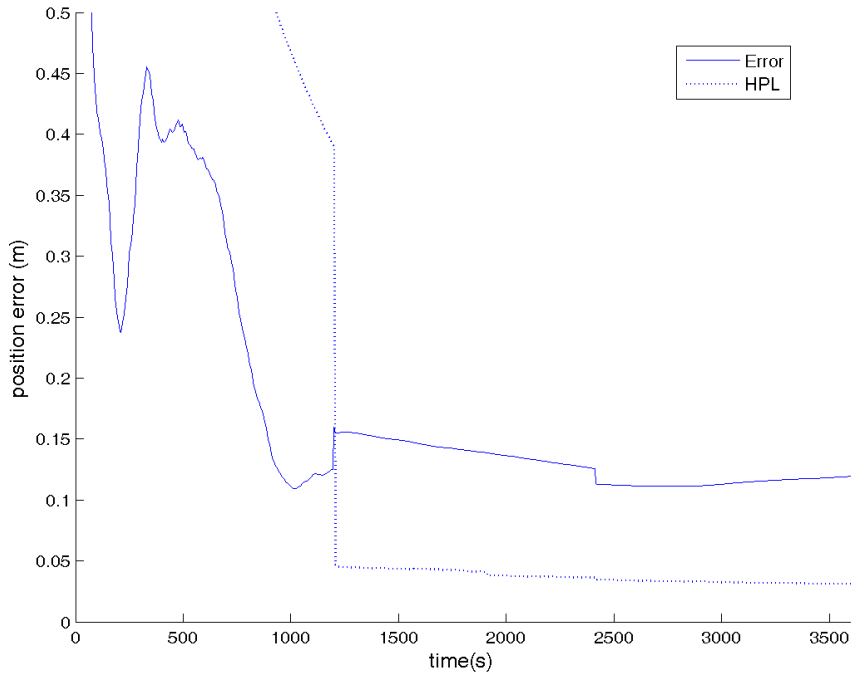

Figure 5.27 Horizontal position error and Protection Level (HPL) in the case of fixing ambiguities incorrectly

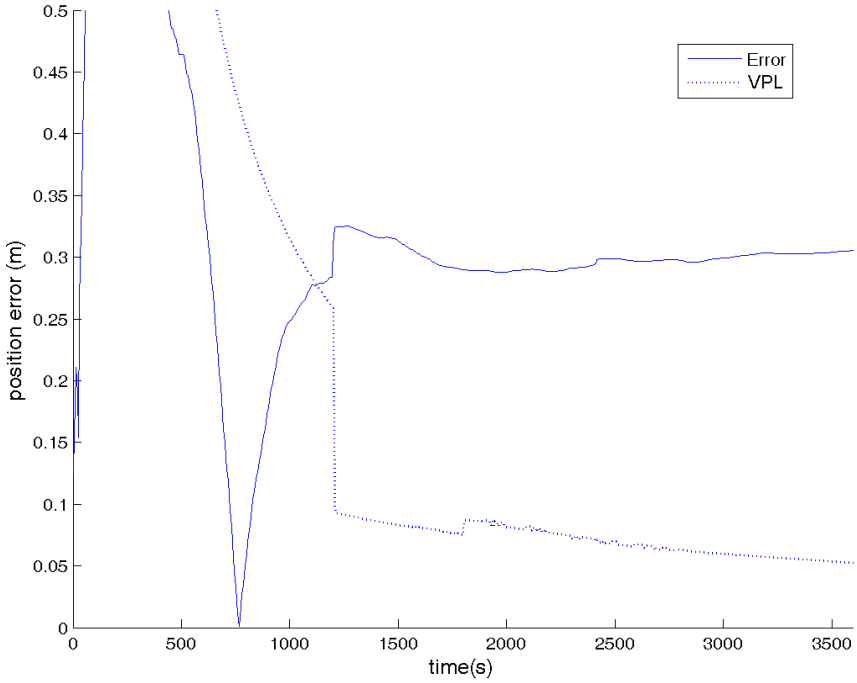

Figure 5.28 Vertical position error and Protection Level (VPL) in the case of fixing ambiguities incorrectly

In general, real-time PPP using the L1 and L2 signals can provide sufficient accuracy when ambiguities are fixed correctly or the solution has converged over a sufficiently long time (at least 30 min). However, the primary issue when using PPP for real-life applications is to guarantee the accuracy, i.e. to monitor the integrity.

5.2.6.4 Integrity monitoring

When employing cRTK with a short, for example, 2 km baseline, most errors in the measurements are removed or mitigated by differencing the measurements across receivers. The significant error sources which are left after the differencing are measurement noise, multipath, satellite orbit and errors caused by satellite or user equipment failures. Ionospheric errors are typically significantly mitigated by differencing measurements across receivers, unless ionosphere conditions are extreme (scintillation or ionosphere storms). Satellite orbit errors are also significantly mitigated, unless there is a significant failure in the broadcast satellite orbit predictions.

When using PPP, errors cannot be cancelled or mitigated by differencing measurements across receivers. Therefore, PPP integrity monitoring is significantly more difficult compared to cRTK. Errors which can impact PPP when using the L1/L2 ionosphere-free combination are satellite orbit, satellite clock, tropospheric, higher-order ionospheric and site-displacement errors. These errors increase the probability of incorrect ambiguity resolution with respect to cRTK.

The ICRAM method (Feng et al., 2010) enables PPP integrity monitoring. However, it may not detect errors which are common to multiple satellites, for example, site-displacement errors. Also slowly changing errors in satellite orbit and clock corrections are difficult to detect using ICRAM, because carrier-phase ambiguity terms become consistent with the errors, if the errors have already occurred during solution convergence. If the ambiguity terms are consistent with the errors, residuals for the problematic satellites are small and ICRAIM integrity monitoring is not triggered. In addition, ICRAM may not detect errors caused by incorrect ambiguity resolution, as discussed in Section 5.2.6.3.

To provide high integrity PPP, integrity must be monitored both during product generation and rover operation. Currently, little research has been carried out on using PPP for safety

critical applications, which have specific requirements in terms of the integrity risk, alert limit and time to alert. Defining the total integrity risk of fixed-ambiguity PPP requires understanding of the integrity risk of product generation, float solution calculation and integer ambiguity resolution. Calculating the integrity risk of ambiguity resolution is particularly difficult, because the correctness of the ambiguity resolution depends on the quality of the float position solution.

The integrity risk of correction product generation is not taken into account by the current PPP methods. Estimating the risk would require correction providers to monitor the integrity of the product generation and transmission of the integrity risk estimates to rover receivers. In addition, the current PPP methods do not address the integrity risk of ambiguity resolution caused by inaccurate float PPP solutions.

5.2.6.5 Availability and performance of correction products

The major challenge in the generation of the correction products is the reliability and accuracy of the products. The accuracy of satellite orbit and clock corrections products can vary by time. Sometimes, the products cannot achieve the specified accuracy.

The orbit corrections used with the CNES real-time satellite clock corrections are based on the ultra-rapid orbit predictions (Laurichesse, 2011). There is a three to nine hour delay between the time of collecting the data, which is used to generate the predictions, and the application of the predictions by the rover. Under specific conditions, for example, when multiple satellites are eclipsing (Section 3.4.10), the long time between collecting the data for product generation and applying the products can make the accuracy of the orbit predictions unacceptable (Laurichesse, 2011).

Based on the float PPP test in Section 5.2.3, it is not possible to obtain 3D position errors smaller than 10 cm in 12.0% of the test cases. The most likely reason for this is insufficient accuracy of the orbit and clock corrections. The CNES corrections are still an experimental product and therefore, their quality cannot be guaranteed.

To increase the suitability of PPP for the applications discussed in Chapter 2, the integrity of real-time satellite orbit and clock correction products must be improved. For example, this

could be achieved by generating satellite orbit corrections in real-time, as achieved by some commercial PPP services (Leandro et al., 2011a). In addition, as discussed in Section 5.2.6.4, integrity monitoring of the correction products generation must be improved and integrity risk estimates must be provided for rover receivers.

5.3 Development steps of the enhanced PPP method

The enhanced PPP method is developed in this thesis to address the limitations of the current methods discussed in the previous sections. The enhanced PPP method uses an approach to the float position computations similar to that described in Section 4.2. Thus, the same PPP error corrections and models, EKF parameters, cycle-slip detection and correction methods and other parameters are used as in the tests presented in Section 5.2.

This enhanced PPP method includes enhanced ambiguity validation, the integration of GPS and GLONASS measurements, improved integrity monitoring and use of NWM based tropospheric corrections when available. The most important novelty of the enhanced PPP method is enhanced ambiguity validation (Section 5.3.2), which consists of time-window based ambiguity validation and additional validations to make incorrect ambiguity resolution less likely. Compared to the current methods in the literature, the enhanced ambiguity validation method can provide significant improvements in terms of the rates of correct and incorrect ambiguity resolution and magnitude of the position error at the initial ambiguity resolution epoch. An additional novelty of the enhanced PPP method is integration of GPS and GLONASS measurements in the case of fixed ambiguity PPP (Section 5.3.3). GPS ambiguity resolution is attempted and GLONASS ambiguities are kept as float. Employing both GPS and GLONASS is beneficial, because it typically improves float solution convergence leading to faster ambiguity resolution. In addition, novel improvements to integrity monitoring (Section 5.3.4) are presented including improved protection level calculation and failure exclusion.

The next sections explain the details of the enhanced PPP method, including its tuneable parameters and the relative improvement achieved.

The enhanced PPP method is designed to be used with the CNES real-time satellite clock and orbit corrections. Therefore, optimal ambiguity validation and measurement weighting

parameters may be different if other products are used. Only the GPS and GLONASS L1 and L2 signals are used by the enhanced PPP method, because the method is designed for real-life applications using the currently available signals.

5.3.1 The Minimum Constellation Method (MCM) with ILSDNCF

Based on the existing fixed ambiguity PPP ambiguity validation method tests presented in Section 5.2.4, the ILSDNCF method with a 1200 s carrier-phase lock-time limitation was chosen as the most reliable. Therefore, this method is also used in the enhanced PPP method. However, the empirically chosen 1200 s lock-time limitation is not used in the enhanced method, because the lock time limitation can only prevent problems caused by inaccurate PPP float solution during the solution convergence period. In addition, the solution convergence, for example, to better than 10 cm 3D position errors can sometimes take more than 1200 s or sometimes the convergence may also be significantly faster. Instead of the 1200 s lock-time limitation, alternative methods are used to enhance the ILSDNCF method.

The Minimum Constellation Method (MCM), developed in Schuster et al (2012), is used when there are more than four float ambiguities available. In general, obtaining full ambiguity resolution is difficult when employing PPP, because float ambiguities are vulnerable to multiple error sources such as FCB and multipath. Therefore, it is often possible that multiple float ambiguities are far from the nearest integers, even though the float position solution has converged.

The principle of the MCM is to attempt ambiguity resolution with all possible sub-set combinations of float ambiguities if the full set cannot be used. For example, if there are five narrow-lane float ambiguities available, ambiguity resolution can be attempted for one five-satellite group and five four-satellite groups. The benefit of employing the MCM is to achieve fast initial ambiguity resolution by exploiting measurement sub-sets that have the required quality and geometry conditions.

The required computation time increases when the number of ambiguity combinations increases. To reduce the amount of computational power required when attempting initial ambiguity resolution, narrow-lane ambiguity groups consisting of low elevation satellites

(below 15 degrees) or narrow-lane ambiguity groups with high Position Dilution Of Precision (PDOP) can be excluded when there are more than nine float narrow-lane ambiguities available. Nine is chosen as the threshold as a compromise between the number of combinations to test and required computational processing power. For example, there are 126 four ambiguity groups to test when there are nine float narrow-lane ambiguities available. The number increases to 210 when there are ten float narrow-lane ambiguities available. The low elevation (below 15 degrees) float narrow-lane ambiguities are often affected by error sources such as multipath. Therefore, they are so far from the nearest integer that resolving them is nearly impossible. Thus, excluding low elevation satellites have a minimal impact on the ambiguity resolution rate. The same applies to the satellite combinations with high PDOP. The processing power requirement is not a limiting factor, if the PPP estimation is done using a desktop computer. Nevertheless, the available processing power is an important design criteria, if the PPP estimation is done using embedded processors, for example, running PPP estimation using a Central Processing Unit (CPU) integrated to a GNSS receiver.

MCM was used in Section 5.2.4 to test the ILSC, ILSDNCF and ILSFFS ambiguity resolution and validation methods. The use of MCM for PPP ambiguity resolution is not completely new: partial ambiguity resolution similar to MCM is used in Geng et al. (2009) and Verhagen and Teunissen (2013). However, MCM is not used in the literature, when ambiguity resolution and validation is based on the ILSDNCF method.

When employing MCM, there may be more than one ambiguity candidate vector accepted by the ratio test. Therefore, the best ambiguity candidate vector is determined as the one with the largest number of fixed ambiguities in the vector and the highest ratio test statistic.

In the enhanced PPP method, MCM is used to test the ambiguity resolution for all possible combinations of float ambiguities, and ambiguity validation is based on the ILSDNCF method. No carrier-phase lock-time requirement is employed.

5.3.2 Enhanced ambiguity validation

The novel enhancements to increase the reliability of the ILSDNCF method are discussed in this section. These include time window based ambiguity validation (Section 5.3.2.1) and

additional validations (Sections 5.3.2.2) to reduce the probability of incorrect ambiguity resolution.

5.3.2.1 Time window based ambiguity validation

The principle of time window based ambiguity validation is to require that the best ambiguity candidate vector is the same over a given number of epochs consecutively and that the ambiguities belonging to that vector can be fixed to the same integers during the chosen time-period. The theory behind this test is that the float ambiguities change when the float solution is converging. Therefore, if for the given time window the best ambiguity candidate vector is the same and the ambiguities in the vector are fixed to the same values, then it is less likely that float ambiguities have not converged to the correct values and are close to the nearest integer.

Ambiguity resolution is tested with multiple time window lengths such as 1, 50, 150, 250 and 500 s using the NOAA dataset and ILSDNCF method. The required confidence level of ambiguity validation is set to 99.9%. The results are shown in Table 5.7 and analysed in terms of the rate of ambiguity resolution, rate of correct ambiguity resolution, rate of incorrect ambiguity resolution, time required to obtain an initial ambiguity resolution and position error at the initial ambiguity resolution epoch.

Time window length (s)	**Rate of ambiguity resolution (%)**	**Rate of correct ambiguity resolution (%)**	**Rate of incorrect ambiguity resolution (%)**	**Average time to obtain an initial ambiguity resolution and its standard deviation (s)**	**Average position error 3D/Horizontal/ Vertical and their standard deviations (cm)**
1	99.9	5.0	94.9	190 (SD: 300 s)	63.8/39.3/43.7 (SD: 46.1/28.6/44.0)
50	97.1	44.8	52.4	850 (SD: 600 s)	17.8/12.4/10.5 (SD: 17.5/13.9/12.8)
150	89.2	72.7	16.4	1460 (SD: 690 s)	7.3/4.6/4.7 (SD: 8.9/7.7/5.5)
250	80.4	74.1	6.3	1830 (SD: 720 s)	4.6/2.6/3.4 (SD: 4.7/3.7/3.5)
500	54.7	53.4	1.3	2290 (SD: 670 s)	3.6/1.8/2.8 (SD: 2.6/1.7/2.5)

Table 5.7 The effect of the selected time window length on ambiguity resolution results

The idea of using the time-window based ambiguity validation for fixed-ambiguity PPP is novel and developed in this thesis. When employing cRTK, the time window based ambiguity validation was used to complement the ILSC method based carrier-phase ambiguity validation in Wei and Schwarz (1995). However, using the time-window based ambiguity validation with the ILSDNCF method has not been attempted, even with cRTK. In addition, time-window based ambiguity validation is not used for PPP ambiguity validation in the literature. Therefore, the time-window based ambiguity validation can be defined a new PPP development, even though the idea of it is not completely novel.

Using the time-window based ambiguity validation is particularly useful for PPP, because it verifies that float narrow-lane ambiguities with 10.7 cm wavelength have stabilised sufficiently before deciding ambiguity fixing. The narrow-lane ambiguities in the PPP estimation are particularly vulnerable to errors in measurements and correction products, because of the short wavelength. The time window based ambiguity validation ensures that ambiguity resolution is not done only based on the one acceptance of the ratio test as in the case of the current methods presented in the literature. It is often possible that float ambiguities are sufficiently close to some (wrong) integers that the ratio test is accepted for a few epochs. Nevertheless, it is significantly less likely that the float ambiguities would remain close to incorrect integers for long time periods such as 150 s.

The time window lengths of 150 and 250 s are selected for further investigation, because they give a good compromise between the rate of correct and incorrect ambiguity resolution, time required to obtain an initial ambiguity resolution and average position error and its standard deviation at the initial ambiguity resolution epoch. For the time window lengths of 1 and 50 s, the magnitude of the average position error at the initial ambiguity resolution epoch is unacceptably large. On the other hand, long time window lengths such as 500 s provide a small average position error, but the obtained rate of ambiguity resolution (54.7%) is unacceptably low.

5.3.2.2 Additional validations to make incorrect ambiguity resolution less likely

When employing the LAMBDA method implementation, the number of float narrow-lane ambiguities in a vector must be at least four. However, requiring that only four narrow-lane

ambiguities are fixed initially is not always optimal, because it is more likely that inaccurate float solution estimation can result in incorrect ambiguity resolution. The probability that all float ambiguities are close to wrong integers decreases when the number of ambiguities to test increases. Therefore, ambiguity resolution is tested by requiring that at least four, five and six ambiguities are fixed initially using the NOAA dataset. The length of the ambiguity validation time window in this test is 150 s and required confidence level is set to 99.9%. The results are shown in Table 5.8. The requirement of fixing initially at least five narrow-lane ambiguities gives a good compromise between the reliability and ambiguity resolution rate when the time window length is 150 s. The reliability is measured in terms of the rate of incorrect ambiguity resolution and average position error and its standard deviation at the initial ambiguity resolution epoch.

Minimum number of narrow-lane ambiguities	**Rate of ambiguity resolution (%)**	**Rate of correct ambiguity resolution (%)**	**Rate of incorrect ambiguity resolution (%)**	**Average time to obtain an initial ambiguity resolution and its standard deviation (s)**	**Average position error 3D/Horizontal/ Vertical and their standard deviations (cm)**
4	89.2	72.7	16.4	1460 (SD: 690 s)	7.3/4.6/4.7 (SD: 8.9/7.7/5.5)
5	78.8	70.9	7.9	1610 (SD: 790 s)	5.5/3.1/3.9 (SD: 6.7/5.3/4.6)
6	60.9	58.0	2.9	1670 (SD: 810 s)	4.2/2.2/3.2 (SD: 5.0/3.7/3.7)

Table 5.8 The effect of requiring initial ambiguity resolution for more than four narrow-lane ambiguities (150 s time window)

Table 5.9 shows the ambiguity resolution results when the length of the time window is 250 s and the required confidence level is 99.9%. The ambiguity resolution rate is already as low as 80.4% when at least four ambiguities are initially required to be fixed. Increasing the minimum number of narrow-lane ambiguities to be fixed would further decrease the fixing rate. That is shown in Table 5.9 when at least five ambiguities are initially required to be fixed.

Minimum number of narrow-lane ambiguities	Rate of ambiguity resolution (%)	Rate of correct ambiguity resolution (%)	Rate of incorrect ambiguity resolution (%)	Average time to obtain an initial ambiguity resolution and its standard deviation (s)	Average position error 3D/Horizontal/ Vertical and their standard deviations (cm)
4	80.4	74.1	6.3	1830 (SD: 720 s)	4.6/2.6/3.4 (SD: 4.7/3.7/3.5)
5	70.1	67.3	2.9	1900 (SD: 780 s)	3.9/2.0/3.0 (SD: 3.3/2.3/2.9)

Table 5.9 The effect of requiring initial ambiguity resolution for more than four narrow-lane ambiguities (250 s time window)

When employing the ILSDNCF method, the ratio test statistic must be larger than the threshold for an integer ambiguity candidate vector to be accepted. The variable confidence level method is developed in this thesis. The variable confidence level method cannot be considered as a new development, but it can be considered as a more optimal way of employing the ILSDNCF method. The principle of the variable confidence level method is to use a confidence level threshold value of 99.99% during the float solution convergence period and 99.00% otherwise. The solution is defined to be in the convergence period when the longest carrier-phase lock time is smaller than 2000 seconds. The reason for using a higher threshold during the float solution convergence period is that the position error is typically larger during this period. Thus, it is more likely that float ambiguities are close to wrong integers.

The results of the comparison of the use of constant confidence levels of 99.00%, 99.90% and 99.99% during the whole test and a variable confidence level are shown in Table 5.10. The results show that the higher confidence level of 99.99% during the convergence period is beneficial in terms of reducing the rate of incorrect ambiguity resolution. On the other hand, it is beneficial to use a lower confidence level (99.00%) after the solution has converged to increase the rate of correct ambiguity resolution. When using a time window length of 250 s and requiring that at least four ambiguities are fixed initially, the variable confidence level method reduced the incorrect ambiguity resolution rate from 6.3% to 4.5% and increased the correct ambiguity resolution rate from 74.1% to 82.0% compared to using the constant confidence level 99.9%. When the time window length is 150 s and an initial fix of five ambiguities is required, the variable confidence level method reduces the rate of incorrect ambiguity resolution from 7.9% to 6.0% and increases the rate of correct

ambiguity resolution from 70.9% to 80.8% compared to using the constant confidence level 99.9%. Employing the variable confidence level method is also beneficial in terms of reducing average position error and its standard deviation at the initial ambiguity resolution epochs.

Confidence level (%)	Confidence level during convergence (%)	Time window (s)	Minimum number of narrow-lane ambiguities	Rate of ambiguity resolution (%)	Rate of correct ambiguity resolution (%)	Rate of incorrect ambiguity resolution (%)	Average time to obtain an initial ambiguity resolution and its standard deviation (s)	Average position error 3D/Horizontal/ Vertical and their standard deviations (cm)
99.00	99.00	250	4	92.1	79.9	12.2	1530 (SD: 670 s)	6.2/3.6/4.3 (SD: 7.4/5.8/5.2)
99.00	99.00	150	5	91.7	71.6	20.2	1270 (SD: 690 s)	8.6/5.3/5.7 (SD: 11.6/9.1/8.1)
99.90	99.90	250	4	80.4	74.1	6.3	1830 (SD: 720 s)	4.6/2.6/3.4 (SD: 4.7/3.7/3.5)
99.90	99.90	150	5	78.8	70.9	7.9	1610 (SD: 790 s)	5.5/3.1/3.9 (SD: 6.7/5.3/4.6)
99.00	99.99	250	4	86.5	82.0	4.5	2190 (SD: 600 s)	4.3/2.4/3.1 (SD: 4.1/3.3/3.1)
99.00	99.99	150	5	86.0	80.8	6.0	1970 (SD: 650 s)	4.5/2.5/3.3 (SD: 4.7/3.8/3.4)
99.99	99.99	250	4	60.8	59.4	1.3	2130 (SD: 730 s)	3.6/1.8/2.7 (SD: 2.9/1.9/2.5)
99.99	99.99	150	5	57.1	55.0	2.1	1870 (SD: 790 s)	3.9/2.0/2.9 (SD: 3.5/2.6/2.8)

Table 5.10 The effect of requiring initial ambiguity resolution for more than four narrow-lane ambiguities

5.3.2.3 Selection of the optimal ambiguity validation parameters

When employing the enhanced PPP method, the ambiguity validation parameters are: the required confidence level during the convergence period and afterwards, length of the validation time-window and minimum number of ambiguities required to be fixed initially. The parameters are selected based on the required performance in terms of the rate of correct and incorrect ambiguity resolution, time required to obtain an initial ambiguity resolution and position error at the initial ambiguity resolution epoch. The required computational power is dependent on the minimum number of narrow-lane ambiguities to fix initially, which determines the number of combinations to be tested with the MCM approach. Ambiguity resolution is attempted immediately since starting PPP, unlike the current methods tested in Section 5.2.4.

Based on the tests with the NOAA dataset, there are two most suitable parameter combinations, shown in Table 5.11. Among the combinations tested, combination 1 gives the highest rate of correct ambiguity resolution, lowest rate of incorrect ambiguity resolution and smallest position error at the initial ambiguity resolution epoch. On the other hand, combination 2 gives a slightly lower rate of correct ambiguity resolution, a higher rate of incorrect ambiguity resolution and larger position error at the initial ambiguity resolution epoch. However, the time required to obtain an initial ambiguity resolution and computational power requirements are lower. Based on the analysis, both combinations are suitable for the enhanced PPP method.

Combination	Confidence level (%)	Confidence level during convergence (%)	Time window (s)	Minimum number of narrow-lane ambiguities
1	99.00	99.99	250	4
2	99.00	99.99	150	5

Table 5.11 The most suitable parameter combinations when using the enhanced PPP method

5.3.3 Using both GPS and GLONASS to calculate float position solution

Only GPS measurements are used when employing the current fixed ambiguity PPP methods presented in the literature. However, adding GLONASS to the position estimation is attractive, because of the current availability of a full constellation of GLONASS satellites (IAC, 2012). Using GLONASS with GPS for position estimation can, for example, improve satellite geometry and increase the number of atmospheric pierce points to better estimate tropospheric delays. Therefore, using GLONASS with GPS is expected to improve float PPP convergence and accuracy over GPS-only approaches.

Although the addition of GLONASS improves the performance of float PPP estimation, it is not used for fixed ambiguity PPP in the literature. The issues on GLONASS PPP ambiguity resolution are discussed in Section 4.3.3. In general, GLONASS PPP ambiguity resolution is difficult, because there are code and phase biases in the measurements, which are difficult to calibrate. On the other hand, employing both GLONASS and GPS measurements to estimate the float position solution is straightforward and expected to provide performance benefits.

BSD GPS and un-differenced GLONASS measurements are used in this thesis. The EKF is updated separately with GPS and GLONASS measurements. Only GPS ambiguity resolution is attempted and GLONASS ambiguities are kept as float.

The impact of employing both GPS and GLONASS to calculate a float PPP solution is tested. The performance between GPS only and GPS with GLONASS cases is compared. For the GPS-only approach, the processing parameters and results are identical to those discussed in Section 5.2.3.

It is assumed that the quality of GLONASS satellite orbit and clock corrections is worse than the quality of the GPS corrections. The reasons for the worse quality of the GLONASS corrections are: the lack of global reference network stations (Laurichesse, 2013), which are used to collect data for orbit and clock estimation, difficulty of calibrating GLONASS carrier-phase and code-phase inter-frequency biases and less advanced processing methods for the generation of the corrections. The issues with GLONASS inter-frequency biases were discussed in Reussner and Wanninger (2011). It is likely that the quality of the GLONASS corrections will likely improve in the future, because organisations maintaining reference networks are upgrading their networks with new GNSS receivers supporting GLONASS.

The standard deviation used for GLONASS carrier-phase measurements is three times larger than for GPS carrier-phase measurements. The value has been chosen empirically based on the performance of the CNES correction products in early 2013 to accommodate the worse quality of the GLONASS orbit and clock correction products compared to the corrections for GPS satellites. It is assumed that the standard deviation of GLONASS code-phase measurements is 20 times larger than for GPS code-phase measurements, because of the uncorrected GLONASS satellite and receiver specific code-phase biases and assumed worse quality of the correction products.

The average success rate in obtaining 3D position errors better than 10 cm at different stations is shown in Figure 5.29. The success rate is highest (98%), at the MIQE station when employing both GPS and GLONASS. The rate is the lowest (73%), at the BDOS station when employing GPS alone. In general, employing both GPS and GLONASS increases the success rate, except at the ICT5 station. At the BJCO and CHIN stations, there are no GLONASS dual-frequency carrier-phase measurements available.

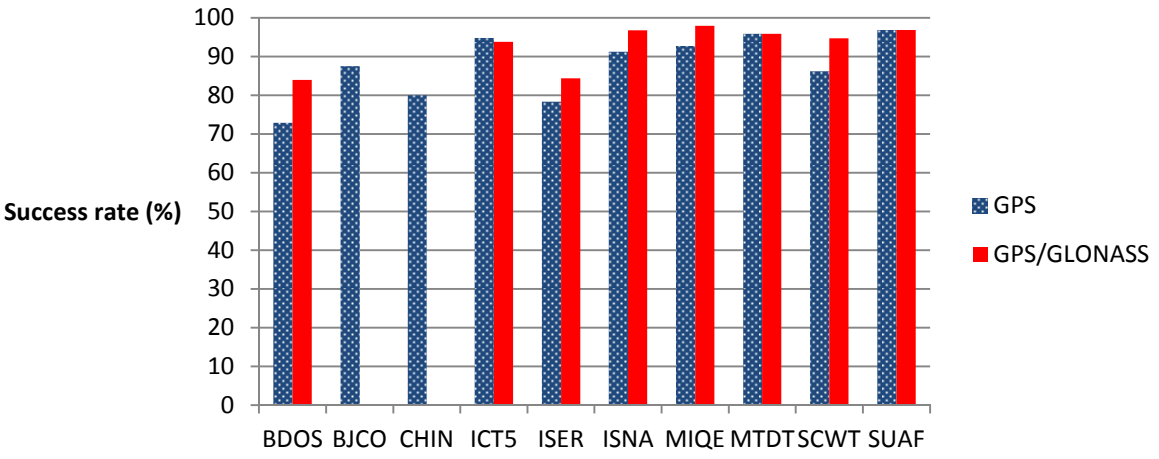

Figure 5.29 The success rate of obtaining smaller than 10 cm 3D position error

The average convergence time to 10 cm 3D position error at different stations is shown in Figure 5.30. The time varies between 2690 and 950 s. It is longest at the BDOS station when employing GPS only and shortest at the MTDT station when employing both GPS and GLONASS. Employing GLONASS provides shorter convergence time at all stations.

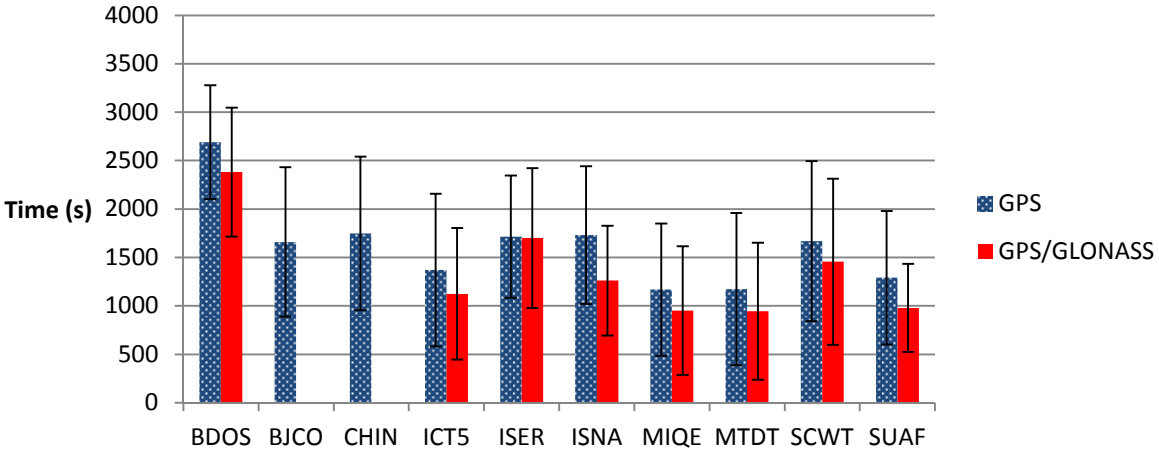

Figure 5.30 The average time required to obtain smaller than 10 cm 3D position error (one sigma standard deviation as error bars)

The success rate of obtaining better than 5 cm 3D position error is shown in Figure 5.31. The success rate is lowest (20%) at the BSDOS station when employing GPS only and highest (85%) at the SUAF station when employing both GPS and GLONASS. Employing both GPS and GLONASS increases the success rate except at the MIQE station.

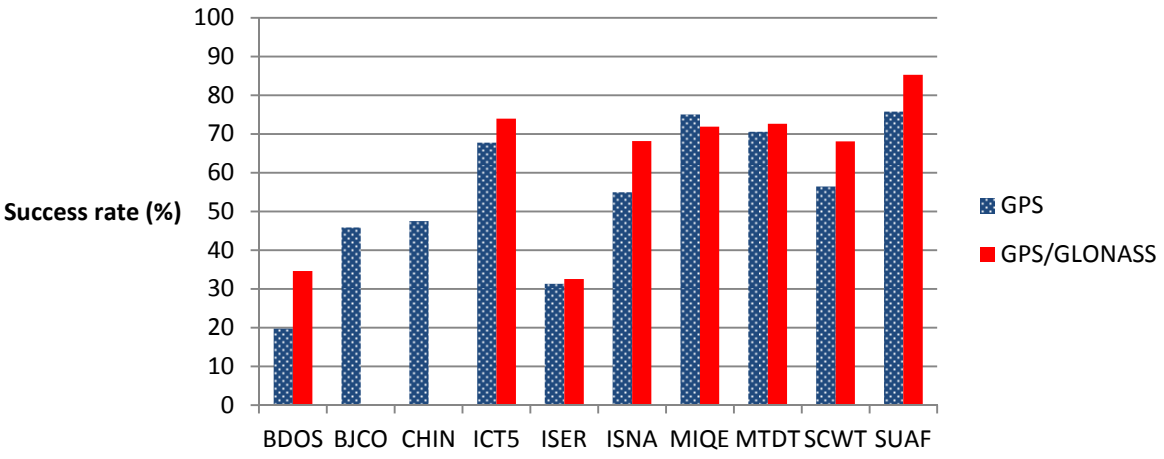

Figure 5.31 The success rate of obtaining better than 5cm 3D position error

The average time required to obtain better than 5 cm 3D position error is shown in Figure 5.32. Employing GPS and GLONASS provides a benefit at all the stations tested. The time is shortest (1770 s) at the MTDT station when using both GPS and GLONASS and longest (3100 s) at the BDOS station when using GPS alone.

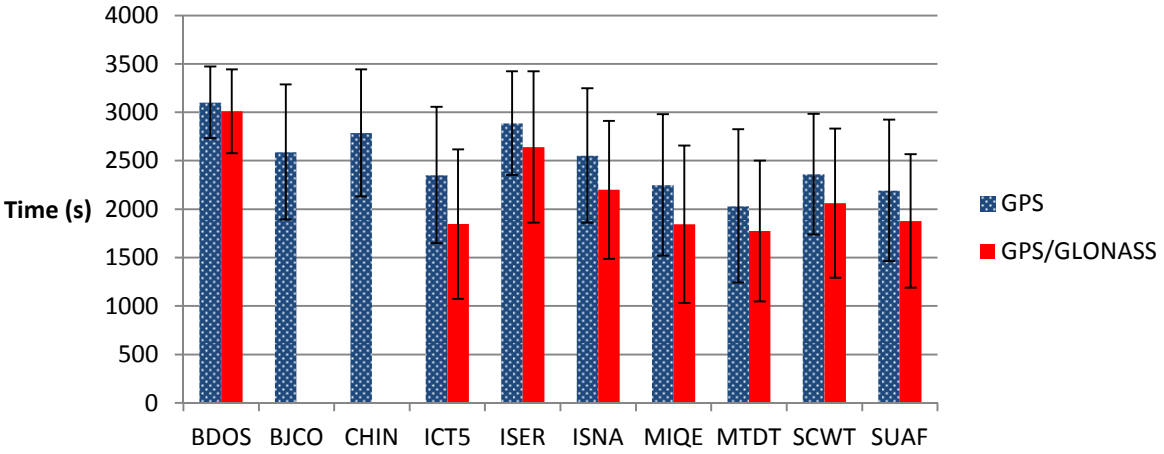

Figure 5.32 The average time required to obtain better than 5 cm 3D position error (one sigma standard deviation as error bars)

The success rate of obtaining better than 10 cm position error based on all tests is shown in Figure 5.33. When employing GPS alone, the success rates of obtaining better than 10 cm 3D, horizontal and vertical position errors are 88%, 93% and 95%, respectively. When employing both GPS and GLONASS, the success rates are 92%, 95% and 98%, respectively. The average convergence time to better than 10 cm position error based on all data is shown in Figure 5.34. Obtaining better than 10 cm 3D, horizontal and vertical position error takes 1570 (SD: 830 s), 1210 (SD: 800 s) and 1080 s (SD: 770 s), respectively, when using GPS

alone. When employing both GPS and GLONASS, the corresponding values are 1360 (SD: 810 s), 1010 (SD: 720 s) and 910 s (SD: 700 s), respectively.

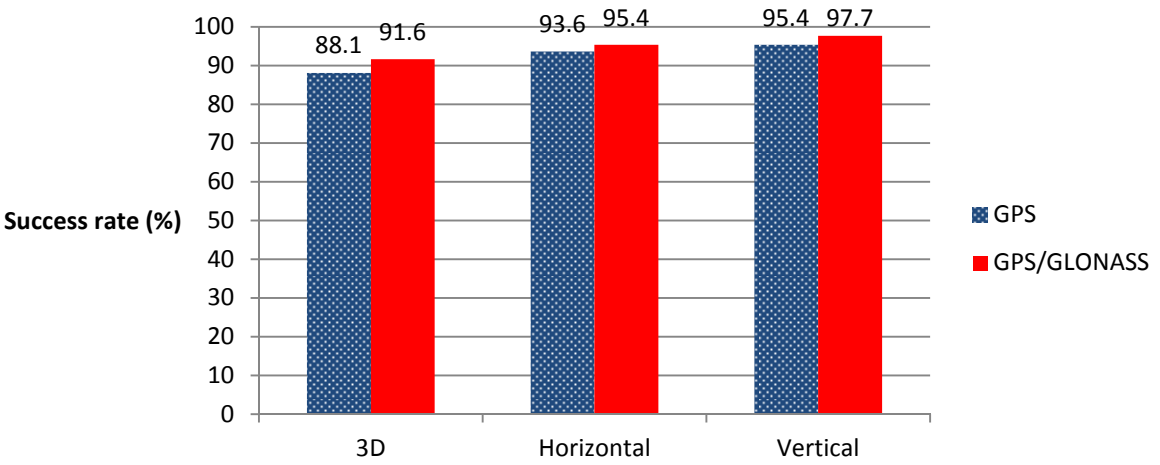

Figure 5.33 The success rate of obtaining better than 10 cm position error

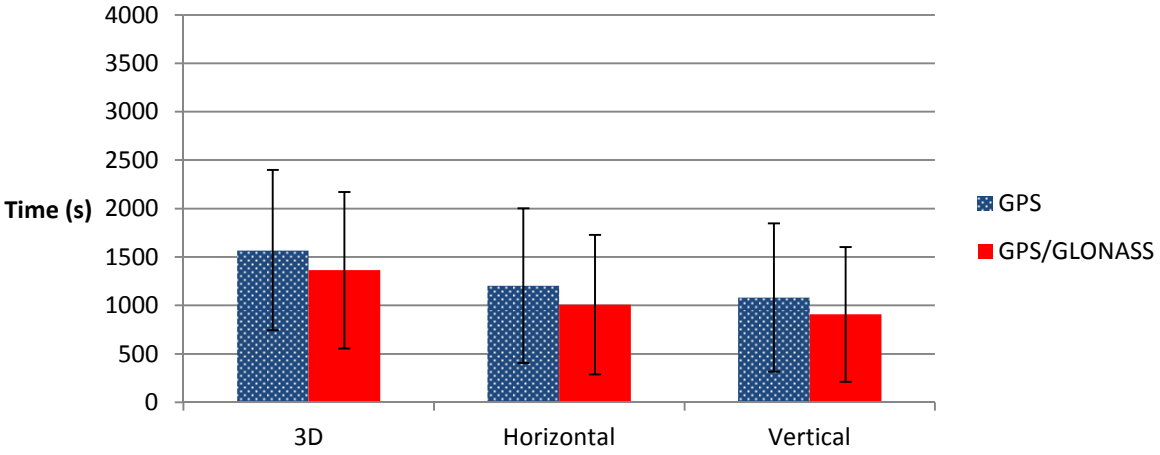

Figure 5.34 The average time required to obtain smaller than 10 cm position error (one sigma standard deviation as error bars)

The success rate of obtaining better than 5 cm 3D, horizontal and vertical position errors is shown in Figure 5.35. When employing GPS alone, the success rates of obtaining better than 5 cm 3D, horizontal and vertical position errors are 55%, 76% and 79%, respectively. In the case of employing both GPS and GLONASS, the success rates are 60%, 81% and 82%, respectively. The average time required to obtain better than 5 cm position error is shown in Figure 5.36. The convergence times to better than 5 cm 3D, horizontal and vertical position errors are 2400 (SD: 740 s), 1940 (SD: 830 s) and 1800 s, (SD: 880 s) respectively, when using GPS alone. The convergence times in the same order are 2100 (SD: 820 s), 1720 (SD: 840 s) and 1610 s (SD: 900 s) when employing both GPS and GLONASS.

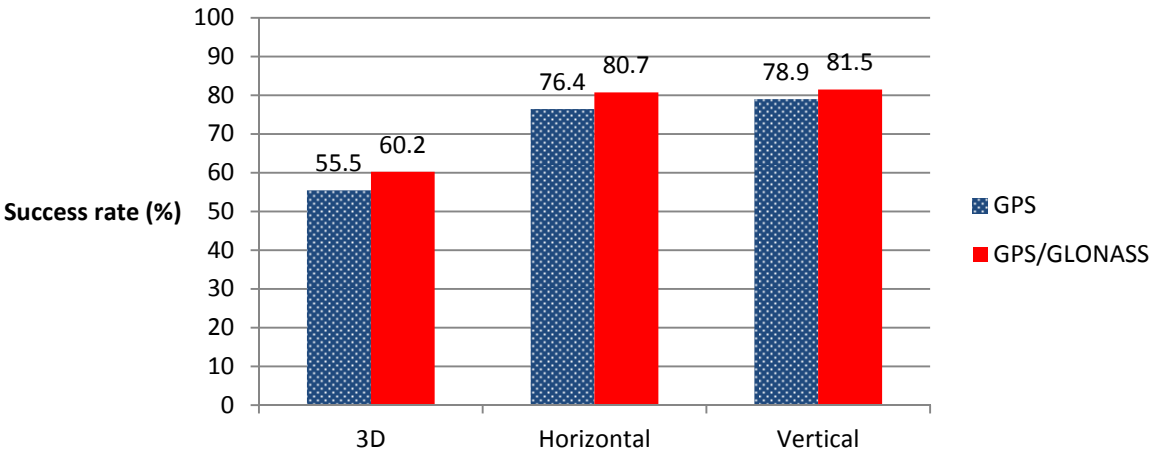

Figure 5.35 The success rate of obtaining better than 5 cm position error

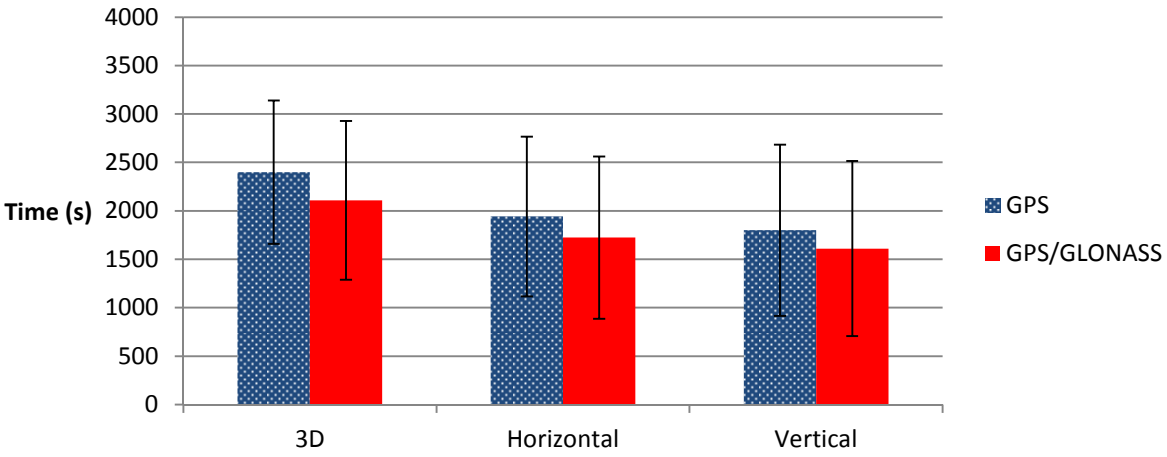

Figure 5.36 The average time required to obtain better than 5 cm position error (one sigma standard deviation as error bars)

Based on the float PPP test, using both GPS and GLONASS reduces the average time required to obtain better than 5 or 10 cm position error. Using GLONASS with GPS is beneficial, because it improves satellite geometry and adds more points for better tropospheric delay estimation. In addition, the increased number of measurements is beneficial for position estimation and integrity monitoring, because of the increased redundancy. For the given dataset, using GLONASS could result in more significant improvement if dual-frequency GLONASS measurements were available at the BJCO and CHIN stations. It is also likely that GLONASS could result in further benefits in the future, if the quality of the GPS and GLONASS orbit and clock corrections are similar and GLONASS inter-frequency biases are calibrated with sufficient accuracy. In a theory, there should be

no significant differences in terms of the quality of the GPS and GLONASS observations, if the correction products and bias calibration have similar accuracy.

In terms of the standard deviation of the average time required to obtain better than 5 and 10 cm position error, employing both GPS and GLONASS reduces the standard deviation of 10 cm convergence time, but increases the standard deviation of the 5 cm convergence time. The increase may be explained by the larger success rate of obtaining better than 5 cm position error when using both GPS and GLONASS. E.g. employing both GPS and GLONASS increases the success rate, but it causes obtaining better than 5 cm position error with long convergence time in some cases when using both GPS and GLONASS while not obtaining better than 5 cm position error at all in these cases when using GPS alone.

The reduction of the standard deviations show that employing both GPS and GLONASS makes results more consistent between different stations and time periods. The reduction can be explained by the similar reasons which reduced the average convergence time when employing both GPS and GLONASS.

There are still few cases where employing both GPS and GLONASS increased the convergence times compared to employing GPS only. This is likely caused by the insufficient quality of the GLONASS orbit and clock corrections during the problematic time-periods. The lower quality of the GLONASS correction products compared to the GPS corrections may be caused by the smaller number of stations tracking GLONASS satellites (Laurichesse, 2013).

The benefit of using both GLONASS and GPS for fixed ambiguity PPP when employing the enhanced PPP method is tested in Chapter 6. The tests are done based the optimal ambiguity validation parameters defined in Section 5.3.2.3.

5.3.4 Improving integrity monitoring

In the literature, little research has been carried out on PPP integrity monitoring, particularly with respect to failure exclusion. Improvements to the ICRAIM method in terms of protection level calculation and failure exclusion are proposed in this Section.

ICRAIM is tested using real GNSS data in Section 5.2.5. Based on the test results, a number of issues were identified with calculating realistic protection levels when the errors are non-

Gaussian. Such errors include, for example, satellite orbit errors and site-displacement effects. In addition, it is not possible to calculate realistic protection levels based on the SLOPE concept when employing EKF, because the Kalman gain values are small when the solution has converged.

To estimate more realistic protection levels, a nominal bias calculated based on the assumed magnitudes of non-Gaussian errors, is added to the protection level estimates. In an ideal case, the magnitude of the nominal bias would be calculated based on the estimated error magnitude in error models (e.g. tropospheric model) and correction products (e.g. satellite orbits and clock). The error estimates of correction products would be provided in the ideal case by the correction products provider such as CNES. However, in practice, information on the error magnitude is not currently available. Therefore, an empirically chosen nominal bias value of 5 cm is used in this thesis. It is selected based on the assumed error in satellite orbit corrections, tropospheric estimation and site-displacement estimation. Adding an empirically derived bias cannot be considered as new development in general, but it can be regarded as an improvement when processing the dataset in this thesis using the CNES orbit and clock corrections.

When taking the nominal bias into account, the horizontal protection level is calculated using equation (5.2) and the vertical protection level using equation (5.3). P_{local} is the EKF P matrix converted into the local (East, North, Up) coordinates; k_H and k_V are factors calculated based on the allowed rate of missed detection and $\mathrm{nominalBias}$ is the chosen nominal bias value. ah is calculated using equation (5.4) and av using equation (5.5). H_{EKF} and R_{EKF} are the EKF design and measurement variance matrices, respectively.

$$HPL = k_H\sqrt{P_{local,11} + P_{local,22}} + \mathrm{nominalBias} * ah \tag{5.2}$$

$$VPL = k_V\sqrt{P_{local,33}} + \mathrm{nominalBias} * av \tag{5.3}$$

$$ah = \sum_{i=1}^{n}\left(\sqrt{{G_{1,i}}^2 + {G_{2,i}}^2}\right), \text{where } G = (H_{EKF}^T R_{EKF}^{-1} H_{EKF})^{-1} H_{EKF}^T R_{EKF}^{-1} \tag{5.4}$$

$$av = \sum_{i=1}^{n}\left|G_{3,i}\right|, \text{where } G = (H_{EKF}^T R_{EKF}^{-1} H_{EKF})^{-1} H_{EKF}^T R_{EKF}^{-1} \tag{5.5}$$

5.3.4.1 Failure exclusion

ICRAIM employs three different test statistics: total, code-phase only and carrier-phase only. Failure exclusion is attempted, if any test statistic exceeds its threshold. The BSD approach used for GPS measurements requires failure exclusion to be applied separately for failures associated with the base-satellite and other satellites. For GLONASS measurements, there is no need for separate handling, because the GLONASS measurements are un-differenced.

It is assumed that a range error (ϵ_1) is added to a carrier-phase signal broadcasted by the satellite i. Thereafter, it is assumed that the impact of the error goes completely to the carrier-phase residual. E.g. the error is not absorbed by the carrier-phase ambiguity or other states estimated. If it is assumed that the satellite i is not the base-satellite and there are no other errors, the magnitude of the carrier-phase residuals for the satellite i is ϵ_1 and for the other satellites the magnitude is zero. On the other hand, if the error occurs for the base-satellite (j), magnitude of the all residuals is $-\epsilon_1$, because the measurements of the base-satellite j are differenced from other satellite's measurements. In this ideal case, the failure can be defined as a non-base-satellite failure, if the magnitude of the residual for one satellite is equal to the total magnitude of all residuals. Otherwise, it can be assumed that the base-satellite has been failed.

When employing the ICRAIM, it is assumed that two failures can happen simultaneously and there are noise and multipath errors. The failure excluding test must be able to separate cases where there are one or two large failures from the cases where the base-satellite has been failed. To enable separating the base-satellite and non-base-satellite failures, the following test is developed in this thesis:

$$\frac{w_{largest} + w_{secondLargest}}{\sum_0^{s\,=\,n_m} w_s} < \frac{3.5}{n_m} \tag{5.6}$$

In the equation, w is a measurement residual and n_m is the number of measurements used to calculate the test statistic. If the test equation (5.6) is true, the failure is with the base-satellite. Otherwise, the failure is with some other satellite. The test is carried out separately for each test statistic such as total and carrier-phase only. The test is designed to handle four different types of failures: a base-satellite failure, one non-base-satellite failure, two simultaneous non-base-satellite failures and the base-satellite and non-base-satellite failing

simultaneously. The primary assumption of the test is that if the combined magnitude of the largest ($w_{largest}$) and second largest ($w_{secondLargest}$) residuals is sufficiently large compared to the total sum of residuals ($\sum_{0}^{s=n_m} w_s$), the failure is not with the base-satellite. The assumption is true, because the base-satellite failures cause residuals to increase for all satellites. In an ideal case when the base-satellite has failed, the residuals would increase equally for all satellites and the magnitude of the residuals for one satellite divided by the total magnitude of residuals would be $\frac{1.0}{n_m}$ and for two satellites the ratio would be $\frac{2.0}{n_m}$. Therefore, the test threshold should be $\frac{2.0}{n_m}$ in the idea case. Nevertheless, $\frac{3.5}{n_m}$ is chosen as the threshold empirically, because the residuals when the base-satellite fails are not typically divided evenly for all satellites when using real GNSS data. That may have been caused by multipath and measurement noise.

If a failure is detected with the base-satellite, it is excluded for 30 s. Otherwise, the satellite with the largest residual is excluded for 30 s. The same approach is used for failure exclusion of GLONASS measurements. The excluding time period of 30 s is chosen based on the assumption that the duration of most failures is not long. For example, multipath or errors in the satellite orbit and clock corrections products can cause short term failures. After excluding the failure, ICRAIM is run again to check for possible multiple-failures. This is run until ICRAIM accepts the solution or there is no sufficient number of measurements available to run ICRAIM again.

The integrity monitoring improvements in terms of failure detection and excluding are tested in Section 6.5.

5.3.5 Conclusion

The enhanced PPP method is a novel fixed ambiguity PPP method developed in this thesis. Compared to the existing methods (tested in 5.2.4), the enhanced PPP method provides the lower rate of incorrect ambiguity resolution, higher rate of correct ambiguity resolution and smaller position error and its standard deviation during the initial ambiguity resolution epoch. The enhanced PPP method will be tested using variety of datasets and compared to the existing PPP methods in Chapter 6.

The development steps of the enhanced PPP method was discussed in this chapter. The first step was employing the MCM method when attempting narrow-lane ambiguity resolution as discussed in 5.5.1.

The second step was employing time window based ambiguity validation as discussed in Section 5.3.2.1. The principle of the validation is checking that the best ambiguity candidate vector is the same over a given number of epochs (for example, 150 s) consecutively and that the ambiguities belonging to that vector can be fixed to the same integers during the chosen time-period. The benefit of employing the time window based ambiguity validation method is making ambiguity resolution less vulnerable for insufficiently accurate float solutions.

The third step was employing the additional validations to make incorrect ambiguity resolution less likely as discussed in 5.3.2.2. This includes limiting the minimum size of narrow-lane vector used for ambiguity resolution and requiring higher ambiguity validation confidence level during solution convergence.

The enhanced PPP method uses both GPS and GLONASS measurements when estimating float solution as discussed in Section 5.3.3. The benefit of employing both GPS and GLOANSS for fixed ambiguity is tested and analysed more in Chapter 6.

Integrity improvements in terms of protection level calculation and failure excluding discussed in Section 5.3.4 are also a part of the enhanced PPP method. The integrity monitoring of the enhanced PPP method in terms of failure exclusion and detection is tested in Section 6.5.

6 The performance of the enhanced PPP method

The performance of the enhanced PPP method is tested both in static and dynamic environments. Static testing is carried out on the NOAA and global datasets. In addition, the impact of employing NWM-based tropospheric corrections is tested using a dataset recorded in the UK. The dynamic performance is tested using data recorded on the University of Nottingham mini-train track (Liu et al., 2013).

The enhanced PPP method developed in Chapter 5 is used in these tests. The parameters of the enhanced PPP methods correspond to those from the most suitable combination 2, defined in Section 5.3.2.3: length of ambiguity validation window is set to 150 s; at least five narrow-lane ambiguities are required to be fixed initially; and the confidence level required during the convergence period is 99.99% and 99.00% post-convergence. The solution is defined to be in the convergence period when the longest carrier-phase lock time of the current tracked satellites is less than 2000 seconds.

6.1 Ideal testing environment

The performance of the enhanced PPP method must be tested both in static and dynamic environments, because the enhanced PPP method is designed both for static (e.g. surveying) and dynamic applications (e.g. agriculture). The performance of PPP is dependent on many factors including, quality of the error correction products, type of rover receiver and antenna used, prevalent atmospheric conditions, rover side PPP method, and receiver location-dependent error sources, such as site-displacement effects and multipath. Therefore, the performance must be tested using carefully selected datasets, covering representative time-periods, rover locations and types of receivers and antennae. GNSS data with shorter or equal than five second data rate should be used to enable reliable cycle-slip detection and correction. The rate of the CNES satellite clock corrections is 5 s. Therefore, using the 5 s GNSS data rate is also beneficial to enable running the PPP estimation at the epochs matching to the satellite clock correction reference epochs to mitigate the error caused by satellite clock correction interpolation. In addition, the dataset must have GPS and GLONASS L1 and L2 observations. It is important to note that the GNSS

observations which have been used to generate the correction products should not be used to test the rover PPP performance in order to prevent correlations from potentially biasing the results.

6.1.1 Static positioning

To test the static performance of the PPP method developed in this thesis, the data used should capture potential spatio-temporal variations. For example, at least one year of GNSS data divided into one hour datasets should be used, with geographical locations all around the world. Ideally, these stations should be located in diverse operational environments to capture the impacts of local specificities on performance. To enable error analysis, the IGS08 coordinates of the GNSS receivers must be known at the level of millimetres.

In practice, it is difficult to achieve such an ideal test scenario. The primary problem is the availability of GNSS data. Whilst not a problem in North America, East-Asia or Europe, there are regions such as Africa where the coverage of GNSS reference stations is low. In addition, it may not be possible to obtain GNSS data from some countries such as the Democratic People's Republic of Korea (North Korea), because of political issues.

GNSS data, for example, from the IGS (IGS, 2009), NOAA (NOAA, 2013), the European Space Agency (ESA) (EGOS, 2013) and the University Navstar Consortium (UNAVCO) (UNAVCO, 2013) can be used in practice. However, ESA and UNAVCO data are not suitable, the former because the ESA EGNOS network does not provide L2 GLONASS observations and the IGS08 coordinates and antenna types of the ESA stations are not known. The data provided by UNAVCO is not suitable, because the low data rate of 30 s. Therefore, only data provided by the IGS and NOAA are used in this thesis. For the IGS data, stations which have been used to generate CNES satellite clock correction products are excluded from the test data.

In addition, the time required to process PPP solutions is a problem. When processing the RINEX data (with 5 s data rate) with the POINT software, it takes typically between one and two minutes to process a one hour dataset for one station, using a laptop with an Intel Core i5 M 450 @ 2.40 GHz processor.

The availability of correction data is also an issue. For example, there may be no suitable CNES orbit and clock corrections available for some time-periods, due to problems associated with the generation of these corrections. Large errors in float PPP solutions often indicate that there are issues with the correction products. The data used in this thesis is selected so that it does not include time-periods with significant corrections issues. In conclusion, the data used in the static tests are chosen to ensure the combined availability of stations and correction products, and realistic processing time.

6.1.2 Kinematic positioning

In an ideal scenario, kinematic PPP should be tested on a variety of data that are able to capture potential spatio-temporal variations. However, recording kinematic GNSS data is significantly more labour intensive and expensive than recording static data. This is because dynamic data cannot be provided by existing reference station networks. Therefore, the number and length of kinematic PPP tests are limited.

A key difficulty in carrying out tests on kinematic data lies in accurately determining the true track. In an ideal case, the true track should be estimated independently of GNSS measurements. For example, in the case of the controlled miniature train test in Section 6.4, the true track of the device can be calculated based on the known railroad track and controlled acceleration and velocity of the train.

In practice, the true track of a kinematic rover receiver is not often known. In this case, positioning methods other than PPP can be used to estimate the track. For example, cRTK with Inertial Navigation System (INS) can be used for the estimation. However, the estimation accuracy of cRTK is typically only at centimetre level and there is a correlation in errors between cRTK and PPP solutions, because the same GNSS measurements are used by both methods.

Kinematic GNSS data recorded using the mini train track located on top of the Nottingham Geospatial Building at the University of Nottingham in the United Kingdom is used in this thesis to test kinematic PPP (Liu et al., 2013). cRTK is used to estimate the true reference solution, because it is the most accurate available method to determine the trajectory of the train. It would have been possible to determine the trajectory of the train based on the

time, speed of the train and location of the track. However, the train movement information was not recorded, because a mistake made by the technical executing the test. It was not possible to repeat the test, because it was performed the by an iNsight project partner and not the author of the thesis. Therefore, this was the most suitable kinematic train dataset available. Using the cRTK solution as a truth track instead of the recorded movements of the train may cause centimetre level position errors.

6.2 Static positioning tests

Static positioning performance is tested using NOAA and Global datasets. The Global dataset is discussed in Section 6.2.2. The length of each test case is one hour. The correctness of the position solutions is evaluated by comparing the computed position estimates with the known IGS08 coordinates of the stations in terms of 3D, horizontal and vertical position errors. For the NOAA dataset, station coordinates are provided by NOAA (NOAA, 2013) and for the Global dataset stations coordinates are provided by the IGS as weekly solution (IGS, 2009). The accuracy of the reference coordinates is at the millimetre-level (Altamimi and Collilieux, 2009).

6.2.1 Fixed ambiguity PPP using the National Oceanic and Atmospheric Administration (NOAA) dataset

The average time required to obtain an initial ambiguity resolution at different stations is shown in Figure 6.1. The time varies between 1660 (the MIQE station when using both GPS and GLONASS) and 2500 s (the BDOS station when using GPS alone). There are no suitable GLONASS carrier-phase measurements available at the BJCO and CHIN stations. Therefore, the impact of employing GLONASS cannot be tested at these stations. At other stations, using GPS with GLONASS provides faster ambiguity resolution compared to using GPS alone. In terms of the standard deviation of the ambiguity fixing time, there are no large differences between the GPS alone and GPS with GLONASS cases.

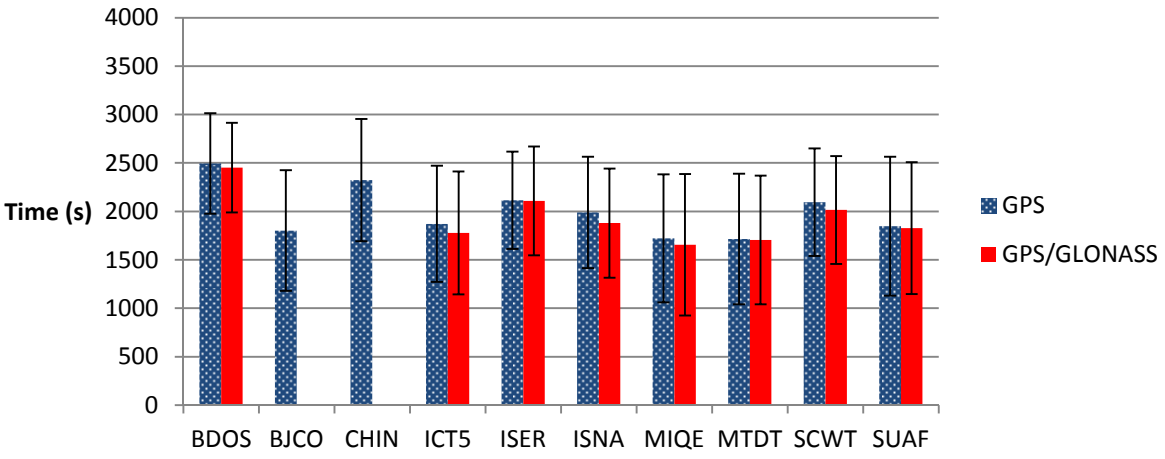

Figure 6.1 The average time required to obtain an initial ambiguity resolution at different stations and its standard deviation (one sigma) shown by the error bars (NOAA dataset)

The average horizontal position error at the initial ambiguity resolution epoch at different stations is shown in Figure 6.2. The average error is calculated by first calculating the difference between the estimated and known coordinates of a station at the time epoch of obtaining an initial ambiguity resolution and then averaging it over all hourly datasets tested. The initial ambiguity resolution epoch follows the definition given before in this thesis (Section 5.2.4): the first epoch of fixing at least four narrow-lane ambiguities to integers. The average horizontal position error varies between 1.4 and 3.7 cm depending on the station. Employing both GPS and GLONASS provides horizontal position errors equal to or better than GPS alone, except at the ISNA and SUAF stations. At the ISNA station, using GLONASS with GPS causes insufficiently accurate float PPP solutions in the test datasets starting at 12 February 2013 at 22:00 and 5 March 2013 at 10:00. This caused large position errors due to wrong ambiguity resolution when employing both GPS and GLONASS. At the SUAF station, a larger average horizontal error is shown, because ambiguity fixing rate is higher when using both GPS and GLONASS (88%) compared to GPS alone (85%). This refers to fixing ambiguities in a larger number of test cases when using both GPS and GLONASS. Using GPS with GLONASS reduces the standard deviation of the horizontal position error at most stations. However, the magnitude of the standard deviation is larger at the BJCO (GPS/GLONASS and GPS alone processing, 6.4 cm) and MTDT (GPS alone processing, 4.0 cm) stations. The large error standard deviations can be explained by the cases where ambiguities were fixed incorrectly.

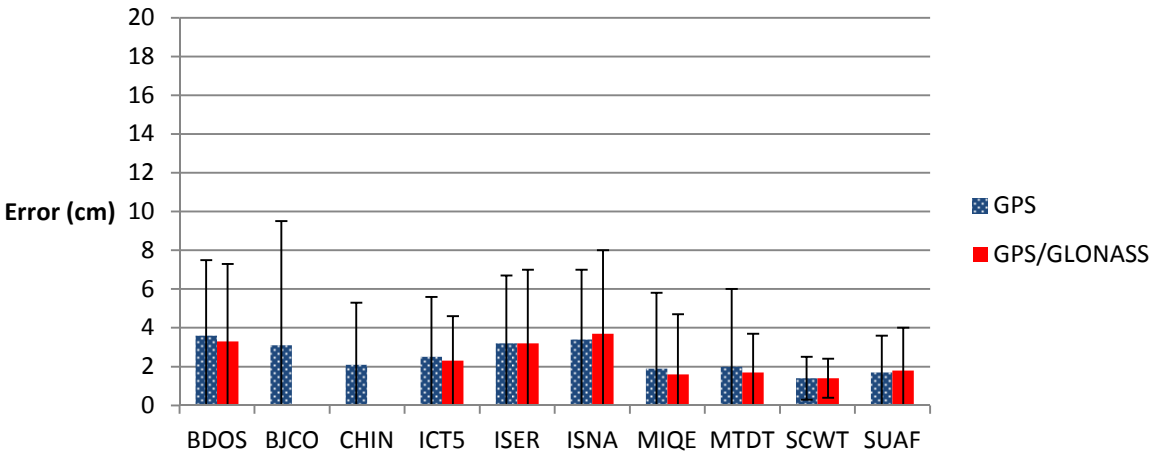

Figure 6.2 The average horizontal position error at the initial ambiguity resolution epoch at different stations (NOAA dataset, one sigma standard deviation shown as error bars)

The average vertical position error at the initial ambiguity resolution epoch at different stations is shown in Figure 6.3. The average vertical error is obtained in a similar style of way as the horizontal average error. The magnitude of the error is largest (5.8 cm) at the BDOS station when using GPS alone and smallest at the ICT5 and MIQE stations when using both GPS and GLONASS. Using GPS with GLONASS provides vertical errors smaller or equal to GPS alone, except at the ISNA and SUAF stations. The reasons for larger average vertical errors at the ISNA and SUAF stations are the same as for the larger horizontal errors. In terms of the vertical error standard deviation, there is no significant difference between GPS alone and GPS with GLONASS processing scenarios. The largest standard deviation (5.2 cm) is at the BJCO station when using GPS alone. This may be caused by an incorrect ambiguity resolution case.

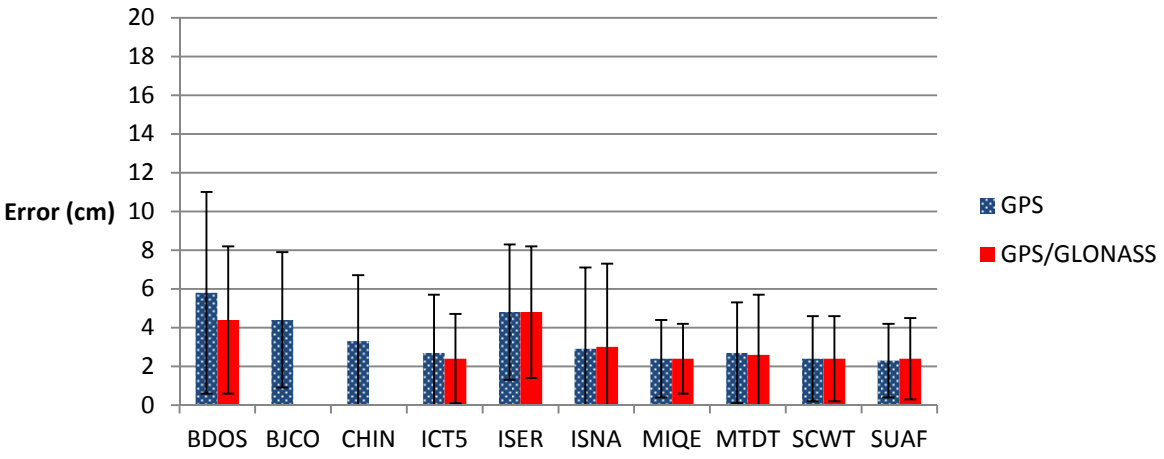

Figure 6.3 The average vertical position error at the initial ambiguity resolution epoch at different stations (NOAA dataset, one sigma standard deviation shown as error bars)

Based on all data, the average time required to obtain an initial ambiguity resolution is shown in Figure 6.4. It takes on average 1970 s (SD: 650 s) when using GPS alone and 1930 s (SD: 660 s) when using both GPS and GLONASS. The difference is not large, but it still shows that employing GLONASS with GPS can improve results slightly.

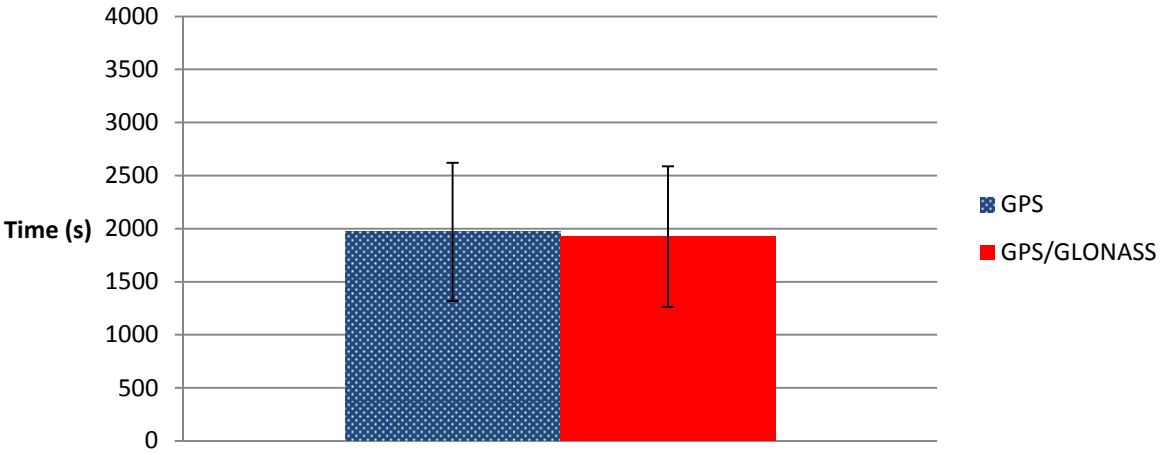

Figure 6.4 The average time required to obtain an initial ambiguity resolution based on all data (NOAA dataset, one sigma standard deviation shown as error bars)

The average 3D, horizontal and vertical position errors at the initial ambiguity resolution epoch based on all data are shown in Figure 6.5. The average 3D, horizontal and vertical errors are 4.5 (SD: 4.7 cm), 2.5 (SD: 3.8 cm) and 3.3 cm (SD: 3.4 cm), respectively, when using GPS alone. When employing both GPS and GLONASS, the average magnitudes of the errors are 4.3 (SD: 4.5 cm), 2.4 (SD: 3.6 cm) and 3.2 (SD: 3.2 cm) cm. Employing GLONASS with GPS provides smaller 3D, horizontal and vertical errors their standard deviations. The

relative large standard deviations such as the 4.5 cm 3D standard deviation when employing both GPS and GLONASS are mostly caused by incorrect ambiguity resolution cases. In addition, the variation of the error magnitude depending on the station and time is usual, because the atmospheric conditions, satellites geometry and quality of the orbit and clock corrections vary.

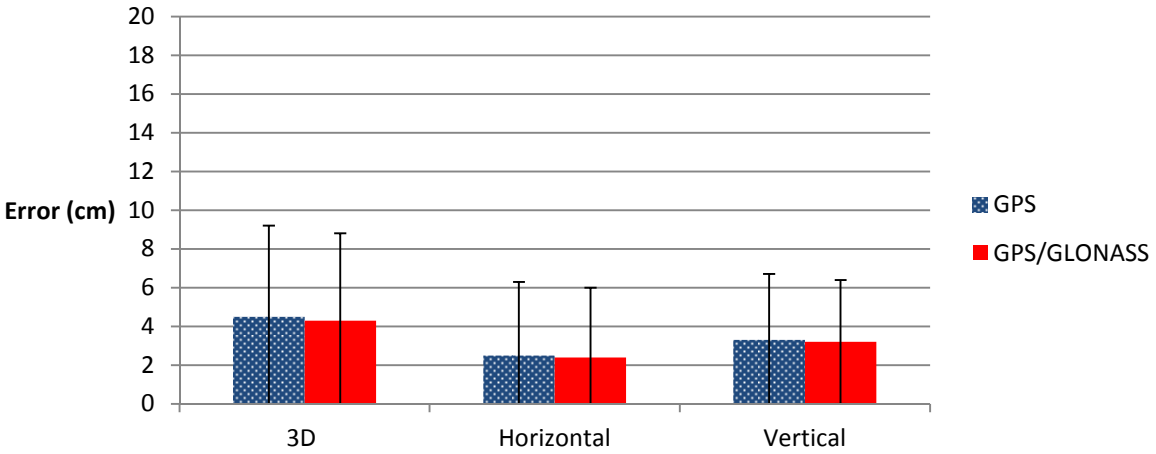

Figure 6.5 The average position error at the initial ambiguity resolution epoch based on all data (NOAA dataset, one sigma standard deviation shown as error bars)

The success rates of obtaining better than 10 cm position error based on all the data is shown in Figure 6.6. The 3D, horizontal and vertical success rates are 89.3%, 94.3% and 94.7%, respectively, when using GPS alone and 90.6%, 94.4% and 96.0% when using both GPS and GLONASS. It can be seen that employing GLONASS provides a small improvement. Ambiguity fixing does not improve the success rates of obtaining better than 10 cm position error compared to float PPP (Figure 5.33), because the wavelength of the narrow-lane combination is 10.7 cm and obtaining correct ambiguity resolution typically requires that the position error is smaller than the wavelength.

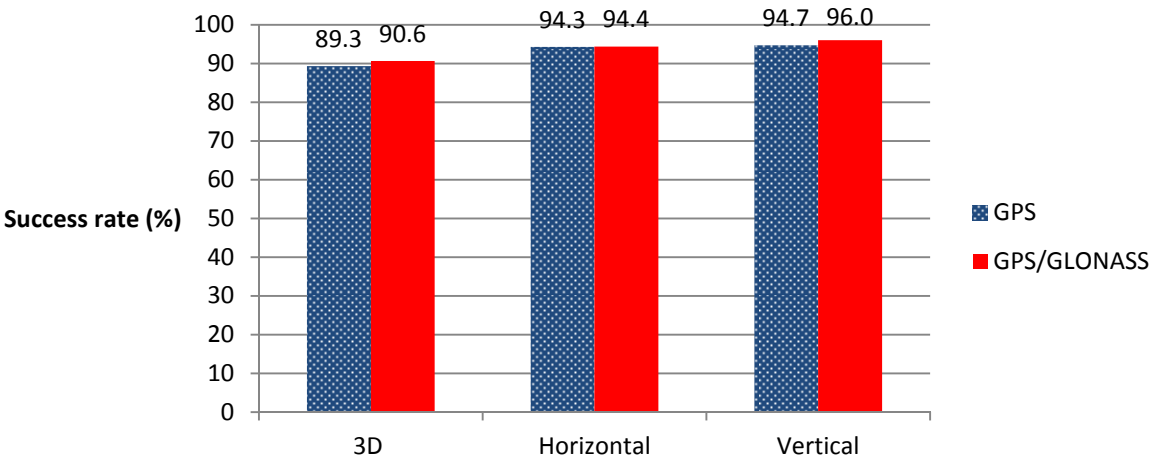

Figure 6.6 The success rate of obtaining smaller than 10 cm position error based on all data (NOAA dataset)

The convergence time required to obtain better than 10 cm position errors is shown in Figure 6.7. It takes 1420 (SD: 730 s), 1120 (SD: 720 s) and 1030 s (SD: 710 s) to obtain better than 10 cm 3D, horizontal and vertical position errors, respectively, when using GPS alone. When using both GPS and GLONASS, it takes 1290 (SD: 710 s), 1010 (SD: 660 s) and 910 s (SD: 650 s) respectively. Compared to float PPP (Figure 5.34), employing the enhanced PPP method reduces the convergence time by 9.5% when using GPS alone and 5.0% when using GPS and GLONASS. This shows a clear improvement given by the enhanced PPP method. However, the enhanced PPP method gives more significant improvement in terms of success rate and time required to obtain better than 5 cm position error, which is discussed next.

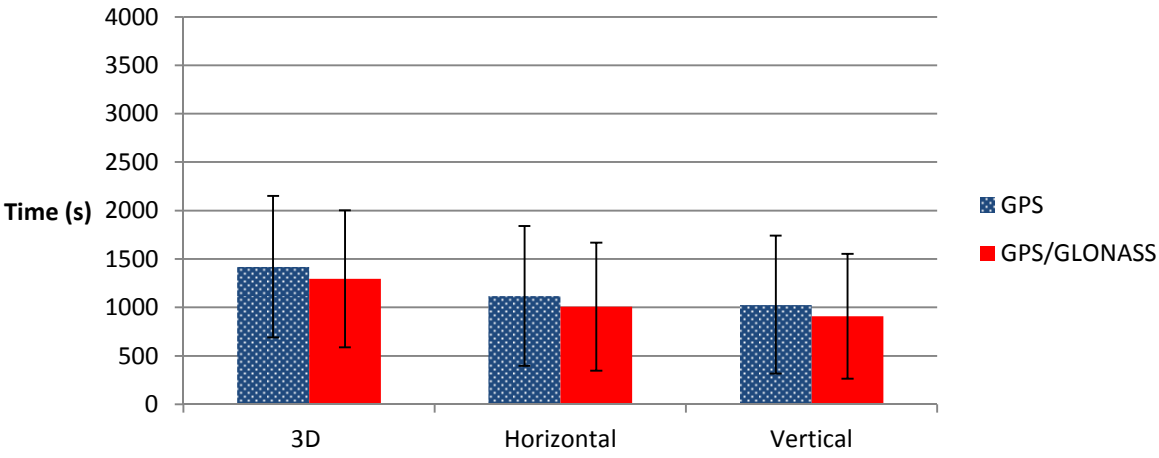

Figure 6.7 The average time required to obtain smaller than 10 cm position errors based on all data (NOAA dataset, one sigma standard deviation shown as error bars)

The success rate of obtaining better than 5 cm position error is shown in Figure 6.8. The figure shows that fixing ambiguities using the enhanced PPP method provides a significant improvement compared to float PPP (Figure 5.35): the success rates of obtaining smaller than 5 cm 3D, horizontal and vertical position errors have increased from 55.5% to 72.5%, 76.4% to 86.4% and 78.9% to 80.7%, respectively, when using GPS alone and from 60.2% to 74.9%, 80.7% to 88.1% and 81.5% to 82.5%, respectively, when using both GPS and GLONASS.

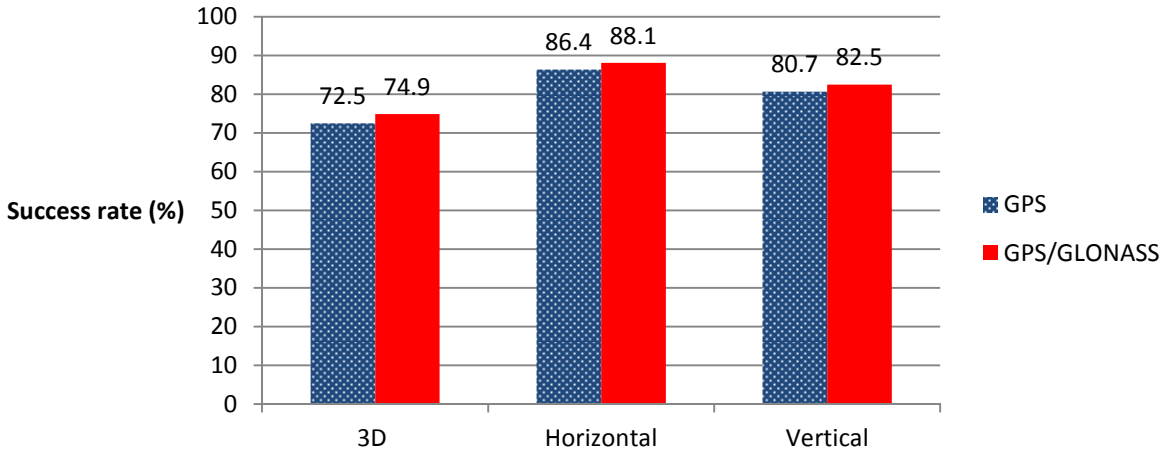

Figure 6.8 The success rate of obtaining smaller than 5 cm position error based on all data (NOAA dataset)

The convergence time required to obtain better than 5 cm position error is shown in Figure 6.9. The figure shows that employing GLONASS with GPS reduces the 5 cm convergence time and its standard deviation. Compared to float PPP (Figure 5.36), fixing ambiguities reduces the convergence times to smaller than 5 cm 3D, horizontal and vertical position errors by 17.4%, 15.9% and 8.8%, respectively, when using GPS alone. When using both GPS and GLONASS, the corresponding convergence times are reduced by 11.7%, 11.5% and 5.8% compared to float PPP.

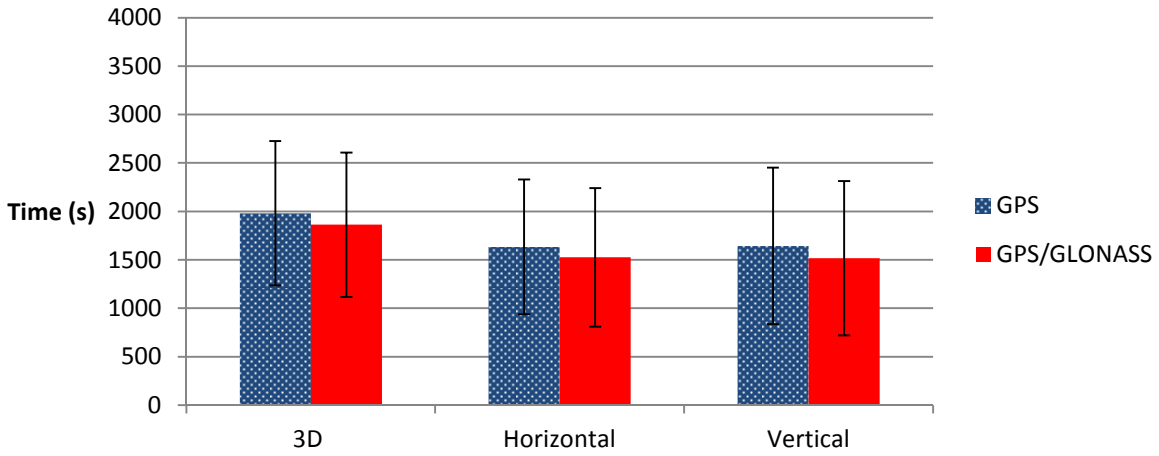

Figure 6.9 The average time required to obtain smaller than 5 cm position errors based on all data (NOAA dataset, one sigma standard deviation shown as error bars)

The distribution of 3D position errors at the initial ambiguity resolution epoch is shown in Figure 6.10. Ambiguity resolution is defined as being incorrect when the 3D position error is larger than 10.7 cm. The rate of incorrect ambiguity resolution is 6.0% when using GPS alone and 5.3% when using both GPS and GLONASS.

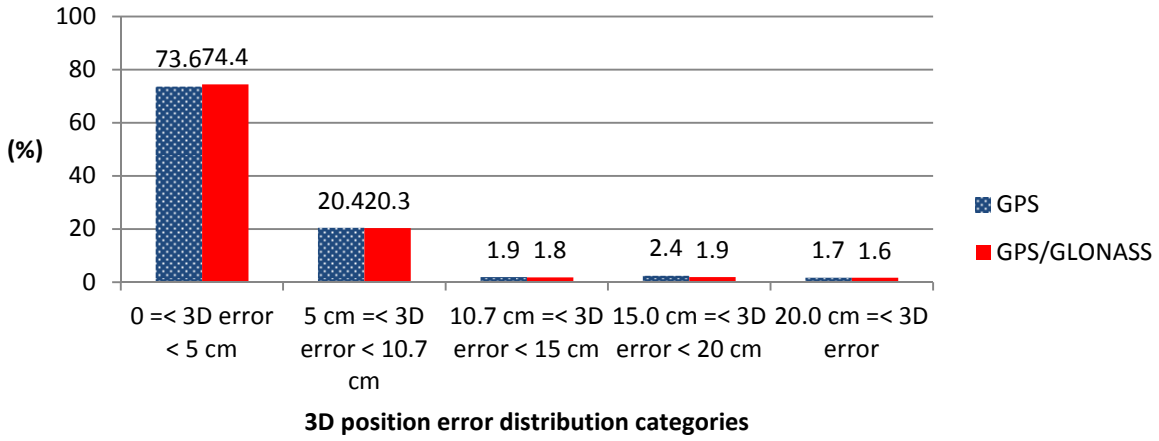

Figure 6.10 The distribution of the 3D position error at the initial ambiguity resolution epoch based on all data (NOAA dataset)

The performance of the enhanced PPP method based on the results obtained using the NOAA dataset is summarised in Table 6.1 and compared to the ILSDNCF method with a 1200 s lock time requirement, which was determined to be the most reliable existing fixed ambiguity PPP method in Section 5.2.4. Compared to the ILSDNCF method with a 1200 s lock time requirement, the enhanced PPP method when using both GPS and GLONASS reduces the rate of incorrect ambiguity resolution by 58.3%, increases the rate of correct

ambiguity resolution by 10.8% and reduces the 3D, horizontal and vertical position errors at the initial ambiguity resolution epoch by 31.7%, 40.0% and 23.8%, respectively. In addition, the standard deviation of the 3D, horizontal and vertical error is reduced by 42.3%, 46.3% and 31.9%, respectively. The only negative aspect compared to ILSDNCF with a 1200 s lock time requirement is the 26.1% increase in the time required to obtain an initial ambiguity resolution. The increase is likely caused by the more strict ambiguity validation when employing the enhanced PPP method. Using the enhanced PPP method with both GPS and GLONASS provided a small improvement compared to using GPS alone. In summary, the enhanced PPP method provides a significantly lower rate of incorrect ambiguity resolution, a higher rate of correct ambiguity resolution and lower position error at the initial ambiguity resolution epoch compared to the existing fixed ambiguity PPP methods.

Method	**Rate of ambiguity resolution (%)**	**Rate of correct ambiguity resolution (%)**	**Rate of incorrect ambiguity resolution (%)**	**Average time to obtain an initial ambiguity resolution and its standard deviation (s)**	**Average position error 3D/Horizontal/ Vertical and their standard deviations (cm)**
Enhanced PPP method (GPS only)	86.0	80.8	6.0	1970 (SD: 650)	4.5/2.5/3.3 (SD: 4.7/3.8/3.4)
Enhanced PPP method (GPS/GLONASS)	86.9	82.2	5.3	1930 (SD: 660)	4.3/2.4/3.2 (SD: 4.5/3.6/3.2)
The most reliable current fixed ambiguity PPP method: ILSDNCF, 1200 s lock time requirement	86.9	74.2	12.7	1560 (SD: 570 s)	6.3/4.0/4.2 (SD: 7.8/6.7/4.7)

Table 6.1: The summary of PPP ambiguity resolution and validation results (NOAA dataset)

The success rate and time required to obtain better than 5 or 10 cm horizontal and vertical position errors are shown in Tables 6.2 and 6.3, respectively. Compared to the most reliable current fixed ambiguity PPP method (ILSDNCF, 1200 s lock time requirement), the enhanced PPP method improves results in all aspects except the convergence time to the 5 cm horizontal error. The convergence time to the 5 cm horizontal error is longer, because

convergence is achieved in a larger number of cases (e.g. the success rate of obtaining the 5 cm horizontal position error is higher when employing the enhanced PPP method).

Compared to float PPP, the enhanced PPP method improves convergence to the 5 cm error level, but does not improve convergence to the 10 cm error level. Convergence to the 5 cm error is improved, because correct narrow-lane ambiguity resolution typically reduces the position error to smaller than 5 cm level. On the other hand, correct narrow-lane ambiguity resolution does typically not improve convergence to the 10 cm level, because a 10 cm level position error is required before narrow-lane ambiguity resolution can be completed. Nevertheless, improvements can be provided in some cases, because there are cases when narrow-lane ambiguity resolution can be done when the 3D position error is slightly larger than 10 cm and the correct ambiguity resolution typically ensures that the position error does not increase to over the 10 cm threshold after ambiguities are fixed. However, ambiguity resolution can also make convergence to the 10 cm error level worse, if ambiguities are fixed incorrectly.

Method	**Convergence time to 10 cm horizontal position error (s)**	**Success rate of obtaining 10 cm horizontal position error (%)**	**Convergence time to 5 cm horizontal position error (s)**	**Success rate of obtaining 5 cm horizontal position error (%)**
Enhanced PPP method (GPS only)	1119	94.3	1633	86.4
Enhanced PPP method (GPS/GLONASS)	1006	94.4	1525	88.1
The most reliable current fixed ambiguity PPP method: ILSDNCF, 1200 s lock time requirement	1036	88.7	1448	80.7
Float PPP (GPS Only)	1205	93.6	1941	76.4
Float PPP (GPS/GLONASS)	1007	95.4	1724	80.7

Table 6.2: Horizontal error convergence comparison

Method	Convergence time to 10 cm vertical position error (s)	Success rate of obtaining 10 cm vertical position error (%)	Convergence time to 5 cm vertical position error (s)	Success rate of obtaining 5 cm vertical position error (%)
Enhanced PPP method (GPS only)	1028	94.7	1642	80.7
Enhanced PPP method (GPS/GLONASS)	909	96.0	1516	82.5
The most reliable current fixed ambiguity PPP method: ILSDNCF, 1200 s lock time requirement	978	91.1	1581	77.2
Float PPP (GPS Only)	1082	95.4	1800	78.9
Float PPP (GPS/GLONASS)	908	97.7	1610	81.5

Table 6.3: Vertical error convergence comparison

In general, using GLONASS with GPS improves ambiguity resolution results through better float PPP estimation, as discussed in Section 5.3.3. However, there are a few cases where using GLONASS with GPS caused worse float PPP estimation, leading to wrong ambiguity resolution. It is likely that using GLONASS with GPS can provide more benefit in the future, if the GLONASS correction products are more accurate and reliable compared to the current CNES correction products.

As discussed in Chapter 5, the enhanced PPP method can also be used with an alternative set of ambiguity validation parameters. For this set, the length of the ambiguity validation time window is set to 250 s; at least four narrow-lane ambiguities are required to be fixed initially and the required confidence level during the convergence period is set to 99.99% and to 99.00% post-convergence. The results obtained using the alternative parameters are shown in Table 6.4. Compared to the results shown in Table 6.1, employing the alternative processing settings increases the rate of correct ambiguity resolution and time required to obtain an initial ambiguity resolution. In addition, employing the alternative settings decreases the rate of incorrect ambiguity resolution and average position error and its standard deviation at the initial ambiguity resolution epoch. Furthermore, employing the alternative validation settings requires more computational power, because of the increased number of float ambiguity groups to test.

Method	Rate of ambiguity resolution (%)	Rate of correct ambiguity resolution (%)	Rate of incorrect ambiguity resolution (%)	Average time to obtain an initial ambiguity resolution and its standard deviation (s)	Average position error 3D/Horizontal/ Vertical and their standard deviations (cm)
Enhanced PPP method (GPS only)	86.5	82.0	4.5	2190 (SD: 600)	4.3/2.4/3.1 (SD: 4.1/3.3/3.1)
Enhanced PPP method (GPS/GLONASS)	87.1	83.2	3.9	2120 (SD: 620)	4.1/2.3/2.9 (SD: 3.5/2.9/2.5)
The most reliable current method: ILSDNCF, 1200 s lock time requirement	86.9	74.2	12.7	1560 (SD: 570 s)	6.3/4.0/4.2 (SD: 7.8/6.7/4.7)

Table 6.4: Summary of the PPP ambiguity resolution and validation results using the enhanced PPP method with the alternative ambiguity validation parameters (NOAA dataset)

6.2.2 Fixed ambiguity PPP using a Global dataset

The performance of the enhanced PPP method is also tested using a Global dataset. The dataset includes 14 IGS stations, which are shown in Table 6.5, and 80 one hour time-periods, which are shown in Table 6.6. The map of the global dataset stations is shown in Figure 6.11. The stations exclude those that are used in generating the CNES satellite clock corrections (Laurichesse, 2013). The same processing settings (combination 2 in Section 5.3.2.3) and error corrections products are used as in the previous NOAA dataset test.

Station code	Location	Receiver	Antenna
CHUR	Manitoba, Canada	TPS NET-G3A	ASH701945E_M NONE
DRAO	British Columbia, Canada	TRIMBLE NETR8	AOAD/M_T NONE
FAA1	Tahiti	SEPT POLARX4	LEIAR25.R4 NONE
GOLD	California, the USA	JPS EGGDT	AOAD/M_T
GMSD	Japan	TRIMBLE NETR9	TRM59800.00 SCIS
JPLM	California, the USA	JPS EGGDT	AOAD/M_T NONE
KIT3	Uzbekistan	JAVAD TRE_G3TH DELTA	JAV_RINGANT_G3T NONE
KOUR	French Guiana	SEPT POLARX4	AOAD/M_B NONE
OUS2	New Zealand	JAVAD TRE_G3TH DELTA	JAV_RINGANT_G3T NONE
PERT	West Australia, Australia	TRIMBLE NETR9	TRM59800.00 NONE
STHL	Saint Helena	TPS NET-G3A	TPSCR.G3 SCIS
STR2	Australia Capital Territory, Australia	TRIMBLE NETR9	TRM59800.00 NONE
UNB3	New Brunswick, Canada	TRIMBLE NETR9	TRM57971.00
ZIM2	Switzerland	TRIMBLE NETR5 4.43	TRM59800.00 NONE

Table 6.5 The Global dataset stations, receivers and antennas

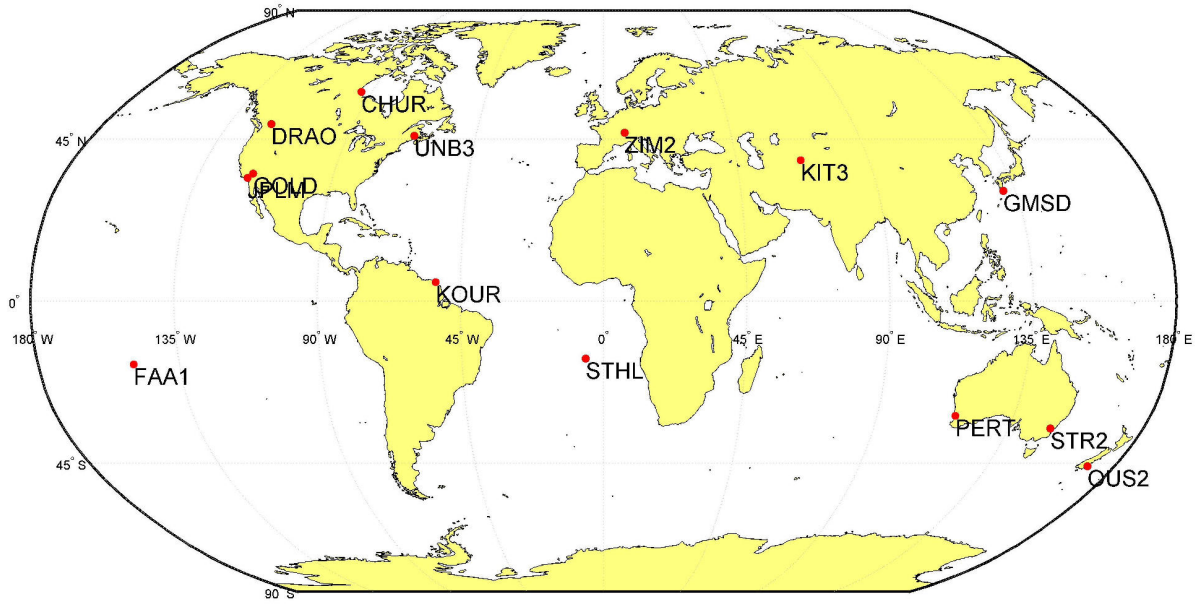

Figure 6.11 The Global dataset stations

Year	Month	Day	Hours
2013	01	19	1-2, 4,-5, 7-8, 10-11, 13-14, 16-17, 19-20 and 22-23
2013	01	20	1-2, 4,-5, 7-8, 10-11, 13-14, 16-17, 19-20 and 22-23
2013	01	21	1-2, 4,-5, 7-8, 10-11, 13-14, 16-17, 19-20 and 22-23
2013	01	22	1-2, 4,-5, 7-8, 10-11, 13-14, 16-17, 19-20 and 22-23
2013	01	23	1-2, 4,-5, 7-8, 10-11, 13-14, 16-17, 19-20 and 22-23
2013	01	24	1-2, 4,-5, 7-8, 10-11, 13-14, 16-17, 19-20 and 22-23
2013	01	25	1-2, 4,-5, 7-8, 10-11, 13-14, 16-17, 19-20 and 22-23
2013	01	26	1-2, 4,-5, 7-8, 10-11, 13-14, 16-17, 19-20 and 22-23
2013	01	27	1-2, 4,-5, 7-8, 10-11, 13-14, 16-17, 19-20 and 22-23
2013	01	28	1-2, 4,-5, 7-8, 10-11, 13-14, 16-17, 19-20 and 22-23

Table 6.6 The Global dataset time-periods

The average time required to obtain an initial ambiguity resolution is shown in Figure 6.12 for the various stations. It varies between 1840 and 2300 s when using GPS alone and between 1760 and 2180 s when using both GPS and GLONASS. The required time is shorter or equal when using GPS with GLONASS compared to the GPS alone case, except at the STR2 station. However, the difference at the STR2 station is explained by the higher ambiguity fixing rate when employing both GPS and GLONASS (66%) compared to employing GPS alone (64%). At the CHUR station, there are no GLONASS measurements available. In terms of the standard deviation of the time required to obtain an initial ambiguity resolution, there is no significant differences between the GPS alone and GPS with GLONASS processing scenarios.

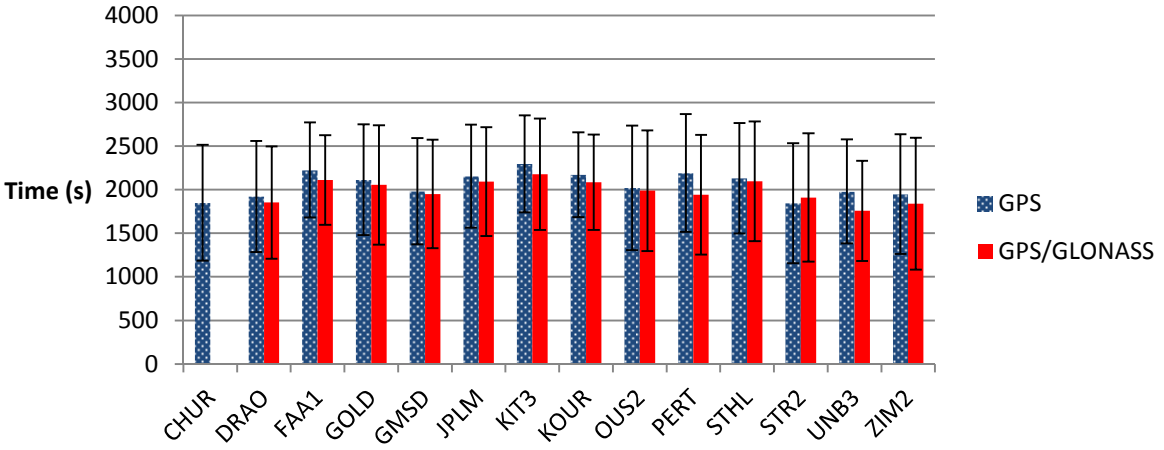

Figure 6.12 The average time required to obtain an initial ambiguity resolution at different stations and standard deviation (one sigma), shown as error bars (Global dataset)

The average horizontal position error at the initial ambiguity resolution epoch at different stations is shown in Figure 6.13. The average magnitude of the error varies between 1.1 and 3.3 cm when using GPS alone and between 1.1 and 2.9 cm when using both GPS and GLONASS. Using GLONASS with GPS provides position errors smaller or equal to GPS alone, except at the KOUR station. The reason why the horizontal position error is larger at the KOUR station is that employing GLONASS with GPS caused insufficiently accurate float PPP solution at 21 January 2013 at 7:00, which caused incorrect ambiguity resolution. The insufficient accuracy of the float solution is caused by errors in the CNES correction products. The standard deviation of the horizontal error is large at the KOUR (GPS/GLONASS processing, 4.7 cm) and ZIM2 (GPS/GLONASS processing, 6.0 cm) stations. The reason for this may be incorrect ambiguity resolution.

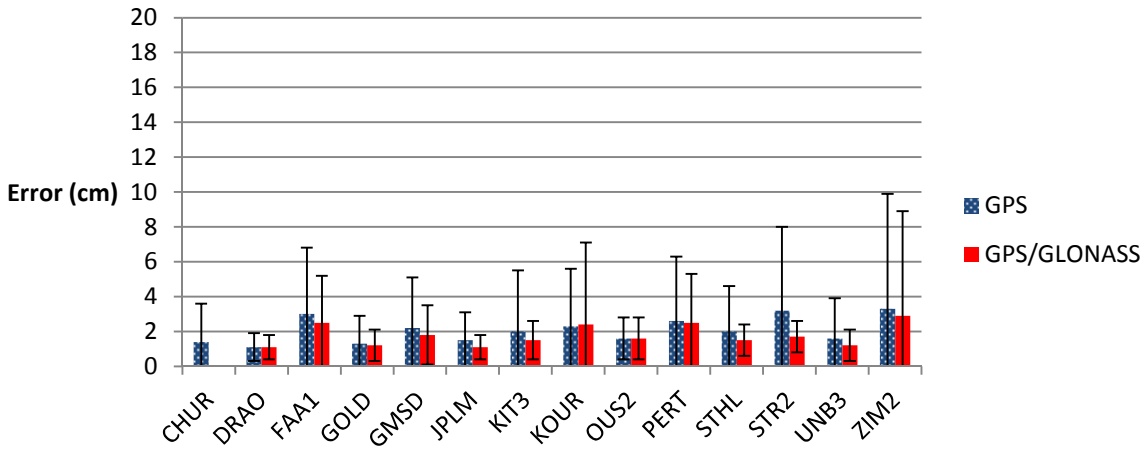

Figure 6.13 The average horizontal position error at the initial ambiguity resolution epoch at different stations (Global dataset, one sigma standard deviation shown as error bars)

The average vertical position error at the initial ambiguity resolution epoch at different stations is shown in Figure 6.14. The error magnitude varies between 1.9 and 5.8 cm when using GPS alone and between 2.1 and 5.0 cm when using both GPS and GLONASS. Using GLONASS with GPS provides vertical errors smaller or equal to GPS alone, except at the GOLD station. The difference at the GOLD station is explained by the higher ambiguity resolution rate when employing both GPS and GLONASS (85%) compared to employing GPS alone (75%).

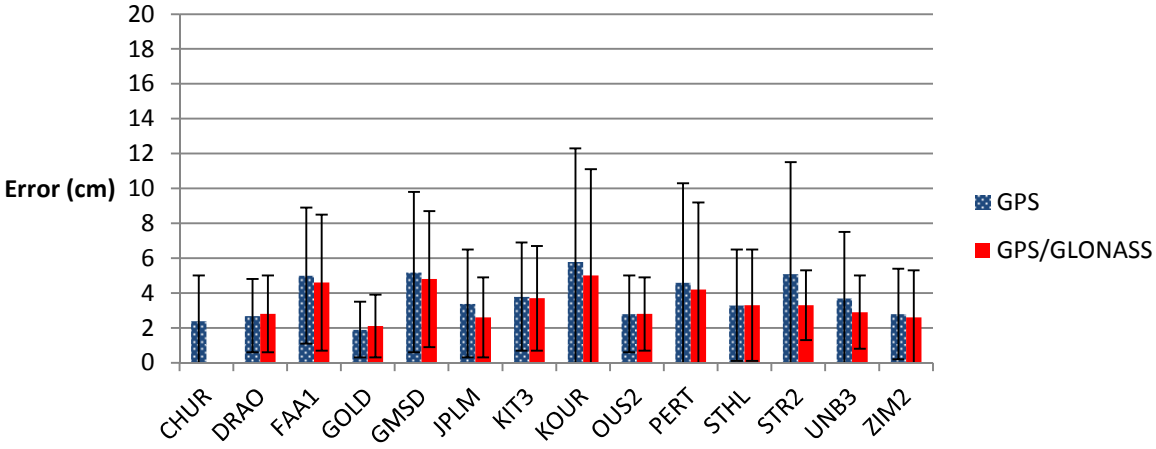

Figure 6.14 The average vertical position error at the initial ambiguity resolution epoch at different stations (Global dataset, one sigma standard deviation shown as error bars)

The average position error at the initial ambiguity resolution epoch based on all data is shown in Figure 6.15. The magnitudes of the average 3D, horizontal and vertical position errors are 4.6 (SD: 4.9 cm), 2.1 (SD: 3.3 cm) and 3.7 cm (SD: 4.0 cm), respectively, when

using GPS alone and 4.1 (SD: 4.1 cm), 1.7 (SD: 2.7 cm) and 3.4 cm (SD: 3.4 cm), respectively, when using both GPS and GLONASS.

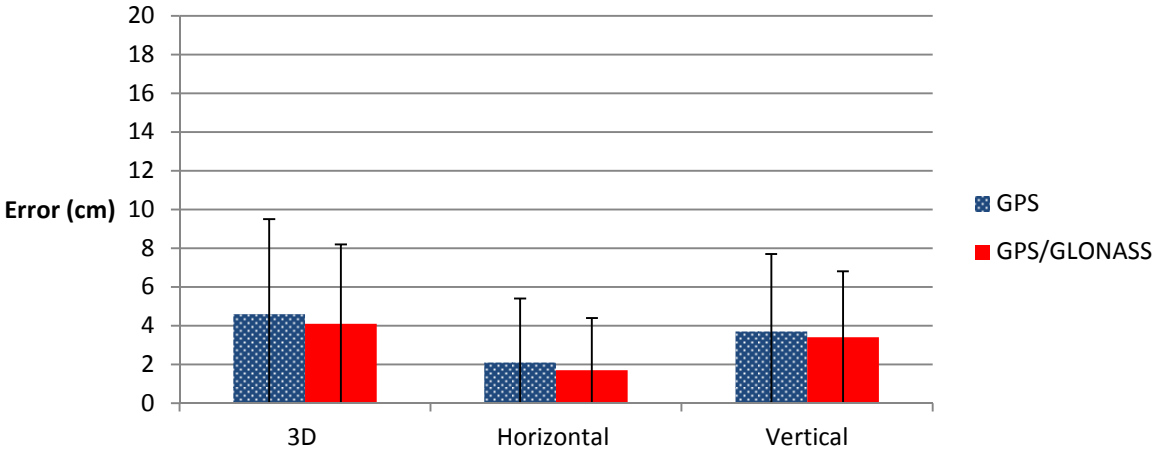

Figure 6.15 The average position errors at the initial ambiguity resolution epoch based on all data (Global dataset, one sigma standard deviation shown as error bars)

The average time required to obtain an initial ambiguity resolution is shown in Figure 6.16 . An average of 2060 s (SD: 630 s) is required to obtain an initial ambiguity resolution when using GPS alone and 1980 s (SD: 660 s) when using both GPS and GLONASS.

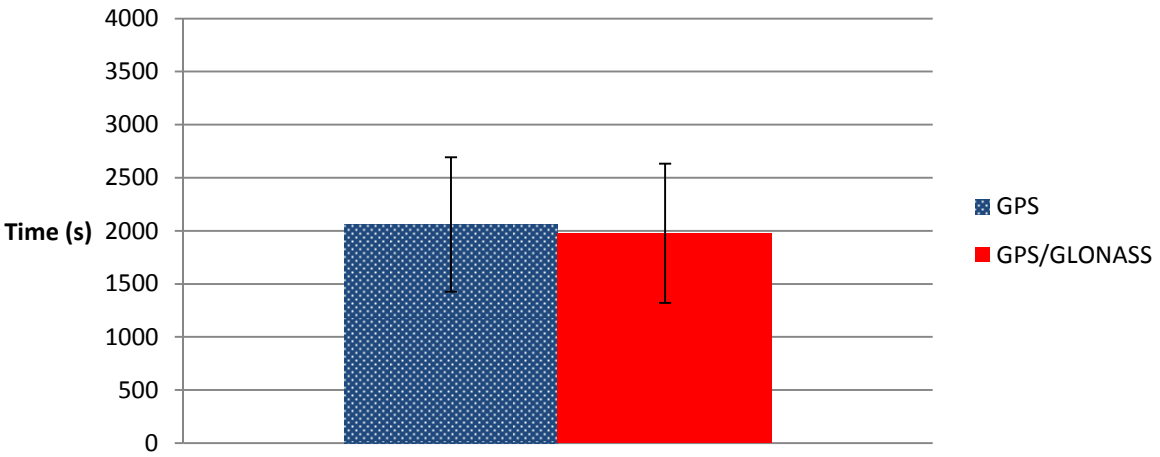

Figure 6.16 The average time required to obtain an initial ambiguity resolution based on all data (Global dataset, one sigma standard deviation shown as error bars)

The distribution of 3D position errors at the initial ambiguity resolution epoch is shown in Figure 6.17. The 3D position error is larger than 10.7 cm in 7.4% cases when using GPS alone and 4.8% cases when using both GPS and GLONASS.

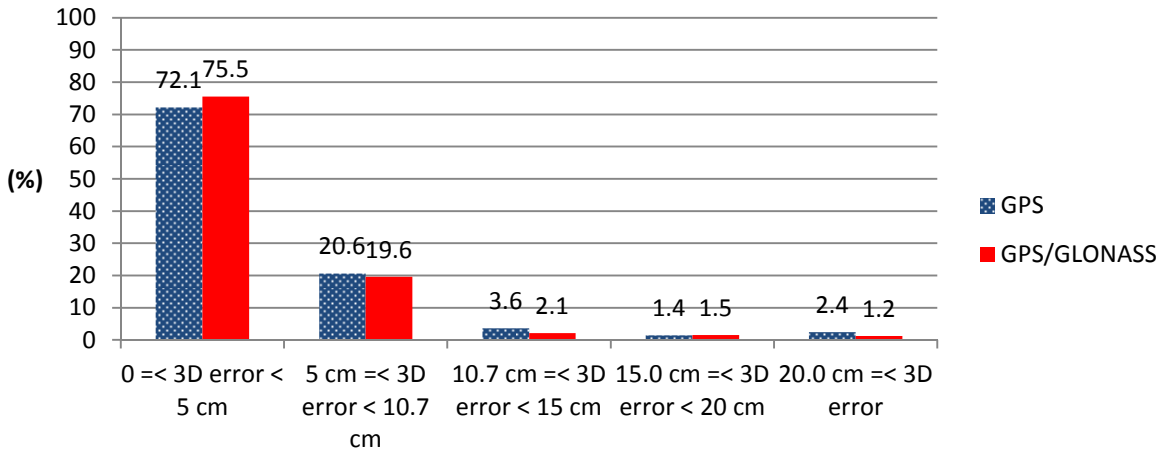

Figure 6.17 The distribution of the 3D position error at the initial ambiguity resolution epoch based on all data (Global dataset)

A summary of the PPP ambiguity resolution and validation results is shown in Table 6.7. The table shows that using GLONASS with GPS improves the results in all aspects. Compared to the NOAA dataset results shown in Table 6.1, using GLONASS with GPS provides more benefit when processing the Global dataset. For example, employing GLONASS with GPS improved the rate of correct ambiguity resolution from 80.8% to 82.2% with the NOAA dataset and 73.6% to 78.0% with the Global dataset.

In general, the rates of ambiguity resolution and correct ambiguity resolution are lower when processing the Global dataset compared to the NOAA dataset. It is expected that there are some differences between the datasets, because the locations of the stations and testing time-periods are different. The NOAA dataset stations (Figure 5.2) are mostly located in North-America or the Middle East as the Global dataset stations (Figure 6.11) are located in a globally diverse way. The differences between the datasets may cause different atmospheric and multipath conditions and varying satellite geometry and performance of the CNES correction products. Thus, it is expected that the PPP results are also different.

Method	Rate of ambiguity resolution (%)	Rate of correct ambiguity resolution (%)	Rate of incorrect ambiguity resolution (%)	Time to obtain an initial ambiguity resolution and its standard deviation (s)	Position error 3D/Horizontal/ Vertical and their standard deviations (cm)
Enhanced PPP method (GPS only)	79.4	73.6	5.9	2060 (SD: 630 s)	4.6/2.1/3.7 (SD: 4.9/3.3/4.0)
Enhanced PPP method (GPS/GLONASS)	81.7	78.0	3.9	1980 (SD: 660 s)	4.1/1.7/3.4 (SD: 4.1/2.7/3.4)

Table 6.7: Summary of PPP ambiguity resolution and validation results using the enhanced PPP method (Global dataset)

6.3 Static positioning using Numerical Weather Modelling (NWM) based tropospheric corrections

The impact of using NWM based tropospheric corrections is tested with the enhanced PPP method. Data recorded at the DARE (Daresbury, UK) and INVR (Inverness, UK) Ordnance Survey stations are used for these tests. One hour datasets are used in each test. The data were recorded during the following time-periods: 30 December 2011 (1am-11pm), 31 December 2011 (1am-7pm) and 3, 4, 5 and 6 January 2012 (1am-11pm). The total number of hourly tests per stations is 128.

NWM-based tropospheric delay is calculated as described in Section 3.4.5.4. The update interval of the corrections is 6 hours and the slant tropospheric delay is calculated for each satellite every 30 s. Thus, the EKF is also updated every 30 s in this test. RINEX data with a 5 s data-rate are used for cycle-slip detection and correction.

Three different types of tropospheric modelling methods are tested. The conventional method employs the UNB3m model, GMF and Chen tropospheric gradient mapping function. The conventional method is the same as used in Section 4.2. The NWM method employs NWM based tropospheric corrections as discussed in Sections 3.4.5.4 without estimating troposphere in EKF. The NWM + wet method employs NWM based corrections while the tropospheric wet delay is estimated as an EKF state and mapped into the satellite to receiver range level using GMF.

The average time required to obtain an initial ambiguity resolution based on all data is shown in Figure 6.18. The times are 1990 (SD: 590 s), 1970 (SD: 640 s) and 2080 s (SD: 620 s) in the conventional, NWM and NWM + wet test cases, respectively. It can be seen that ambiguities are fixed fastest in the NWM case. It is likely that ambiguity resolution is faster, because there is no need to wait for the tropospheric delay estimate in EKF to converge to sufficient accuracy. On the other hand, the standard deviation of the time required to fix ambiguities is largest in the NWM case. This is likely caused by the time and location specific variation of the NWM correction quality.

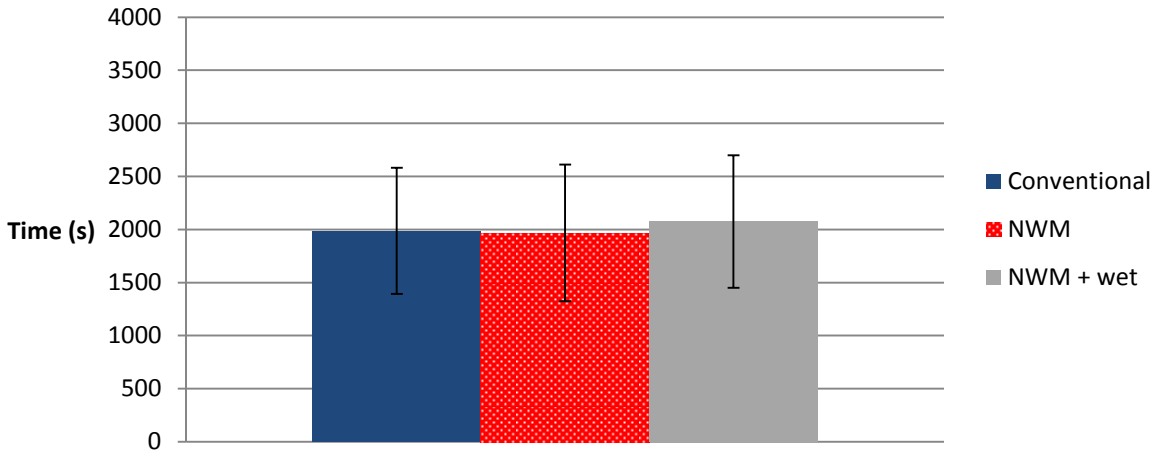

Figure 6.18 The average time required to obtain an initial ambiguity resolution when employing the enhanced PPP method (one sigma standard deviation shown as error bars)

The average 3D, horizontal and vertical position errors at the initial ambiguity resolution epoch based on all data are shown in Figure 6.19. The figure shows that using NWM based corrections increases the errors. For example, the 3D position error is 3.2 (SD: 2.3 cm), 4.4 (SD: 4.5 cm) and 5.6 cm (SD: 5.3 cm) when employing the conventional, NWM and NWM + wet methods, respectively. The reason for the increased error magnitudes is that the tropospheric delay correction is inaccurate when employing NWM based corrections, compared to the conventional method. The same issue can also be seen when looking the standard deviation of the errors.

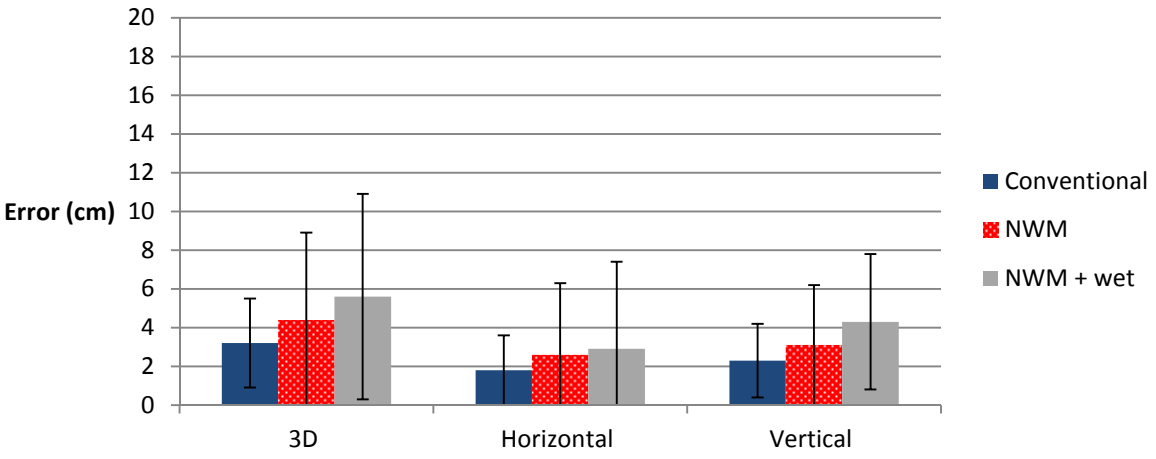

Figure 6.19 The average position error at the initial ambiguity resolution epoch when employing the enhanced PPP method (one sigma standard deviation shown as error bars)

When employing the enhanced PPP method, the satellite elevation mask used is five degrees. However, the quality of the NWM based corrections is not sufficient for low elevation satellites (satellites below 10 degrees). For conventional tropospheric estimation, using low elevation data is useful. However, this is not necessary when employing NWM based tropospheric corrections.

To understand the impact of elevation mask and code and carrier-phase measurement weighting, the NWM test is run again using an elevation mask of ten degrees and the measurement weighting formula (Black and Eisner, 1984) shown in (6.1). When employing this formula, less weight is given to low elevation measurements compared to the weighting associated with equation (4.12) otherwise employed with the enhanced PPP method. The base-standard deviation used for carrier-phase measurements in this test is 1 cm and for code-phase measurements 4.5 m. The standard deviation of a measurement is obtained by multiplying the base-standard deviation with the value obtained using equation (6.1), where E is the elevation of the the satellite. The other processing settings are the same as those used in the enhanced PPP method.

$$ratio = \frac{1.001}{\sqrt{(0.002001 + \sin^2(E))}} \tag{6.1}$$

The average times required to obtain an initial ambiguity resolution are shown in Figure 6.20. The times are 1980 (SD: 630 s), 2020 (SD: 670 s) and 2030 s (SD: 630 s) when

employing the conventional, NWM and NWM + wet methods, respectively. The results show that NWM based tropospheric corrections do not improve the speed of ambiguity resolution.

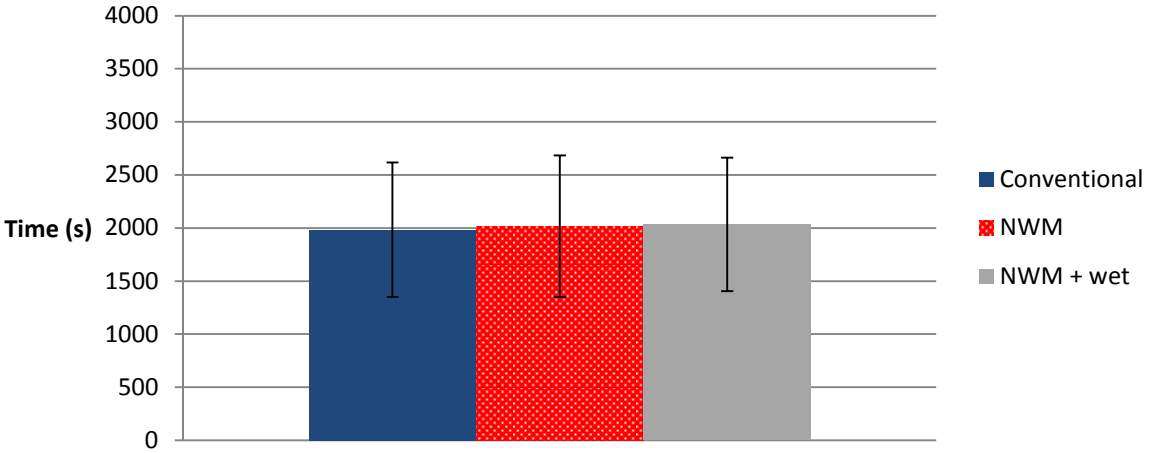

Figure 6.20 The average times required to initial ambiguity resolution when employing the enhanced PPP method with a 10 degree elevation mask and Black and Eisner measurement weighting (one sigma standard deviation shown as error bars)

The magnitudes of the average 3D, horizontal and vertical position errors at the initial ambiguity resolution epoch based on all data are shown in Figure 6.21. The results show that using NWM based corrections decreases the 3D and vertical position errors compared to the conventional and NWM + wet methods. For example, the 3D position error is 4.5 (SD: 5.0 cm), 3.9 (SD: 3.7 cm) and 4.0 cm (SD: 4.2 cm) when employing the conventional, NWM and NWM + wet methods, respectively. However, the error and its standard deviation are still larger compared to the case of employing the conventional method and using the weighting formula associated with equation (4.12).

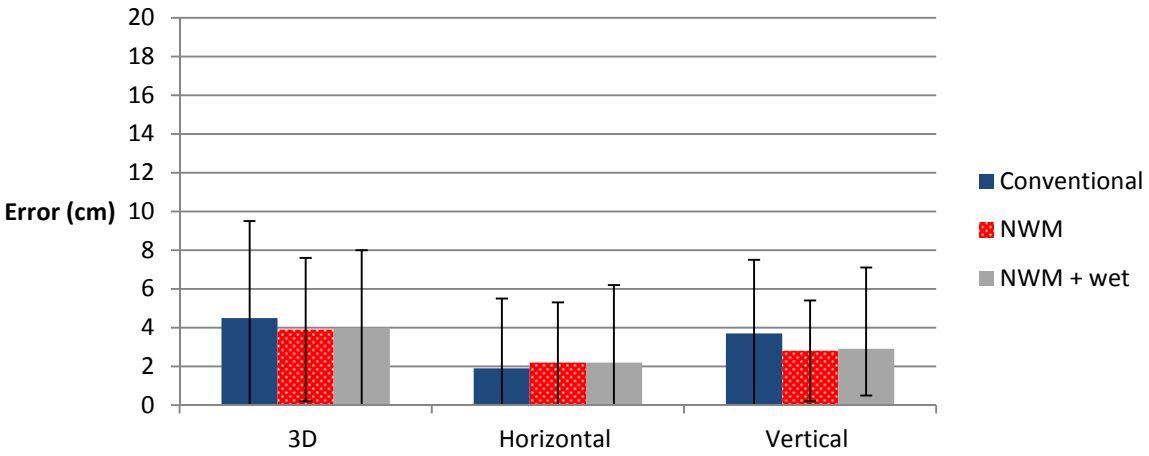

Figure 6.21 The average position error at the initial ambiguity resolution epoch when employing the enhanced PPP method with a 10 degree elevation mask and Black and Eisner measurement weighting (one sigma standard deviation shown as error bars)

Table 6.8 shows a comparison between the methods in terms of the ambiguity fixing rates, time required to initial ambiguity resolution and position error at the initial ambiguity resolution epoch. The rate of ambiguity resolution is highest (91.4%) when using the enhanced PPP method with a 10 degree elevation mask, Black and Eisner measurement weighting and conventional tropospheric estimation. The rate of correct ambiguity resolution is highest (89.1%) when employing the enhanced PPP method with a 10 degree elevation mask, Black and Eisner measurement weighting and NWM + wet tropospheric estimation. The rate of incorrect ambiguity resolution is lowest when employing the enhanced PPP method with conventional tropospheric estimation. There are no significant differences in the time required to obtain an initial ambiguity resolution between the methods. The position error and its standard deviation at the initial ambiguity resolution epoch are smallest when using the enhanced PPP method with conventional tropospheric estimation.

Method	Tropospheric estimation	Rate of ambiguity resolution (%)	Rate of correct ambiguity resolution (%)	Rate of incorrect ambiguity resolution (%)	Time to obtain an initial ambiguity resolution and its standard deviation (s)	Position error 3D/Horizontal/ Vertical and their standard deviations (cm)
Enhanced PPP method	Conventional	89.9	88.7	1.2	1990 (SD: 590 s)	3.2/1.8/2.3 (SD: 2.3/1.8/1.9)
Enhanced PPP method	NWM	87.1	81.6	5.5	1970 (SD: 640 s)	4.4/2.6/3.1 (SD: 4.5/3.7/3.1)
Enhanced PPP method	NWM + wet	84.8	76.2	8.6	2080 (SD: 620 s)	5.6/2.9/4.3 (SD: 5.3/4.5/3.5)
Enhanced PPP method, 10 degree elevation mask and Black and Eisner measurement weighting	Conventional	91.4	88.3	3.1	1980 (SD: 630 s)	4.5/1.9/3.7 (SD: 5.0/3.6/3.8)
Enhanced PPP method, 10 degree elevation mask and Black and Eisner measurement weighting	NWM	88.3	85.9	2.3	2020 (SD: 670 s)	3.9/2.2/2.8 (SD: 3.7/3.1/2.6)
Enhanced PPP method, 10 degree elevation mask and Black and Eisner measurement weighting	NWM + wet	90.6	89.1	1.6	2030 (SD: 630 s)	4.0/2.2/2.9 (SD: 4.2/3.8/2.4)

Table 6.8: Summary of PPP ambiguity resolution and validation results for the NWM test

The results show that using NWM based tropospheric corrections is useful when employing the enhanced PPP method with a 10 degree elevation mask and the Black and Eisner measurement weighting. When using the enhanced PPP method with the default parameters, using NWM based corrections degrades the results. The reason for this can be attributed to the quality of the NWM based corrections, which may not be sufficient for low elevation satellites.

Employing the current NWM based corrections does not result in noticeable benefit. However, with improved accuracy and quality in the future, using NWM based tropospheric

corrections has potential. Currently, the problems are the long six hour update intervals of meteorological data, quality of the NWM products and lack of real-time processing capability. Particularly, the accuracy of the corrections must be improved to make them suitable for fixed-ambiguity PPP.

6.4 Kinematic positioning tests

Kinematic PPP is tested using data recorded by a GNSS receiver installed on a miniature train. The miniature train track is located on top of the Geospatial building at the University of Nottingham, UK (Liu et al., 2013). The length of the train track is 120 m and its width is 184.15 mm.

A Leica GNSS GS10 receiver and Leica AS10 antenna were used. The data were recorded on 26 October 2012. The receiver was static between 11:12:47 and 13:19:25. Thereafter, the receiver was turned off for 24 s between 13:19:25 and 13:19:49. Kinematic data recording began at 13:19:49 and ends at 15:21:47. The train was stopped for a while during the kinematic test, because low battery power. Both GPS and GLONASS measurements were recorded with a data-rate of 1 Hz. The EKF constant velocity model, which assumes that the rover has constant velocity, is employed in the PPP processing. The assumed standard deviation of the velocity is 10 m/s to allow fast accelerations. In general, it is important to not underestimate standard deviations, because this may lead the EKF to converge to a wrong solution. Overestimating the standard deviation of velocity is typically not as harmful as underestimating it. The overestimation may cause slower solution convergence, but it does not cause solution to convergence to a wrong solution.

A cRTK solution from the NovAtel GrafNav software is used as the reference track. The KEYW Ordnance survey reference station is used as the cRTK base-station. It is assumed that the position accuracy of the cRTK solution is at the level of centimetres.

Horizontal position error at the latitude/longitude level is shown in Figure 6.22 when using GPS alone and in Figure 6.23 when using both GPS and GLONASS. The figures show that the position error is larger during the initial convergence phase. During the kinematic phase, the position error is typically smaller than 10 cm. However, it is larger than 10 cm when the solution is re-converging after a signal outage.

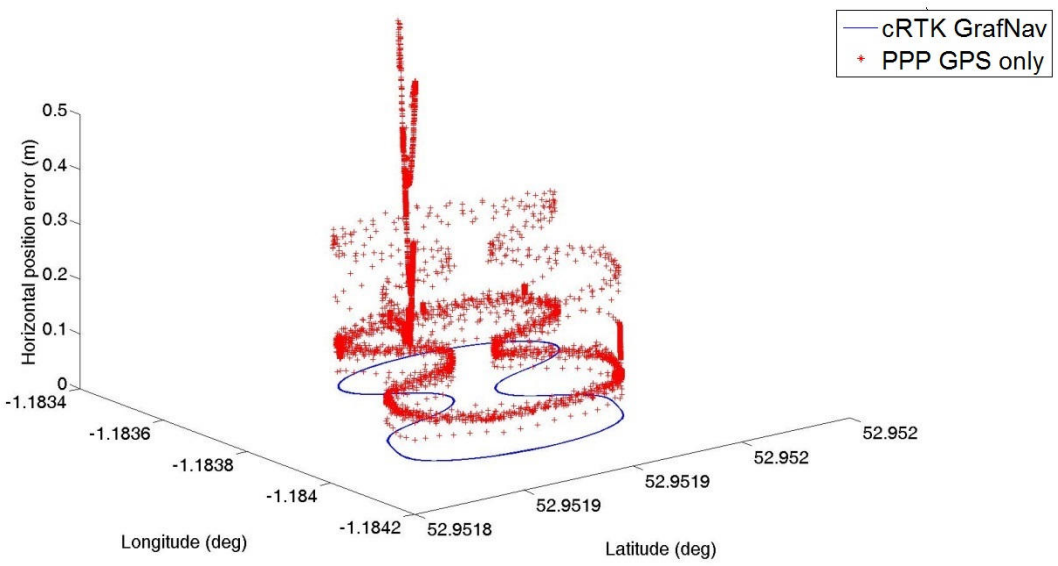

Figure 6.22 Horizontal position errors at the latitude/longitude level when using GPS only (Kinematic test)

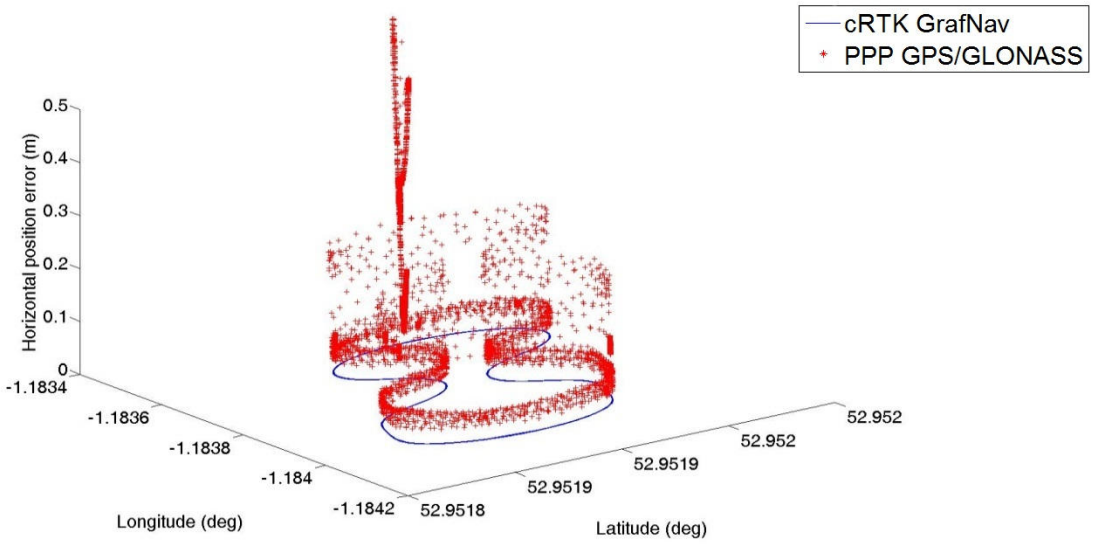

Figure 6.23 Horizontal position errors at the latitude/longitude level when using both GPS and GLONASS (Kinematic test)

Horizontal position errors based on all data is shown in Figure 6.24. The error associated with the kinematic portion is shown in Figure 6.25. The figures show that better than 10 cm position errors are achieved before the signal outage. It takes 2333 s to resolve the narrow-lane carrier phase ambiguities following the signal outage when using GPS alone and 2156 s when using both GPS and GLONASS. The magnitude of the horizontal position errors is 10

cm or less when the ambiguities are fixed. Using GLONASS with GPS provides faster initial ambiguity resolution and smaller horizontal position errors.

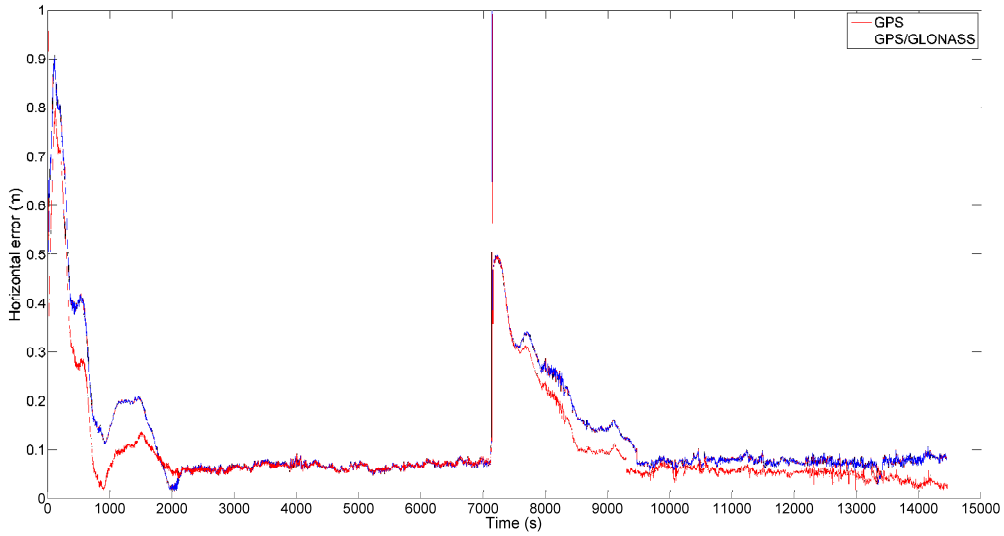

Figure 6.24 Horizontal position error (Kinematic test)

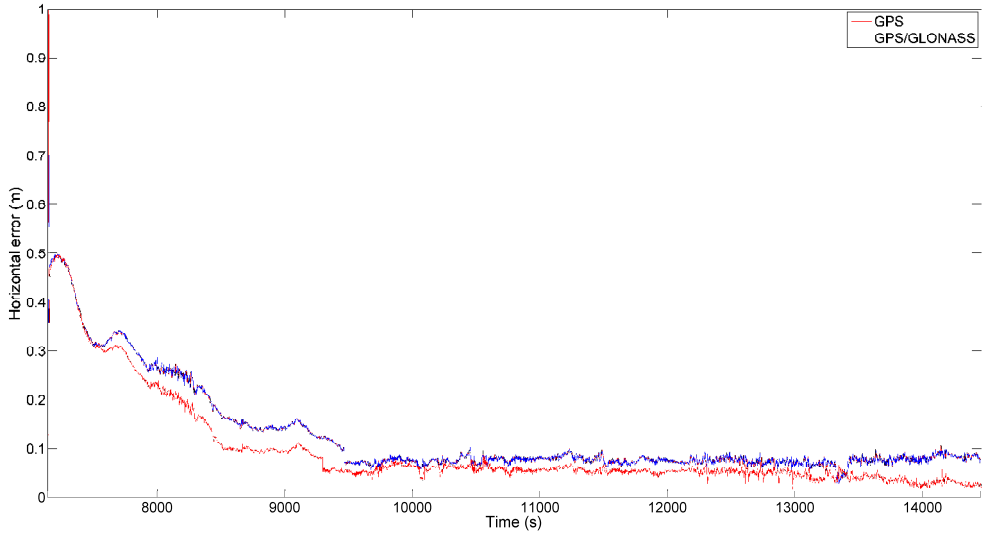

Figure 6.25 Horizontal position error for the kinematic portion (Kinematic test)

The vertical position error based on all data is shown in Figure 6.26. The error for the kinematic portion is shown in Figure 6.27. The results show that vertical position errors are larger than horizontal errors for most epochs and that employing GLONASS with GPS does not reduce vertical position errors. However, the potentially insufficient vertical accuracy of the reference cRTK solution may make the GPS with GLONASS solution look worse than it

actually is. The accuracy of the cRTK solution may be insufficient, because of the coordinates of the cRTK base-station may be inaccurate or the cRTK solution may have issues such as wrong ambiguity resolution. In addition, the larger vertical error for the GPS with GLONASS solution may have been caused by the insufficient quality of the satellite orbit and clock correction products.

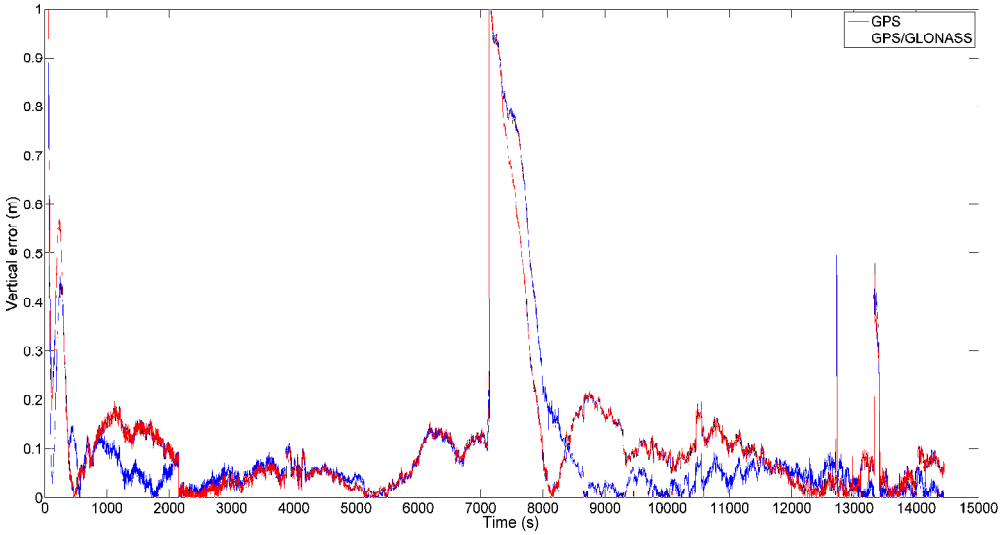

Figure 6.26 Vertical position errors (Kinematic test)

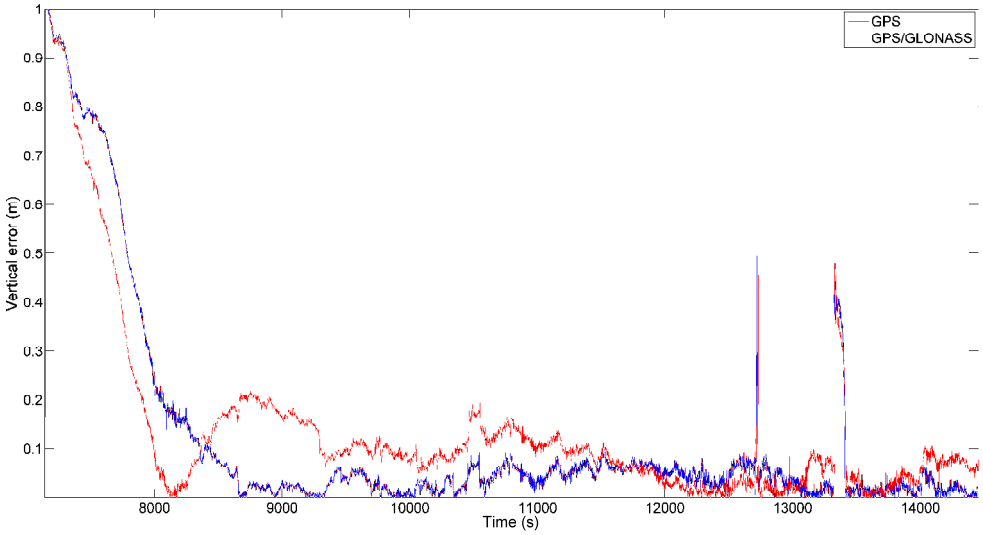

Figure 6.27 Vertical position errors for the kinematic portion (Kinematic test)

The kinematic test shows that fixed ambiguity PPP can provide sufficient accuracy after the position solution has converged and ambiguities are fixed. However, a problem was identified with the solution re-convergence after the signal outage.

The rapid re-convergence method discussed in Section 4.3.2.3 is used. The method is based on saving wide-lane slant ionospheric delays before a signal outage and then using the saved ionospheric delay values after the signal outage to enable geometry dependent wide-lane ambiguity resolution (Geng et al., 2010a). However, the method is not suitable, if ionospheric activity is high during the signal outage. In this kinematic test, rapid PPP re-convergence failed likely because of high ionospheric activity, multipath environment or the insufficient quality of the CNES orbit and clock correction.

Errors in satellite orbit and clock corrections impact kinematic PPP to a larger extent than static PPP, because the errors translate directly into the position domain when the assumed position process noise is large in the EKF. This can explain the discontinuities in the position plots and the long time required for re-convergence.

6.5 Integrity tests

Failure detection and exclusion using the ICRAIM method is tested using data recorded on 8 March 2013 between 13:00 and 14:00 at the BDOS, ICT5, MIQE, MTDT, SCWT and SUAF NOAA stations. The performance of integrity monitoring is analysed in terms of the time required to generate an integrity alert and exclude the failure correctly since the time when the errors appeared in the data. The enhanced PPP method is used with both GPS and GLONASS measurements. In the tests, errors are added to raw measurements.

6.5.1 Case1: GPS PRN 26 L1 carrier-phase failure when it is the base-satellite

A 0.01 m/s ramp type of failure is added between 13:53:40 and 13:55:20 to the L1 carrier-phase signal received from the GPS satellite PRN 26, which is used as the base-satellite. The time required to generate an integrity alert and to exclude the failure correctly since the first appearance of the error is shown in Figure 6.28. The former varies between 5 and 40 s

and the latter between 10 and 90 s depending on the station. The failed satellite is not available at the SCWT and SUAF stations, explaining the lack of results.

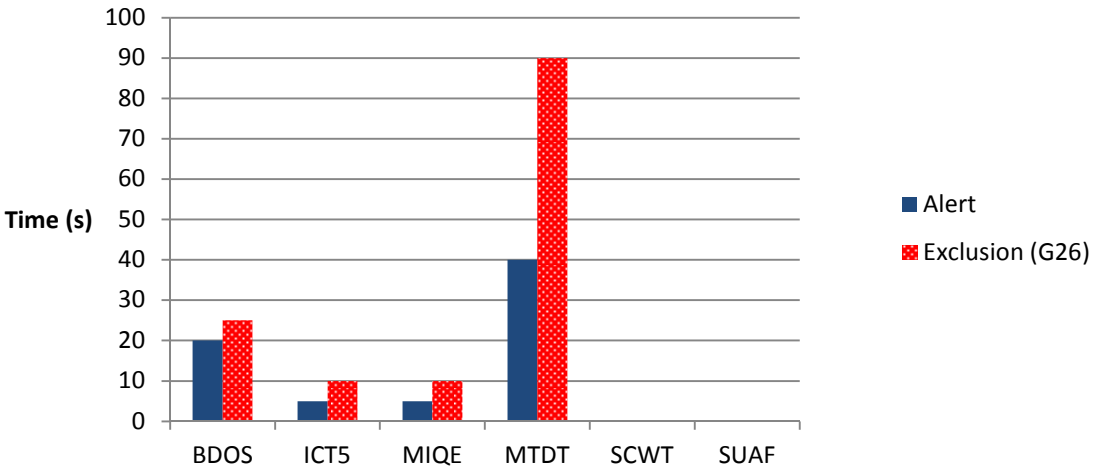

Figure 6.28 The time required to alert and exclude failures (Test case 1)

6.5.2 Case2: GPS PRN 5 and 29 L2 carrier-phase failure

A 0.01 m/s ramp type of carrier-phase failure is added between 13:52:00 and 13:53:40 to the L2 carrier-phase signals received from the GPS satellites PRN 5 and 29. Failure detection and correct exclusion results since the first appearance of the errors are shown in Figure 6.29. It takes between 10 and 50 s to generate an integrity alert, between 10 and 65 s to exclude PRN 5 and between 10 and 50 s to exclude PRN 29.

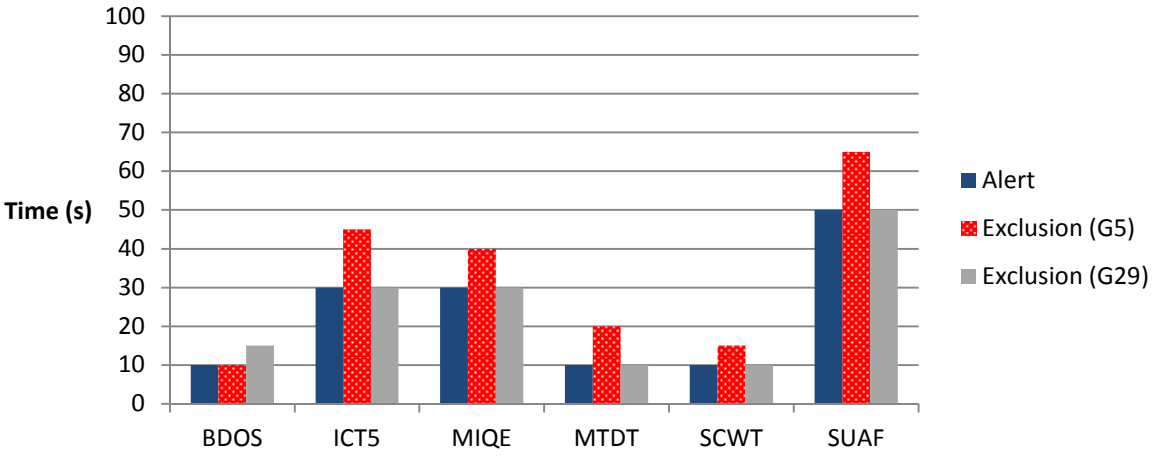

Figure 6.29 The time required to alert and exclude failures (Test case 2)

6.5.3 Case3: GPS PRN 5 and 29 L2 carrier-phase failure and GLONASS PRN 1 and 24 L1 carrier-phase failure

In this test case, GPS satellites PRN 5 and 29 and GLONASS satellites PRN1 and 24 are made to fail simultaneously between 13:52:00 and 13:53:40. The magnitude of the ramp type failure is 0.01 m/s, added to the GPS L2 and GLONASS L1 carrier-phase signals. The integrity alert and correct failure exclusion results since the first appearance of the errors are shown in Figure 6.30. It takes between 5 and 75 s to generate an integrity alert. Excluding GPS PRN 5 takes between 10 and 85 s, GPS PRN 29 between 15 and 75 s, GLONASS PRN 24 between 10 and 40 s and PRN 01 between 10 and 40 s. At the BDOS, MTDT and SCWT stations, the magnitudes of the GLONASS failures are not causing sufficiently large position errors to cause the exclusion of the failed satellites from the solution.

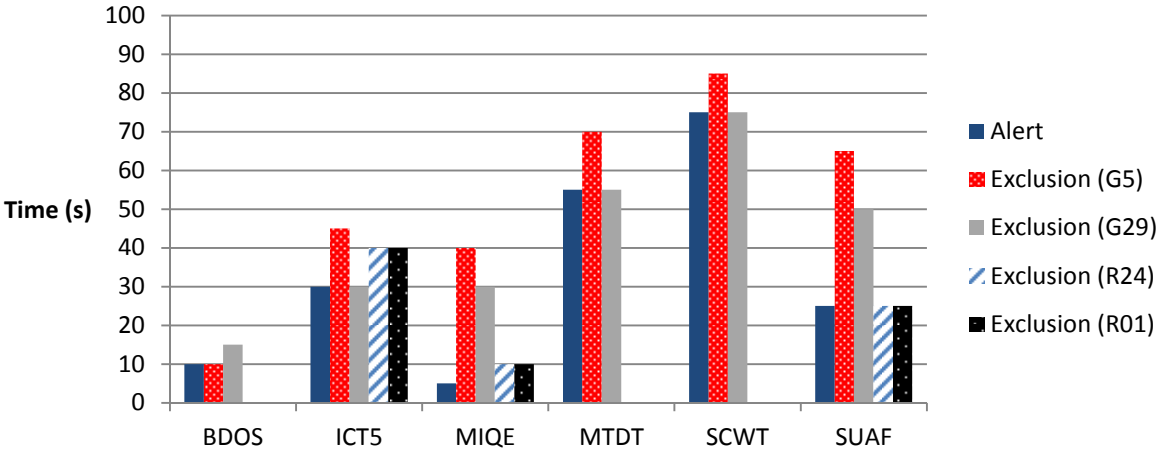

Figure 6.30 The time required to alert and exclude failures (Test case 3)

6.5.4 Case4: GLONASS PRN 1 and 24 L1 carrier-phase failures

The GLONASS satellites PRN 1 and 24 are made to fail in this test. A 0.01 m/s ramp type of failure is added to the L1 carrier-phase signals received from the satellites between 13:52:00 and 13:53:40. This test is similar to test case 3, except that GPS satellites are not made to fail. The failure alert and correct exclusion results since the first appearance of the errors are shown in Figure 6.31. The time required to generate an integrity alert varies between 5 and 25 s, and the GLONASS satellites 1 and 24 are excluded in a time-frame varying between 10 and 40 s. At the MTDT and SCWT stations, the failures do not cause sufficiently large position errors to cause an integrity alert. At the BDOS station, an integrity alert is

generated, but failure exclusion is not carried out. The reason is the low magnitude of the failures.

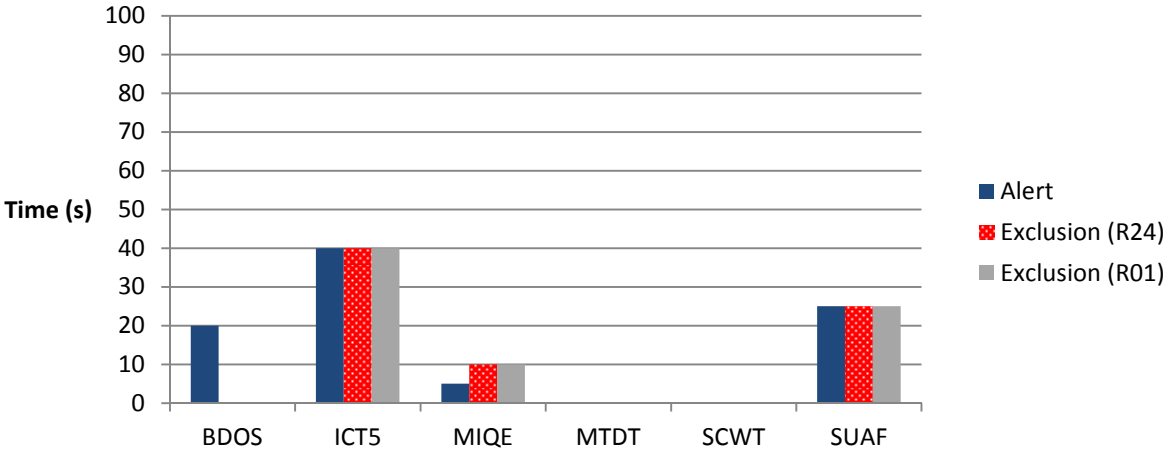

Figure 6.31 The time required to detect and exclude failures (Test case 4)

6.5.5 Case5: GPS PRN 5 and 29 and GLONASS PRN 24 L1 code-phase failures

The impact of code-phase failures is tested in this case. A ramp type code-phase failure with a magnitude of 0.1 m/s is added to the L1 code-phase signals received from the GPS PRN 5 and 29 and GLONASS PRN 24 satellites. The failure alert and correct exclusion results since the first appearance of the errors are shown in Figure 6.32. It takes between 25 and 45 s to generate an integrity alert. Excluding GPS PRN 05, GPS PRN 29 and GLONASS PRN 24 takes between 25 and 45 s, 25 and 60 s and 40 and 45 s, respectively.

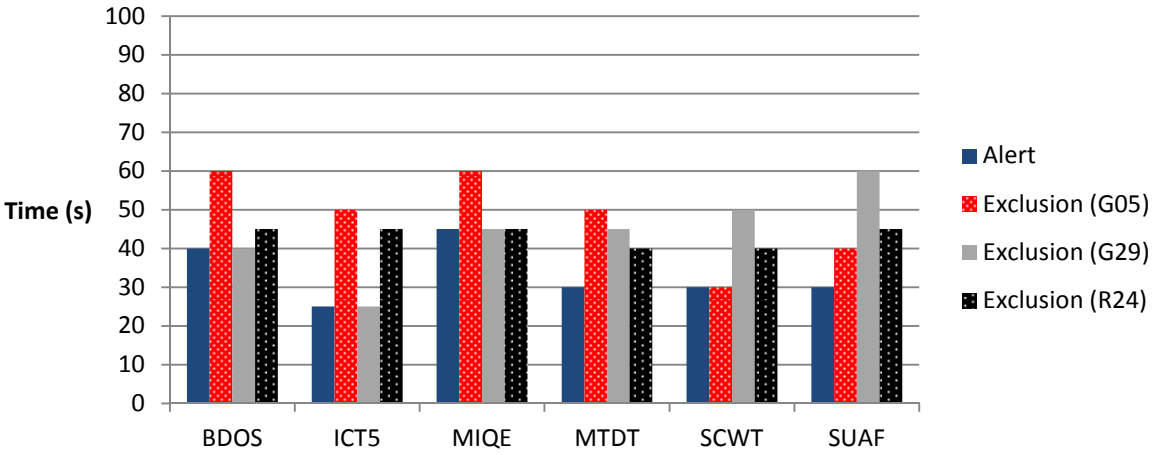

Figure 6.32 The time required to detect and exclude failures (Test case 5)

6.5.6 Summary of the integrity test results

Based on the results, raising an integrity alert took between 5 and 75 s and failure exclusion between 10 and 90 s depending on the magnitude of the failure and satellite geometry. Therefore, it can be concluded that ICRAIM is a suitable method to alert and exclude the tested failures. Based on this, ICRAIM is a suitable method for monitoring integrity against multiple types of errors such as satellite clock failures and cycle-slips. It was even demonstrated that ICRAM can alert and exclude multiple failures simultaneously.

The weakness of the ICRAIM method is that it calculates test statistics based on measurement residuals. Therefore, ICRAIM cannot detect and exclude errors which are consistent with the PPP estimation. Wrong carrier-phase ambiguity resolution (as discussed in Section 5.2.6.2) is an example of this kind of error situation, because the PPP filter solution becomes consistent with the wrongly fixed ambiguities after the ambiguity resolution is accepted. In addition, ICRAIM may not be able to detect centimetre-level constant or slowly growing errors which appeared already during the solution convergence, because the estimated ambiguity terms are consistent with the errors.

To improve PPP integrity monitoring, monitoring integrity during correction product generation (as discussed in Section 5.2.6.4) is necessary. In addition, detecting wrong carrier-phase ambiguity resolution is necessary. As future work, for example, parallel independent float and fixed ambiguity PPP solutions can be used to detect wrong ambiguity resolutions.

Because of the weakness of ICRAIM, PPP cannot currently be used for safety critical applications, which have specific integrity requirements. Nevertheless, ICRAIM is still a useful method for ensuring that failures are not causing unnecessary decrease of PPP performance, when PPP is used for non-safety critical applications such as agriculture. In addition, the improvements in terms of failure exclusion and protection level calculation presented in this thesis can still make ICRAIM more useful for practical applications as shown by the results.

6.6 Feasibility of the enhanced PPP method

The requirements of the applications are defined in Chapter 2. The feasibility of the enhanced PPP method to fulfil the requirements is discussed hereafter.

6.6.1 Static applications

As discussed in Chapter 2, positioning accuracies between 1 and 10 cm are required for detailed surveying. For control surveying, the required accuracy is at sub-centimetre level. There are no specific integrity or time criticality requirements for surveying applications. Based on the requirements of detail surveying, the enhanced PPP method (as tested in Section 6.2) is able to fulfil these. For control surveying, the accuracy of the enhanced PPP method or any other current PPP method is not sufficient at least when the surveying is done using only one hour of GNSS data as discussed Section 6.2. The reason is that sub-centimetre level positioning accuracy cannot be obtained using the enhanced PPP method. In addition, the total sum of errors (Section 3.5) when employing the most accurate currently available PPP error correction products and models is not sufficiently small that sub-centimetre level positioning could be obtained.

In general, the enhanced PPP method can fulfil the requirements of static applications which require accuracy similar to that of detail surveying. However, if a static application requires centimetre-level position accuracy and immediate convergence, the enhanced PPP method or any currently available PPP method which is available globally is not suitable. The immediate convergence requirement can currently only be achieved using correction data such as ionospheric corrections from local reference networks as discussed in Section 4.3.2.3.

Furthermore, the enhanced PPP method can be used to determine the position of reference stations with centimetre-level accuracy in areas where no permanent GNSS networks are available. Thereafter, the cRTK method can be used to estimate positions of rover receivers, because the position of the temporary reference station is known with centimetre level accuracy based on the PPP solution. Using PPP to calculate the coordinates of temporary

reference stations is beneficial in areas where there are no permanent GNSS networks available.

In conclusion, the enhanced PPP method is suitable for most static applications, provided the required convergence time for the application is not more stringent than the convergence time required to obtain centimetre-level accuracy. It is particularly useful in remote areas where there are no local reference networks available, and therefore, cRTK approaches cannot be used.

6.6.2 Kinematic and scientific applications

In general, the requirements for most kinematic applications are stricter than for static applications. Many kinematic applications require centimetre positioning with immediate convergence. In addition, some kinematic applications such as automatic landing have stringent integrity requirements, as discussed in Section 2.2. Nevertheless, there are still a large number of kinematic applications such as agriculture and marine applications which benefit from centimetre level positioning, but do not have strict accuracy or integrity requirements.

In general, PPP cannot fulfil the requirements of most aviation, military or intelligent transport applications, due to the long convergence times to reach the required accuracy. When employing the enhanced PPP method, the time required to fix ambiguities and obtain centimetre level positioning accuracy is typically between 20 and 30 minutes, not sufficient for these applications. In addition, the enhanced PPP method or any other current PPP method cannot satisfy the integrity requirements of the most aviation, military or intelligent transport applications as discussed in 6.5.6. The major reason is that there is no guarantee on the quality of the correction products.

However, the enhanced PPP method may be useful for kinematic applications which can tolerate a larger error during the convergence period or which are able to keep the receiver static during the initial ambiguity fix. The enhanced PPP method is suitable, for example, for many agricultural, transport or marine applications as discussed in Chapter 2, because the required convergence times are sufficiently long or because they have less stringent accuracy requirements. The suitable marine applications can include oil and gas (offshore)

applications, because decimetre to centimetre level accuracy is typically sufficient for these applications.

Re-convergence is a challenge for kinematic applications, because the signals from all satellites may be blocked temporarily. It is possible to use the rapid re-convergence method as discussed in Section 4.3.2.3 and tested in Section 6.4. However, this may increase the integrity risk, because ionospheric conditions may change rapidly during the data gap.

The enhanced PPP method and PPP in general are suitable, for example, for tsunami or earthquake prediction, because the applications do not require immediate solution convergence and the accuracy obtained is sufficient. Furthermore, the enhanced PPP method can also be used for research applications, for example, for LEO satellite orbit determination (Section 2.1).

In conclusion, the enhanced PPP method or in general any current PPP method which does not employ external ionospheric corrections cannot fulfil the requirements of dynamic applications which require cm-level accuracy and cannot afford 20 to 30 min convergence period. On the other hand, the enhanced PPP method is suitable for many kinematic applications such as agriculture which do not have strict requirements. For example, obtaining centimetre level positioning is beneficial for agricultural applications, but many of the agricultural applications can tolerate larger magnitude of the position error temporally.

6.6.3 Real-time and commercial implementation feasibility

All correction products used by the enhanced PPP method are generated in real-time, thereby enabling real-time positioning. For example, CNES provides satellite orbit and clock correction products in real-time. However, the long time required to obtain an initial ambiguity resolution may limit the suitability of the enhanced PPP method for some applications, because centimetre level positioning cannot be obtained immediately after turning on a receiver.

From the perspective of computational power requirements, the enhanced PPP method is suitable for real-time use. However, implementing it in embedded devices in practice

requires implementing matrix operations and mathematic operations used in ambiguity resolution in a computationally efficient way.

The enhanced PPP method is useful for commercial applications provided that the quality of the correction products can be assured. Therefore, it may be necessary to develop commercial-specific correction products that can guarantee a quality at a level enabling the correct resolution of GPS narrow-lane ambiguities. In addition, the reliability of the global GNSS reference network which is used to collect data for correction product generation must be guaranteed.

Satellite orbit and clock corrections must be delivered to rover receivers in real-time. If real-time positioning is required in remote areas, the corrections can be delivered using telecommunication satellites as is currently done by commercial PPP services, discussed in Section 4.6.2. Furthermore, mobile networks may also be used.

In all aspects, it is possible to build a real-time commercial PPP service, which can provide similar performance as the enhanced PPP method. However, it requires investments to develop a reliable satellite orbit and clock correction service and means to deliver the corrections to end-users.

7 Conclusions and recommendations

This chapter summarises the conclusions that can be drawn from the research in this thesis and provides recommendations for future work with the aim to further improve PPP in terms of convergence time, accuracy and ambiguity resolution performance.

7.1 Conclusion

This thesis has focussed on fixed ambiguity PPP using existing GPS and GLONASS L1 and L2 signals, because of the aim to develop solutions for systems and signals that are currently available for real-life applications. In addition, the aim was also to demonstrate the performance of the developed algorithms using real-GNSS data. Therefore, the new GNSS signals and systems were not employed in this thesis. Furthermore, the goal was to develop a globally applicable model. It was therefore, assumed that there are no local area specific error correction products such as ionospheric or tropospheric correction available.

The CNES real-time generated satellite orbit, clock, FCB and code-bias correction products were used. The correction products are openly available on the Internet for any user. The CNES products were used in this thesis, because they are the only openly available correction product in early 2013 which enables PPP carrier-phase ambiguity resolution. For the other error sources, the current error correction models and products were employed as discussed in Section 3.5.

Existing fixed ambiguity PPP methods including ambiguity resolution and validation were analysed and tested using the NOAA dataset in Chapter 5. Based on the tests, the ILSDNCF method with a 1200 s lock time requirement was chosen as the most suitable existing method, because it provided the lowest rate (12.7%) of incorrect ambiguity resolution and smallest 3D (6.3 cm), horizontal (4.0 cm) and vertical (4.2 cm) position errors at the initial ambiguity resolution epoch.

The large rate of incorrect ambiguity resolution and positioning accuracy obtained using existing methods are not acceptable for real-life applications. Therefore, novel methods to enhance ambiguity resolution and validation were developed in this thesis. This includes the

time window based ambiguity validation and variable confidence level methods and finding the most optimal ambiguity validation parameters discussed in Chapter 5. When employing the enhanced PPP method, which uses enhanced ambiguity resolution and validation, significant improvements were obtained compared to the results obtained the most reliable existing method (the ILSDNCF method with a 1200 s lock time requirement). Based on the results, the rate of incorrect ambiguity resolution was reduced from 12.7% to 6.0%, rate of correct ambiguity resolution increased from 74.2% to 80.8% and 3D, horizontal and vertical position errors were improved from 6.3, 4.0 and 4.2 cm to 4.5, 2.5, 3.3 cm, respectively. The new PPP method developed in this thesis thus provides a clear improvement over the existing PPP methods.

Results were further improved (in Chapter 6) by employing both GLONASS and GPS to estimate a float position solution while attempting GPS ambiguity resolution. GLONASS ambiguities are kept float, because of the code and phase biases in the GLONASS measurements. The rate of incorrect ambiguity resolution was further improved to 5.3%, the rate of correct ambiguity resolution to 82.2% and the 3D, horizontal and vertical positions errors at the initial ambiguity resolution epoch were reduced to 4.3, 2.4, and 3.2 cm, respectively, when employing both GPS and GLONASS on the NOAA dataset. Compared to the most reliable existing method (the ILSDNCF method with a 1200 s lock time requirement), the enhanced PPP method reduced the 3D error by 31.8%, horizontal error by 40.0% and vertical error by 23.8%. Using GLONASS with GPS provides improvements at minimal cost, because GLONASS is already supported by most geodetic quality GNSS receivers.

Existing PPP integrity monitoring methods were also analysed in this thesis. Novel methods to estimate more realistic protection levels and exclude multiple failures were developed in Chapter 5 and tested in Chapter 6. In terms of protection level calculation, a novel method to calculate more realistic protection levels based on the nominal bias assumption was proposed. In terms of failure exclusion, a novel method to make failure exclusion in the case of multiple simultaneously failures or a base-satellite failure was developed.

Employing NWM based tropospheric corrections with the enhanced PPP method was tested in Chapter 6. However, based on the results, NWM based corrections are currently not

providing major improvements in terms of positioning accuracy, solution convergence and ambiguity resolution. Whether further improvements in the quality, latency and update rate of NWM data can be beneficial for PPP remains to be investigated.

In conclusion, novel methods have been developed to improve PPP in terms of ambiguity validation, accuracy, convergence time and integrity. The methods proposed are designed for the existing GPS and GLONASS signals and the openly available CNES correction products. Therefore, the work presented in this thesis is readily implementable for real-life applications, such as many surveying, agriculture and marine applications.

7.2 Recommendations for future work

The modernisation of GPS and GLONASS and development of the Galileo, BeiDou and QZSS systems will be the most important changes to GNSS-based positioning in the next 10 years. New signals and systems are expected to significantly improve PPP. However, there are only a few satellites broadcasting the modernised and new constellations' signals to-date (in 2013). Thus, more research is required to further explore the benefits of the new constellations and signals as and when they become available. This includes both rover side processing and product generation.

A particularly interesting topic is the benefit of the new signals and constellations for PPP ambiguity resolution. It is speculated in the literature that the existence of the triple-frequency GNSS signals enables fast PPP ambiguity resolution referring to obtaining an initial ambiguity resolution within 5 minutes. This would make PPP more practical for a wide range of applications. In addition, the availability of the new constellations such as BeiDou and Galileo will increase the number of satellites in a view, which can improve PPP in challenging environments such as urban canyons and add redundancy to the solution estimation.

The modernisation of GPS and Galileo brings new signals such as L1C and E5, which have better noise and multipath properties compared to the current GPS C and P-code signals. This can make PPP more suitable to use in environments with significant multipath. In addition, the improved noise and multipath properties can reduce PPP convergence time and reduce the likelihood of wrong ambiguity resolution, because errors in float ambiguity

solutions are often caused by multipath. The addition of CDMA signals to GLONASS facilitates ambiguity resolution, because receiver specific biases discussed in Section 4.3.3 are eliminated.

More work is required to improve the accuracy and reliability of satellite orbit and clock and fractional cycle bias correction products. This would include monitoring integrity of the product generation and providing integrity information for rovers. In addition, generating real-time satellite orbit corrections with shorter update and prediction intervals than the currently used IGS Ultra-rapid correction would improve the reliability and accuracy of the corrections. It would also be necessary to generate the corrections for the GNSS systems and signals.

GLONASS PPP ambiguity resolution is a suitable topic for future work. Enabling it would require receiver manufactures to provide calibration information on the phase and code biases of their receivers.

PPP integrity is also an important topic for future research. Little work has been carried out to-date on estimating the integrity risk of the whole PPP processing chain, including product generation and rover side processing. Integrity issues in correction products can seriously decrease accuracy, convergence and ambiguity resolution performance on the rover side.

Improving local or regional ionospheric and tropospheric correction products is also a suitable topic for future research. For example, the future research can include the development of local or regional products for fast PPP ambiguity resolution. Employing NWM based tropospheric corrections was tested in this thesis, but more work is required to improve the quality of the corrections in terms of the accuracy, update rate and real-time availability.

More work is still required to improve the ratio test threshold calculation methods. The issue with the ILSFFS method is that it uses ILS failure rate for the ratio test threshold calculation. However, it is not possible to estimate realistic ILS failure rates when employing EKF. For the ILSDNCF method, the issue is that the assumption of the Doubly Non-Central F-distribution of the ratio test statistic requires further justification. Based on the analysis, more work is still required to find the most optimal ambiguity validation method in terms of

the time required to obtain an initial ambiguity resolution and rate of correct and incorrect ambiguity resolution. An additional challenge in the future is to find the most optimal ambiguity validation method when employing the new GNSS systems and signals.

8 References

ABDEL-SALAM, M. 2005. *Precise Point Positioning using un-differenced code and carrier phase observations.* PhD thesis, University of Calgary

ALTAMIMI, Z. & COLLILIEUX, X. 2009. IGS contribution to the ITRF. *Journal of Geodesy,* 83**,** 375-383.

ALTAMIMI, Z., COLLILIEUX, X. & MÉTIVIER, L. 2011. ITRF2008: an improved solution of the international terrestrial reference frame. *Journal of Geodesy,* 85**,** 457-473.

BAKKER, P. F. D., TIBERIUS, C. C. J. M., MAREL, H. V. D. & BREE, R. J. P. V. 2012. Short and zero baseline analysis of GPS L1 C/A, L5Q, GIOVE E1B, and E5aQ signals. *GPS Solutions,* 16**,** 53-64.

BANVILLE, S. & LANGLEY, R. B. 2009. Improving Real-Time Kinematic PPP with Instantaneous Cycle-Slip Correction. *Proceedings of the 22nd International Technical Meeting of The Satellite Division of the Institute of Navigation (ION GNSS 2009).* Savannah, GA.

BANVILLE, S. & TANG, H. 2010. Antenna Rotation and Its Effects on Kinematic Precise Point Positioning. *Proceedings of the 23rd International Technical Meeting of The Satellite Division of the Institute of Navigation (ION GNSS 2010).* Portland, OR

BAR-SEVER, Y. E., KROGER, P. M. & BORJESSON, J. A. 1997. Estimating Horizontal Gradients of Tropospheric Path Delay with a Single GPS Receiver. *Journal of Geophysical research,* 103**,** 5019-5035.

BEIDOU 2011. BeiDou Navigation Satellite System signal In Space Interface Control Document (Test Version). China Satellite Navigation Office

BEIDOU. 2012a. *BeiDou Navigation Satellite System Signal In Space Interface Control Document released today* [Online]. Available: http://www.beidou.gov.cn [Accessed 15 January 2013].

BEIDOU 2012b. BeiDou Navigation Satellite System Signal In Space Interface Control Document,Open Service Signal B1I (Version 1.0). *In:* OFFICE, C. S. N. (ed.).

BEIDOU. 2013. *BeiDou Navigation Satellite System* [Online]. Available: http://www.beidou.gov.cn/ [Accessed 29 July 2013].

BERN. 2012. *IGS - International GNSS Service* [Online]. Available: http://cmslive3.unibe.ch/unibe/philnat/aiub/content/research/satellite_geodesy/code___research/igs/index_eng.html [Accessed 21 August 2012].

BERTIGER, W., DESAI, S. D., HAINES, B., HARVEY, N., MOORE, A. W., OWEN, S. & WEISS, J. P. 2010. Single receiver phase ambiguity resolution with GPS data. *Journal of Geodesy* 84**,** 327-337.

BILICH, A. & MADER, G. L. 2010. GNSS Absolute Antenna Calibration at the National Geodetic Survey. *Proceedings of the 23rd International Technical Meeting of The Satellite Division of the Institute of Navigation (ION GNSS 2010).* Portland, OR

BISNATH, S. & GAO, Y. 2009. Precise Point Positioning A powerful Technique with a Promising Future. *GPS World.*

BLACK, H. D. & EISNER, A. 1984. Correcting satellite Doppler data for tropospheric effects. *Journal of Geophysical Research: Atmospheres* 89**,** 2616–2626.

BLEWITT, G. 1989. Carrier Phase Ambiguity Resolution for the Global Positioning System Applied to Geodetic Baselines up to 2000 km. *Journal of Geosphysical research,* 94**,** 10,187-10,203

BLEWITT, G., HAMMOND, W. C., KREEMER, C., PLAG, H.-P., STEIN, S. & OKAL, E. 2009. GPS for real-time earthquake source determination and tsunami warning systems. *Journal of Geodesy,* 83**,** 335-343.

BOEHM, J., HEINKELMANN, R. & SCHUH, H. 2007. Short Note: A global model of pressure and temperature for geodetic applications. *Journal of Geodesy,* 81**,** 679-683.

BOEHM, J., NIELL, A., TREGONING, P. & SCHUH, H. 2006a. Global Mapping Function (GMF): A new empirical mapping function based on numerical weather model data. *Geophysical Research Letters,* 33.

BOEHM, J., WERL, B. & SCHUH, H. 2006b. Troposphere mapping functions for GPS and very long baseline interferometry from European Centre for Medium-Range Weather Forecasts operational analysis data *Journal of Geosphysical research* 111.

BOS, M. S. & SCHERNECK, H.-G. 2011. *Ocean tide loading provider*

[Online]. Available: http://froste.oso.chalmers.se/loading//index.html [Accessed 21 June 2011].

BROWN, R. G. & CHIN, G. Y. 1998. GPS RAIM: Calculation of Threshold and Protection Radius Using Chi-Square Methods-A Geometric Approach. *Global positioning system, ION,* 5**,** 155–178.

BUICK, R. 2006. RTK base station networks driving adoption of GPS +/- 1 inch automated steering among crop growers. Westminster, CO: Trimble.

CAI, C. & GAO, Y. 2013. Modeling and assessment of combined GPS/GLONASS precise point positioning *GPS Solutions,* 17**,** 223-236.

CAISSY, M., AGROTIS, L., WEBER, G., HERNANDEZ-PAJARES, M. & HUGENTOBLER, U. 2012. The International GNSS Real-Time Service. *GPS World*

CHANG, X., PAIGE, C. & PEREPETCHAI, V. 2001. Integrity methods using carrier phase. *Proceedings of International Symposium on Kinematic Systems in Geodesy, Geomatics and Navigation.* Banff, Alberta, Canada.

CHEBOTAREV, V. E. 2007. Navigation Satellite Systems. *Information Satellite Systems.* Reshetnev company.

CHEN, G. & HERRING, T. A. 1997. Effects of atmospheric azimuthal asymmetry on the analysis of space geodetic data. *Journal of Geophysical Research,* 102**,** 20,489-20,502.

CHEN, X., ALLISON, T., CAO, W., FERGUSON, K., GRÜNIG, S., GOMEZ, V., KIPKA, A., KÖHLER, J., LANDAU, H., LEANDRO, R., LU, G., STOLZ, R. & TALBOT, N. 2011. Trimble RTX, an Innovative New Approach for Network RTK. *Proceedings of the 24th International Technical Meeting of The Satellite Division of the Institute of Navigation (ION GNSS 2011).* Portland, OR.

CHEN, X., LANDAU, H. & VOLLATH, U. 2003. New Tools for Network RTK Integrity Monitoring *Proceedings of the 16th International Technical Meeting of the Satellite Division of The Institute of Navigation (ION GPS/GNSS 2003).* Portland, OR.

CODE. 2012. *INTERNATIONAL GNSS SERVICE CODE Analysis Strategy Summary*

[Online]. Available: http://igscb.jpl.nasa.gov/igscb/center/analysis/code.acn [Accessed 24 August 2012].

COLLINS, P. 2008. Isolating and Estimating Undifferenced GPS Integer Ambiguities. *Proceedings of the 2008 National Technical Meeting of The Institute of Navigation.* San Diego, CA

COLLINS, P., LAHAYE, F. & BISNATH, S. 2012. External Ionospheric Constraints for Improved PPP-AR Initialisation and a Generalised Local Augmentation Concept. *Proceedings of the 25th International Technical Meeting of The Satellite Division of the Institute of Navigation (ION GNSS 2012).* Nashville, TN.

COLLINS, P., LAHAYE, F., HEROUX, P. & BISNATH, S. 2008. Precise Point Positioning with Ambiguity Resolution using the Decoupled Clock Model. *Proceedings of the 21st International Technical Meeting of the Satellite Division of The Institute of Navigation (ION GNSS 2008).* Savannah, GA

COUNSELMAN, C. C. & GOUREVITCH, S. A. 1981. Miniature Interferometer Terminals for Earth. Surveying: Ambiguity and Multipath with. Global Positioning System. *IEEE Transactions on Geoscience and Remote Sensing,* GE-19.

DACH, R., HUGENTOBLER, U., FRIDEZ, P. & MEINDL, M. 2007. *Bernese GPS Software Version 5.0 user manual*

DAVIS, J. L., HERRING, T. A., SHAPIRO, I. I., ROGERS, A. E. E. & ELGERED, G. 1985. Geodesy by radio interferometry: effects of atmospheric modeling errors on estimates of baseline length. *Radio Science,* 20**,** 1593-1607.

DESAI, S. D., BERTIGER, W., M. GARCIA-FERNANDEZ, HAINES, B., MURPHY, D., C. SELLE, SIBOIS, A., SIBTHORPE, A. & WEISS, J. P. 2014. Status and Plans at the JPL IGS Analysis Center. *IGS Workshop.* Pasadena, CA

DGMOVE. 2007. *GALILEO European Satellite Navigation System:Frequently asked questions* [Online]. Available: http://ec.europa.eu/dgs/energy_transport/galileo/faq/index_en.htm#12 [Accessed 20 August 2012].

DILSSNER, F., SPRINGER, T., GIENGER, G. & DOW, J. 2010. The GLONASS-M satellite yaw-attitude model. *Advances in Space Research,* 47**,** 160-171.

DIXON, K. 2006. StarFire™: A Global SBAS for Sub-Decimeter Precise Point Positioning. *Proceedings of the 19th International Technical Meeting of the Satellite Division of The Institute of Navigation (ION GNSS 2006).* Fort Worth, TX

DONG, D. & BOCK, Y. 1989. Global Positioning System Network Analysis With Phase Ambiguity Resolution Applied to Crustal Deformation Studies in California. *Journal of Geophysical research,* 94**,** 3949-3966.

DOUCET, K., HERWIG, M., KIPKA, A., KREIKENBOHM, P., LANDAU, H., LEANDRO, R., MOESSMER, M. & PAGELS, C. 2012. Introducing Ambiguity Resolution in Web-hosted Global Multi-GNSS Precise Point Positioning with Trimble RTX-PP. *Proceedings of the 25th International Technical Meeting of The Satellite Division of the Institute of Navigation (ION GNSS 2012).* Nashville, TN.

DRAKE, S. P. 2004. Converting GPS Coordinates (φλh) to Navigation Coordinates (ENU). Edinburgh, South Australia, Australia: DSTO Electronics and Surveillance Research Laboratory.

EGNOS. 2011. *What is SBAS?* [Online]. Available: http://www.egnos-portal.eu/discover-egnos/about-egnos/what-sbas [Accessed 2 May 2013].

EGOS. 2013. *EGNOS Data Access Service (EDAS)* [Online]. Available: http://egnos-user-support.essp-sas.eu/egnos_ops/edas_intro [Accessed 16 April 2013].

ELMAS, Z. G., AQUINO, M., MARQUES, H. A. & MONICO, J. F. G. 2011. Higher order ionospheric effects in GNSS positioning in the European region. *Annales Geophysicae,* 29.

ELSOBEIEY, M. & EL-RABBANY, A. 2009. Effect of Second-Order Ionospheric Delay on GPS Orbit and Precise Point Positioning. *Proceedings of the 22nd International Technical Meeting of The Satellite Division of the Institute of Navigation (ION GNSS 2009).* Savannah, GA

ELSOBEIEY, M. & EL-RABBANY, A. 2010. On stochastic modeling of the modernized global positioning system (GPS) L2C signal. *Measurement science and technology* 21.

ELSOBEIEY, M. & EL-RABBANY, A. 2011. GPS Precise Point Positioning: Some Recent Developments. *Geomatics Technologies in The City.* Jeddah, Saudi-Arabia.

ENDERLE, W., AGROTIS, L., ZANDBERGEN, R., KINTS, M. V. & MARTIN, J. 2013. Real-Time GNSS Activities at ESA. *GPS World.*

ESA 2010. European GNSS (Galileo) Open Service Signal In Space Interface Control Document European Union.

ESA. 2011. *ESA GNSS products* [Online]. Available: ftp://dgn6.esoc.esa.int/products/ [Accessed 16 June 2011].

ESA. 2013. *Fact Sheet* [Online]. Available: http://download.esa.int/docs/Galileo_IOV_Launch/Galileo_factsheet_2012.pdf [Accessed 3 August 2013].

EU. 2011. *Launch of first 2 operational Galileo satellites* [Online]. Available: http://ec.europa.eu/enterprise/policies/satnav/galileo/satellite-launches/index_en.htm [Accessed 20 August 2012].

EU. 2013. *Why Galileo?* [Online]. Available: http://ec.europa.eu/enterprise/policies/satnav/galileo/why/index_en.htm [Accessed 3 August 2013].

EULER, H. J. & SCHAFFRIN, B. 1990. On a measure of the discernibility between different ambiguity solutions in the static-kinematic GPS mode. *Kinematic Systems in Geodesy, Surveying and Remote Sensing, IAG Symposium No. 107.* Banff, Alberta.

FENG, S., OCHIENG, W., MOORE, T., HILL, C. & HIDE, C. 2009. Carrier phase-based integrity monitoring for high-accuracy positioning. *GPS Solutions,* 13**,** 13-22.

FENG, S., OCHIENG, W., SAMSON, J., TOSSAINT, M., HERNANDEZ-PAJARES, M., JUAN, J. M., SANZ, J., ARAGÓN-ÀNGEL, À., RAMOS-BOSCH, P. & JOFRE, M. 2012. Integrity Monitoring for Carrier Phase Ambiguities. *Journal of Navigation* 65**,** 41-58

FENG, S., OCHIENG, W., SAMSON, J., TOSSAINT, M., HERNANDEZ-PAJARES, M., JUAN, J. M., SANZ, J., ARAGÓN-ÀNGEL, À., RAMOS, P. & JOFRE, M. 2010. Integrity Monitoring for Carrier Phase Ambiguities. *Proceedings of the 23rd International Technical Meeting of The Satellite Division of the Institute of Navigation (ION GNSS 2010).* Portland, OR

GABOR, M. J. & NEREM, R. S. 1999. GPS carrier phase ambiguity resolution using satellite-satellite single differences *Proceedings of the 12th International Technical Meeting of the Satellite Division of The Institute of Navigation (ION GPS 1999).* Nashville, TN

GAO, Y. & SHEN, X. 2001. Improving Ambiguity Convergence in Carrier Phase-Based Precise Point Positioning. *Proceedings of the 14th International Technical Meeting of the Satellite Division of The Institute of Navigation (ION GPS 2001).* Salt Lake City, UT

GE, M., CHEN, J., DOUŠA, J., GENDT, G. & WICKERT, J. 2012. A computationally efficient approach for estimating high-rate satellite clock corrections in realtime. *GPS Solutions,* 16**,** 9-17.

GE, M., GENDT, G. & ROTHACHER, M. 2006. Integer Ambiguity Resolution For Precise Point Positioning: Applied To Fast Integrated Estimation of Very Huge GNSS Networks. *VI Hotine-Marussi Symposium of Theoretical and Computational Geodesy:Challenge and Role of Modern Geodesy.* Wuhan, China.

GE, M., GENDT, G., ROTHACHER, M., SHI, C. & LIU, J. 2008. Resolution of GPS carrier-phase ambiguities in Precise Point Positioning (PPP) with daily observations. *Journal of Geodesy* 82**,** 389-399.

GENG, J. 2009. Rapid Re-convergence in Real-time Precise Point Positioning with Ambiguity Resolution *Proceedings of the 22nd International Technical Meeting of The Satellite Division of the Institute of Navigation (ION GNSS 2009).* Savannah, GA

GENG, J., MENG, X., ALAN H. DODSON, GE, M. & TEFERLE, F. N. 2010a. Rapid re-convergences to ambiguity-fixed solutions in precise point positioning. *Journal of Geodesy,* 84**,** 705-714.

GENG, J., MENG, X., DODSON, A. H. & TEFERLE, F. N. 2010b. Integer ambiguity resolution in precise point positioning: method comparison. *Journal of Geodesy,* 84**,** 569-581.

GENG, J., SHI, C., GE, M., DODSON, A. H., LOU, Y., ZHAO, Q. & LIU, J. 2012. Improving the estimation of fractional-cycle biases for ambiguity resolution in precise point positioning. *Journal of Geodesy,* 86**,** 579-589.

GENG, J., TEFERLE, F. N., MENG, X. & DODSON, A. H. 2010c. Kinematic precise point positioning at remote marine platforms. *GPS Solutions,* 14**,** 343-350.

GENG, J., TEFERLE, F. N., MENG, X. & DODSON, A. H. 2010d. Towards PPP-RTK: Ambiguity resolution in real-time precise point positioning *Advances in Space Research,* 47**,** 1664–1673.

GENG, J., TEFERLE, F. N., SHI, C., MENG, X., DODSON, A. H. & LIU, J. 2009. Ambiguity resolution in precise point positioning with hourly data. *GPS Solutions,* 13**,** 263-270.

GIBBONS, G. 2013. BeiDou to Restart Satellite Launches Next Year, Shift B1 Signal Frequency after 2016. *GPS World*.

GPS. 2013a. *LightSquared and GPS* [Online]. Available: http://www.gps.gov/spectrum/lightsquared/ [Accessed 4 May 2013].

GPS 2013b. Official U.S. Government information about the Global Positioning System (GPS) and related topics.
GPS. 2014. *Official U.S. Government information about the Global Positioning System (GPS) and related topics* [Online]. Available: http://www.gps.gov/ [Accessed 29 November 2014].
GPS, N. 2010a. GLOBAL POSITIONING SYSTEM WING (GPSW) SYSTEMS ENGINEERING & INTEGRATION INTERFACE SPECIFICATION IS-GPS-200 Revision E.
GPS, N. 2010b. GLOBAL POSITIONING SYSTEM WING (GPSW) SYSTEMS ENGINEERING & INTEGRATION INTERFACE SPECIFICATION IS-GPS-705 Revision A.
GPS, N. 2010c. GLOBAL POSITIONING SYSTEM WING (GPSW) SYSTEMS ENGINEERING & INTEGRATION INTERFACE SPECIFICATION IS-GPS-800 Revision A.
GPS_WORLD 2012a. Massive GPS Jamming Attack by North Korea. *GPS World.*
GPS_WORLD 2012b. Transmissions from Galileo Satellite IOV-3 Have Begun. *GPS World*
GRIFFITHS, J. & RAY, J. R. 2009. On the precision and accuracy of IGS orbits. *Journal of Geodesy,* 83**,** 277-287.
GRIMES, J. 2007. GLOBAL POSITIONING SYSTEM PRECISE POSITIONING SERVICE PERFORMANCE STANDARD *In:* DEPARTMENT OF DEFENSE, U. S. O. A. (ed.).
GRINTER, T. & ROBERTS, C. 2011. Precise Point Positioning: Where are we now? *International Global Navigation Satellite Systems Society IGNSS Symposium 2011.* Sydney, NSW, Australia.
GROVES, P. D., JIANG, Z., SKELTON, B., CROSS, P. A., LAU, L., ADANE, Y. & KALE, I. 2010. Novel Multipath Mitigation Methods using a Dual-polarization Antenna *Proceedings of the 23rd International Technical Meeting of The Satellite Division of the Institute of Navigation (ION GNSS 2010).* Portland, OR
GSA 2012. GNSS market report issue 2. The European GNSS Agency (GSA).
GSA. 2013. *Galileo Services* [Online]. Available: http://www.gsa.europa.eu/galileo/services [Accessed 3 August 2013].
GSI 2004. The New Geodetic Reference System of Japan-Its adoption and application to our products. *Bull Geogr Surv Inst,* 50**,** 33-36.
GSI. 2011. *Japanese Geodetic Datum 2011 (JGD2011)* [Online]. Available: http://www.gsi.go.jp/ENGLISH/page_e30030.html [Accessed 24 August 2012].
HADAS, T. & BOSY, J. 2014. IGS RTS precise orbits and clocks verification and quality degradation over time. *GPS Solutions,* February.
HAMMOND, W. C., BROOKS, B. A., BÜRGMANN, R., HEATON, T., JACKSON, M., LOWRY, A. R. & ANANDAKRISHNAN, S. 2011. Scientific Value of Real-Time Global Positioning System Data. *Eos, Transactions American Geophysical Union,* 92**,** 125–126.
HEROUX, P., CAISSY, M. & GALLACE, J. 1993. Canadian Active Control System Data Acquisition and Validation. *IGS Workshop.* University of Berne, Berne, Switzerland
HÉROUX, P. & KOUBA, J. 2001. GPS Precise Point Positioning Using IGS Orbit Products. *Physics and Chemistry of the Earth, Part A: Solid Earth and Geodesy,* 26**,** 573-578.
HERRING, T. A. 1992. Modeling atmospheric delays in the analysis of space geodetic data. *Proceedings of the Symposium on Refraction of Transatmospheric Signals in Geodesy.* Delft, Netherlands.
HILLA, S. & CLINE, M. 2003. Evaluating pseudorange multipath effects at stations in the National CORS Network. *GPS Solutions,* 7**,** 253-267.
HOFMANN-WELLENHOF, B., LICHTENEGGER, H. & WALSE, E. 2008. *GNSS Global Navigation Satellite Systems; GPS, Glonass, Galileo & more,* New York, Springer Wien.
HOQUE, M. M. & JAKOWSKI, N. 2008. Mitigation of higher order ionospheric effects on GNSS users in Europe *GPS Solutions* 12**,** 87-97.
IAC. 2012. *Information-Analytical Centre* [Online]. Available: http://www.glonass-ianc.rsa.ru/en/ [Accessed 1 February 2012].
IAC. 2013. *Information-Analytical Centre* [Online]. Available: http://glonass-iac.ru/en/ [Accessed 2 May 2013].

IAC. 2014. *Information analytical centre of GLONASS and GPS controlling* [Online]. Available: https://glonass-iac.ru/en/index.php [Accessed 29 November 2014].
ICAO 2005. Global Navigation Satellite System (GNSS) Manual.
IERS 2003. IERS Technical Note No. 32. International Earth Rotation and Reference Systems Service.
IFADIS, I. M. 1992. The excess propagation path of radio waves: Study of the influence of the atmospheric parameters on its elevation dependence. *Survey Review,* 31**,** 289-298.
IGS. 2009. *IGS Products* [Online]. Available: http://igscb.jpl.nasa.gov/components/prods.html [Accessed 17 December 2012].
INSIDE_GNSS 2013. Japan Awards Contracts for QZSS Space, Ground Segments. *Inside GNSS.*
IWABUCHI, T., ROCKEN, C., LUKES, Z., MERVART, L. & JOHNSON, J. 2006. PPP and Network True Real-time 30 sec Estimation of ZTD in Dense and Giant Regional GPS Network and the Application of ZTD for Nowcasting of Heavy Rainfall. *Proceedings of the 19th International Technical Meeting of the Satellite Division of The Institute of Navigation (ION GNSS 2006).* Fort Worth, TX
JAXA 2013. Quasi-Zenith Satellite System Navigation Service, Interface Specification for QZSS V1.5. *In:* AGENCY, J. A. E. (ed.).
JOERGER, M. & PERVAN, B. 2011. Integrity Risk of Kalman Filter-Based RAIM. *Proceedings of the 24th International Technical Meeting of The Satellite Division of the Institute of Navigation (ION GNSS 2011).* Portland, OR.
JOERGER, M. & PERVAN, B. 2012. Kalman Filter Residual-Based Integrity Monitoring Against Measurement Faults. *AIAA Guidance, Navigation, and Control Conference.* Minneapolis, MN.
JONGE, P. D. & TIBERIUS, C. 1996. The LAMBDA method for integer ambiguity estimation: implementation aspects. *Publications of the Delft Geodetic Computing Centre,* 12.
JPL. 2014. *GIPSY-OASIS* [Online]. Available: https://gipsy-oasis.jpl.nasa.gov/index.php?page=home [Accessed 29 November 2014].
JUAN, J. M., HERNÁNDEZ-PAJARES, M., SANZ, J., RAMOS-BOSCH, P., ARAGÓN-ÀNGEL, A., ORÚS, R., OCHIENG, W., FENG, S., JOFRE, M., COUTINHO, P., SAMSON, J. & TOSSAINT, M. 2012. Enhanced Precise Point Positioning for GNSS users. *IEEE transactions on geoscience and remote sensing,* PP**,** 1 - 11
KALMAN, R. E. 1960. A New Approach to Linear Filtering and Prediction Problems. *Journal of Basic Engineering,* 82**,** 35-45.
KAPLAN, E. D. & HEGARTY, C. J. 2006. *Understanding GPS principles and applications second edition* Norwood, MA, Artech House, Inc.
KATO, T., TERADA, Y., ITO, K., HATTORI, R., ABE, T., MIYAKE, T., KOSHIMURA, S. I. & NAGAI, T. 2005. Tsunami due to the 2004 September 5th off the Kii peninsula earthquake,Japan, recorded by a new GPS buoy. *Earth Planets Space,* 57**,** 297–301.
KERKHOFF, A., HARRIS, R. B., PETERSEN, C. P. & PICKARD, A. 2010. Modifications to GPS Reference Station Antennas to Reduce Multipath. *Proceedings of the 23rd International Technical Meeting of The Satellite Division of the Institute of Navigation (ION GNSS 2010).* Portland, OR.
KIM, U. S., LORENZO, D. D., GAUTIER, J., ENGE, P. & ORR, J. A. 2004. Phase Effects Analysis of Patch Antenna CRPAs for JPALS. *Proceedings of the 17th International Technical Meeting of the Satellite Division of The Institute of Navigation (ION GNSS 2004).* Long Beach, CA.
KLEIJER, F. 2004. *Troposphere Modeling and Filtering for Precise GPS Leveling.* PhD thesis, The NCG, Nederlandse Commissie voor Geodesie, Netherlands Geodetic Commission is an institute of the Royal Netherlands Academy of Arts and Sciences (KNAW).
KOUBA, J. 2009a. Guide to using International GNSS service (IGS) products. Ottawa, Ontario: Geodetic Survey Division, Natural Resources Canada.
KOUBA, J. 2009b. A simplified yaw-attitude model for eclipsing GPS satellites. *GPS Solutions,* 13**,** 1-12.
KOUBA, J. 2009c. Testing of global pressure/temperature (GPT) model and global mapping function (GMF) in GPS analyses. *Journal of Geodesy,* 83**,** 199-208.

LANGEL, S., KHANAFSEH, S. & PERVAN, B. 2012. Assessing the Impact of Time Correlation Uncertainty on Cycle Ambiguity Resolution for High Integrity Aviation Applications. *Proceedings of the 25th International Technical Meeting of The Satellite Division of the Institute of Navigation (ION GNSS 2012).* Nashville, TN.

LARSON, R. E., DRESSLER, R. M. & RATNER, R. S. 1967. Application of the Extended Kalman filter to ballistic trajectory estimation. Menlo Park, CA: Stanford Res. Inst.

LAU, L. & CROSS, P. 2006. A New Signal-to-Noise-Ratio Based Stochastic Model for GNSS High-Precision Carrier Phase Data Processing Algorithms in the Presence of Multipath Errors. *Proceedings of the 19th International Technical Meeting of the Satellite Division of The Institute of Navigation (ION GNSS 2006).* Fort Worth, TX

LAURICHESSE, D. 2011. The CNES Real-time PPP with undifferenced integer ambiguity resolution demonstrator. *Proceedings of the 24th International Technical Meeting of The Satellite Division of the Institute of Navigation (ION GNSS 2011).* Portland, Oregon.

LAURICHESSE, D. 2012. Phase Biases Estimation for Undifferenced Ambiguity Resolution. *PPP-RTK & Open Standards Symposium.* Frankfurt am Main, Germany.

LAURICHESSE, D. 2013. *RE: Personal communication:Map of CNES stations*

LAURICHESSE, D. & MERCIER, F. 2007. Integer ambiguity resolution on undifferenced GPS phase measurements and its applications to PPP. *Proceedings of the 20th International Technical Meeting of the Satellite Division of The Institute of Navigation (ION GNSS 2007).* Fort Worth, TX

LAURICHESSE, D., MERCIER, F. & BERTHIAS, J. P. 2009a. Real Time GPS Constellation and Clocks Estimation using Zero-difference Integer Ambiguity Fixing. *Proceedings of the 2009 International Technical Meeting of The Institute of Navigation.* Anaheim, CA.

LAURICHESSE, D., MERCIER, F. & BERTHIAS, J. P. 2009b. Zero-difference integer ambiguity fixing on single frequency receivers. *Proceedings of the 22nd International Technical Meeting of The Satellite Division of the Institute of Navigation (ION GNSS 2009).* Savannah, GA

LAURICHESSE, D., MERCIER, F. & BERTHIAS, J. P. 2010. Real-time PPP with undifferenced integer ambiguity resolution, experimental results. *Proceedings of the 23rd International Technical Meeting of The Satellite Division of the Institute of Navigation (ION GNSS 2010).* Portland, Or.

LAURICHESSE, D., MERCIER, F., BERTHIAS, J. P. & BIJAC, J. 2008. Real Time Zero-difference Ambiguities Blocking and Absolute RTK. *Proceedings of the 2008 National Technical Meeting of The Institute of Navigation.* San Diego, California.

LAURICHESSE, D., MERCIER, F., BERTHIAS, J. P., BROCA, P. & CERRI, L. 2009c. Integer Ambiguity Resolution on Undifferenced GPS Phase Measurements and its Application to PPP and Satellite Precise Orbit Determination. *Navigation,* 56.

LEANDRO, R., GOMEZ, V., STOLZ, R., LANDAU, H. & GLOCKER, M. 2012a. Developments on Global Centimeter-level GNSS Positioning with Trimble CenterPoint RTX/TM. *Proceedings of the 25th International Technical Meeting of The Satellite Division of the Institute of Navigation (ION GNSS 2012).* Nashville, TN.

LEANDRO, R., LANDAU, H., NITSCHKE, M., GLOCKER, M., SEEGER, S., CHEN, X., DEKING, A., BENTAHAR, M., ZHANG, F., FERGUSON, K., STOLZ, R., TALBOT, N., LU, G., ALLISON, T., BRANDL, M., GOMEZ, V., CAO, W. & KIPKA, A. 2011a. RTX Positioning: The Next Generation of cm-accurate Real-Time GNSS Positioning. *Proceedings of the 24th International Technical Meeting of The Satellite Division of the Institute of Navigation (ION GNSS 2011).* Portland, OR.

LEANDRO, R., SANTOS, M. & LANGLEY, R. B. 2006. UNB Neutral Atmosphere Models: Development and Performance. *Proceedings of ION NTM 2006, the 2006 National Technical Meeting of The Institute of Navigation.* Monterey, California.

LEANDRO, R. F., LANDAU, H., NITSCHKE, M., GLOCKER, M., SEEGER, S., CHEN, X., DEKING, A., TAHAR, M. B., ZHANG, F., FERGUSON, K., STOLZ, R., TALBOT, N., LU, G., ALLISON, T., BRANDL, M., GOMEZ, V., CAO, W. & KIPKA, A. 2012b. Real-Time Extended GNSS Positioning. *GPS World*

LEANDRO, R. F., SANTOS, M. C. & LANGLEY, R. B. 2011b. Analyzing GNSS data in precise point positioning software. *GPS Solutions,* 15**,** 1-13.

LEE, Y. C. 1986. Analysis of Range and Position Comparison Methods as a Means to Provide GPS Integrity in the User Receiver. *Institute of Navigation, Annual Meeting, 42nd.* Seattle, WA.

LI, B., FENG, Y. & SHEN, Y. 2010. Three carrier ambiguity resolution: distance-independent performance demonstrated using semi-generated triple frequency GPS signals. *GPS Solutions,* 10**,** 177-184.

LI, W., YUAN, Y., OU, J., LI, H. & LI, Z. 2012. A new global zenith tropospheric delay model IGGtrop for GNSS applications. *Chinese Science bulleting,* 57**,** 2132-2139.

LI, X. 2012. Improving Real-time PPP Ambiguity Resolution with Ionospheric Characteristic Consideration. *Proceedings of the 25th International Technical Meeting of The Satellite Division of the Institute of Navigation (ION GNSS 2012).* Nashville, TN.

LI, X. & ZHANG, X. 2012. Improving the Estimation of Uncalibrated Fractional Phase Offsets for PPP Ambiguity Resolution. *Journal of Navigation,* 65**,** 513-529.

LI, X., ZHANG, X. & GUO, F. 2009. Study on Precise Point Positioning Based on Combined GPS and GLONASS. *Proceedings of the 22nd International Technical Meeting of The Satellite Division of the Institute of Navigation (ION GNSS 2009).* Savannah, GA

LIU, C., MENG, X. L., LI, N. & RYDING, J. 2013. Precise 3D Measurements of the Roof Lab Railway Track with Ground Base Laser Scanning Technology and Its Relevance to High Speed Railway Track Monitoring. *Joint International Symposium on Deformation Monitoring.* Hong Kong.

LIU, Z. 2011. A new automated cycle slip detection and repair method for a single dual-frequency GPS receiver. *Journal of Geodesy,* 85**,** 171–183.

MACLEOD, K. & CAISSY, M. 2010. Real Time IGS Pilot Project (RT-PP) Status Report. *IGS Workshop.* Newcastle UK.

MACMILLAN, D. S. 1995. Atmospheric gradients from very long baseline interferometry observations. *Geophysical Research Letters,* 22**,** 1041-1044.

MELBOURNE, W. G. 1985. The Case for Ranging in GPS Based Geodetic Systems. *Proceedings of the 1st International Symposium on Precise Positioning with the Global Positioning System.* Rockville, Maryland.

MENDES, V. B. 1999. Modeling the neutral-atmosphere propagation delay in radiometric space techniques. *Technical report no. 199.* Fredericton, New Brunswick, Canada: Department of Geodesy and Geomatics Engineering, University of New Brunswick.

MERCIER, F. & LAURICHESSE, D. 2008. Zero-Difference Ambiguity Fixing - Properties of satellite/receiver widelane biases. *Toulouse Space Show'08, European Navigation Conference ENC-GNSS.* Toulouse, France.

MERVART, L. 1995. *Ambiguity Resolution Techniques in Geodetic and Geodynamic Applications of the Global Positioning System.* PhD University of Bern.

MONTENBRUCK, O., GILL, E. & KROES, R. 2005. Rapid orbit determination of LEO satellites using IGS clock and ephemeris products. *GPS Solutions,* 9**,** 226-235.

MORADI, R., SCHUSTER, W., FENG, S. & OCHIENG, W. 2013. Reducing GPS wide lane ambiguity resolution time: a novel carrier phase multipath mitigation technique. *Proceedings of the 2013 International Technical Meeting of The Institute of Navigation.* San Diego, CA.

NAVCOM. 2012. *StarFire* [Online]. Available: http://www.navcomtech.com/wps/dcom/navcom_en_US/technology/augmentation/starfire/starfire.page? [Accessed 13 December 2012].

NIELL, A. E. 1996. Global Mapping Functions for the Atmosphere Delay at Radio Wavelengths. *Journal of Geophysical Research,* 101**,** 3227-3246.

NOAA. 2013. *The National Oceanic and Atmospheric Administration (NOAA)* [Online]. Available: http://www.noaa.gov/ [Accessed 20 March 2013].

NOVATEL. 2012. *GrafNav/GrafNet®* [Online]. Available: http://www.novatel.com/products/software/waypoint-products/post-processing-software/grafnav/#overview [Accessed 13 December 2012].

ODIJK, D., TEUNISSEN, P. J. G. & ZHANG, B. 2012. Single-frequency integer ambiguity resolution enabled precise point positioning *Journal of Surveying Engineering*

OMNISTAR. 2012. *OmniSTAR G2* [Online]. Available: http://www.omnistar.com/SubscriptionServices/OmniSTARG2.aspx [Accessed 14 December 2012].

ORLIAC, E. J. 2009. *Development of azimuth dependent tropospheric mapping functions, based on a high resolution mesoscale numerical weather model, for GNSS data processing.* PhD thesis, University of Nottingham.

PALESTINI, C. 2014. Current status of Galileo PRS service and user segment development. *Satellite Masters Conference.* Berlin, Germany.

PARKINSON, B. W., JR., J. J. S., AXELRAD, P. & ENGE, P. 1996. *Global Positioning System: Theory and Applications, Volume I*, American Institute of Aeronautics and Astronautics

PENNA, N., DODSON, A. & CHEN, W. 2001. Assessment of EGNOS Tropospheric Correction Model. *The Journal of Navigation* 54**,** 37-55

PERVAN, B. S., LAWRENCE, D. G., COHEN, C. E. & PARKINSON, B. W. 1996. Parity Space Methods for Autonomous Fault Detection and Exclusion using GPS Carrier Phase. *Position Location and Navigation Symposium.* Atlanta, GA.

PERVAN, B. S., LAWRENCE, D. G. & PARKINSON, B. W. 1998. Autonomous Fault Detection and Removal Using GPS Carrier Phase. *IEEE Transactions on Aerospace and Electronic Systems,* 34**,** 897–906.

PHAM, N. D. 2011. The Economic Benefits of Commercial GPS Use in the U.S. and The Costs of Potential Disruption. NDP Consulting Group.

PORRETTA, M., MILNER, C. & OCHIENG, W. 2009. GAARDIAN Project WP1.ICL03 - User Requirements Document.

RAY, J. 2011. [IGSMAIL-6384] REMINDER: switch to IGS08/igs08.atx on 17 April 2011. International GNSS Service.

REBISCHUNG, P., GRIFFITHS, J., RAY, J., SCHMID, R., COLLILIEUX, X. & GARAYT, B. 2012. IGS08: the IGS realization of ITRF2008. *GPS Solutions,* 16**,** 483-494.

REMONDI, B. W. 1984. *Using the global positioning system (GPS) phase observable for relative geodesy: Modeling, processing, and results* PhD thesis University of Texas.

REUSSNER, N. & WANNINGER, L. 2011. GLONASS Inter-frequency Biases and Their Effects on RTK and PPP Carrier-phase Ambiguity Resolution. *Proceedings of the 24th International Technical Meeting of The Satellite Division of the Institute of Navigation (ION GNSS 2011).* Portland, OR.

REVNIVYKH, S. 2012. GLONASS Status and Modernization. *International GNSS Committee IGC-7.* Beijing, China.

RICS 2010. Guidelines for the use of GNSS in land surveying and mapping. Royal Institution of Chartered Surveyors (RICS).

ROCKWELL_COLLINS. 2012. *Rockwell Collins launches Real Time Kinematic technology solution for secure GPS receivers* [Online]. Available: http://www.rockwellcollins.com/sitecore/content/Data/News/2012_Cal_Yr/GS/FY12GSNR33-RTK.aspx [Accessed 25 February 2013].

RTCA 1999. Minimum operational performance standards for Global Positioning System / Wide Area Augmentation System airborne equipment. *RTCA DO-229B*.

RTCM. 2013. *The Radio Technical Commission for Maritime Services* [Online]. Available: http://www.rtcm.org/ [Accessed 16 August 2014].

SAASTAMOINEN, J. 1973. Contributions to the theory of atmospheric refraction, Part II. Refraction Corrections in Satellite Geodesy. *Bulletin Géodésique,* 107.

SCHAER, S. & DACH, R. 2010. Biases in GNSS Analysis. *IGS Workshop.* Newcastle England

SCHMID, R., ROTHACHER, M., THALLER, D. & STEIGENBERGER, P. 2005. Absolute phase center corrections of satellite and receiver antennas Impact on global GPS solutions and estimation of azimuthal phase center variations of the satellite antenna. *GPS Solutions,* 9**,** 459-476

SCHÜLER, T., DIESSONGO, H. & POKU-GYAMFI, Y. 2011. Precise ionosphere-free single-frequency GNSS positioning. *GPS Solutions,* 15**,** 139-147.

SCHUSTER, W., BAI, J., FENG, S. & OCHIENG, W. 2012. Integrity monitoring algorithms for airport surface movement. *GPS Solutions,* 16**,** 65-75.

SCHWARZ, C. R. & WADE, E. B. 1990. The North American datum of 1983: Project methodology and execution. *Journal of Geodesy,* 64**,** 28-62.

SEPTENTRIO. 2011. PolaRx4/PolaRx4TR :Multi-frequency GNSS Reference Station.

SHI, C., ZHAO, Q., GE, M., LIU, J., LOU, Y., ZHANG, H., GENG, J. & LI, M. 2010. Introduction to PANDA Software and the Latest Development for High Precision GNSS Data Processing and Application. *GS Analysis Center Workshop 2010.* Newcastle upon Tyne, UK.

SHI, J. 2012. *Precise Point Positioning Integer Ambiguity Resolution with Decoupled Clocks.* PhD thesis, University of Calgary.

SHI, J. & GAO, Y. 2010. Analysis of the integer property of ambiguity and characteristics of code and phase clocks in PPP using a decoupled clock model. *Proceedings of the 23rd International Technical Meeting of The Satellite Division of the Institute of Navigation (ION GNSS 2010).* Portland, OR

SHI, J. & GAO, Y. 2012. A Fast Integer Ambiguity Resolution Method for PPP. *Proceedings of the 25th International Technical Meeting of The Satellite Division of the Institute of Navigation (ION GNSS 2012).* Nashville, TN.

SNAY, R. & PEARSON, C. 2010. Coping with Tectonic Motion *The American Surveyor,* 7.

STEPHENSON, S., MENG, X., MOORE, T., BAXENDALE, A. & EDWARDS, T. 2012. Implementation of V2X with the Integration of Network RTK: Challenges and Solutions. *Proceedings of the 25th International Technical Meeting of The Satellite Division of the Institute of Navigation (ION GNSS 2012).* Nashville, TN.

TAKAC, F. & LIENHART, W. 2008. SmartRTK: A Novel Method Of Processing Standardised RTCM Network RTK Information For High Precision Positioning. *Proceedings of ENC GNSS 2008.* Toulouse, France.

TAKASU, T. 2012. *RTKLIB: An Open Source Program Package for GNSS Positioning* [Online]. Available: http://www.rtklib.com/ [Accessed 17 December 2012].

TERRASTAR. 2013. *TerraStar services* [Online]. Available: http://www.terrastar.net/services.html [Accessed 17 August 2014].

TEUNISSEN, P. 1998. A class of unbiased integer GPS ambiguity estimators. *Artificial Satellites,* 33**,** 4-10.

TEUNISSEN, P. J. G. 1993. Least-Squares Estimation of the Integer GPS Ambiguities. *The General Meeting of the International Association of Geodesy.* Beijing, China.

TEUNISSEN, P. J. G. 1999. An optimality property of the integer least-squares estimator. *Journal of Geodesy,* 73**,** 587-593.

TEUNISSEN, P. J. G. & VERHAGEN, S. 2008. GNSS Carrier Phase Ambiguity Resolution: Challenges and Open Problems. *Observing our changing Earth International Association of Geodesy Symposia,* 133**,** 785-792.

TEUNISSEN, P. J. G. & VERHAGEN, S. 2009. The GNSS ambiguity ratio-test revisited: a better way of using it *Survey Review,* 41**,** 138-151.

TIBERIUS, C. C. J. M. & JONGE, P. J. D. 1995. Fast positioning using the LAMBDA method. *Proceedings of the 4th International Symposium on Differential Satellite Navigation Systems DSNS'95.* Bergen, Norway.

TOLMAN, B., HARRIS, R. B., GAUSSIRAN, T., MUNTON, D., LITTLE, J., MACH, R., NELSEN, S., RENFRO, B. & SCHLOSSBERG, D. 2004. The GPS Toolkit -- Open Source GPS Software. *Proceedings of the*

17th International Technical Meeting of the Satellite Division of the Institute of Navigation (ION GNSS 2004). Long Beach, California.

UNAVCO. 2013. *Data - GNSS & Archive Glossary* [Online]. Available: http://facility.unavco.org/data/glossary.html [Accessed 16 April 2013].

URQUHART, L. 2009. Atmospheric Pressure Loading and its Effects on Precise Point Positioning. *Proceedings of the 22nd International Technical Meeting of The Satellite Division of the Institute of Navigation (ION GNSS 2009).* Savannah, GA

VERHAGEN, S. 2005. *The GNSS integer ambiguities: estimation and validation.* PhD thesis, Delft University of Technology (TUDelft)

VERHAGEN, S. & TEUNISSEN, P. J. G. 2013. The ratio test for future GNSS ambiguity resolution. *GPS Solutions,* 17**,** 535-548.

VERIPOS. 2013. *VERIPOS Apex 2* [Online]. Available: http://www.veripos.com/veripos-apex2.html [Accessed 5 March 2014].

WANG, L., GROVES, P. D. & ZIEBART, M. K. 2012. Multi-Constellation GNSS Performance Evaluation for Urban Canyons Using Large Virtual Reality City Models. *Journal of Navigation,* 65**,** 459-476

WANG, M. & GAO, Y. 2006. GPS Un-Differenced Ambiguity Resolution and Validation. *Proceedings of the 19th International Technical Meeting of the Satellite Division of The Institute of Navigation (ION GNSS 2006).* Fort Worth, TX

WARREN, D. L. M. & RAQUET, J. F. 2003. Broadcast vs. precise GPS ephemerides: a historical perspective. *GPS Solutions,* 7**,** 151-156.

WEI, M. & SCHWARZ, K.-P. 1995. Fast Ambiguity Resolution Using an Integer Nonlinear Programming Method. *Proceedings of the 8th International Technical Meeting of the Satellite Division of The Institute of Navigation (ION GPS 1995).* Palm Springs, CA

WEINBACH, U. & SCHÖN, S. 2011. GNSS receiver clock modeling when using high-precision oscillators and its impact on PPP. *Advances in Space Research,* 47**,** 229–238.

WISHNER, R. P., TABACZYNSKI, J. A. & ATHANS, M. 1969. A comparison of three non-linear filters. *Automatica,* 5**,** 487–496.

WMO 1988. WMO technical regulations. *WMO-NO 49, Vol I.*

WU, J. T., WU, S. C., HAJJ, G. A., BERTIGER, W. I. & LICHTEN, S. M. 1992. Effects of antenna orientation on GPS carrier phase. *Astrodynamics,* 18**,** 91-98.

WUBBENA, G. 1985. Software Developments for Geodetic Positioning with GPS Using TI 4100 Code and Carrier Measurements. *Proceedings First International Symposium on Precise Positioning with the Global Positioning System.* Rockville, Maryland.

YANG, L., ELMAS, Z., HILL, C., AQUINO, M. & MOOREA, T. 2011. An Innovative Approach for Atmospheric Error Mitigation Using New GNSS Signals. *Journal of Navigation,* 64**,** 211-S232

ZHANG, Y. & GAO, Y. 2006. Influence Analysis of Tropospheric Model and Mapping Function on Precise Tropospheric Delay Estimation Using PPP. *Proceedings of the 19th International Technical Meeting of the Satellite Division of The Institute of Navigation (ION GNSS 2006).* Fort Worth, Texas.

ZUMBERGE, J. F., HEFTIN, M. B., JEFFERSON, D. C., WATKINS, M. M. & WEBB, F. H. 1997. Precise point positioning for the efficient and robust analysis of GPS data from large networks. *Journal of Geophysical Research,* 102**,** 5005-5017.